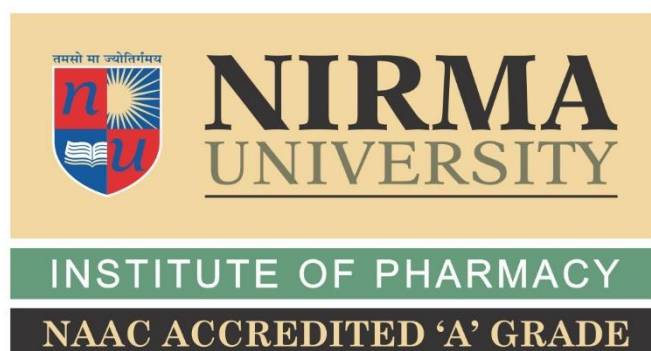


“Computational Studies And Design of Novel Molecules
As Potential Glycogen Synthase Kinase Inhibitors”

A Thesis Submitted To
Nirma University
In Partial Fulfillment of the Requirements For
The Degree of
Doctor of Philosophy
In
Pharmacy
By

Navneet F. Chauhan (09EXTPHDP37)



Department of Pharmaceutical Chemistry
Institute of Pharmacy
Nirma University
Ahmedabad-382481
Gujarat, India
(May 2017)

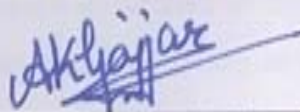
Thesis Approval for Ph.D.

Nirma University Institute of Pharmacy

Certificate

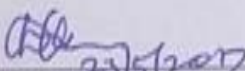
This is to certify that the thesis entitled "Computational Studies And Design of Novel Molecules As Potential Glycogen Synthase Kinase Inhibitors" has been prepared by Navneet Fatehsingh Chauhan under my supervision and guidance. The thesis is his own original work completed after careful research and investigation. The work of the thesis is of the standard expected of a candidate for Ph.D. Programme in Pharmaceutical Sciences and I recommend that it be sent for evaluation.

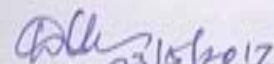
Date: 23rd May, 2017



Prof. Anuradha K. Gajjar, Guide

Forwarded Through:


(i) Prof. Manjunath Ghate
Dean, Faculty of Pharmacy


(ii) Prof. Manjunath Ghate
Dean, Faculty of Doctoral Studies and Research

To:
Executive Registrar
Nirma University


23/5

Nirma University
Institute of Pharmacy


Declaration

I, Navneet Fatehsingh Chauhan, registered as Research Scholar, bearing Registration No. 09EXTPHDP37 for Doctoral Programme under the Faculty of Pharmacy of Nirma University do hereby declare that I have completed the course work, pre-synopsis seminar and my research work as prescribed under R. Ph.D. 6.4.

I do hereby declare that the thesis submitted is original and is the outcome of the independent research carried out by me and contains no plagiarism. The research is leading to the discovery of new techniques / correlation of scientific facts already known. This work has not been submitted to any other University or Body in quest of a degree, diploma or any other kind of academic award.

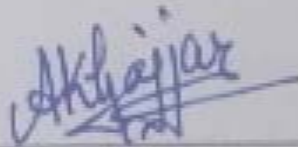
I do hereby further declare that the text, diagrams or any other material taken from other sources (including but not limited to books, journals and web) have been acknowledged, referred and cited to the best of my knowledge and understanding.

Date: 23rd May 2017



Navneet Fatehsingh Chauhan

I endorse the above declaration made by the student.



Prof. Anuradha K. Gajjar
Guide

Acknowledgement

However much you succeed in your life, you should never forget the good wishes and the help of many around you who smoothened your path and helped you to jump the toughest hurdles of life. Today, at the acme of my dissertation, I remember my parents, teachers, friends, colleagues, relatives and well wishers without whom this project would not have taken shape.

It gives me profound pleasure to express my deep sense of gratitude to my guide and mentor Dr. Anuradha K. Gajjar, Professor, L.M. College of Pharmacy, Ahmedabad, under whose esteemed guidance and supervision, the work presented in this thesis was carried out. The high standards and expectations set by her always urged me to strive harder and perform the best. For me she is the person who has knocked the door of Medicinal Chemistry research work. It would have been certainly difficult to accomplish the project work without her guidance and positive motivation.

I would like to sincerely thank my RPC members Prof. C. J. Shishoo, Honorary Director, B.V. Patel PERD Centre, Ahmedabad and Dr. C. T. Rao, Vice President, Sun Pharma Advanced Research Centre, Vadodara, for their insightful feedback and encouragement, which inspired me to widen my research from various perspectives.

I sincerely express my gratitude to Institute of Pharmacy, Nirma University for enlightening me the first glance of research. I thankfully acknowledge Dr. Karsanbhai K. Patel, President, Nirma University for establishing a robust and growing educational environment.

I would also like to thank Prof. Manjunath Ghate, Director, Institute of Pharmacy for his continuous support. I sincerely express my gratitude to all Heads of the departments and faculties of Institute of Pharmacy, Nirma University for their continuous support of my Ph.D study and related research. I would like to thank Dr. Nrupesh Patel for helping me in writing my Ph.D thesis, Professor Tejal Mehta for her continuous motivation and Ms. Krishna Gajjar for her help and support in the journey of this project work.

I am thankful to Oxygen Healthcare Research Private Limited, Ahmedabad and Piramal Discovery Solutions, Ahmedabad for providing Mass spectral analysis, ^1H NMR and ^{13}C NMR spectral analysis.

I specially thank Dr. Premkumar Arumugam, Dr. Rueban Jacob Anicattu Issac & Mr. Sravan Kumar Pucha, GVK Biosciences Private Limited, Hyderabad for providing necessary requirements and their laboratory facility to carry out in-vitro screening for biological assays.

I am thankful to Schrödinger Inc. and Open eye scientific software for providing software for this project. I sincerely thank Dr. Ravikumar Muttineni & Mr. Vinod Devaraji, Application Scientist, Schrödinger and Mr. Sunil Chawla, Open eye Scientific Software for helpful suggestions.

Also I thank my friends in the following institution Mr. Davinder Tuli, Torrent Research Centre, Mr. Tushar Patel, Piramal Discovery Solutions and Mr. Jagat Upadhyay Dharmsinh Desai University. Without their precious support it would not be possible to conduct this project.

I would like to thank Saraswati Institute of Pharmaceutical Sciences for providing me the necessary infrastructure and facility to pursue this project work. Further, I am thankful for cooperation of all non-teaching staff, account and establishment department of college for providing timely assistance. I am deeply thankful to my colleagues from Saraswati Institute of Pharmaceutical Sciences, Dr. Ankit Chaudhary, Professor, & Dr. Dhaval Patel Professor, for their kind help and motivation. Finally, I would like to express my sincere gratitude to the Ph.D. section of Nirma University, Dr A. S. Patel, Ms. A. P. Prashya and Mr. Sachin for helping me in all the Ph.D related guidelines and support.

Last but not least, I would like to thank my family for supporting me and showering their blessing, love and good wishes. Without them, I would not have reached at this stage of my life.

Date:

Navneet F. Chauhan

Abstract

The present thesis titled “Computational Studies and Design of Novel Molecules as Potential Glycogen Synthase Kinase Inhibitors” is divided into 7 chapters as described in brief.

Chapter 1 describes the disease condition associated with the over expression of GSK-3 β enzyme, its structure, various strategies implemented for designing selective GSK-3 β inhibitors and clinical status of GSK-3 β inhibitors.

Chapter 2 outlines the aim and objectives of the present work. The aim of the work is to identify new chemical moieties as GSK-3 β inhibitors by rational drug design based on *in-silico* fragment-based and docking approach as well as to identify novel inhibitors via virtual screening of chemical databases.

Chapter 3 covers detailed literature review of various class of compounds available as GSK-3 β inhibitors. They are further classified based on their mode of inhibition as non-ATP competitive, substrate competitive and ATP-competitive GSK-3 β inhibitors. A review on patent literature is also covered.

Chapter 4 describes prediction of binding sites and druggability assessment of GSK-3 β by SiteMap software tool. The ligand-binding characteristics and druggability of each site of GSK-3 β was assessed with SiteScore (SScore) and Druggability score (Dscore) respectively. Eight sites were identified on the surface of GSK-3 β . The ATP-binding site (pocket 1) and allosteric site (pocket 7) were predicted as top scoring sites of GSK-3 β . Application of combined *in-silico* fragment-based and molecular docking approach yielded the design of new chemical series of allosteric pocket 7 targeted N^{1,3}-disubstituted imidazolidin-2-one derivatives. These hits displayed strong H-bond and pi-stacking interactions with Ser236 and His173 residues.

Application of virtual screening methodology based on structural features of Tideglusib; identified new heterocyclic compounds via shape-based similarity screening using ROCS followed by molecular docking, electrostatic similarity search using EON and pharmacophore feature-based searching and molecular dynamics simulation approach. Three virtual hits AO-476/41610153, AT-057/43486355 and AK-080/40907857 (ZINC4192390) were identified from the SPECS and ZINC database.

Chapter 5 describes synthesis and characterization of 21 designed compounds under a series of N^{1,3}-disubstituted imidazolidin-2-one derivatives. The final synthesized compounds

were purified by 100 - 200 mesh silica gel by column chromatography. Structural characterization was carried through FT-IR, Mass (ESI-MS), ^1H NMR and ^{13}C NMR analysis. LC-MS analysis of compound 2d was also performed for confirmation of synthesized compound.

Chapter 6 describes *in-vitro* screening of 24 test compounds and Tideglusib on GSK-3 β target using ADP-GloTM Kinase assay. Assay standardization was performed to find the optimal concentration of GSK-3 β (7.5 ng), ATP (10 μM) and substrate (2 μM) for the entire study. The inhibitory effect of test compounds and Tideglusib was studied. Compounds 1i, 1n, 2d and AO-476/41610153 have very weak inhibition on GSK-3 β compared to the standard drug Tideglusib. Out of the four identified hits, compounds 1i and AO-476/41610153 showed the highest GLIDE XP scores in the allosteric and substrate sites of GSK-3 β respectively. Here, our docking computations are in perfect agreement with the *in-vitro* results.

Chapter 7 describes the summary and future prospects, which can be further explored with this study.

Table of Contents

Chapter 1. Introduction	1
1.1 Introduction	1
1.2 GSK-3 in Signaling Pathways	2
1.3 Structure of GSK-3	4
1.4 Current Strategies for Designing Selective GSK-3 β Inhibitors	5
1.5 Clinical status of GSK-3 Inhibitors	6
1.6 References	9
Chapter 2. Aim and Objectives	12
Chapter 3. Literature Review	13
3.1 Literature Review of GSK-3 Inhibitors	13
3.1.1 Non-ATP competitive GSK-3 Inhibitors	13
3.1.1.1 Thiadiazolidinones (TDZDs)	14
3.1.1.2 Furanosesquiterpenoids (Palinurin)	15
3.1.1.3 Quinoline Derivative (V.P 0.7)	16
3.1.1.4 Thienyl and Phenyl α -Halomethyl Ketones as Irreversible GSK-3 β Inhibitors	16
3.1.1.5 Benzothiazepinones (BTZs) and Benzothiazinone (BTO)	17
3.1.2 Substrate competitive GSK-3 Inhibitors	19
3.1.2.1 Manzamine alkaloids	20
3.1.2.2 5-Imino-1,2,4-Thiadiazoles (ITDZs)	21
3.1.2.3 Peptides	21
3.1.2.4 Benzothiazinone (BTO)	22
3.1.3 ATP Competitive GSK-3 Inhibitors	23
3.1.3.1 Lithium	24
3.1.3.2 Pyrazolopyridines	24
3.1.3.3 Paullones	25
3.1.3.4 Thiazoles	25
3.1.3.5 Maleimides	26
3.1.3.6 Oxadiazole	28
3.1.3.7 Acylaminopyridine	29
3.1.3.8 Indirubins	29

3.1.3.9	Hymenialdisine	30
3.2	Recent Patents on GSK-3	31
3.3	Conclusion	35
3.4	References	36
Chapter 4. <i>In-Silico</i> Design of Novel GSK-3β Inhibitors		43
4.1	<i>In-Silico</i> Druggability Assessment	43
4.1.1	Material and Methods	43
4.1.1.1	Protein Preparation	43
4.1.1.2	Site Identification	43
4.1.1.3	Druggability assessment by SiteMap	44
4.1.2	Results and Discussion	45
4.1.2.1	Classifying ligand-binding sites of GSK-3 β	46
4.1.2.2	Classifying druggable binding sites of GSK-3 β	46
4.1.2.3	Computational Validation of Generated Pockets with SiteMap	51
4.1.3	Summary of SiteMap Analysis	56
4.2	<i>In-Silico</i> Fragment-Based Approach and Molecular Docking	58
4.2.1	Material and Methods	58
4.2.1.1	Database Preparation	58
4.2.1.2	Molecular Docking	58
4.2.2	Results and Discussion	60
4.2.2.1	Identification of New Chemical Series of N ^{1,3} -disubstituted imidazolidin-2-one	60
4.2.2.2	Prediction of Physicochemical Properties of N ^{1,3} -disubstituted imidazolidin-2-one Compounds	68
4.2.3	Summary of <i>In-Silico</i> Fragment-Based Approach and Molecular Docking	70
4.3	Virtual Screening	71
4.3.1	ROCS Shape Based Similarity Screening and Molecular Docking	71
4.3.1.1	Material and Methods	71
4.3.1.2	Results and Discussion	72
4.3.2	Electrostatic Similarity Search	73
4.3.2.1	Material and Methods	73
4.3.2.2	Results and Discussion	73
4.3.3	Pharmacophore Feature-Based Virtual Screening	74
4.3.3.1	Material and Methods	74

4.3.3.2	Results and Discussion	75
4.3.4	Predication of Physicochemical Properties of Identified Virtual Hits	78
4.4	Conclusion	79
4.5	References	80
Chapter 5. Synthesis and Characterization of Designed Molecules		83
5.1	Chemicals and Instruments	83
5.2	Synthetic Scheme	84
5.3	Reaction Mechanism	85
5.4	Experimental Procedure	86
5.4.1	General procedure for synthesis of 1-(2-chloroethyl)-3-substituted aryl-urea (A ₁ -H ₁)	86
5.4.2	General procedure for synthesis of N ¹ -substituted imidazolidin-2-ones (A ₂ -H ₂)	86
5.4.3	General procedure for synthesis of N ^{1,3} -disubstituted imidazolidin-2-ones (1a-1p, 2a-2e)	89
5.4.3.1	1-benzyl-3-(naphthalen-1-yl) imidazolidin-2-one (1a)	89
5.4.3.2	1-(5-fluoro-2-methylbenzyl)-3-(naphthalen-1-yl)imidazolidin-2-one (1b)	89
5.4.3.3	1-(3-bromobenzyl)-3-(4-chloronaphthalen-1-yl)imidazolidin-2-one (1c)	89
5.4.3.4	1-(4-chloronaphthalen-1-yl)-3-(5-fluoro-2-methylbenzyl)imidazolidin-2-one (1d)	90
5.4.3.5	1-(4-chloronaphthalen-1-yl)-3-(2-methylbenzyl)imidazolidin-2-one (1e)	90
5.4.3.6	1-(4-chloronaphthalen-1-yl)-3-(2,5-difluorobenzyl)imidazolidin-2-one (1f)	90
5.4.3.7	1-(4-chloronaphthalen-1-yl)-3-(2-(trifluoromethyl)benzyl)imidazolidin-2-one (1g)	90
5.4.3.8	1-(4-bromonaphthalen-1-yl)-3-(5-fluoro-2-methylbenzyl)imidazolidin-2-one	90
5.4.3.9	1-(4-bromonaphthalen-1-yl)-3-(3-methylbenzyl)imidazolidin-2-one (1i)	91
5.4.3.10	1-(4-bromonaphthalen-1-yl)-3-(3-chlorobenzyl)imidazolidin-2-one (1j)	91
5.4.3.11	1-(4-bromonaphthalen-1-yl)-3-(2,5-difluorobenzyl)imidazolidin-2-one (1k)	91
5.4.3.12	1-(4-bromonaphthalen-1-yl)-3-(2-fluorobenzyl)imidazolidin-2-one (1l)	91
5.4.3.13	1-(3,5-bis(trifluoromethyl)phenyl)-3-(2-fluorobenzyl)imidazolidin-2-one (1m)	92
5.4.3.14	1-(4-chloro-3-(trifluoromethyl)phenyl)-3-(3-fluorobenzyl)imidazolidin-2-one (1n)	92

5.4.3.15	1-(2-methylbenzyl)-3-(2-(methylthio)phenyl)imidazolidin-2-one (1o)	92
5.4.3.16	1-(2-fluorobenzyl)-3-(4-(trifluoromethyl)phenyl)imidazolidin-2-one (1p)	92
5.4.3.17	1-(naphthalen-1-yl)-3-phenethylimidazolidin-2-one (2a)	92
5.4.3.18	1-(4-chloro-3-(trifluoromethyl)phenyl)-3-(4-fluorophenethyl)imidazolidin-2-one (2b)	93
5.4.3.19	1-(3,5-bis(trifluoromethyl)phenyl)-3-phenethylimidazolidin-2-one (2c)	93
5.4.3.20	1-(2-chloro-5-(trifluoromethyl)phenyl)-3-(2-phenylethyl)imidazolidin-2-one (2d)	93
5.4.3.21	1-(2-chloro-5-(trifluoromethyl)phenyl)-3-(2-(4-fluorophenyl)ethyl)imidazolidin-2-one (2e)	93
5.5	Representative Spectra	95
5.5.1	¹ H NMR Spectrum (400 MHz, DMSO) of compound 1a	95
5.5.2	ESI-MS Spectrum of compound 1a	95
5.5.3	¹ H NMR Spectrum (400 MHz, DMSO) of compound 1b	96
5.5.4	ESI-MS Spectrum of compound 1b	96
5.5.5	¹ H NMR Spectrum (400 MHz, DMSO) of compound 1c	97
5.5.6	ESI-MS Spectrum of compound 1c	97
5.5.7	¹ H NMR Spectrum (400 MHz, DMSO) of compound 1d	98
5.5.8	ESI-MS Spectrum of compound 1d	98
5.5.9	¹ H NMR Spectrum (400 MHz, DMSO) of compound 1e	99
5.5.10	ESI-MS Spectrum of compound 1e	99
5.5.11	¹ H NMR Spectrum (400 MHz, DMSO) of compound 1f	100
5.5.12	ESI-MS Spectrum of compound 1f	100
5.5.13	¹ H NMR Spectrum (400 MHz, DMSO) of compound 1g	101
5.5.14	ESI-MS Spectrum of compound 1g	101
5.5.15	¹ H NMR Spectrum (400 MHz, DMSO) of compound 1h	102
5.5.16	ESI-MS Spectrum of compound 1h	102
5.5.17	IR Spectrum (KBr, cm ⁻¹) of compound 1i	103
5.5.18	ESI-MS Spectrum of compound 1i	103
5.5.19	¹ H NMR Spectrum (400 MHz, DMSO) of compound 1i	104
5.5.20	¹³ C NMR Spectrum of compound (101 MHz, DMSO) of compound 1i	105
5.5.21	¹ H NMR Spectrum (400 MHz, DMSO) of compound 1j	106
5.5.22	ESI-MS Spectrum of compound 1j	106
5.5.23	¹ H NMR Spectrum of compound (400 MHz, DMSO) of compound 1k	107
5.5.24	ESI-MS Spectrum of compound 1k	107
5.5.25	¹ H NMR Spectrum of compound (400 MHz, DMSO) of compound 1l	108

5.5.26	ESI-MS Spectrum of compound 1l	108
5.5.27	¹ H NMR Spectrum of compound (400 MHz, DMSO) of compound 1m	109
5.5.28	ESI-MS Spectrum of compound 1m	109
5.5.29	IR Spectrum (KBr, cm ⁻¹) of compound 1n	110
5.5.30	ESI-MS Spectrum of compound 1n	110
5.5.31	¹ H NMR Spectrum (400 MHz, DMSO) of compound 1n	111
5.5.32	¹³ C NMR Spectrum of compound (101 MHz, DMSO) of compound 1n	112
5.5.33	¹ H NMR Spectrum (400 MHz, DMSO) of compound 1o	113
5.5.34	ESI-MS Spectrum of compound 1o	113
5.5.35	¹ H NMR Spectrum (400 MHz, DMSO) of compound 1p	114
5.5.36	ESI-MS Spectrum of compound 1p	114
5.5.37	IR Spectrum (KBr, cm ⁻¹) of compound 2a	115
5.5.38	ESI-MS Spectrum of compound 2a	115
5.5.39	¹ H NMR Spectrum (400 MHz, DMSO) of compound 2a	116
5.5.40	IR Spectrum (KBr, cm ⁻¹) of compound 2b	117
5.5.41	ESI-MS Spectrum of compound 2b	117
5.5.42	¹ H NMR Spectrum (400 MHz, DMSO) of compound 2b	118
5.5.43	¹ H NMR Spectrum (400 MHz, DMSO) of compound 2c	119
5.5.44	ESI-MS Spectrum of compound 2c	119
5.5.45	IR Spectrum (KBr, cm ⁻¹) of compound 2d	120
5.5.46	ESI-MS Spectrum of compound 2d	120
5.5.47	¹ H NMR Spectrum (400 MHz, DMSO) of compound 2d	121
5.5.48	¹³ C NMR Spectrum (101 MHz, DMSO) of compound 2d	122
5.5.49	LC-MS Spectrum of compound 2d	123
5.5.50	¹ H NMR Spectrum (400 MHz, DMSO) of compound 2e	124
5.5.51	ESI-MS Spectrum of compound 2e	124
5.6	TLC analysis of synthesized compounds	125
5.7	Conclusion	126
5.8	References	127

Chapter 6. Screening For GSK-3β Inhibitory Activity **128**

6.1	<i>In-Vitro</i> Screening for GSK-3β Inhibitory Activity	128
6.1.1	Principle of ADP-Glo™ Kinase Assay	128
6.1.2	Materials and Reagents	129
6.1.3	Assay Procedure	129

6.1.3.1	Assay Standardization of GSK-3 β	129
6.1.3.2	Protocol for assay validation of GSK-3 β	132
6.1.3.3	Data Analysis	132
6.1.4	Results and Discussion	133
6.1.4.1	Determination of optimal enzyme concentration (protocol I)	133
6.1.4.2	Determination of optimal ATP concentration (protocol II)	134
6.1.4.3	Determination of optimal substrate concentration (protocol III)	135
6.1.4.4	Results of DMSO Tolerance Test	136
6.1.4.5	Results of GSK-3 β assay validation	137
6.2	Results of GSK-3 β screening of 24 test compounds	138
6.3	Conclusion	141
6.4	References	142
Chapter 7. Summary and Future Prospects		143
7.1	Summary	143
7.2	Future Prospects	145

Publications

List of Tables

Table No.	Title	Page No.
1.1	GSK-3 inhibitors in human clinical trials	08
3.1	Classification of non-ATP competitive GSK-3 inhibitors	14
3.2	Classification of substrate competitive GSK-3 inhibitors	20
3.3	Classification of ATP competitive GSK-3 inhibitors	23
4.1	Performance in classifying binding sites of glycogen synthase kinase-3 β based on SiteScore	48
4.2	Performance in classifying binding sites of GSK-3 β based on Dscore	49
4.3	SiteMap property values of pocket 7 (Allosteric site) of GSK-3 β	50
4.4	Representative structures of N ^{1,3} -disubstituted imidazolidin-2-one	63
4.5	Docking results of N ^{1,3} -disubstituted imidazolidin-2-one designed compounds in the allosteric pocket 7 of GSK-3 β (PDB ID: 1PYX)	65
4.6	Predicted physicochemical properties of N ^{1,3} -disubstituted imidazolidin-2-one compounds using QikProp	68
4.7	Predicted physicochemical properties of identified hit compounds and Tideglusib using QikProp	78
5.1	Structure and physical properties of substituted arylurea derivatives (A ₁ -H ₁)	87
5.2	Structure and physical properties of N ¹ -substituted imidazolidin-2-ones derivatives (A ₂ -H ₂)	88
5.3	Structure and physical properties of N ^{1,3} -disubstituted imidazolidin-2-ones derivatives (1a-1p and 2a-2e)	94
6.1	Enzyme titration protocol for standardization of GSK-3 β	130
6.2	ATP titration protocol for standardization of GSK-3 β	131
6.3	Determination of substrate (K _m) protocol for standardization of GSK-3 β	131
6.4	Protocol for determination of 1C ₅₀ for the reference compound (Tideglusib)	132
6.5	Determination of optimal enzyme concentration	133
6.6	Determination of optimal ATP concentration	134
6.7	Determination of optimal substrate concentration	135
6.8	Determination of optimal DMSO concentration	136
6.9	GSK-3 β inhibitory activity of four test compounds	140

List of Figures

Figure No.	Title	Page No.
1.1	Role of Glycogen Synthase Kinase-3 (GSK-3) in various disorders in humans	1
1.2	Schematic representation of insulin signaling pathway involved in GSK-3 activity	2
1.3	The different structural regions of GSK-3 β	4
1.4	GSK-3 inhibitors that reached human clinical trials	6
3.1	Structures of selected TDZD analogs as non-ATP competitive GSK-3 β inhibitors	15
3.2	Palinurin as non-ATP competitive GSK-3 β inhibitor	15
3.3	Compound V.P 0.7 as non-ATP competitive GSK-3 β inhibitors	16
3.4	Comparison of reversible and irreversible binding modes of GSK-3 β inhibitors after addition of halomethylketones	17
3.5	Benzothiazepinone (BTZ) hit compounds identified through virtual screening	18
3.6	Design strategy of selected benzothiazepinone and benzothiazinone analogs as non-ATP competitive GSK-3 β inhibitors	19
3.7	Manzamine A as substrate competitive GSK-3 β inhibitors	20
3.8	Selected ITDZ analogs as substrate competitive GSK-3 β inhibitors	21
3.9	BTO-5s as a potent substrate competitive GSK-3 β inhibitor	22
3.10	Identification of 6-aryl pyrazolo[3,4- <i>b</i>]pyridine as potent GSK-3 inhibitor	24
3.11	Structures of various paullone congeners	25
3.12	Structure of thiazole derivative AR-A014418 as potent GSK-3 β inhibitor	25
3.13	Selected potent maleimide analogs as potent GSK-3 β inhibitors	26
3.14	Selected macrocyclic bisindolylmaleimide and azaindolylmaleimide analogs as GSK-3 β inhibitors	27
3.15	1,3,4-oxadiazole core structure based potent GSK-3 inhibitors	28
3.16	Selected examples of compounds designed around acylaminopyridine core scaffold	29
3.17	Optimization of 6-bromo indirubin-3'-oxime (6-BIO)	30
3.18	Structure of hymenialdisine	30

3.19	Pyrimidine compounds developed by Chiron Corporation	31
3.20	New analogs patented by Noscira with thiadiazolidinone scaffold	32
3.21	Some urea analogs as potent GSK-3 β inhibitors	32
3.22	Isonicotinamide analog as potent GSK-3 β inhibitor	33
3.23	Quinoline derivatives as potent GSK-3 β inhibitors	33
3.24	Analogues with diverse scaffolds patented as GSK-3 inhibitors	34
3.25	Novel oxadiazole based GSK-3 inhibitor	35
4.1	Representation of eight surface pockets of GSK-3 β identified by SiteMap	45
4.2	Comparison of the surface maps of pockets of GSK-3 β identified by SiteMap (A) druggable pocket (B) difficult pocket	47
4.3	Representation of pS9 auto-inhibitory peptide in the substrate site of GSK-3 β	52
4.4	A hydrophobic patch identified by SiteMap within the peptide-binding channel of pocket 3	53
4.5	Axin (A) and Fratide (B) peptides recognize the peptide binding channel inside pocket 3 of GSK-3 β	53
4.6	Surface view of glycerol molecule occupying pocket 4 of GSK-3 β	54
4.7	Surface view of glycerol molecule occupying pocket 5 of GSK-3 β	54
4.8	The total surface of pocket 6 represented as gray and the site points as white spheres (PDB ID: 1O9U, blue cartoon representation)	55
4.9	Surface view of DTT (Dithiothreitol) molecule occupying pocket 7 of GSK- 3 β	55
4.10	Surface view of glycerol molecule occupying pocket 8 of GSK-3 β	56
4.11	Validation of pocket 7 with V.P 0.7 structure represented as green ball and stick model. H-bonds are labeled as yellow dotted lines (PDB ID: 1PYX)	59
4.12	LigPlot view of the docked complex 1,3-dimethylbenzimidazol-2-one in the allosteric pocket 7 of GSK-3 β (PDB ID: 1PYX)	60
4.13	A) LigPlot view of 1-benzyl-3-(naphthalen-1-yl)benzimidazol-2-one docked complex in the allosteric pocket 7 of GSK-3 β . B) Solvent exposed region of 1-benzyl-3-(naphthalen-1-yl)benzimidazol-2-one represented as spherical shape	61

4.14	A) LigPlot view of 1-benzyl-3-(naphthalen-1-yl)imidazolidin-2-one docked complex in the allosteric pocket 7 of GSK-3 β . B) Solvent exposed region of 1-benzyl-3-(naphthalen-1-yl)imidazolidin-2-one represented as spherical shape	61
4.15	Schematic diagram of designed template by <i>in-silico</i> fragment-based and molecular docking approach	62
4.16	Docked conformation of 21 designed N ^{1,3} -disubstituted imidazolidin-2-one compounds in the allosteric pocket 7 of GSK-3 β (PDB ID: 1PYX)	66
4.17	Docked conformation of compound 1i in the allosteric pocket 7 of GSK-3 β . A) H-bond interaction is represented as dotted lines and the ligand as ball and stick model. B) LigPlot view of the docked compound 1i in the allosteric pocket 7 of GSK-3 β	66
4.18	Docked conformation of compound 1n in the allosteric pocket 7 of GSK-3 β	67
4.19	Docked conformation of compound 2d in the allosteric pocket 7 of GSK-3 β	67
4.20	Overlay of Tideglusib reference compound (green stick representation) and SPECS database compound AO-476/41610153 (gray stick representation) with ROCS similarity screening	72
4.21	A) Docked complex of SPECS database compound [7,10-dioxo-4,5-dihydro-7H,10H-pyrano[3,2,1- <i>ij</i>]quinolin-8-yl acetate] in the substrate binding site of GSK-3 β . B) LigPlot interaction view of the SPECS database compound in the substrate binding site	72
4.22	Predicted top-scoring virtual hit AT-057/43486355 of SPECS database identified by electrostatic screening. Contour maps of positive and negative charges are shown as blue and red maps respectively	73
4.23	A) Pharmacophore features of Tideglusib which was used for finding structurally similar compounds for virtual screening; B) docking snapshot of Tideglusib in the active site; C) docking snapshot of ZINC4192390 compound at the active binding site of GSK-3 β ; D) MD simulation energy plots for the GSK-3 β complexed with Tideglusib and ZINC4192390	76
4.24	Chemical structure of A) Tideglusib and chemical structure of B) ZINC4192390 compound (2-benzylindeno[1,2,3- <i>de</i>]phthalazin-3(2H)-one)	76
4.25	A) Root mean square deviation (RMSD) of GSK-3 β protein in presence of Tideglusib (red) and ZINC4192390 compound (blue) B) Root mean square fluctuations (RMSF) of GSK-3 β protein in presence of Tideglusib (red) and ZINC4192390 (blue) C) Superimposition of the final snapshots of MD simulations	77

5.1	Synthetic scheme of N ^{1,3} -disubstituted imidazolidin-2-one derivatives	84
5.2	TLC analysis of synthesized compounds	125
6.1	Principle of ADP-Glo TM Kinase Assay	128
6.2	Plot of relative light unit (RLU) versus different concentrations of GSK-3 β enzyme (ng)	133
6.3	Plot of relative light unit (RLU) versus different concentrations of ATP (μ M)	134
6.4	Plot of relative light unit (RLU) versus different concentrations of substrate (GS1) (μ M)	135
6.5	Plot of relative light unit (RLU) versus percentage of DMSO	136
6.6	Concentration response curve of Tideglusib using ADP-Glo TM Kinase assay	137
6.7	Concentration response plot of reference compound Tideglusib (A, plate 1 IC ₅₀ : 16 μ M and B, plate 2 IC ₅₀ : 26 μ M)	139
6.8	Concentration response plots of compound AO-476/41610153, 1i, 1n and 2d using ADP-Glo TM Kinase assay	139

List of Abbreviation

A β	Amyloid beta
AD	Alzheimer's disease
ADP	Adenosine diphosphate
AML	Acute myeloid leukemia
AMP	Adenosine monophosphate
APP	Amyloid precursor protein
ASD	Autism spectrum disorder
ATP	Adenosine triphosphate
AUC	Area under curve
BBB	Blood brain barrier
BEH-C18	Ethylene bridged hybrid-column 18
6-BIO	6-bromoindirubin-3'-oxime
BTO	Benzothiazinone
BTZ	Benzothiazepines
CDK	Cyclin-dependent kinase
CHARMM	Chemistry at Harvard Macromolecular Mechanics
CK-2	Casein kinase-2
CNS	Central nervous system
CRC	Concentration response curve
CREB	Cyclic-AMP response element binding protein
δ	Delta
3D	3-Dimensional
DMF	Dimethyl formamide
DMSO	Dimethyl sulphoxide
DTT	Dithiothreitol
EDTA	Ethylene diamine tetra acetic acid
EGTA	Ethylene glycol-bis(β -aminoethylether)-N,N,N',N'-tetraacetic acid
ESI-MS	Electrospray ionization mass spectrometry
ExACD	Exciting academic database
FRET	Fluorescence resonance energy transfer
FTIR	Fourier-transform infrared spectroscopy
GLIDE	Grid-based Ligand Docking with Energetics

GS-1	Glycogen synthase-1
GSK-3	Glycogen synthase kinase-3
HEPES	Hydroxyethyl piperazine ethane sulphonic acid
HPLC	High-performance liquid chromatography
HSF-1	Heat shock factor-1
Hz	Hertz
IC ₅₀	Half maximal inhibitory concentration
IR	Infrared
IRS-1	Insulin receptor substrate-1
ITDZ	5-Imino-1,2,4-Thiadiazoles
LC-MS	Liquid chromatography-mass spectrometry
MAPKs	Mitogen activated protein kinases
MD	Molecular dynamics
MEKK-1	Mitogen activated protein kinase kinase 1
MHz	Megahertz
mL	Millilitre
μL	Microlitre
mp	Melting point
μM	Micromolar
mmol	Millimole
μV	Microvolt
m/z	Mass-to-charge ratio
NC	Negative control
NCI	National Cancer Institute
NFTs	Neurofibrillary tangles
ng	Nanogram
nm	Nanometer
nM	Nanomolar
NMR	Nuclear magnetic resonance
ns	Nanosecond
OMEGA	Optimized Ensemble Generation Application
OPLS	Optimized Potential For Liquid Simulations
PC	Positive control
PDA	Photo diode array

PDB	Protein data bank
PI 3-kinase	phosphatidylinositol 3-kinase
PIP3	Phosphatidylinositol-3,4,5-triphosphate
PKA	Protein kinase A
PKC	Protein kinase C
ppm	Parts per million
PSA	Polar surface area
PSP	Progressive supranuclear palsy
R _f	Retention factor
RLU	Relative light unit
RMSD	Root mean square deviation
RMSF	Root mean square fluctuation
ROCS	Rapid Overlay of Chemical Structures
RT	Room temperature
RU	Relative unit
SAR	Structure activity relationship
S/B	Signal-to-background ratio
Σ	Standard deviation
σ _M	Standard error of the mean
TDZD	Thiadiazolidinone
THF	Tetrahydrofuran
TIP3P	Three-site transferable intermolecular potential
TLC	Thin layer chromatography
TMS	Tetramethylsilane
T2DM	Type 2 diabetes mellitus
UFF	Universal Force Field
UPLC	Ultra performance liquid chromatography
UV	Ultraviolet
Wnt	Wingless
XP	Extra precision

1.1 Introduction

Protein kinases represent the largest known family of enzymes (Huang et al.). 518 kinase genes had been recognized in the human genome till date. These kinases, by adding a phosphate group from adenosine triphosphate (ATP) to substrates, direct the activity and overall function of several proteins, and thus serve to organize the activity of almost all cellular processes (Vulpetti and Bosotti). An abnormal kinase signaling is implicated in various human diseases such as diabetes, neurodegenerative disorders and diverse forms of cancer (Eldar-Finkelman and Ana Martinez).

Glycogen synthase kinase-3 (GSK-3) is a serine/threonine kinase identified three decades ago. GSK-3 was initially known for its role in regulating the metabolic enzyme glycogen synthase (GS) (Cohen and Frame). The enzyme provides a phosphate group from the ATP to a range of known target substrates such as glycogen synthase, tau-protein, β -catenin etc. Many pathologies such as neurodegenerative diseases, chronic inflammatory processes, type 2 diabetes, mood disorders, various types of cancer such as colon, liver, ovarian and pancreatic tumors are developed by over-activity of GSK-3; which are summarised in figure 1.1 (Cormier and Woodgett). More recently, a new role of GSK-3 antagonists have been identified for dentine restoration and tooth repair (Neves et. al.).

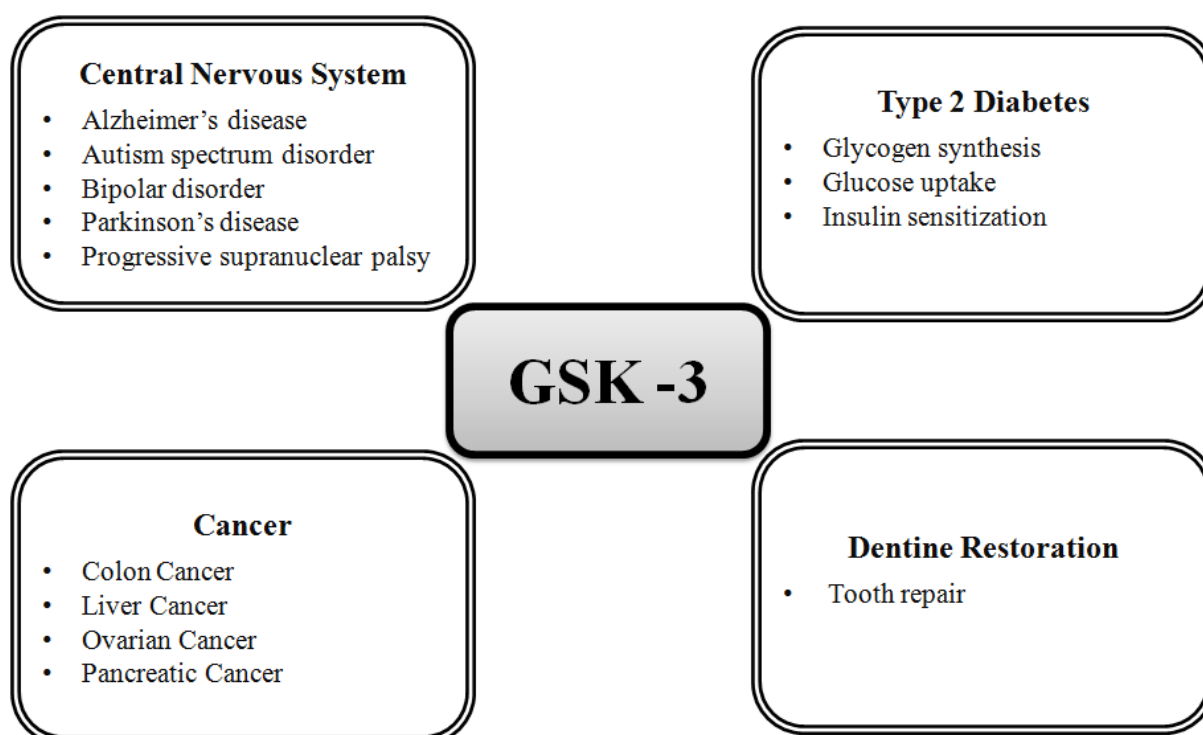


Figure 1.1 Role of Glycogen Synthase Kinase-3 (GSK-3) in various disorders in humans

1.2 GSK-3 in Signaling Pathways

GSK-3 plays an important role as a downstream regulatory switch that determines the output of signaling pathways initiated through diverse stimuli. GSK-3 is primarily located in cell organelles such as cytosol, cell membrane, nucleus and cytoskeleton. Signaling pathways in which GSK-3 acts as a key regulator, when unregulated, have been involved in the development of Alzheimer's disease, bipolar disorder, diabetes and diverse forms of cancer (Khan et al.; Phukan et al.).

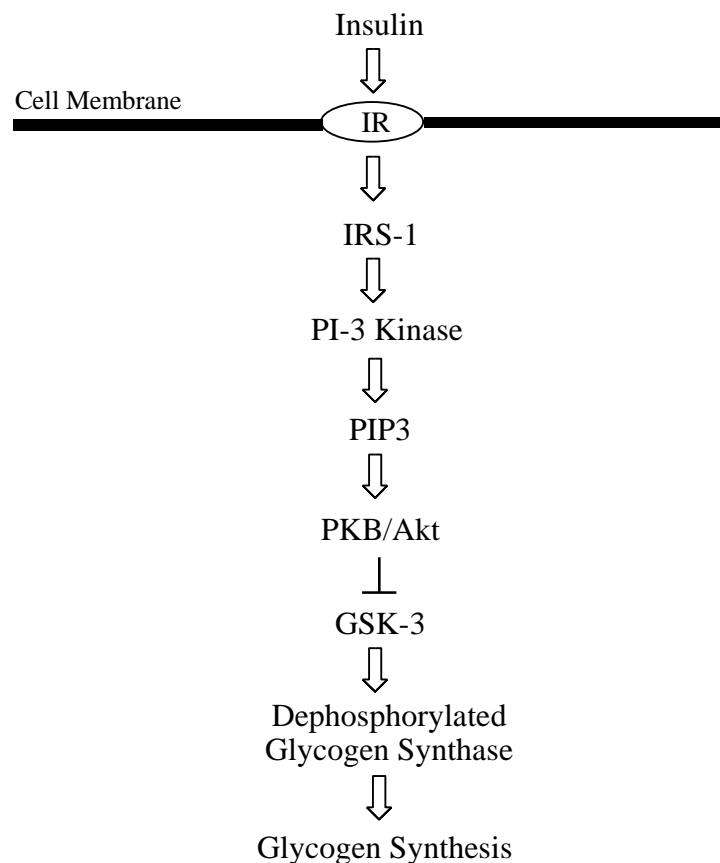


Figure 1.2 Schematic representation of insulin signaling pathway involved in GSK-3 activity

Abbreviations: IR, insulin receptor; IRS-1, insulin receptor substrate-1; PI-3 kinase, phosphatidyl inositol-3-kinase; PIP3, phosphatidyl inositol (3,4,5) trisphosphate, PKB/Akt, protein kinase B; GSK-3, glycogen synthase kinase-3.

Malfunctioning of insulin signaling pathway leads to diabetes (Manning and Toker). Type 2 diabetes was the first disease linked to GSK-3, due to its negative regulation on insulin signaling pathway (Figure 1.2). Insulin receptors in most peripheral tissues as well as in the brain stimulate a signaling cascade via insulin receptor substrate-1 (IRS-1), phosphatidyl inositol-3-kinase (PI3-kinase) and phosphatidylinositol (3,4,5) trisphosphate (PIP3) and

subsequent activation of PKB/Akt which phosphorylates and inhibits GSK-3 leading to dephosphorylation of glycogen synthase and stimulation of glycogen synthesis. As a result GSK-3 is considered a negative modulator of insulin action on glycogen synthase. At the molecular level, GSK-3 may be overexpressed in peripheral tissues during diabetes, and inhibition of GSK-3 might contribute to the control of glucose levels in diabetic subjects (Henriksen and Dokken). Potential drugs that inhibit GSK-3 activity could mimic the ability of insulin to promote the conversion of glucose to glycogen overcoming insulin resistance.

Alzheimer's disease (AD) is an irreversible and progressive neurodegenerative disorder characterized with memory loss and impaired cognitive functions. One of the hallmark of AD is accumulation of neurofibrillary tangles (NFTs) and amyloid beta plaques (A β) between neurons in the mammalian brain. NFTs are hyperphosphorylated forms of the microtubule-associated protein tau, while amyloid beta plaques are derived from the proteolytic cleavage of the amyloid precursor protein (APP). In AD patients, these protein fragments collectively form hard, insoluble plaques between neurons in the brain (Hooper et al.).

Genetic and epidemiological studies indicate that GSK-3 acts as a key player in the etiology of Alzheimer's disease (AD). GSK-3 function is deregulated in AD patients through alterations in upstream of both Wntless (Wnt) and insulin signaling pathway intermediates. In AD, the over-expression of GSK-3 β accounts for tau hyperphosphorylation, increased amyloid beta production and local plaque-associated microglial-mediated inflammatory responses which leads to progressive memory loss and thinking ability (Jope). Pharmacological inhibitors of GSK-3 such as Tideglusib has shown to decrease the amount of altered tau protein in animal studies (Eldar-Finkelman and Ana Martinez). This drug reached phase 2 clinical trial for the treatment of Alzheimer's disease.

Several functions of GSK-3 in cancer as a 'tumor promoter' or 'tumor suppressor' has been identified but still remains controversial. GSK-3 as a 'tumor promoter' may play a significant role in cell-proliferation. Overexpression of GSK-3 has been linked with various tumor types including colon, pancreatic, liver and ovarian cancers. Inhibition of GSK-3 may play a positive role in these cancer types (McCubrey et al.).

On the contrary, GSK-3 also plays significant role as 'tumour suppressor'. GSK-3 can restrain the Wnt/ β -catenin pathway by phosphorylating β -catenin which results in the ubiquitin/proteasome-dependent degradation of β -catenin (Luo et al.). β -catenin is a co-transcription factor and its high expression leads to cancer progression. Furthermore,

suppression of GSK-3 expression stabilizes three cell-cycle regulators namely cyclin D1, cyclin E and c-Myc, the over-expression of which is linked with tumorigenesis (Shang et al.).

1.3 Structure of GSK-3

In mammals, two different isoforms have been found, GSK-3 α and GSK-3 β that share 98 % identity within the kinase catalytic domain. A splice variant, GSK-3 β 2 is also found in brain (Meijer et. al.). GSK-3 α has an additional glycine-rich N-terminal extension that relates to its larger mass (molecular weight is 51 kDa for GSK-3 α and 47 kDa for GSK-3 β) (Force and Woodgett). Although, the two isoforms share high degree of structural similarity they are functionally non-equivalent. As an example, GSK-3 β primarily regulates glycogen storage in the skeletal muscle whereas GSK-3 α does so in the liver (Doble).

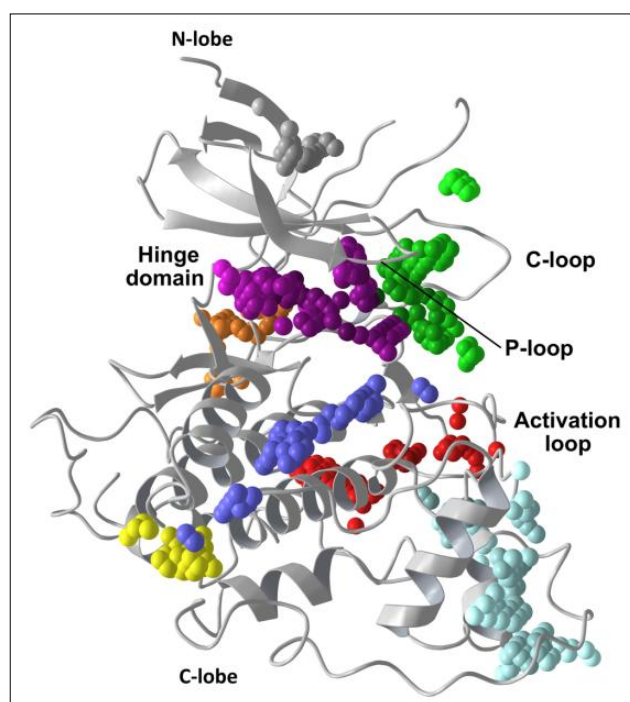


Figure 1.3 The different structural regions of GSK-3 β

Reprinted from Acta Pharmaceutica Scientia [Chauhan and Gajjar, “Classifying Druggability on Potential Binding Sites of Glycogen Synthase Kinase-3 β : An in-Silico Assessment.” *Acta Pharmaceutica Scientia*, vol. 55, no. 3, 2017, pp. 43–60] with permission from publisher.

Structurally, GSK-3 is a two-domain kinase fold comprising a β -strand domain and an α -helix domain. The β -strand domain is present at the N-lobe between the amino acid residues 25 - 138 and an α -helical domain is present at the C-lobe between amino acid residues 139 - 343. The ATP-binding site (labeled a pink spheres) is sandwiched inside, deep-within the interface of the α -helix and β -strand domains that is surrounded by a hinge region and a

glycine-rich loop, which is often referred to as “P-loop”. The substrate binding region, labelled as green spheres is surrounded by the C-loop and the activation loop as shown in figure 1.3 (Beurel et al.).

The catalytic activity of GSK-3 β is regulated by phosphorylation at two different sites, including Ser9 and Tyr216 residues. Phosphorylation of Ser9 inactivates GSK-3 β , whereas phosphorylation at Tyr216 within the activation loop increases its catalytic activity. For GSK-3 α , phosphorylation at Ser21 renders it inactive (Pandey and DeGrado). Before phosphorylation, the β -strand and the α -helical domains must adjust in a catalytically active conformation for effective binding of the substrate. In certain circumstances, GSK-3 β pre-phosphorylates few substrates such as axin, tau, β -catenin, c-Jun and c-Myc whereas under other circumstances, priming of the substrate by another kinase is required before phosphorylating the target (Sutherland).

1.4 Current Strategies for Designing Selective GSK-3 β Inhibitors

A vast majority of GSK-3 β inhibitors currently available are ATP-competitive. The binding mode of such inhibitors have been identified by crystallographic studies. They form critical H-bond contacts with the backbone amino acid residues of Asp133 and Val135. Moreover, Pro136 is observed to strengthen the interaction between ligand and the hinge-backbone in several complexes. The hinge region is highly conserved in nearly every kinase (Chun et al.).

High selectivity can be reached by targeting the substrate and allosteric pockets of GSK-3 β . This can be explained by the fact that inhibitors targeting Arg96, Arg180, and Lys205 and nearby residues within the substrate site hinder binding of substrates to its proper site (Martinez et al.; Patel et al.). The allosteric modulators bind to specific regions of GSK-3 β , induces conformational changes and resist substrate binding to its proper site. Researchers at Institute of Quimica Medica identified an allosteric GSK-3 β inhibitor V.P. 0.7 (Palomo et al.). This approach resulted in selective inhibition of GSK-3 β .

Martinez et al. reported selective inhibition of GSK-3 β with Tideglusib. As indicated by this theory, Tideglusib binds to the active site by covalent interaction with Cys199 residue which inactivates the enzyme. Non-ATP competitive, substrate competitive and allosteric modulators of GSK-3 β are expected to be the most promising leads to overcome the issues of cross-kinase effects.

1.5 Clinical Status of GSK-3 Inhibitors

Over the past years, a huge number of diverse moieties have been designed and claimed to inhibit GSK-3. However, insights into the current status of clinical development of GSK-3 inhibitors turns up with very few compounds in clinical pipeline. Three drug candidates AZD1080 (Astra Zeneca), Tideglusib (Noscria) and LY2090314 (Eli Lilly) have reached clinical trials in human subjects (Figure 1.4) (Palomo and Ana Martinez). Two small molecules AZD1080, an indolyl derivative and Tideglusib, targeting GSK-3 have reached clinical trials for Alzheimer's disease (AD) (Georgievska et al.; Lovestone et al.). However, AZD1080 was withdrawn from AD therapeutic development due to the nephrotoxic side effect in phase I clinical trials (Han and Inhee Mook-Jung). LY2090314, a GSK-3 inhibitor reached phase 2 clinical trial for the treatment of acute myeloid leukemia (Rizzieri et al.; Gray et al.). An overview of GSK-3 inhibitors in human clinical trials is shown in table 1.1. It is possible that few GSK-3 inhibitors which are under clinical development administered to humans is short and one possible cause could be the off-target effects due to binding to other kinases. A GSK-3 inhibitor with more selectivity could potentially circumvent some of these issues.

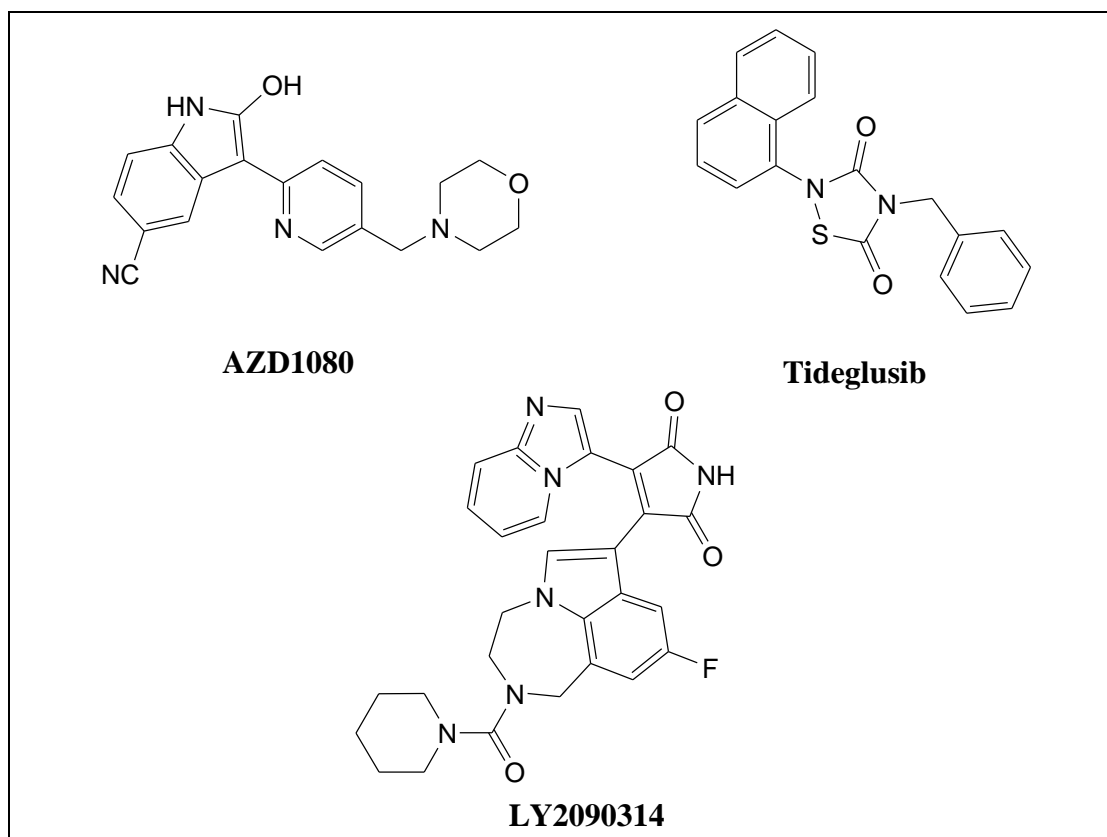


Figure 1.4 GSK-3 Inhibitors that reached human clinical trials

Drug candidates in clinical pipeline were extracted from the database of clinical trials (<http://www.clinicaltrials.gov>). Tideglusib is the only known non-ATP competitive and selective GSK-3 β inhibitor that has reached clinical trials for various neurological disorders such as Alzheimer's disease, progressive supranuclear palsy and autism spectrum disorder. Clinical study outcome of Tideglusib and LY2090314 are summarized as under:

- i) *Autism Spectrum Disorder (ASD)*: A neurological disorder that begin early in childhood and lasts throughout a person's life. Patients with ASD have difficulty in communicating and interacting with other people. At present, Tideglusib is in Phase 2 clinical trials for ASD.
- ii) *Alzheimer's Disease*: Tideglusib reached Phase IIa clinical trial (NCT00948259) for the treatment of Alzheimer's disease (AD). The treatment was well tolerated with patients of AD, but showed some transient, and fully reversible serum transaminase elevations in a few 6 active subjects enrolled in the study. The side effects of Tideglusib have been reported as adverse events which includes diarrhoea and abnormal liver function. In conclusion, short term treatment with Tideglusib was acceptably safe but failed to show any clinical efficacy in mild-to-moderate AD patients.
- iii) *Progressive Supranuclear Palsy (PSP)*: PSP is a rare brain disorder characterized by difficulty in walking, balance and regular eye movements. The disorder results from deterioration of cells in areas of brain such as the brainstem, cerebral cortex, cerebellum and basal ganglia that control body movement and thinking. Tideglusib reached Phase 2 clinical trials (NCT01049399) for the treatment of mild-to-moderate progressive supranuclear palsy. Tideglusib was found to be safe, but showed some transient, and fully reversible serum transaminase elevations (9 % patients) and diarrhoea (13 % patients). It was found to be safe but failed to show any clinical efficacy in mild-to-moderate PSP patients.
- iv) *Acute Myeloid Leukemia (AML)*: Acute Myeloid Leukemia is a type of cancer that affects blood and bone marrow. LY2090314 reached phase 2 safety study (NCT01214603) in AML patients. The study suggest that although LY2090314 might be well tolerated in patients with AML; however, decreased appetite, nausea, febrile neutropenia, dyspnea, thrombocytopenia, anemia, atrial flutter, QT interval prolongation, visual disturbances were the most common observed side effects.

Chapter 1

Moreover, because of the limited clinical benefit further development in this indication as a single agent was not justified. Therefore, further studies of LY2090314 in combination with other chemotherapeutic agents could be of interest in the future (Rizzieri et al.).

Table 1.1 GSK-3 inhibitors in human clinical trials

Sr. No	Drug	Clinical Trial	Disease Condition	Starting Date	Status*
1	Tideglusib	Tideglusib versus Placebo in the Treatment of Adolescents with Autism Spectrum Disorders	Autism Spectrum Disorders	December 2015	Recruiting (Phase II)
2	Tideglusib	Efficacy, Safety and Tolerability of Tideglusib to Treat Mild-to-Moderate Alzheimer's Disease Patients	Alzheimer's Disease	April 2011	Completed (Phase II)
3	Tideglusib (NP031112)	Safety, Tolerability and Efficacy of Two Different Oral Doses of NP031112 Versus Placebo in the Treatment of Patients With Mild-to-Moderate PSP	Progressive Supranuclear Palsy	December 2009	Completed (Phase II)
4	LY2090314	A Phase 2 Study of LY2090314 in Participants With Acute Leukemia	Leukemia	November 2010	Completed (Phase II)
* The clinical trial data were accessed from http://www.clinicaltrials.gov , on 10-01-2018					

1.6 References

- Beurel, Eleonore, et al. "Glycogen synthase kinase-3 (GSK-3): Regulation, actions, and diseases." *Pharmacology & Therapeutics*, vol. 148, 2015, pp. 114–131.
- Cohen, Philip, and Sheelagh Frame. "The renaissance of GSK3." *Nature Reviews Molecular Cell Biology*, vol. 2, no. 10, 2001, pp. 769–776.
- Cormier, Kevin W., and James R. Woodgett. "Recent advances in understanding the cellular roles of GSK-3." *F1000Research*, vol. 6, 2017.
- Chauhan, Navneet, and Anuradha Gajjar. "Classifying Druggability on Potential Binding Sites of Glycogen Synthase Kinase-3 β : An in-Silico Assessment." *Acta Pharmaceutica Scientia*, vol. 55, no. 3, 2017, pp. 43–60.
- Chun, Kwangwoo, et al. "Synthesis and evaluation of 8-Amino-[1,2,4]Triazolo[4,3-*a*]Pyridin-3(2H)-One derivatives as glycogen synthase kinase-3 (GSK-3) inhibitors." *Bioorganic & Medicinal Chemistry Letters*, vol. 23, no. 13, 2013, pp. 3983–3987.
- Doble, B. W. "GSK-3: tricks of the trade for a multi-Tasking kinase." *Journal of Cell Science*, vol. 116, no. 7, 2003, pp. 1175–1186.
- Eldar-Finkelman, Hagit, and Ana Martinez. "GSK-3 Inhibitors: Preclinical and Clinical Focus on CNS." *Frontiers in Molecular Neuroscience*, vol. 4, 2011.
- Force, Thomas, and James R. Woodgett. "Unique and Overlapping Functions of GSK-3 Isoforms in Cell Differentiation and Proliferation and Cardiovascular Development." *Journal of Biological Chemistry*, vol. 284, no. 15, 2008, pp. 9643–9647.
- Gray, Jhanelle E., et al. "A first-In-Human phase I dose-Escalation, pharmacokinetic, and pharmacodynamic evaluation of intravenous LY2090314, a glycogen synthase kinase 3 inhibitor, administered in combination with pemetrexed and carboplatin." *Investigational New Drugs*, vol. 33, no. 6, 2015, pp. 1187–1196.
- Han, Sun-Ho, and Inhee Mook-Jung. "Diverse Molecular Targets for Therapeutic Strategies in Alzheimer's Disease." *Journal of Korean Medical Science*, vol. 29, no. 7, 2014, pp. 893–902.
- Henriksen, Erik, and Betsy Dokken. "Role of Glycogen Synthase Kinase-3 in Insulin Resistance and Type 2 Diabetes." *Current Drug Targets*, vol. 7, no. 11, 2006, pp. 1435–1441.

Chapter 1

- Hooper, Claudie, et al. "The GSK-3 hypothesis of Alzheimer's disease." *Journal of Neurochemistry*, vol. 104, no. 6, 2007, pp. 1433–1439.
- Huang, Danzhi, et al. "Kinase selectivity potential for inhibitors targeting the ATP binding site: a network analysis." *Bioinformatics*, vol. 26, no. 2, 2009, pp. 198–204.
- Joep, Richard Scott. "Glycogen Synthase Kinase-3 in the Etiology and Treatment of Mood Disorders." *Frontiers in Molecular Neuroscience*, vol. 4, 2011.
- Khan, Imran, et al. "Natural and synthetic bioactive inhibitors of glycogen synthase kinase." *European Journal of Medicinal Chemistry*, vol. 125, 2017, pp. 464–477.
- Luo, Jia. "Glycogen synthase kinase 3 β (GSK3 β) in tumorigenesis and cancer chemotherapy." *Cancer Letters*, vol. 273, no. 2, 2009, pp. 194–200.
- Lovestone, Simon, et al. "A phase II trial of tideglusib in Alzheimer's disease." *Journal of Alzheimer's Disease* vol. 45, no.1, 2015, pp. 75-88.
- Manning, Brendan D., and Alex Toker. "AKT/PKB Signaling: Navigating the Network." *Cell*, vol. 169, no. 3, 2017, pp. 381–405.
- Maqbool, Mudasir, et al. "Pivotal role of glycogen synthase kinase-3: A therapeutic target for Alzheimers disease." *European Journal of Medicinal Chemistry*, vol. 107, 2016, pp. 63–81.
- Martinez, Ana, et al. "First Non-ATP Competitive Glycogen Synthase Kinase 3 β (GSK-3 β) Inhibitors: Thiadiazolidinones (TDZD) as Potential Drugs for the Treatment of Alzheimers Disease." *Journal of Medicinal Chemistry*, vol. 45, no. 6, 2002, pp. 1292–1299.
- Mccubrey, James A., et al. "GSK-3 as potential target for therapeutic intervention in cancer." *Oncotarget*, vol. 5, no. 10, 2014, pp. 2881-2911.
- Medina, Miguel, and Francisco Wandosell. "Deconstructing GSK-3: The Fine Regulation of Its Activity." *International Journal of Alzheimers Disease*, vol. 2011, 2011, pp. 1–12.
- Meijer, L, et al. "Pharmacological inhibitors of glycogen synthase kinase 3." *Trends in Pharmacological Sciences*, vol. 25, no. 9, 2004, pp. 471–480.
- Neves, Vitor C. M., et al. "Promotion of natural tooth repair by small molecule GSK-3 antagonists." *Scientific Reports*, vol. 7, 2017.

- Palomo, Valle, et al. “Exploring the Binding Sites of Glycogen Synthase Kinase 3. Identification and Characterization of Allosteric Modulation Cavities.” *Journal of Medicinal Chemistry*, vol. 54, no. 24, 2011, pp. 8461–8470.
- Palomo, Valle, and Ana Martinez. “Glycogen synthase kinase 3 (GSK-3) inhibitors: a patent update (2014-2015).” *Expert Opinion on Therapeutic Patents*, vol. 27, no. 6, 2016, pp. 657–666.
- Pandey, Mukesh K., and Timothy R. Degrado. “Glycogen Synthase Kinase-3 (GSK-3) Targeted Therapy and Imaging.” *Theranostics*, vol. 6, no. 4, 2016, pp. 571–593.
- Patel, Dhilon S., et al. “Structure-Based Approaches in the Design of GSK-3 Selective Inhibitors.” *Current Protein & Peptide Science*, vol. 8, no. 4, 2007, pp. 352–364.
- Phukan, S, et al. “GSK3 β : role in therapeutic landscape and development of modulators.” *British Journal of Pharmacology*, vol. 160, no. 1, 2010, pp. 1–19.
- Rizzieri, David A., et al. “An open-Label phase 2 study of glycogen synthase kinase-3 inhibitor LY2090314 in patients with acute leukemia.” *Leukemia & Lymphoma*, vol. 57, no. 8, 2016, pp. 1800–1806.
- Shang, Shuang, et al. “The regulation of β -Catenin activity and function in cancer: therapeutic opportunities.” *Oncotarget*, vol. 8, no. 20, 2017, pp. 33972-33989.
- Sutherland, Calum. “What Are the bonafide GSK-3 Substrates?” *International Journal of Alzheimers Disease*, vol. 2011, 2011, pp. 1–23.
- Vulpetti, Anna, and Roberta Bosotti. “Sequence and structural analysis of kinase ATP pocket residues.” *Il Farmaco*, vol. 59, no. 10, 2004, pp. 759–765.

2.1 Aim and Objectives

In the field of discovery of novel GSK-3 β inhibitors the basic challenge is to design selective and potent inhibitors.

The aim of the study was to explore various computational approaches in the design of selective GSK-3 β inhibitors.

The aim was proposed to be achieved with the following objectives:

- a. To identify new scaffold based on *in-silico* fragment-based and docking approach.
 - b. To design new heterocyclic molecules based on the results of docking computations and virtual screening and to predict their *in-silico* binding affinity and physicochemical properties.
 - c. To synthesize new heterocyclic derivatives and to characterize them with IR spectra, Mass spectra, ^1H NMR and ^{13}C NMR.
 - d. To evaluate the potency of designed compounds by *in-vitro* GSK-3 β inhibition assay.
-

3.1 Literature Review of GSK-3 Inhibitors

A huge amount of information regarding GSK-3 as a drug discovery target have appeared in scientific literature. Many published research focus on the medicinal chemistry aspect of GSK-3 inhibitor development and few focus on the biology of GSK-3. Several reviews have been published with their potential role of GSK-3 in drug discovery, but there has not been a comprehensive review covering both medicinal chemistry and patent literature. This literature review presents the information about small molecule inhibitors of GSK-3 with an emphasis on medicinal chemistry, lead optimization, patent literature and recent clinical development.

Broadly, three distinct classes of inhibitors are covered; they have been classified as, non-ATP competitive, substrate competitive and ATP-competitive GSK-3 inhibitors. A wide variety of molecules capture the ATP-binding site of GSK-3 that might offer unfavourable cross-kinase effects. Therefore, non-ATP competitive and substrate competitive GSK-3 inhibitors are expected to be the most promising leads to overcome the issues of cross-kinase effects. Several binding sites on the surface of GSK-3 have been explored and validated recently. Hence, the possibility of designing selective lead molecules has rapidly advanced by the application of *in-silico* molecular modeling tools.

3.1.1 Non-ATP Competitive GSK-3 Inhibitors

Currently, six diverse classes of non-ATP competitive GSK-3 inhibitors available from marine sources as well as synthetic origin are reported in literature. Majority of the non-ATP competitive kinase inhibitors identified so far has largely been as a result of serendipity. For example, Tideglusib belongs to the class of thiadiazolidinone (TDZD). TDZD analogs were initially recognized as potassium channel openers and were later on repurposed as irreversible GSK-3 β inhibitors with non-ATP competitive mode of inhibition (Martinez et al.). Furthermore, researchers at Institute of Quimica Medica identified a quinoline moiety V.P 0.7 as non-ATP competitive GSK-3 β inhibitor through specific screening of in-house synthesized chemical library (Palomo et al.). Typical representative examples of non-ATP competitive GSK-3 inhibitors are outlined in table 3.1.

Table 3.1 Classification of non-ATP competitive GSK-3 inhibitors

Source	Chemical Class	Inhibitor Potency (IC ₅₀)	Pharmacological Activity
Molecules from marine sources	Furanosesquiterpenoids	4.5 - 7.5 μ M	Decrease tau protein hyperphosphorylation
Small organic synthesized molecules	Thiadiazolidinediones (TDZD)	2 - 4 μ M	Decrease tau protein hyperphosphorylation Neuroprotection Antidepressant Dentine restoration
	Benzothiazepines (BTZ)	8 - 25 μ M	GSK-3 β inhibition
	Benzothiazinone (BTO)	8 - 10 μ M	GSK-3 β inhibition
	Thienyl and Phenyl α -Halomethyl Ketones	0.5 μ M	GSK-3 β inhibition
	Quinoline Derivative (V.P 0.7)	3.01 \pm 0.4 μ M	GSK-3 β inhibition
Abbreviations: IC ₅₀ , half maximal inhibitory concentration; μ M, micromolar.			

3.1.1.1 Thiadiazolidinones (TDZDs)

In early 2002, Martinez et al. reported TDZD analogs as first non-ATP competitive GSK-3 β inhibitors. Several TDZD analogs have been tested for their non-ATP competitive nature that selectively inhibits GSK-3 β with an IC₅₀ value with concentrations ranging between 2 - 4 μ M. TDZD class of compounds were unable to show significant inhibition over a panel of kinases including PKC, PKA, CK-2 and CDK1/cyclinB. Till date, crystallographic studies have not been published on TDZD compounds. However, two independent studies published the possible binding modes of TDZD analogs. Martinez and her team proposed the initial hypothesis with the help of molecular docking and suggested TDZD binding site was sandwiched between the glycine-rich loop, often referred to as the “P-loop”, the activation loop and the C-loop, which has been proposed to be the substrate binding pocket of GSK-3 (Site 2). Domínguez et al. reported an irreversible inhibition of GSK-3 β with Tideglusib. As indicated by this theory, Tideglusib binds to the active site by covalent interaction with Cys199 residue which inactivates the enzyme and resists binding of substrates to its proper site. However, this irreversibility apparently was not characterized by covalent binding of Tideglusib (Osolodkin et al.).

Tideglusib and TDZD-8 are the two analogs currently under clinical investigation as indicated in figure 3.1. Tideglusib is the only known non-ATP competitive GSK-3 β inhibitor that has reached clinical trials for various neurological disorders such as Alzheimer's disease, progressive supranuclear palsy and autism spectrum disorder (Berg et al.; Silva et al.). TDZD-8 is now being tested in combination with other drugs for the treatment of malignant gliomas, which are considered to be one of the deadliest types of cancers (Palomo and Ana Martinez).

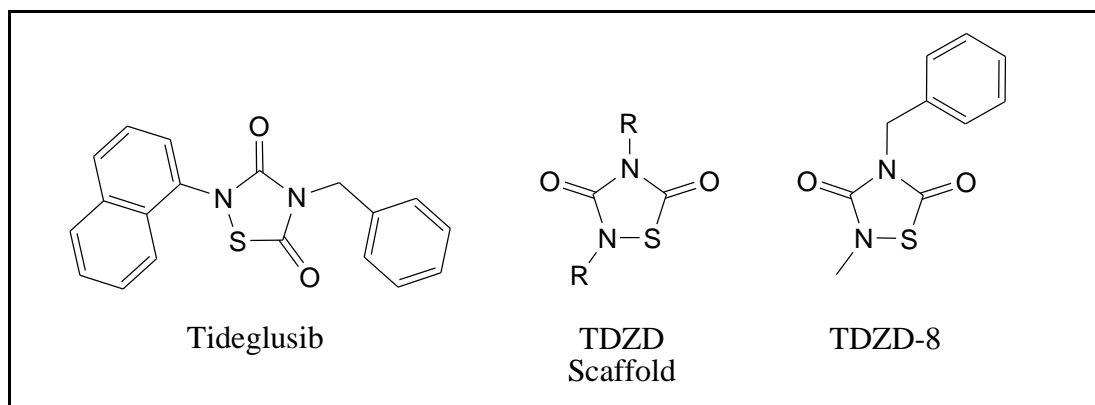


Figure 3.1 Structures of selected TDZD analogs as non-ATP competitive GSK-3 β inhibitors

3.1.1.2 Furanosesquiterpenoids (Palinurin)

Palinurin is a furanosesquiterpenoid isolated from Mediterranean sponge *Ircinia variabilis*. Bidon-Chanal et al. suggested the allosteric binding mode of palinurin at the N-terminal lobe of GSK-3 β . Palinurin is reported to inhibit human recombinant GSK-3 α (IC₅₀: 1.6 μ M) and GSK-3 β (IC₅₀: 1.9 μ M). Moreover, palinurin was unable to show significant inhibition over a panel of other four protein kinases such as CDK1, CDK5, MAPK and CK2 when tested at a concentration between 25 - 100 μ M.

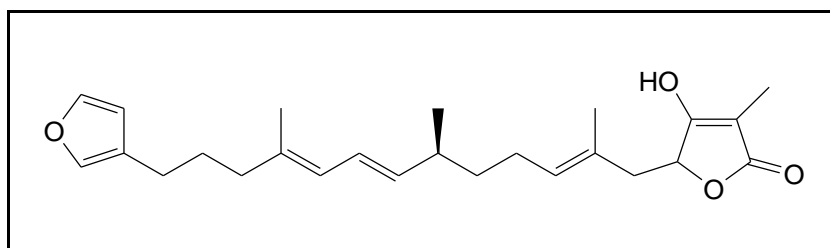


Figure 3.2 Palinurin as non-ATP competitive GSK-3 β inhibitor

3.1.1.3 Quinoline Derivative (V.P 0.7)

Researchers at Institute of Quimica Medica identified compound V.P 0.7 as non-ATP competitive GSK-3 β inhibitor via specific screening of in-house synthesized chemical library. Structurally, this compound comprises a polar heterocyclic head with a long aliphatic hydrophobic tail and inhibits GSK-3 β with an IC₅₀ value of 3.01 ± 0.4 μ M (Figure 3.3).

Palomo et al. reported the molecular docking studies and demonstrated that the polar head of compound V.P 0.7 was sandwiched between Arg209 and Thr235 residues and a hydrogen bond interaction was recognized with Ser236 residue. Furthermore, the hydrophobic tail was extended towards the hydrophobic region of the pocket. Kinetic experiments and molecular docking studies of V.P 0.7 supported the allosteric mode of inhibition. The *in-vivo* efficacy of V.P 0.7 has been shown in pre-clinical models of fragile X and multiple sclerosis (Palomo and Ana Martinez).

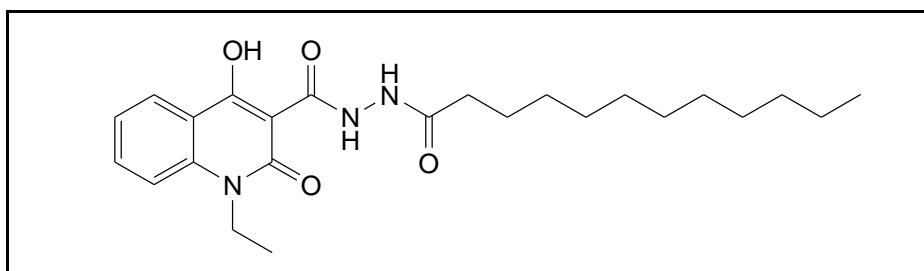


Figure 3.3 Compound V.P 0.7 as non-ATP competitive GSK-3 β inhibitor

3.1.1.4 Thienyl and Phenyl α -Halomethyl Ketones as Irreversible GSK-3 β Inhibitors

Conde et al. designed and synthesized chloromethyl thienyl ketones and halomethylphenyl ketones congeners as irreversible, non-ATP competitive GSK-3 β inhibitors. Among these variants the most potent compounds were reported with an IC₅₀ value of 0.5 μ M in cell-free assays (Morales-Garcia et al.). As indicated by the irreversible inhibition mechanism; inactivation of the enzyme is due to irreversible covalent bond formed between the halomethyl ketone moiety and Cys199 residue in the active site of GSK-3 β . Perez et al. identified that substitution of methyl ketone moiety by halomethyl ketone moiety conferred an ability to switch a reversible GSK-3 β inhibitor to an irreversible GSK-3 β inhibitor. The same is illustrated in figure 3.4

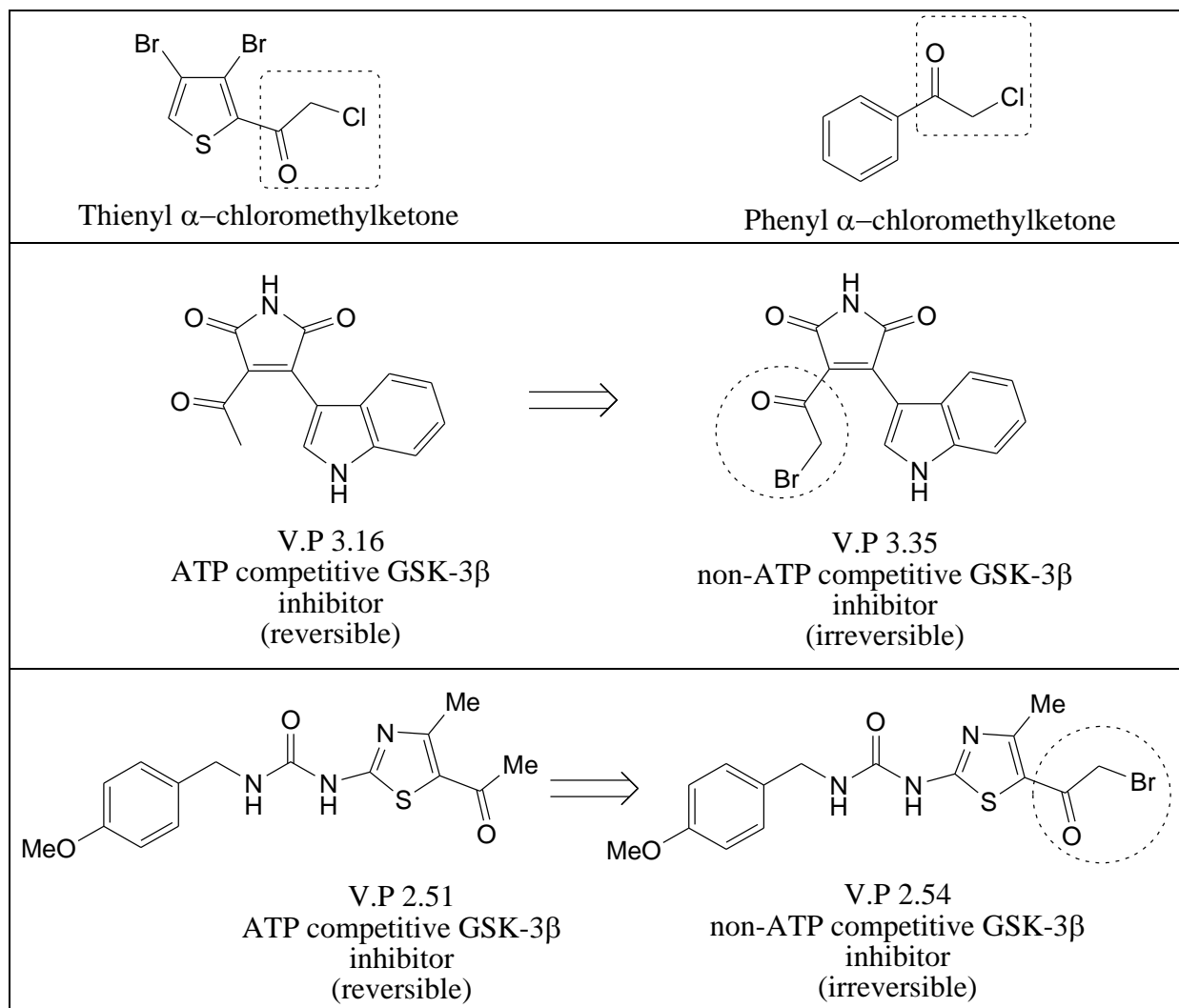


Figure 3.4 Comparison of reversible and irreversible binding modes of GSK-3β inhibitors after addition of halomethylketones

3.1.1.5 Benzothiazepinone (BTZ) and Benzothiazinone (BTO)

Zhang et al. reported benzothiazepinone (BTZ) derivatives as non-ATP competitive GSK-3β inhibitors. Two BTZ hit compounds (IC_{50} : 830 μ M and 480 μ M) were initially identified through virtual screening utilizing Maybridge database shown in figure 3.5. Further, hit-to-lead optimization yielded twenty six BTZ derivatives and the most potent compound 6v of the synthesized series exhibited IC_{50} value of 23 μ M in cell-free assays (Figure 3.6).

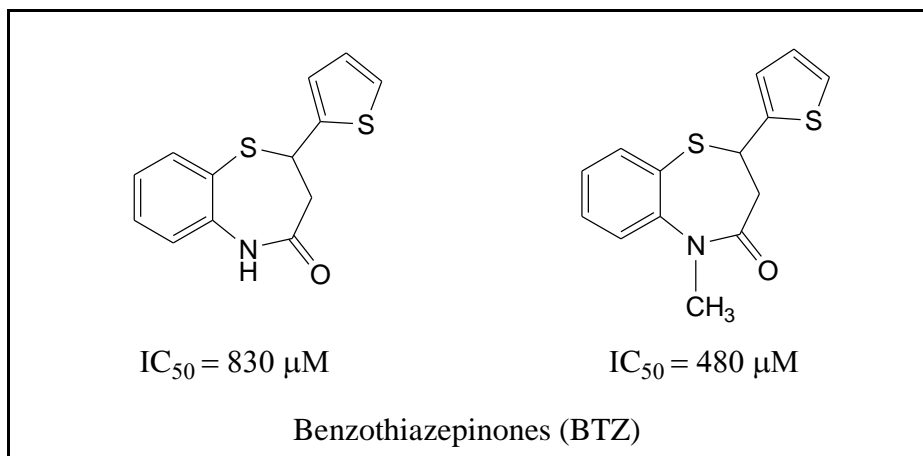


Figure 3.5 Benzothiazepinone (BTZ) hit compounds identified through virtual screening

Zhang and co-workers also reported novel benzothiazinone (BTO) compounds as non-ATP competitive GSK-3 β inhibitors. BTO derivatives were designed based on merge strategy. The benzothiazinone core scaffold was obtained from previously synthesized BTO-jb (a weak allosteric inhibitor of GSK-3 β), and the long hydrophobic side chain was borrowed from compound V.P 0.7 (a potent allosteric inhibitor of GSK-3 β) as outlined in figure 3.6. Over fifty BTO variants were synthesized and the two best compounds BTO-5h (IC_{50} : 8.0 μM) and BTO-5s (IC_{50} : 10 μM) were reported with allosteric and substrate competitive inhibition mechanism of GSK-3 β , respectively. Docking studies of compound BTO-5h and BTZ derivatives supported the allosteric mode of inhibition similar to the binding mode of V.P 0.7 as mentioned in the previous section.

Both class of compounds displayed good efficacy on GSK-3 β and selectivity against a panel of ten related protein kinases. Cellular assays performed on BTO-5h compound showed a decline in phosphorylation level of glycogen synthase in HpG2 cells. Moreover, an improved glucose uptake in both HpG2 and 3T3-L1 cells lines were also observed suggesting that BTO-5h may have a potential therapeutic value for the treatment of T2DM.

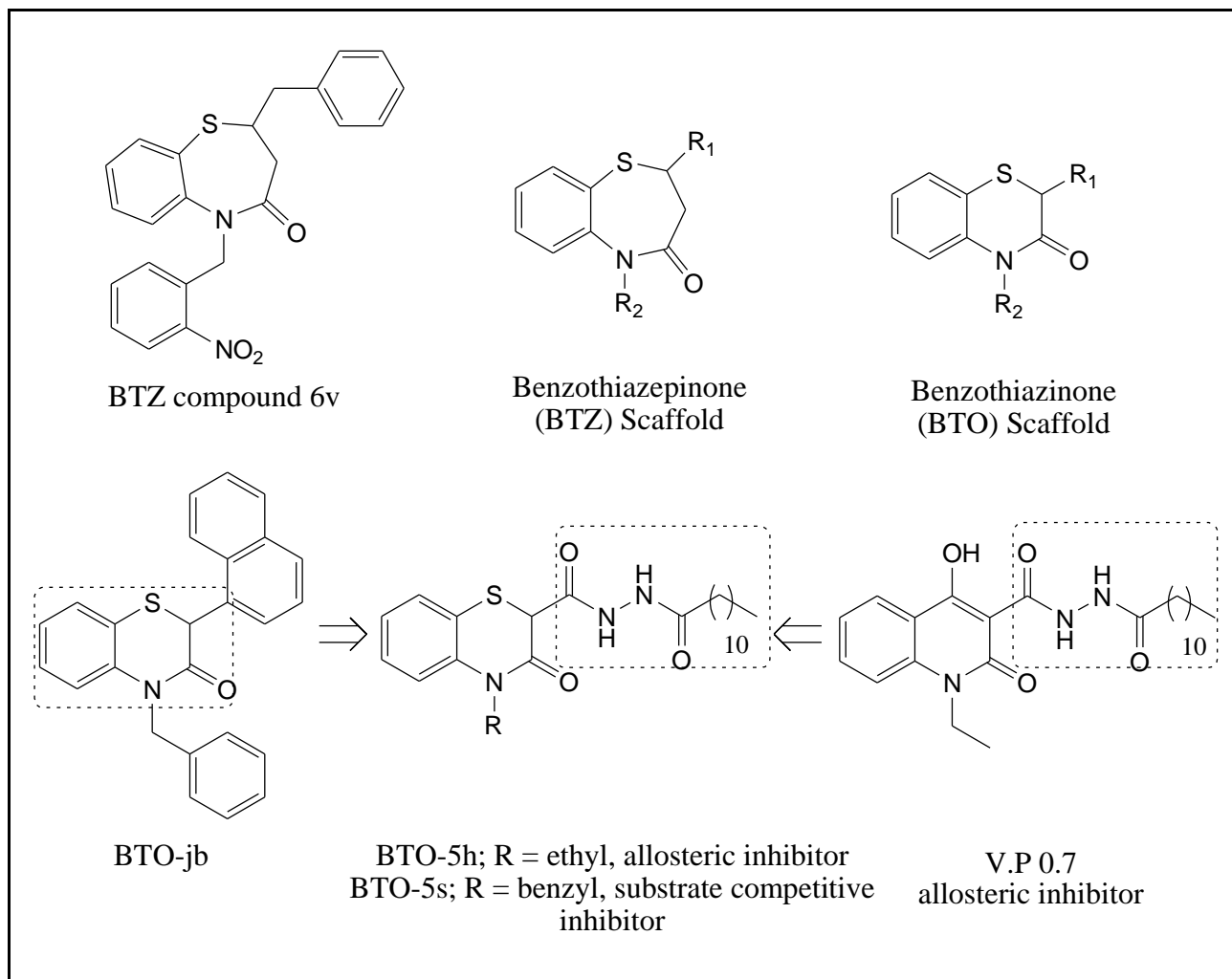


Figure 3.6 Design strategy of selected benzothiazepinone and benzothiazinone analogs as non-ATP competitive GSK-3 β inhibitors

3.1.2 Substrate Competitive GSK-3 Inhibitors

Another viable approach for designing selective inhibitors is by blocking the interaction of the substrate with the kinase via targeting the substrate binding site of GSK-3. Few promising lead molecules have been discovered that target the substrate pocket and inhibit the functioning of GSK-3. It is hypothesized that primed phosphate groups interact with three basic residues Arg96, Arg180 and Lys205 (hydrogen bond and electrostatic interactions) in the substrate pocket, resulting in proper orientation and functioning of GSK-3. Moreover, it was demonstrated that residues Phe67, Gln89, Phe93 and Asn95 were essential for optimal binding of substrates in the substrate binding pocket. Nearly 100 substrates are known to recognize GSK-3; therefore this enzyme is considered to be a prime regulator of almost every physiological process in the cells and tissues of humans (Sutherland; Eldar-Finkelman et al.). Currently, four distinct categories of substrate competitive GSK-3

Chapter 3

inhibitors are reported in literature and their typical representative examples are summarized in table 3.2.

Table 3.2 Classification of substrate competitive GSK-3 inhibitors

Source	Chemical Class	Inhibitor Potency (IC ₅₀)	Pharmacological Activity
Molecules from marine organisms	Manzamines	1.5 μ M	Decrease tau protein hyperphosphorylation
Small organic synthetic molecules	5-Imino-1,2,4-Thiadiazoles (ITDZS)	0.3 - 7 μ M	GSK-3 β inhibition
	Benzothiazinone (BTO-5s)	10 μ M	GSK-3 β inhibition
	Peptide like Inhibitors L803mts L807mts	20 μ M 1 μ M	Inhibits phosphorylation of GSK-3, IRS-1 and β -catenin
Abbreviations: IC ₅₀ , half maximal inhibitory concentration; μ M, micromolar; IRS-1, insulin receptor substrate 1.			

3.1.2.1 Manzamine alkaloids

Manzamine, is a complex polycyclic alkaloid isolated from marine sponge. One of its derivative Manzamine A was reported as dual inhibitor of GSK-3 β (IC₅₀: 10 μ M) and CDK5 (IC₅₀: 1.5 μ M). Kinetic experiments demonstrate Manzamine A as a substrate competitive GSK-3 β inhibitor. Hamann et al. applied molecular dynamics simulations and suggested that the substrate pocket is the most favorable site for interaction of Manzamine A. Cellular assays performed on these alkaloids showed a decline in tau hyperphosphorylation.

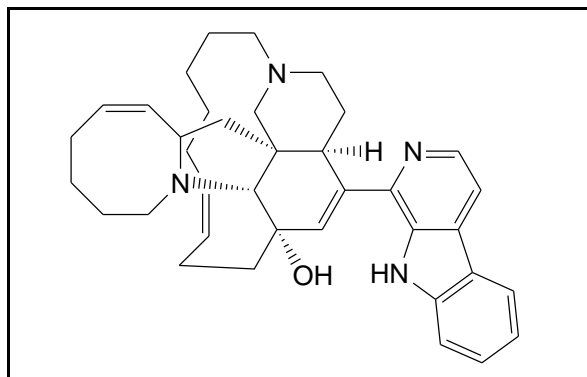


Figure 3.7 Manzamine A as substrate competitive GSK-3 β inhibitor

3.1.2.2 5-Imino-1,2,4-Thiadiazoles (ITDZs)

Palomo et al. reported first synthetic derivatives of 5-Imino-1,2,4-Thiadiazole as substrate competitive GSK-3 β inhibitors. Kinetic studies confirmed a reversible binding of ITDZ analogs to the substrate site. In support of this hypothesis docking studies established the binding mode of ITDZ analogs that interacts within the substrate binding pocket of GSK-3 β by forming a hydrogen-bond interaction connecting the proton of the imino charged group of thiadiazole scaffold with the backbone oxygen atom of Phe67 residue. In addition, an aromatic S- π interaction connecting the heterocyclic scaffold and the aromatic ring of Phe67 residue confirmed the substrate binding interactions. Thirty one synthesized ITDZ analogs were reported to have greater than 60 % of enzyme inhibition at 10 μ M concentrations. The IC₅₀ values of these variants were found in the concentration range of 0.3 to 7.0 μ M. Structures of the most potent ITDZ compounds are shown in figure 3.8.

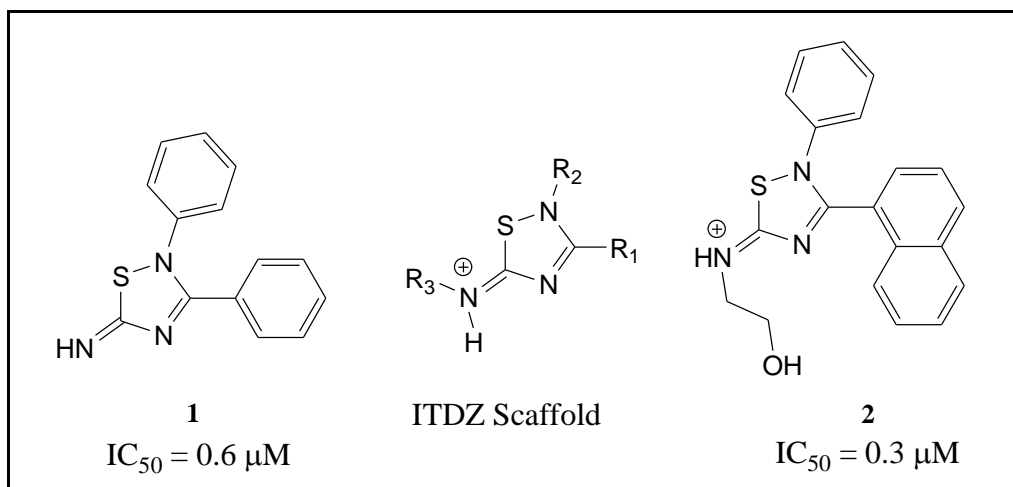


Figure 3.8 Selected ITDZ analogs as substrate competitive GSK-3 β inhibitors

3.1.2.3 Peptides

Researchers at Tel Aviv University designed peptides as substrate competitive GSK-3 inhibitors. Peptide L803-mts targets both isozymes of GSK-3 (α/β isozymes). The peptide was synthesized using heat shock factor-1 (HSF-1) sequence, attached with a myristic acid. Myristoylation improved the cellular permeability of the peptide. The peptide inhibitory binding mode was studied by docking and molecular dynamics simulation techniques; suggesting that the interaction of phosphorylated serine of the peptide with the phosphate binding pocket (Arg96, Arg180 and Lys205) and the remaining part of the peptide was flanked between the glycine-rich loop (P-loop), the activation loop and the C-loop (Licht-Murava and Hagit). The *in-vivo* efficacy of L803-mts has been shown in pre-clinical animal

models of Alzheimer's disease, cancer, diabetes, depressive behavior and multiple sclerosis (Eldar-Finkelman and Ana Martinez).

Recently, a next-generation peptide L807-mts was synthesized that acts *in-situ* as a substrate and an inhibitor of GSK-3. This peptide binds to GSK-3 and becomes phosphorylated, which acts as a substrate and converts the phosphorylated peptide itself to an inhibitor of GSK-3 (Licht-Murava et al.). These next generation peptides are more potent and highly selective GSK-3 α/β inhibitors when compared against a panel of other related protein kinases. Furthermore, the *in-vivo* efficacy of L807-mts, showed better cognitive behavior when tested with experimental mouse models of Alzheimer's disease.

3.1.2.4 Benzothiazinone (BTO)

Zhang et al. reported benzothiazinone derivatives (BTO-5s) as substrate competitive GSK-3 β inhibitors with an IC₅₀ value of 10.0 μ M. BTO-5s showed good efficacy on GSK-3 β and selectivity against a panel of ten related protein kinases (Figure 3.9). Docking studies suggested the substrate binding mode of the inhibitor.

Cellular assays performed on BTO-5s compound displayed a decline in phosphorylation levels of glycogen synthase in HpG2 cells. Moreover, an improved glucose uptake was reported in both HpG2 and 3T3-L1 cells. BTO-5s may have a potential therapeutic value for the treatment of T2DM.

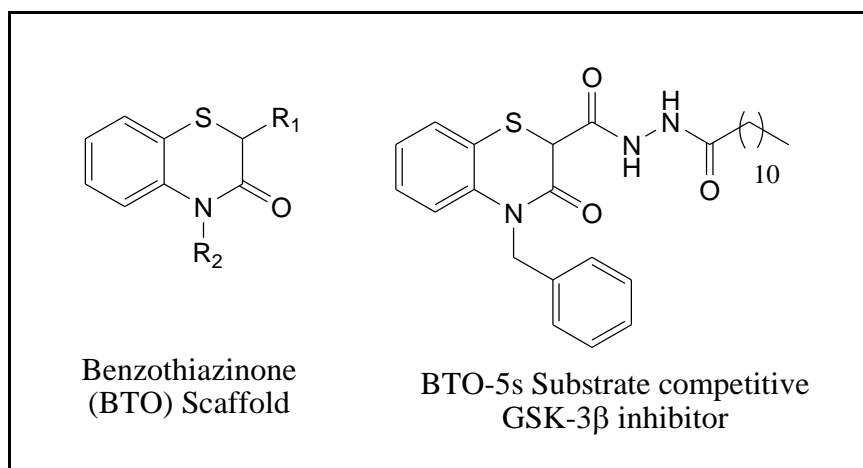


Figure 3.9 BTO-5s as a potent substrate competitive GSK-3 β inhibitor

3.1.3 ATP Competitive GSK-3 Inhibitors

ATP competitive GSK-3 β inhibitors are widely developed with an impressive number of available crystal structures in the Protein Data Bank (PDB). However, the most prominent challenge with developing these inhibitors is "specificity". The kinase family share a highly conserved catalytic pocket. Few compounds extracted from natural sources such as Staurosporine, Paullones, Indirubins and Hymenialdisine were the first-generation compounds reported as GSK-3 β inhibitors (Kramer et al.; Khan et al. and Patel et al.). These compounds are non-selective with other phylogenetically related kinases.

Moderate to high selectivity was achieved with a better understanding of the binding features of first-generation GSK-3 β inhibitors. Synthetic compounds such as 3-Anilino-4-arylmaleimides, 3-(7-Azaindolyl)-4-arylmaleimides, 6-heteroaryl-pyrazolo[3,4-*b*]pyridine and CHIR-98023 were claimed to show fair selectivity for GSK-3 β (Arfeen and Bharatam). The development of next-generation GSK-3 β inhibitors is still needed to overcome the puzzling hurdle of selectivity. Following section comprises representative classes of ATP competitive GSK-3 β inhibitors as outlined in table 3.3.

Table 3.3 Classification of ATP competitive GSK-3 inhibitors

Source	Chemical Class	Inhibitor Potency (IC ₅₀)	Pharmacological Activity
Inorganic compounds	Lithium	2 mM	Mood stabilizer and Neuroprotection
Small organic molecules	Pyrazolopyridines	0.8 nM	GSK-3 inhibition
	Paullones	4 - 80 nM	Decrease tau protein hyperphosphorylation
	Thiazoles	104 nM	Antidepressant and anti-manic
	Maleimides	34 - 77 nM	Neuroprotection
	Oxadiazole	2 - 14 nM	GSK-3 inhibition
	Acylaminopyridines	0.29 - 30 nM	Decrease tau protein hyperphosphorylation
Compounds from marine organisms	Indirubins, 6-bromoindirubin-3'-oxime	5 - 50 nM 1.5 μ M	Decrease tau protein hyperphosphorylation
	Hymenialdisine	10 nM	Decrease tau protein hyperphosphorylation
Abbreviations: IC ₅₀ , half maximal inhibitory concentration; μ M, micromolar; mM, millimolar; nM, nanomolar.			

3.1.3.1 Lithium

Lithium, a known mood-stabilizer was the first metal cation discovered as GSK-3 inhibitor (Geddes et al.). Ryves et al. hypothesized lithium effects on GSK-3 β activity and proposed two modes of GSK-3 β inhibition: directly by competing with magnesium ions and indirectly via serine phosphorylation. Its pharmacological effects by inhibition of GSK-3 β reduces tau hyperphosphorylation, β -amyloid-induced neurotoxicity and overproduction of β -amyloid peptide. These effects support its substantial role in Alzheimer's disease, bipolar disorder and other neurodegenerative disorders (De Ferrari et al.; Klein and Melton).

3.1.3.2 Pyrazolopyridines

Witherington et al. identified pyridazine scaffold as potent inhibitor of human GSK-3 α via pharmacophore screening of the SmithKline Beecham in-house chemistry database. Further, optimization of hits, synthesis and SAR studies afforded a series of potent and selective 6-arylpyrazolo[3,4-*b*]pyridines as indicated in figure 3.10. Kinase profiling studies revealed that 6-phenol analogues with 5-Bromo pyrazolopyridines displayed 20-fold increase in GSK-3 α potency (IC_{50} : 0.8 nM) and improved selectivity over CDK-2 (IC_{50} : 5 nM) compared with previously synthesized pyridazine moieties.

Molecular modeling analysis of binding mode of pyrazolopyridines displayed H-bond interactions with Asp133 and Val135 at hinge region of the ATP-binding site. Furthermore, the phenol moiety formed additional H-bonding interaction with Glu97 and Asp200 with better selectivity on GSK-3 β .

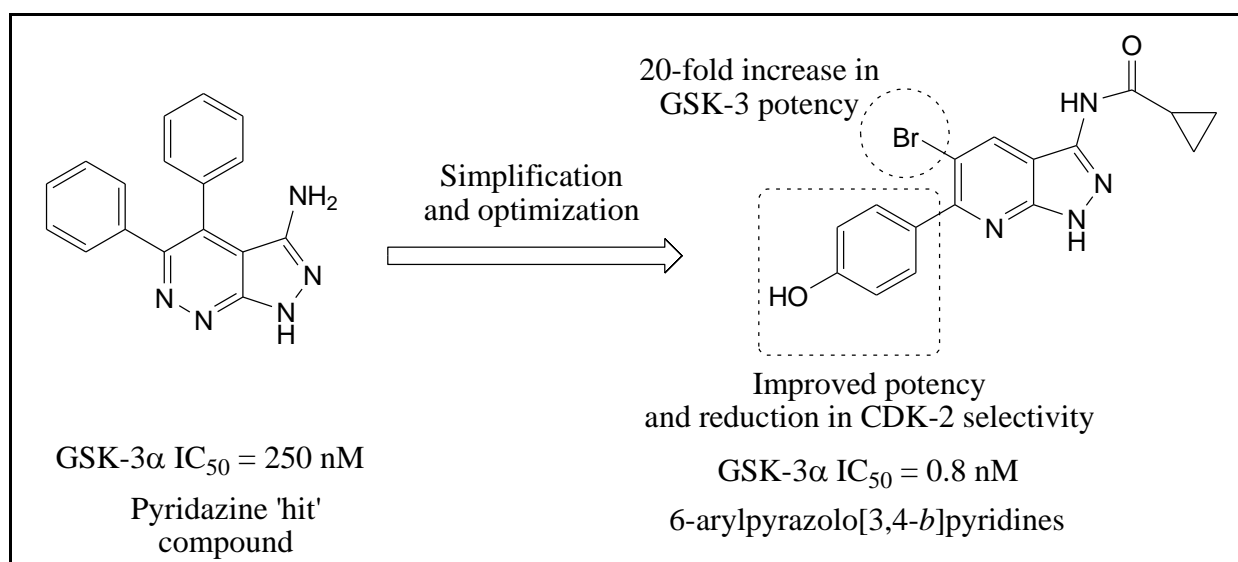


Figure 3.10 Identification of 6-aryl pyrazolo[3,4-*b*]pyridine as potent GSK-3 inhibitor

3.1.3.3 Paullones

Paullones were identified through National Cancer Institute (NCI) drug screening database against CDKs. This benzazepinone class of compounds appear to be specific dual inhibitors of GSK-3 β (IC₅₀: 4 - 80 nM) and CDKs (IC₅₀: 20 - 200 nM). Paullones were described as ATP competitive inhibitors that bind within the active site of these kinases (Conrad; Meijer et al.). More than 60 paullone congeners have been designed and synthesized; alsterpaullone, kenpaullone and cazpaullone were the most potent paullones reported in literature. Bertrand et al. reported the co-crystal structure of GSK-3 β bound with Alsterpaullone (PDB ID: 1Q3W). The ligand formed H-bond interactions with Val135, Asp200 and Lys85 in the ATP-binding site of GSK-3 β . Leost et al. reported the ability of paullones to inhibit phosphorylation of tau by GSK-3 β and described a potential role in treating neurodegenerative disorders. Paullones are poorly soluble in aqueous media which precluded their further development.

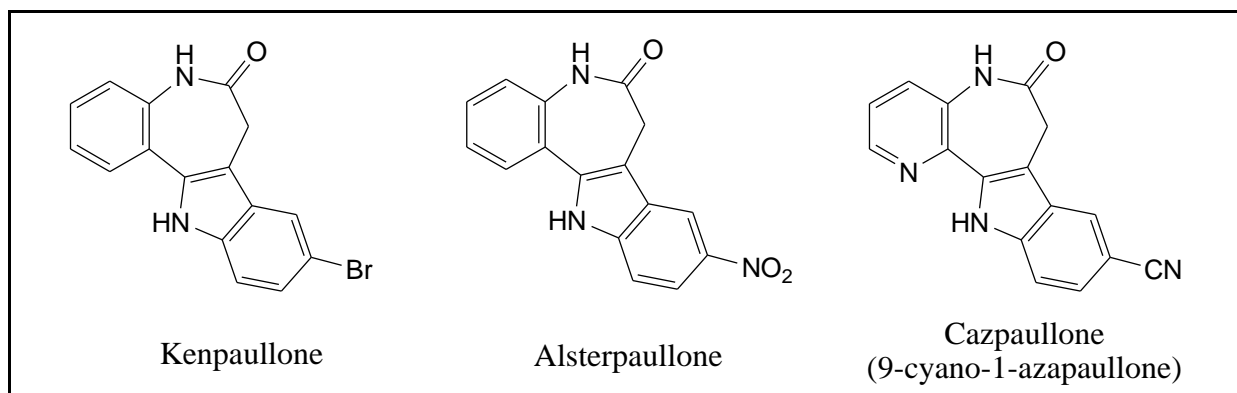


Figure 3.11 Structures of various paullone congeners

3.1.3.4 Thiazoles

Astra Zeneca developed compound AR-A014418 and claimed to be selective ATP-competitive GSK-3 β inhibitor. Cellular assays showed AR-A014418 could inhibit tau phosphorylation and β -amyloid mediated neurodegeneration. This inhibitor interacted with residues Cys199 and Leu132 with an improved selectivity for GSK-3 β (Bhat et al.).

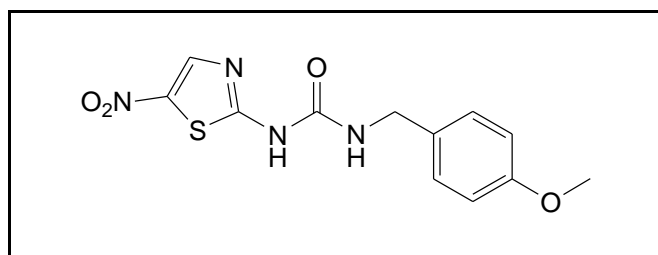


Figure 3.12 Structure of thiazole derivative AR-A014418 as potent GSK-3 β inhibitor

3.1.3.5 Maleimides

Maleimides are simplified scaffold of staurosporine. High-throughput screening assays conducted by Smith and his team reported anilino-maleimides as potent inhibitors of GSK-3 β . Maleimides (Figure 3.13) were demonstrated as competitive inhibitors via an ATP-binding site of GSK-3 β . The crystal structure of maleimides bound with GSK-3 β were shown to form H-bonds with Asp133 and Val135 in the active site. Compound SB-415286 (IC₅₀: 20 nM) from anilino-maleimide series was reported to be highly potent, selective and cell permeable GSK-3 β inhibitor.

A new series of structurally distinct aryl-indolyl maleimides was developed and the most potent compound SB-216763 from the designed series exhibited an IC₅₀ value of 34 nM. SB-415286 and SB216763 have shown *in-vivo* efficacy in different animal models of diabetes mellitus and neurodegenerative diseases.

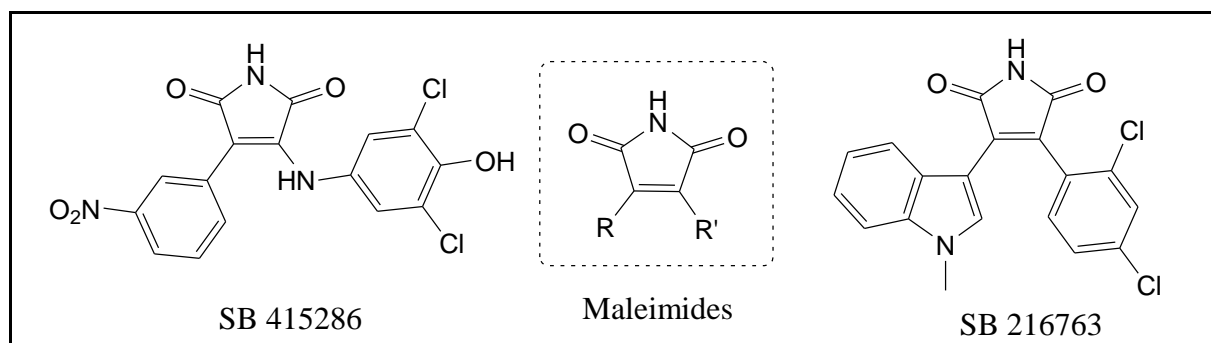


Figure 3.13 Selected potent maleimide analogs as potent GSK-3 β inhibitors

Johnson and Johnson Pharmaceuticals developed a novel macrocyclic bisindolyl maleimide containing linkers having multiple heteroatoms such as compounds 1 - 3 (Figure 3.14), with potent dual inhibition against both PKC- β II and GSK-3 β , indicating high homology in their ATP binding sites between these two kinases (O'Neill et al.). Replacement of both indole rings with 7-azaindole yielded a series of macrocyclic bis-7-azaindolylmaleimides (compound 5) as GSK-3 β inhibitors as indicated in figure 3.14 (Kuo et al.). These compounds showed excellent selectivity against a broad panel of about 60 protein kinases. However, achieving high selectivity over PKC- β II proved to be a challenge. Shen and co-workers synthesized macrocyclic bis-7-azaindolylmaleimide congeners. However, compound 4 (Figure 3.14) with a tetra-ethylene glycol linked ring exhibited good selectivity for GSK-3 β over PKC- β II (200-fold selectivity).

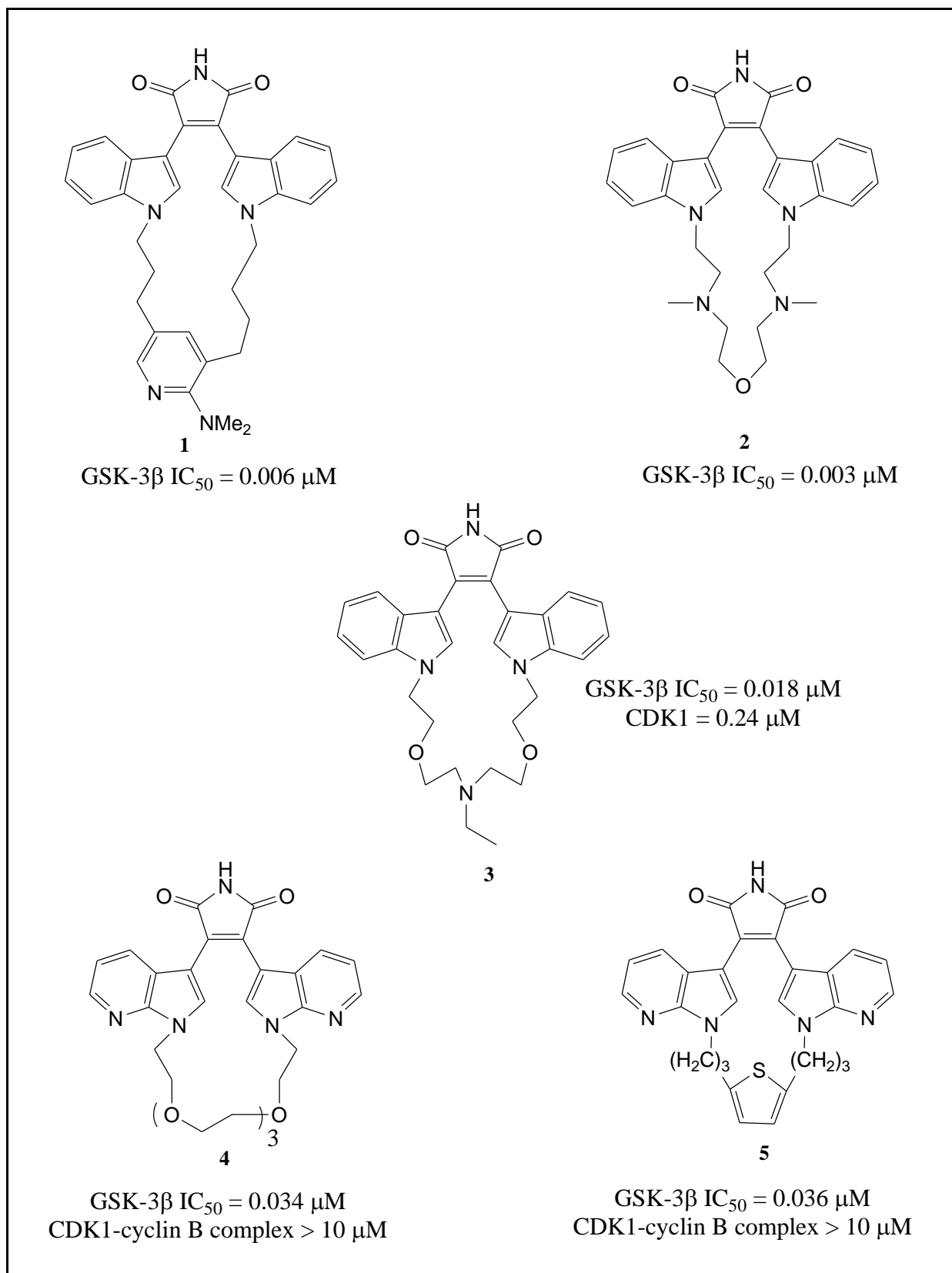


Figure 3.14 Selected macrocyclic bisindolylmaleimide and azaindolylmaleimide analogs as GSK-3β inhibitors

3.1.3.6 Oxadiazole

Siatoh et al. identified 1,3,4-oxadiazole based scaffold as GSK-3 β inhibitor through high-throughput screening as shown in figure 3.15. In lead optimization process, synthesis and SAR, the most potent compound 20x inhibited GSK-3 β with an IC₅₀ value of 2.3 nM. The co-crystal structure of compound 20x revealed that the benzimidazole and oxadiazole nitrogen formed H-bond interactions with Val135 and Asp200 in the ATP-binding pocket. The selectivity of compound 20x with GSK-3 β was compared with 23 protein kinases with greater than 1000-fold higher selectivity except for CDK-1 (IC₅₀: 4.6 μ M), MEKK-1 (IC₅₀: 8.1 μ M) and PKC (IC₅₀: 3.5 μ M).

F Monte et al. synthesized a series of "scorpion shaped" GSK-3 α inhibitors. Among all synthesized compounds, biphenyl-oxadiazole based compound 14d (GSK-3 α IC₅₀: 0.006 μ M; GSK-3 β IC₅₀: 0.316 μ M) and compound 15b (GSK-3 α IC₅₀: 0.002 μ M; GSK-3 β IC₅₀: 0.185 μ M) displayed the highest GSK-3 α selectivity reported so far. Moreover, compound 14d was found to be selective with GSK-3 when tested against a panel of 48 out of 50 protein kinases.

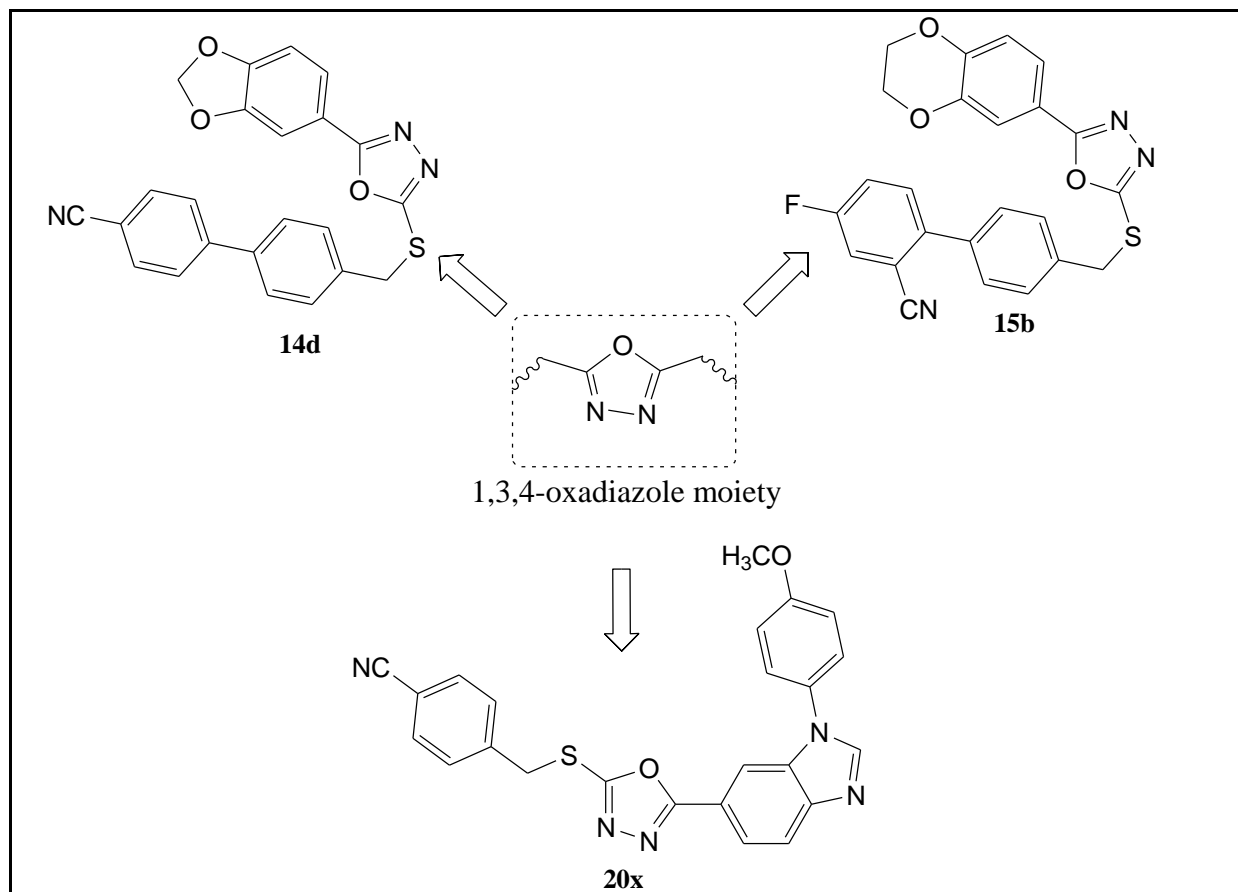


Figure 3.15 1,3,4-oxadiazole core structure based potent GSK-3 inhibitors

3.1.3.7 Acylaminopyridine

Sivaprakasam et al. identified acylaminopyridine linked pyrrolopyridinone lead compounds as potent GSK-3 β inhibitors with nanomolar potency. Systemic exploration of the chemical space around the spacer of the lead molecule guided the development of novel series of acylaminopyridine containing heterocycles with pyridylpyridines, thiazolylpyridines, phenyl and fused phenyl pyridines and miscellaneous heterocyclic pyridines. These ligands showed typical H-bond interactions in the ATP-binding site of GSK-3 β which are represented in figure 3.16. These compounds were capable of lowering tau phosphorylation at phosphorylating site (Ser396) of GSK-3 β in experimental animal models of Alzheimer's disease.

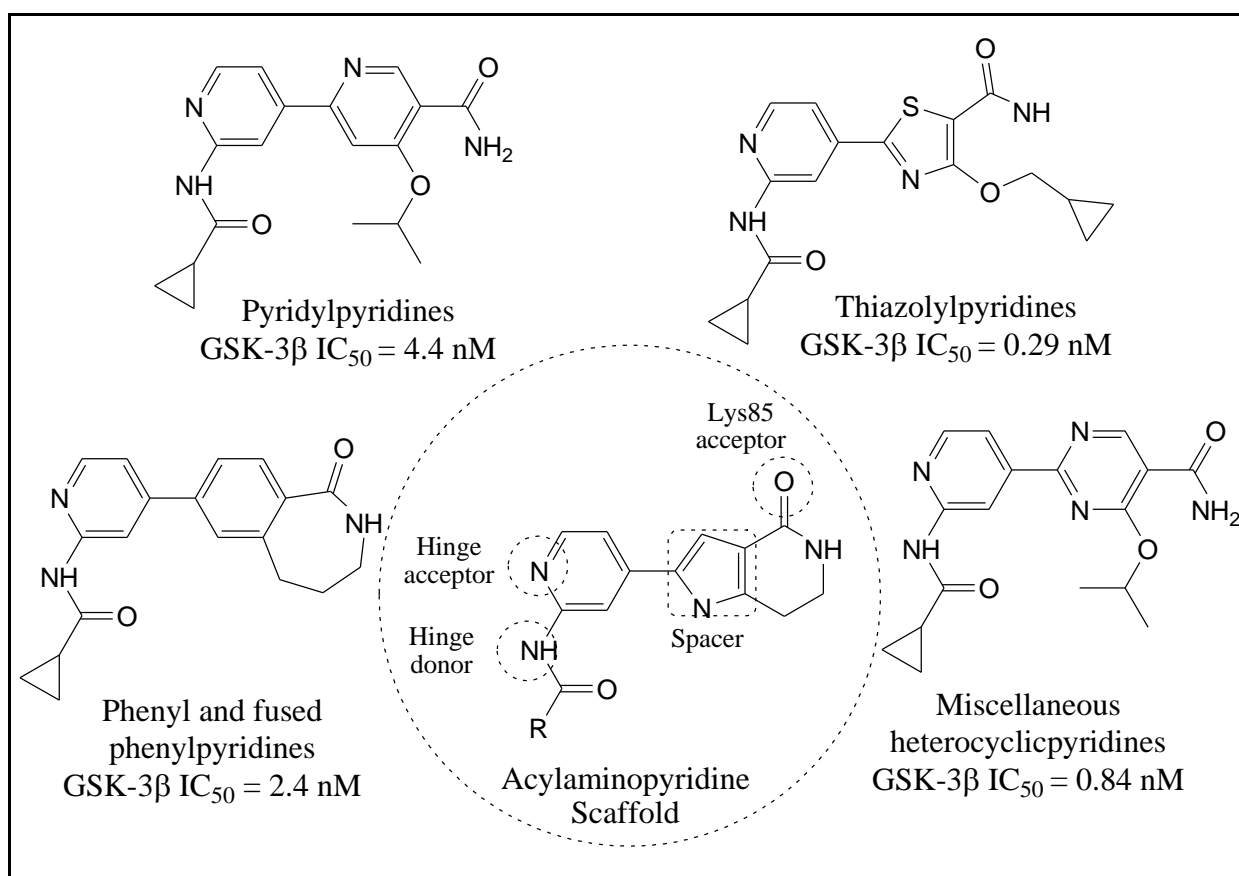


Figure 3.16 Selected examples of compounds designed around acylaminopyridine core scaffold (Sivaprakasam et al.)

3.1.3.8 Indirubins

Indirubins constitute a key ingredient of traditional chinese medicinal recipe for the treatment of chronic myelocytic leukemia. Indirubins are dual inhibitors of two protein kinase families: CDK and GSK-3 β , by competing with ATP in the active site in a nanomolar range (Leclerc et al.).

Polychronopolous and Meijer independently studied diversity-oriented synthesis of indirubin scaffold; the general substitution of 3'-oxime moiety and halogen were placed into the core of the molecule. Newer derivatives with 6-bromo substituted indirubin-3-oxime showed 16-fold better selectivity towards GSK-3 β over CDKs. Co-crystallized structure (PDB: 1UV5) analysis data of GSK-3 β with 6-BIO showed formation of H-bonds with Val135 and Asp133. In addition, a 6-bromo substituent displayed hydrophobic interactions with Met101 and Leu132 and improved the inhibiting capability in the ATP-binding site of GSK-3 β .

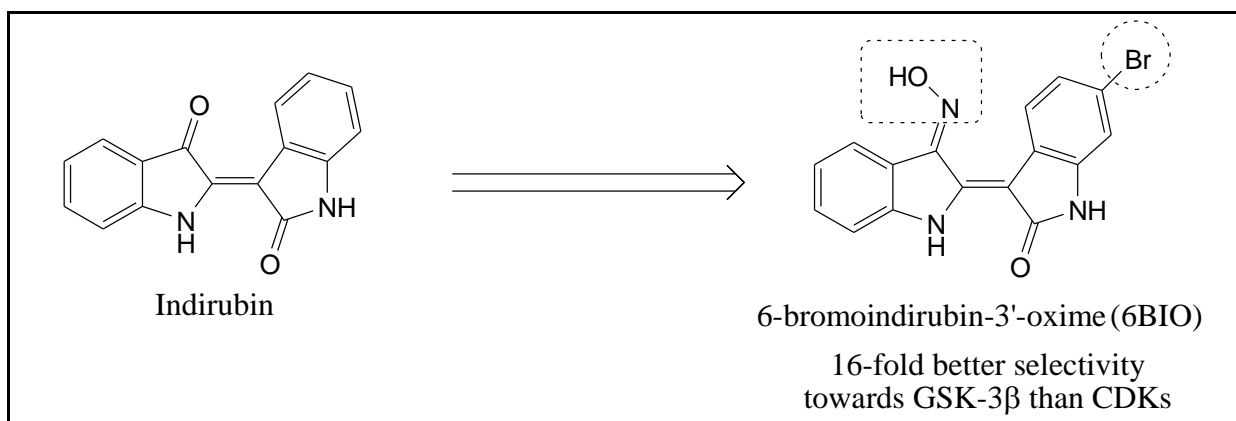


Figure 3.17 Optimization of 6-bromo indirubin-3'-oxime (6-BIO)

3.1.3.9 Hymenialdisine

Meijer et al. first reported hymenialdisine through screening of a large collection of marine derived natural products. Structurally, hymenialdisine is a bromopyrrole compound isolated from marine sponge. The naturally occurring alkaloid inhibits three protein kinase families in nanomolar range: GSK-3 β , cyclin-dependent kinases (CDK's such as CDK-1/cyclinB, CDK-2/cyclinA, CDK-2/cyclinE, CDK-5/p25) and casein kinase 1 (CK-1). It competes with ATP for binding inside the active site of the kinase. Its pharmacological effects inhibit phosphorylation of tau at phosphorylating sites of GSK-3 β and CDK5/p35 in experimental animal models of Alzheimer's disease.

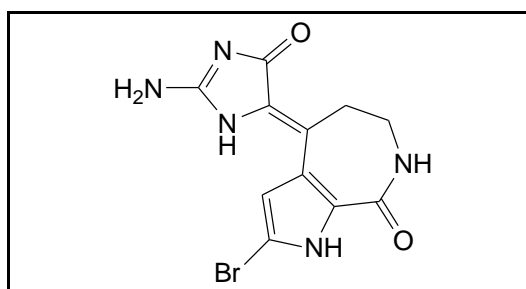


Figure 3.18 Structure of hymenialdisine

3.2 Recent Patents on GSK-3

Numerous patents on GSK-3 have been claimed in recent years due to the exploration of the X-ray crystal structures, virtual screening, molecular modeling techniques, hit-to-lead optimization. Patent searching on GSK-3 was done with PatSeer database.

Previously, Dorronsoro and his team published patent literature on the discovery of novel glycogen synthase kinase inhibitors and their screening methods. Phukan et al. performed patent analysis and classified chemotypes and substructures of GSK-3 β inhibitors. Recently, Palomo and Martinez have published a patent update on GSK-3 inhibitors summing up their applications in various therapeutic disorders. This section provides a report on highly potent GSK-3 inhibitors extracted from patent database and recent patent reviews.

Researchers at Chiron Corporation (acquired by Novartis) claimed first synthetic pyrimidine derivatives as ATP-competitive GSK-3 β inhibitors (Nuss et al.). Some advanced compounds like CHIR99021, CHIR98023 and CHIR98014 were developed as anti-diabetic agents through medicinal chemistry optimization of hits from filtered databases as shown in figure 3.19.

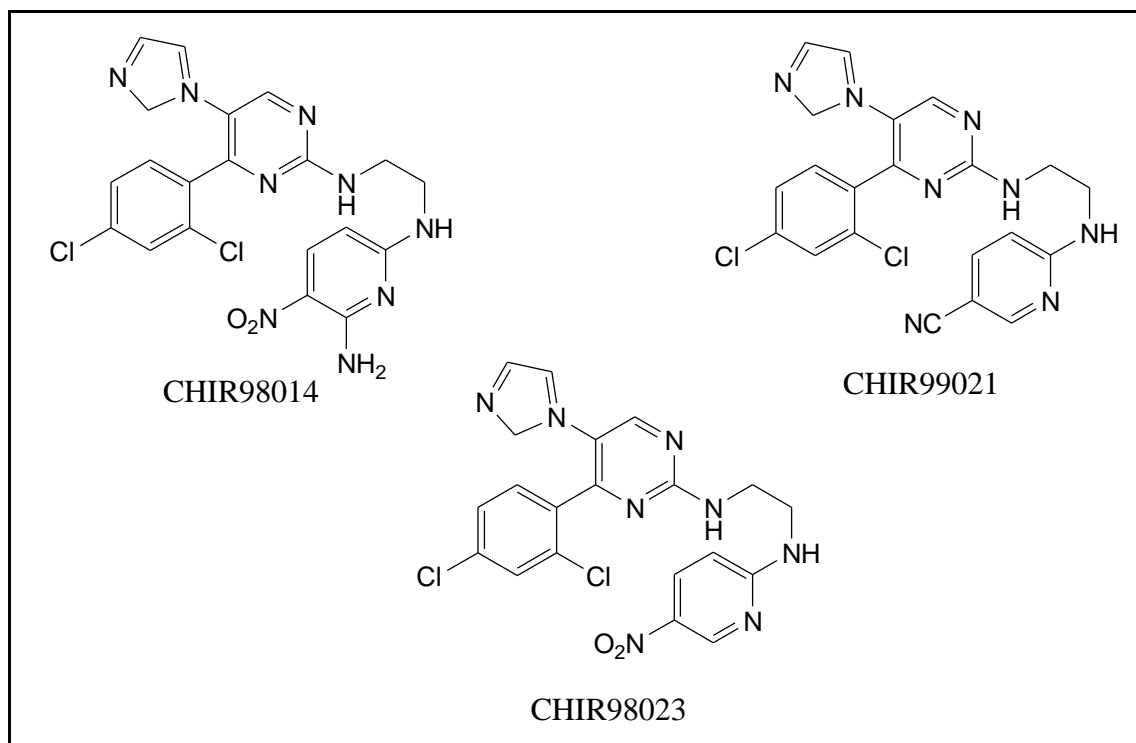


Figure 3.19 Pyrimidine compounds developed by Chiron Corporation

Recently, Noscira company patented next-generation thiadiazolidinone compounds 1, 2 and 3, with an aim to improve thermodynamic solubility of Tideglusib as shown in figure 3.20. As compared to Tideglusib, these newer derivatives showed better solubility and plasma exposure after oral administration (Medina et al.).

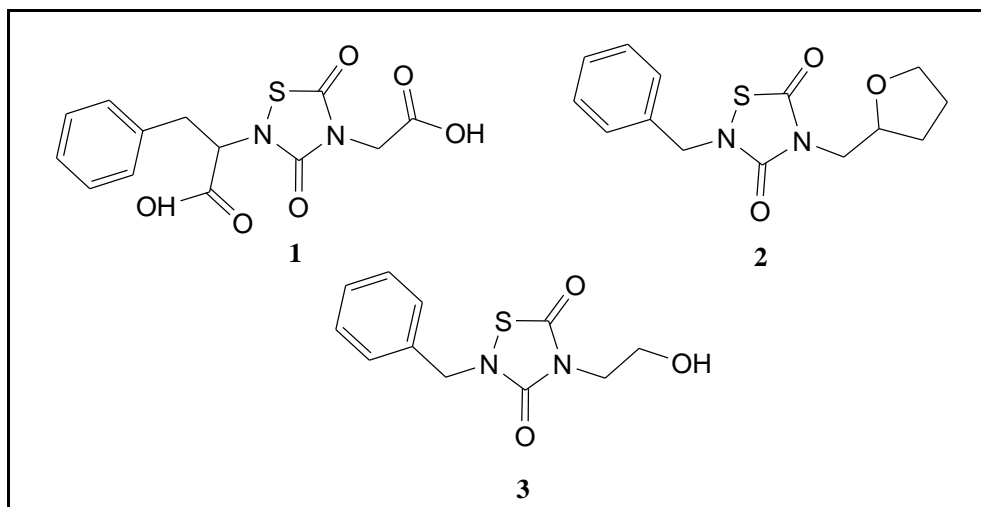


Figure 3.20 New analogs patented by Noscira with thiadiazolidinone scaffold

NeuroPharma claimed a urea derivative N-naphthyl-N'-benzylurea (compound 4) that inhibits GSK-3 β with an IC₅₀ value of 17.1 μ M. More recently, quinolinylpyrazinylureas (compound 5 and 6) were claimed by company Abbvie as potent GSK-3 β inhibitors (Martinez et al.; Turner et al.).

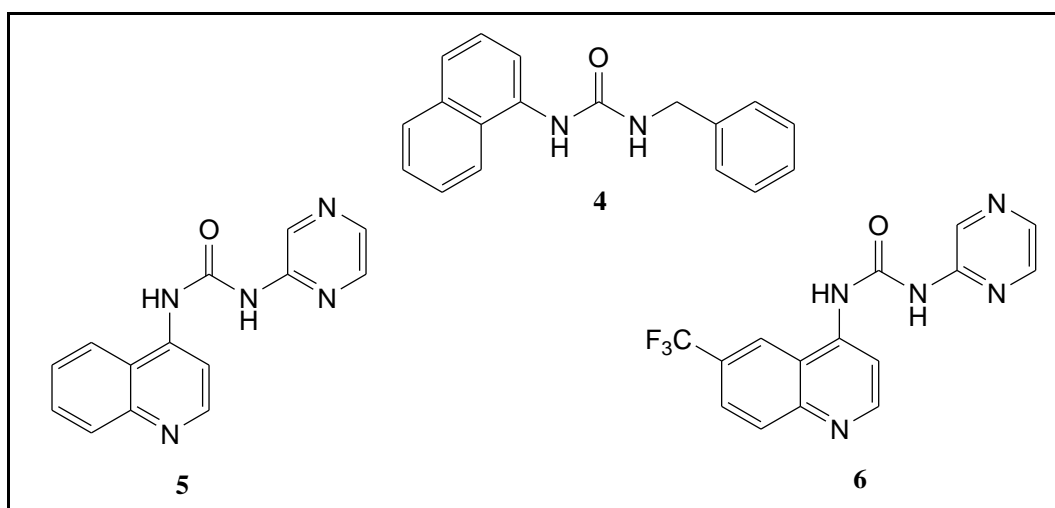


Figure 3.21 Some urea analogs as potent GSK-3 β inhibitors

Bristol-Myers Squibb recently patented novel isonicotinamide derivative (compound 7; figure 3.22) with three characteristic features reported as; orally active, excellent brain permeability and highly selective GSK-3 β inhibitor. The claimed molecule was capable of

lowering tau phosphorylation at phosphorylating site (Ser396) of GSK-3 β in experimental animal models of Alzheimer's disease (Luo et al.).

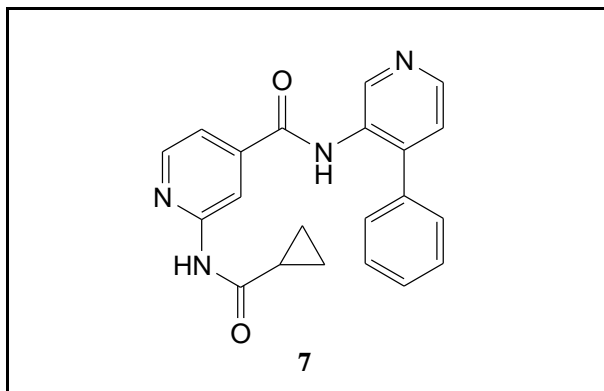


Figure 3.22 Isonicotinamide analog as potent GSK-3 β inhibitor

Recently, quinoline derivatives have been claimed as potential pharmacotherapy agents targeting GSK-3 β . A spiroquinolone derivative (compound 8; figure 3.23) inhibits GSK-3 β with an IC₅₀ value of 36 nM. These derivatives have been proposed as potential candidates for the treatment of diabetes mellitus. Another compound of the same family, a tricyclic 5-quinolone (compound 10; figure 3.23) has been shown to inhibit GSK-3 β and possess antitumor activity *in-vitro* and *in-vivo* (Seto et al.). The third quinoline compound V.P 0.7 is an allosteric inhibitor of GSK-3 β . V.P 0.7 (compound 10; figure 3.23) has been recently granted to Consejo Superior de Investigaciones Científicas (CSIC) (Martínez et al.).

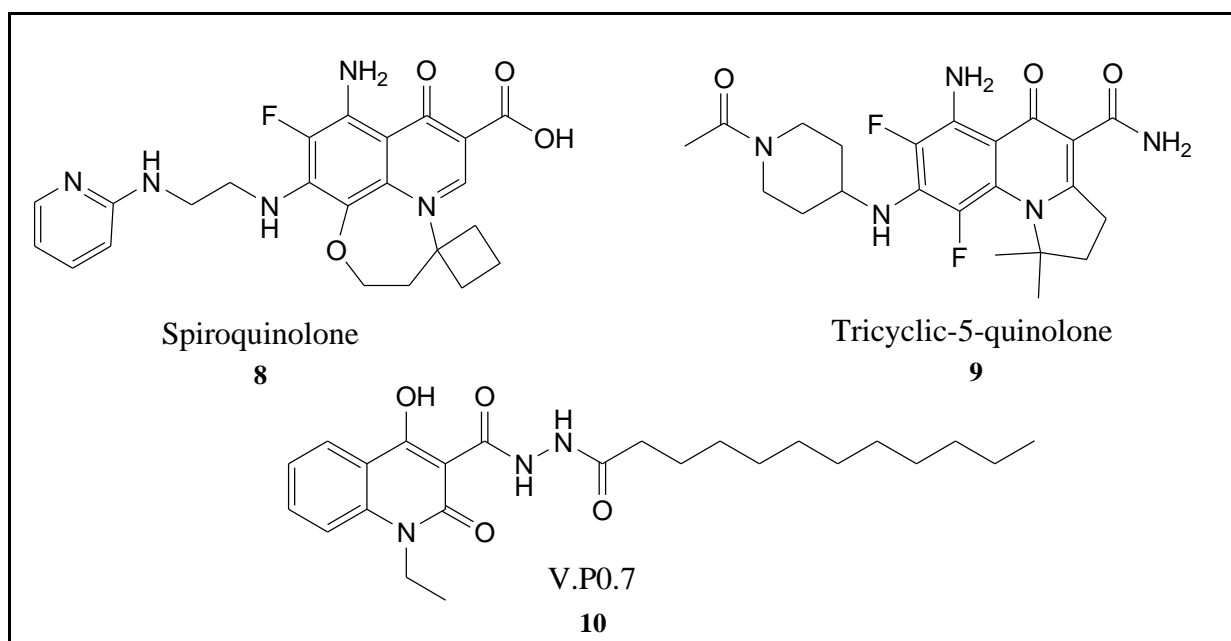


Figure 3.23 Quinoline derivatives as potent GSK-3 β inhibitors

Astex Therapeutics have claimed benzimidazole derivative such as compound 11 (Figure 3.24) that has the ability to modulate GSK-3, Aurora and CDK kinases (Berdini et al.). These derivatives have shown antiproliferative activity in a number of cancer cell lines. Abbvie patented compound 12 (Figure 3.24) as potent inhibitor on fourteen kinases including GSK-3. These compounds are claimed for the treatment of different types of cancers (Turner et al.). Teijin Pharma (compound 13; figure 3.24), Vertex Pharma (compounds 14 and 15; figure 3.24) and Abbot (compounds 16 and 17; figure 3.24) have recently patented diverse classes of potent compounds targeting GSK-3 where GSK-3 upregulation is involved (Figure 3.24) (Bebbington et al.; Green et al. and Tsutsumi et al.).

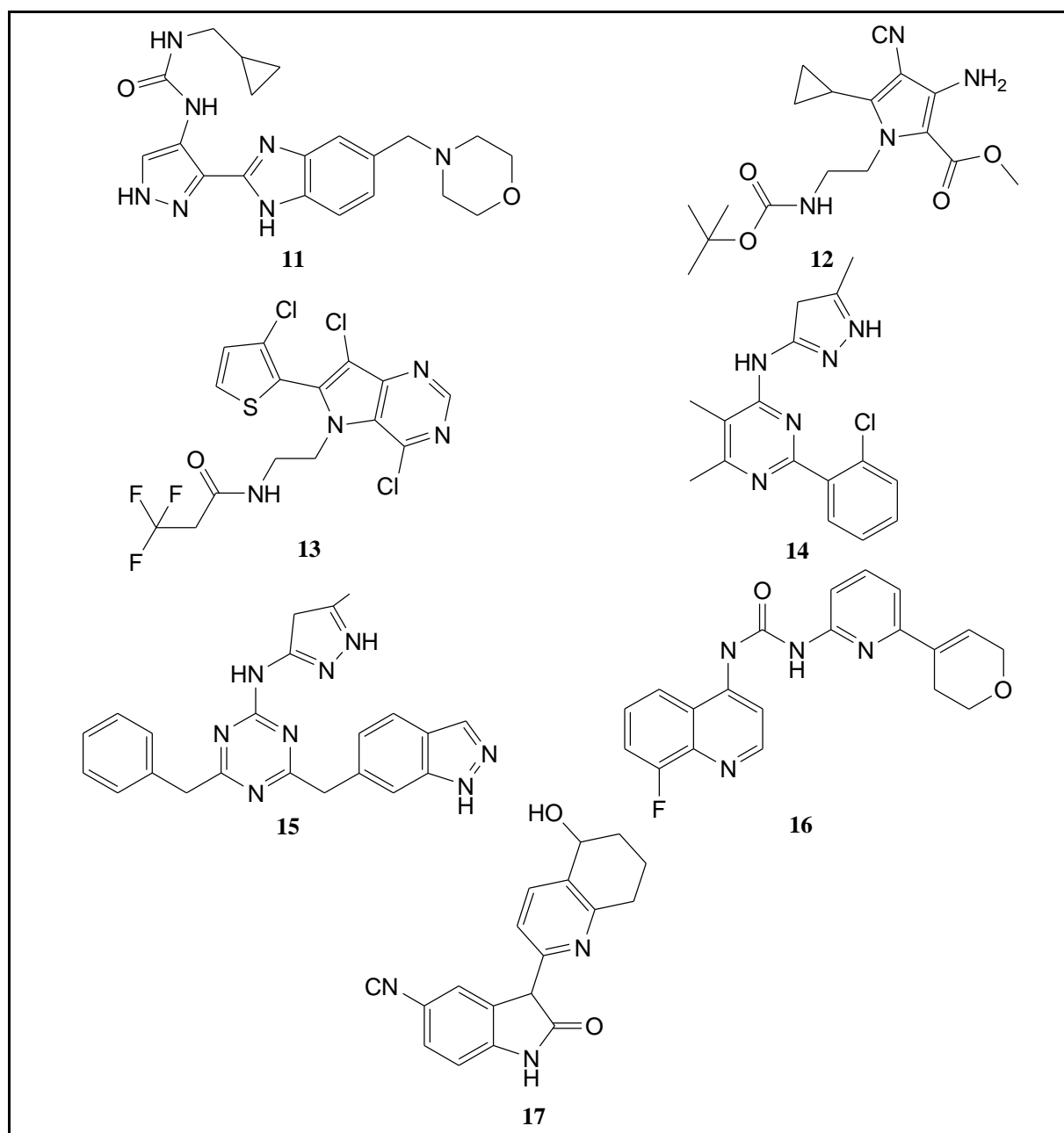


Figure 3.24 Analogs with diverse scaffolds patented as GSK-3 inhibitors

Technische Universität Darmstadt claimed oxadiazole derivatives like compound 18 (Figure 3.25) as ATP competitive inhibitor, which showed 92-fold selectivity for GSK-3 α over β -isoform (Schmidt et al.). The α -isoform specific targeting may require in some diseases such as acute myeloid leukemia (AML).

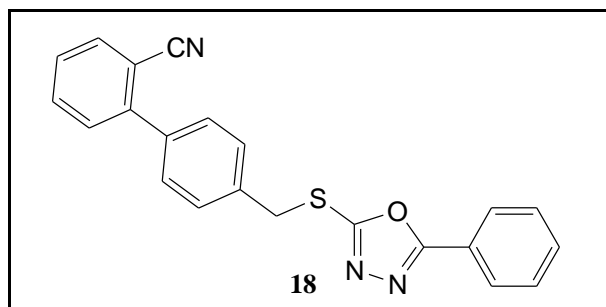


Figure 3.25 Novel oxadiazole based GSK-3 inhibitor

3.3 Conclusion

The drug discovery program in academia and industry exclusively focus on the development of potent and selective GSK-3 β inhibitors. Compounds that inhibit GSK-3 β with high affinity are generally ATP-competitive inhibitors. The similarity of ATP pocket indeed leads to multi-targeting kinase modulators. The advancement from first-generation to second-generation GSK-3 β inhibitors contributed to the development from non-selective to fairly selective GSK-3 β inhibitors. The two major concerns which preclude their further development for the treatment of various therapeutic disorders are 'specificity' and 'weak brain penetrating capacity'. However, next-generation GSK-3 β inhibitors such as isonicotinamide derivatives are claimed to overcome these drawbacks.

Substrate competitive inhibitors, non-ATP competitive inhibitors such as Tideglusib, and purely allosteric modulators, on the other hand, are more specific but inhibits GSK-3 β in micromolar range. However, such inhibitors have largely been identified as a result of serendipity. The development of non-ATP competitive GSK-3 β inhibitors with high potency is still challenging. Tideglusib is the only known compound that has reached clinical stages of development for various neurodegenerative disorders. The development of next-generation GSK-3 β inhibitors is still required to overcome the puzzling hurdle of potency and selectivity.

3.4 References

- Arfeen, Minhajul, and Prasad Bharatam. "Design of Glycogen Synthase Kinase-3 Inhibitors: An Overview on Recent Advancements." *Current Pharmaceutical Design*, vol. 19, no. 26, 2013, pp. 4755–4775.
- Bebbington et al. "Pyrazole compounds useful as protein kinase inhibitors". US8697698, 2014.
- Berdini et al. "Pyrazole compounds that modulate the activity of CDK, GSK and aurora kinases". US8778936, 2014.
- Berg, Stefan, et al. "Discovery of Novel Potent and Highly Selective Glycogen Synthase Kinase-3 β (GSK3 β) Inhibitors for Alzheimer's Disease: Design, Synthesis, and Characterization of Pyrazines." *Journal of Medicinal Chemistry*, vol. 55, no. 21, 2012, pp. 9107–9119.
- Bhat, Ratan, et al. "Structural Insights and Biological Effects of Glycogen Synthase Kinase 3-Specific Inhibitor AR-A014418." *Journal of Biological Chemistry*, vol. 278, no. 46, 2003, pp. 45937–45945.
- Bidon-Chanal, Axel, et al. "Evidence for a New Binding Mode to GSK-3: Allosteric Regulation by the Marine Compound Palinurin." *European Journal of Medicinal Chemistry*, vol. 60, 2013, pp. 479–489.
- Conde, Santiago, et al. "Thienyl and Phenyl α -Halomethyl Ketones: New Inhibitors of Glycogen Synthase Kinase (GSK-3 β) from a Library of Compound Searching." *Journal of Medicinal Chemistry*, vol. 46, no. 22, 2003, pp. 4631–4633.
- De Ferrari, G. V., et al. "Activation of Wnt signaling rescues neurodegeneration and behavioral impairments induced by β -amyloid fibrils." *Molecular Psychiatry*, vol. 8, no. 2, 2003, pp. 195-208.
- Domínguez, Juan Manuel, et al. "Evidence for Irreversible Inhibition of Glycogen Synthase Kinase-3 β by Tideglusib." *Journal of Biological Chemistry*, vol. 287, no. 2, 2011, pp. 893–904.
- Dorronsoro, Isabel, et al. "Inhibitors of Glycogen Synthase Kinase-3: Future Therapy for Unmet Medical Needs?" *Expert Opinion on Therapeutic Patents*, vol. 12, no. 10, 2002, pp. 1527–1536.

- Eldar-Finkelman, Hagit, et al. "Substrate Competitive GSK-3 Inhibitors Strategy and Implications." *Biochimica At Biophysica Acta (BBA) - Proteins and Proteomics*, vol. 1804, no. 3, 2010, pp. 598–603.
- Eldar-Finkelman, Hagit, and Ana Martinez. "GSK-3 Inhibitors: Preclinical and Clinical Focus on CNS." *Frontiers in Molecular Neuroscience*, vol. 4, 2011.
- Eldar-Finkelman et al. "Glycogen synthase kinase-3 inhibitors". WO2012101601, 2013.
- Ferrari, G V De, et al. "Activation of Wnt Signaling Rescues Neurodegeneration and Behavioral Impairments Induced by β -Amyloid Fibrils." *Molecular Psychiatry*, vol. 8, no. 2, 2003, pp. 195–208.
- Geddes, John R., et al. "Long-Term Lithium Therapy for Bipolar Disorder: Systematic Review and Meta-Analysis of Randomized Controlled Trials." *American Journal of Psychiatry*, vol. 161, no. 2, 2004, pp. 217–222.
- Green et al. "Compositions useful as inhibitors of protein kinases". US8653088, 2014.
- Hamann, Mark, et al. "Glycogen Synthase Kinase-3 (GSK-3) Inhibitory Activity and Structure–Activity Relationship (SAR) Studies of the Manzanamine Alkaloids. Potential for Alzheimer's Disease." *Journal of Natural Products*, vol. 70, no. 9, 2007, pp. 1397–1405.
- Khan, Imran, et al. "Natural and Synthetic Bioactive Inhibitors of Glycogen Synthase Kinase." *European Journal of Medicinal Chemistry*, vol. 125, 2017, pp. 464–477.
- Klein, P. S., and D. A. Melton. "A Molecular Mechanism for the Effect of Lithium on Development." *Proceedings of the National Academy of Sciences*, vol. 93, no. 16, June 1996, pp. 8455–8459.
- Kramer, Thomas, et al. "Small-Molecule Inhibitors of GSK-3: Structural Insights and Their Application to Alzheimers Disease Models." *International Journal of Alzheimers Disease*, vol. 2012, 2012, pp. 1–32.
- Kunick, Conrad, et al. "Structure-Aided Optimization of Kinase Inhibitors Derived from Alsterpaullone." *Chem Bio Chem*, vol. 6, no. 3, Apr. 2005, pp. 541–549.
- Kunick, Conrad, et al. "1-Azakenpaullone Is a Selective Inhibitor of Glycogen Synthase Kinase-3 β ." *Bioorganic & Medicinal Chemistry Letters*, vol. 14, no. 2, 2004, pp. 413–416.

- Kuo, Gee-Hong, et al. "Synthesis and Discovery of Macrocyclic Polyoxygenated Bis-7-Azaindolylmaleimides as a Novel Series of Potent and Highly Selective Glycogen Synthase Kinase-3 β Inhibitors." *Journal of Medicinal Chemistry*, vol. 46, no. 19, 2003, pp. 4021–4031.
- Leclerc, Sophie, et al. "Indirubins Inhibit Glycogen Synthase Kinase-3 β and CDK5/P25, Two Protein Kinases Involved in Abnormal Tau Phosphorylation in Alzheimers Disease." *Journal of Biological Chemistry*, vol. 276, no. 1, 2000, pp. 251–260.
- Leost, Maryse, et al. "Paullones Are Potent Inhibitors of Glycogen Synthase Kinase-3 β and Cyclin-Dependent Kinase 5/p25." *European Journal of Biochemistry*, vol. 267, no. 19, 2000, pp. 5983–5994.
- Licht-Murava, Avital, et al. "Elucidating Substrate and Inhibitor Binding Sites on the Surface of GSK-3 β and the Refinement of a Competitive Inhibitor." *Journal of Molecular Biology*, vol. 408, no. 2, 2011, pp. 366–378.
- Licht-Murava, Avital, and Hagit Eldar-Finkelman. "Exploiting Substrate Recognition for Selective Inhibition of Protein Kinases." *Current Pharmaceutical Design*, vol. 18, no. 20, 2012, pp. 2914–2920.
- Licht-Murava, A., et al. "A Unique Type of GSK-3 Inhibitor Brings New Opportunities to the Clinic." *Science Signaling*, vol. 9, no. 454, 2016.
- Luo, Guanglin, et al. "Discovery of Isonicotinamides as Highly Selective, Brain Penetrable, and Orally Active Glycogen Synthase Kinase-3 Inhibitors." *Journal of Medicinal Chemistry*, vol. 59, no. 3, 2016, pp. 1041–1051.
- Martínez, Ana, et al. "Arylimino-1,2,4-Thiadiazolidinones: A New Family of Potassium Channel Openers." *Bioorganic & Medicinal Chemistry*, vol. 5, no. 7, 1997, pp. 1275–1283.
- Martínez et al. "GSK-3 inhibitors". US08686042, 2014.
- Martínez et al. "Heterocyclic GSK-3 allosteric modulators". EP2769720, 2014.
- Martinez, Ana, et al. "First Non-ATP Competitive Glycogen Synthase Kinase 3 β (GSK-3 β) Inhibitors: Thiadiazolidinones (TDZD) as Potential Drugs for the Treatment of Alzheimer's Disease." *Journal of Medicinal Chemistry*, vol. 45, no. 6, 2002, pp. 1292–1299.

- Martinez, Ana, et al. "SAR and 3D-QSAR Studies on Thiadiazolidinone Derivatives: Exploration of Structural Requirements for Glycogen Synthase Kinase 3 Inhibitors." *Journal of Medicinal Chemistry*, vol. 48, no. 23, 2005, pp. 7103–7112.
- Martinez, Ana, et al. "Glycogen Synthase Kinase 3 (GSK-3) Inhibitors as New Promising Drugs for Diabetes, Neurodegeneration, Cancer, and Inflammation." *Medicinal Research Reviews*, vol. 22, no. 4, 2002, pp. 373–384.
- Medina et al. "Thiadiazolidinediones as GSK-3 inhibitors". WO2013124413, 2013.
- Meijer, L., et al. "The Paullones: A Family of Pharmacological Inhibitors of Cyclin-Dependent Kinases and Glycogen Synthase Kinase 3." *Inhibitors of Protein Kinases and Protein Phosphates Handbook of Experimental Pharmacology*, pp. 47–64.
- Meijer, Laurent, et al. "GSK-3-Selective Inhibitors Derived from Tyrian Purple Indirubins." *Chemistry & Biology*, vol. 10, no. 12, 2003, pp. 1255–1266.
- Meijer, L., et al. "Inhibition of Cyclin-Dependent Kinases, GSK-3 β and CK1 by Hymenialdisine, a Marine Sponge Constituent." *Chemistry & Biology*, vol. 7, no. 1, 2000, pp. 51–63.
- Monte, Fabio Lo, et al. "Structure-Based Optimization of Oxadiazole-Based GSK-3 Inhibitors." *European Journal of Medicinal Chemistry*, vol. 61, 2013, pp. 26–40.
- Monte, Fabio Lo, et al. "Identification of Glycogen Synthase Kinase-3 Inhibitors with a Selective Sting for Glycogen Synthase Kinase-3 α ." *Journal of Medicinal Chemistry*, vol. 55, no. 9, 2012, pp. 4407–4424.
- Morales-Garcia, Jose A., et al. "Glycogen Synthase Kinase 3 Inhibition Promotes Adult Hippocampal Neurogenesis *in Vitro* and *in Vivo*." *ACS Chemical Neuroscience*, vol. 3, no. 11, 2012, pp. 963–971.
- Nuss JM, et al. "Preparation of aminopyrimidines and pyridines as glycogen synthase kinase 3 inhibitors". WO2002020495, 2002.
- Osolodkin, Dmitry I., et al. "Glycogen Synthase Kinase 3 as an Anticancer Drug Target: Novel Experimental Findings and Trends in the Design of Inhibitors." *Current Pharmaceutical Design*, vol. 19, no. 4, 2012, pp. 665–679.

- O'Neill, David J., et al. "Design, Synthesis, and Biological Evaluation of Novel 7-Azaindolyl-Heteroaryl-Maleimides as Potent and Selective Glycogen Synthase Kinase-3 β (GSK-3 β) Inhibitors." *Bioorganic & Medicinal Chemistry*, vol. 12, no. 12, 2004, pp. 3167–3185.
- Palomo, Valle, and Ana Martinez. "Glycogen Synthase Kinase 3 (GSK-3) Inhibitors: a Patent Update (2014-2015)." *Expert Opinion on Therapeutic Patents*, vol. 27, no. 6, 2016, pp. 657–666.
- Palomo, Valle, et al. "Exploring the Binding Sites of Glycogen Synthase Kinase 3. Identification and Characterization of Allosteric Modulation Cavities." *Journal of Medicinal Chemistry*, vol. 54, no. 24, 2011, pp. 8461–8470.
- Palomo, Valle, et al. "5-Imino-1,2,4-Thiadiazoles: First Small Molecules As Substrate Competitive Inhibitors of Glycogen Synthase Kinase 3." *Journal of Medicinal Chemistry*, vol. 55, no. 4, 2012, pp. 1645–1661.
- Patel, Dhilon S., et al. "Structure-Based Approaches in the Design of GSK-3 Selective Inhibitors." *Current Protein & Peptide Science*, vol. 8, no. 4, 2007, pp. 352–364.
- Phukan, S, et al. "GSK-3 β : Role in Therapeutic Landscape and Development of Modulators." *British Journal of Pharmacology*, vol. 160, no. 1, 2010, pp. 1–19.
- Perez, Daniel I., et al. "Switching Reversibility to Irreversibility in Glycogen Synthase Kinase 3 Inhibitors: Clues for Specific Design of New Compounds." *Journal of Medicinal Chemistry*, vol. 54, no. 12, 2011, pp. 4042–4056.
- Polychronopoulos, Panagiotis, et al. "Structural Basis for the Synthesis of Indirubins as Potent and Selective Inhibitors of Glycogen Synthase Kinase-3 and Cyclin-Dependent Kinases." *Journal of Medicinal Chemistry*, vol. 47, no. 4, 2004, pp. 935–946.
- Ryves, W Jonathan, et al. "Glycogen Synthase Kinase-3 Inhibition by Lithium and Beryllium Suggests the Presence of Two Magnesium Binding Sites." *Biochemical and Biophysical Research Communications*, vol. 290, no. 3, 2002, pp. 967–972.
- Saitoh, Morihisa, et al. "Design, Synthesis and Structure–Activity Relationships of 1,3,4-Oxadiazole Derivatives as Novel Inhibitors of Glycogen Synthase Kinase-3 β ." *Bioorganic & Medicinal Chemistry*, vol. 17, no. 5, 2009, pp. 2017–2029.

- Saitoh, Morihisa, et al. "2-{3-[4-(Alkylsulfinyl)Phenyl]-1-Benzofuran-5-Yl}-5-Methyl-1,3,4-Oxadiazole Derivatives as Novel Inhibitors of Glycogen Synthase Kinase-3 β with Good Brain Permeability." *Journal of Medicinal Chemistry*, vol. 52, no. 20, 2009, pp. 6270–6286.
- Schmidt et al. "Glycogen synthase kinase-3 inhibitors". WO2012101601, 2013.
- Seto, Shigeki, et al. "Quinolone Derivatives Containing Strained Spirocycle as Orally Active Glycogen Synthase Kinase 3 β (GSK-3 β) Inhibitors for Type 2 Diabetics." *Bioorganic & Medicinal Chemistry*, vol. 20, no. 3, 2012, pp. 1188–1200.
- Shen, Lan, et al. "Synthesis and Biological Evaluation of Novel Macrocyclic Bis-7-Azaindolylmaleimides as Potent and Highly Selective Glycogen Synthase Kinase-3 β (GSK-3 β) Inhibitors." *Bioorganic & Medicinal Chemistry*, vol. 12, no. 5, 2004, pp. 1239–1255.
- Silva, Tiago, et al. "Alzheimers Disease, Enzyme Targets and Drug Discovery Struggles: From Natural Products to Drug Prototypes." *Ageing Research Reviews*, vol. 15, 2014, pp. 116–145.
- Sivaprakasam, Prasanna, et al. "Discovery of New Acylaminopyridines as GSK-3 Inhibitors by a Structure Guided in-Depth Exploration of Chemical Space around a Pyrrolopyridinone Core." *Bioorganic & Medicinal Chemistry Letters*, vol. 25, no. 9, 2015, pp. 1856–1863.
- Smith, David G., et al. "3-Anilino-4-Arylmaleimides: Potent and Selective Inhibitors of Glycogen Synthase Kinase-3 (GSK-3)." *Bioorganic & Medicinal Chemistry Letters*, vol. 11, no. 5, 2001, pp. 635–639.
- Sutherland, Calum. "What Are The bonafide GSK-3 Substrates?" *International Journal of Alzheimers Disease*, vol. 2011, 2011, pp. 1–23.
- Tsutsumi et al. "Pyrrolopyrimidine thion derivatives". US2005153992, 2005.
- Turner et al. "Heterocyclic compounds and their use as glycogen synthase kinase-3 inhibitors". US8642598, 2014.
- Witherington, Jason, et al. "5-Aryl-Pyrazolo[3,4-*b*]Pyridazines: Potent Inhibitors of Glycogen Synthase Kinase-3 (GSK-3)." *Bioorganic & Medicinal Chemistry Letters*, vol. 13, no. 9, 2003, pp. 1581–1584.

- Witherington, Jason, et al. "6-Aryl-Pyrazolo[3,4-*b*]Pyridines: Potent Inhibitors of Glycogen Synthase Kinase-3 (GSK-3)." *Bioorganic & Medicinal Chemistry Letters*, vol. 13, no. 18, 2003, pp. 3055–3057.
- Witherington, Jason, et al. "6-Heteroaryl-Pyrazolo[3,4-*b*]Pyridines: Potent and Selective Inhibitors of Glycogen Synthase Kinase-3 (GSK-3)." *Bioorganic & Medicinal Chemistry Letters*, vol. 13, no. 18, 2003, pp. 3059–3062.
- Zhang, Peng, et al. "Novel Benzothiazinones (BTOs) as Allosteric Modulator or Substrate Competitive Inhibitor of Glycogen Synthase Kinase 3 β (GSK-3 β) with Cellular Activity of Promoting Glucose Uptake." *Bioorganic & Medicinal Chemistry Letters*, vol. 24, no. 24, 2014, pp. 5639–5643.
- Zhang, Peng, et al. "Design, Synthesis and Biological Evaluation of Benzothiazepinones (BTZs) as Novel Non-ATP Competitive Inhibitors of Glycogen Synthase Kinase-3 β (GSK-3 β)." *European Journal of Medicinal Chemistry*, vol. 61, 2013, pp. 95–103.

4.1 *In-silico* Druggability Assessment

Binding site identification and its characterization is a key process in structure-based drug design. Putative binding sites of a target protein can be identified by various *in-silico* tools but their druggability still remains unidentified. In this study, the druggability of GSK-3 β binding sites was analyzed with a pocket detection tool SiteMap from Schrödinger Inc. SiteMap is an energy-based pocket detection algorithm that finds, visualizes, and evaluates protein binding sites (Halgren T). Energy-based methods identify binding sites by docking small organic probes, typically methane or water molecules, on a given target protein to evaluate whether a given protein region interacts favorably (Wagner et al.). Based on the druggability criteria assigned by the developers of SiteMap, this computational tool helps to differentiate between "druggable", "difficult" and "undruggable sites" of a target protein.

4.1.1 Materials and Methods

All computational studies were performed using Schrödinger suite, version 9.3.5 on a windows Dell workstation.

4.1.1.1 Protein Preparation

A dataset of 24 X-ray crystal structures of human GSK-3 β were extracted from the Brookhaven Protein Data Bank (www.rcsb.org). GSK-3 β is a dimer structure consisting of chains A and B. The monomer chain A was first separated from each crystal structure as SiteMap may generate unphysical sites over the entire dimer structure. Likewise, in a few cases of the crystallographic structures, chain A monomers were crystallized with Axin and Fratide peptides and in few cases they were deposited as monomer chains. Each individual chain A monomers were pre-processed with the Protein Preparation Wizard in the Maestro program, with the following default options selected: "assign bond orders," "add hydrogen atoms," "create zero-order bonds to metals," "create disulphide bonds," and "delete water molecules beyond 5Å from heteroatom groups." The optimal protonation states of each ionizable residue were assigned and the hydrogen-bonding network was optimized for each protein with structural ambiguity. A restrained minimization with an OPLS 2005 force field was performed to attain the relaxed state of each refined complex. The prepared structures were validated using Ramachandran plots.

4.1.1.2 Site Identification

A dataset of 24 refined chain A monomers were submitted to SiteMap (v2.6) for druggability assessment. All crystallographic water molecules, ligands, metal ions,

heteroatom groups, unwanted chains, and peptides were removed prior to the site search. SiteMap protocol was set to return up to 10 sites (default settings: 5 sites), considering an average of seven previously identified putative binding sites of GSK-3 β (Palomo et al.).

4.1.1.3 Druggability assessment by SiteMap

The druggability of a protein binding pocket was assessed by various physical descriptors in SiteMap, which were calibrated for submicromolar tight-binding sites (Halgren TA). These include:

- i) The size and the volume of a protein binding site (case-sensitive terms).
- ii) Enclosure property which indicates the degree to which a site is sheltered from the solvent (calibrated scores: ~ 0.76).
- iii) The exposure property measures the degree of exposure to solvent (calibrated scores ≤ 0.49).
- iv) The degree of contact measures the relative tightness between the site points and the protein site via Van der Waals non-bonding interactions (calibrated scores ~ 1.0).
- v) The phobic/philic character is a measure of the relative hydrophobic and hydrophilic nature of the site (calibrated scores ~ 1.0).
- vi) The balance term indicates the ratio of hydrophobic to hydrophilic character of the site (the calibrated ratio of the two scores is approximately 1.6).
- vii) The donor/acceptor character measures the hydrogen-bonding possibility between a ligand and protein site where a ligand donates, and the protein accepts hydrogen bonds within a site (calibrated scores ~ 0.76).

SiteMap computes two output scores for each binding site known as the SiteScore (SScore) and the Druggability score (Dscore). Both scores are defined as:

$$\text{SiteScore} = 0.0733n^{1/2} + 0.6688e - 0.20p$$

$$\text{Dscore} = 0.094n^{1/2} + 0.60e - 0.324p$$

where,

n = number of site points (capped at 100)

e = enclosure score, and

p = hydrophilic score (capped at 1.0).

For SiteScore the hydrophilic score is capped at 1.0 whereas the hydrophilic score is uncapped in Dscore to penalize highly polar sites. This critical feature in Dscore classifies binding sites between “druggable,” “difficult,” and “undruggable” sites on a protein structure.

4.1.2 Results and Discussion

A dataset of twenty-four X-ray crystal structures of GSK-3 β were prepared and submitted to SiteMap for druggability assessment, as described in the methods section 4.1.1.1. An average of eight surface pockets were found on the structure of GSK-3 β . Among them, three pockets (1, 4 and 7) were consistently retrieved in all crystal structures analyzed by SiteMap represented in figure 4.1.

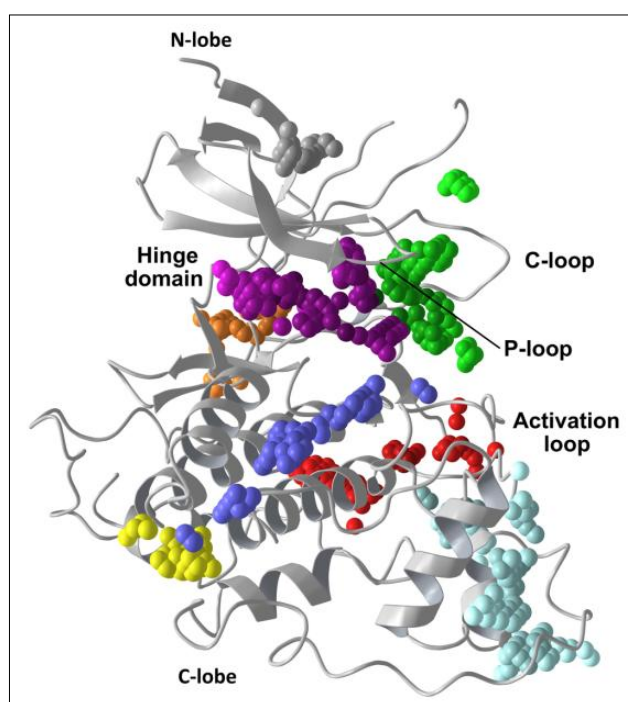


Figure 4.1 Representation of eight surface pockets of GSK-3 β identified by SiteMap. [Protein Data Bank (PDB) ID: 4NU1; gray cartoon representation]: pocket 1 (pink spheres), pocket 2 (green spheres), pocket 3 (turquoise spheres), pocket 4 (blue spheres), pocket 5 (gray spheres), pocket 6 (brown spheres), pocket 7 (red spheres) and pocket 8 (yellow spheres)

The X-ray crystal structures revealed three well-known binding sites of GSK-3 β : (i) the ATP site, (ii) the substrate binding site, and (iii) the Axin/Fratide binding site. In addition, four allosteric pockets (pockets 4 - 7) on GSK-3 β were recently reported (Palomo et al.). SiteMap identified an additional small pocket at the C-lobe of GSK-3 β (pocket 8).

4.1.2.1 Classifying ligand-binding sites of GSK-3 β

The SiteScore data was initially analyzed to identify plausible ligand-binding sites. Based on the recommended cut-off scores, SiteScore can be applied as a classifier to predict ligand-binding sites (SiteScore ≥ 0.80) or non-ligand-binding sites (SiteScore < 0.80) and a score higher than 1.01 indicates highly potential binding sites (Halgren TA). Pockets 1 and 7 demonstrated SiteScore values higher than 0.80 with promising ligand-binding capabilities, as shown in table 4.1. Interestingly, for site 7 the PDB entry 1I09 (SiteScore: 0.734 and 0.674) and 4NM0 (SiteScore: 0.754 and 0.680) revealed two separate pockets very close in space surrounded by the same region. In both cases, the observed low scores were correlated with small cavity volume of each pocket. In the present SiteMap computations, six pockets (2, 3, 4, 5, 6, and 8) have median SiteScores less than the cut-off range.

4.1.2.2 Classifying druggable binding sites of GSK-3 β

In addition to SiteScore, the druggability of each site of GSK-3 β was analyzed by Druggability score (Dscore) (Table 4.2). Considering the Dscore criteria, binding sites of a protein can be classified into “druggable,” “undruggable,” and “medium druggable/difficult” sites (Halgren TA).

(i) Druggable Site (Dscore > 0.98)

A typical druggable site is recognized by its good size, deeply buried pocket and often hydrophobic character. Among the eight sites identified, pocket 1 was the highest predicted site with a median Dscore higher than 0.98 (83 % cases). Moreover, undruggable sites (Dscore < 0.83) were not identified in any case of PDB for pocket 1, indicating a druggable pocket of GSK-3 β . All other pockets, in most cases, failed the druggability criteria of SiteMap.

(ii) Difficult sites (Dscore between 0.83 and 0.98)

SiteMap druggability scores recognize pocket 7 as a “difficult” site with the highest predicted cases scoring between 0.83 and 0.98. Despite the adequate size and volume of the site, with exceptional hydrophilicity, an important reason to classify site 7 as an “intermediate site” is the low hydrophobic nature of the site (quantitative median phobic score is approximately 0.3) (Table 4.3). To facilitate comparison, the surface maps of a “druggable” site (pocket 1) and a “difficult” site (pocket 7) were visualized as identified by SiteMap (Figure 4.2). A clear difference is observed for pocket 7, which lacks sufficient sized hydrophobic regions (yellow maps). The hydrogen-bond donor and acceptor regions of this pocket (blue and red maps,

respectively) are scattered over the entire cavity while these regions are more concentrated surrounding the entire hydrophobic region of pocket 1.

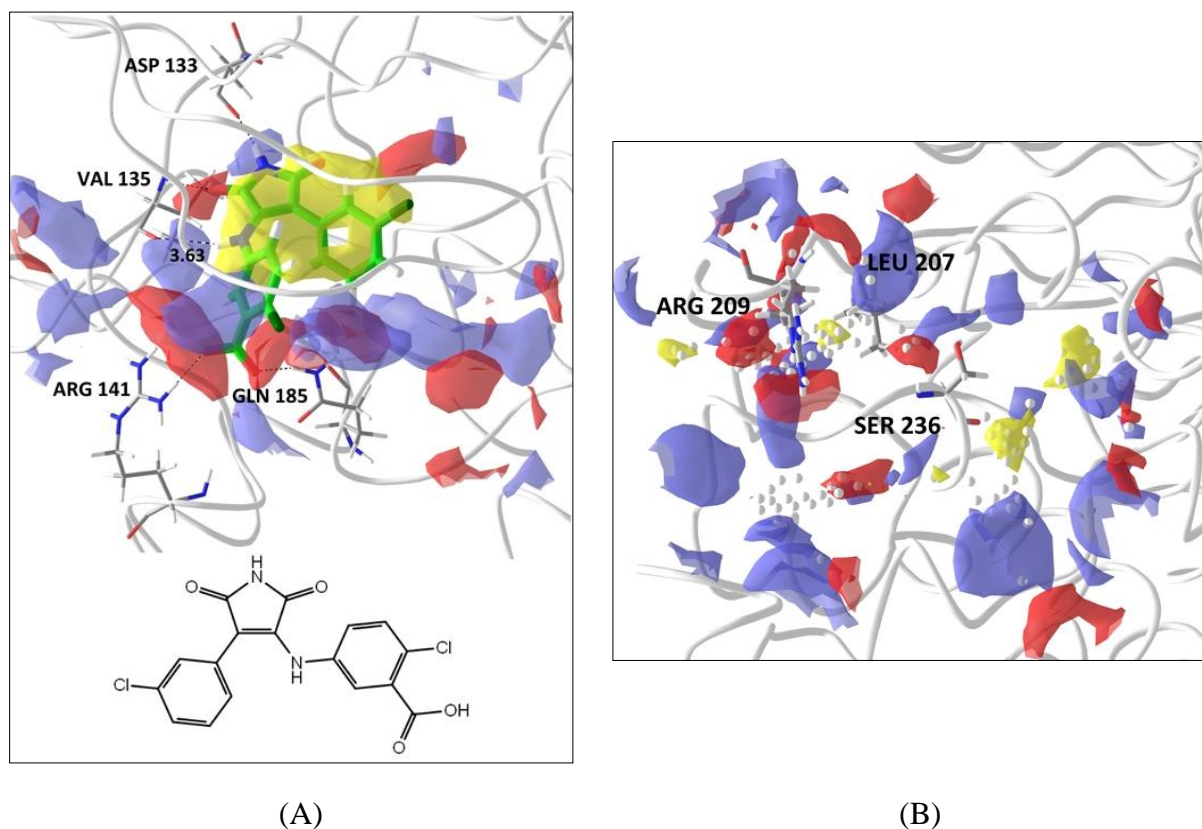


Figure 4.2 Comparison of the surface maps of pockets of GSK-3 β identified by SiteMap
(A) druggable pocket (B) difficult pocket

(iii) Undruggable sites (Dscore < 0.83)

The undruggable sites are shallow protein surface pockets, extremely hydrophilic with negligible hydrophobic nature, characterized with Dscores below 0.80. The druggability scores recognize pockets 5, 6, and 8 as undruggable sites (100 % cases). Pocket 2 (95 % cases) and pocket 4 (87 % cases) were also categorized as undruggable sites in several cases shown in table 4.2. SiteMap identified pocket 3 as having two or three distinct cavities within the same binding region, annotated with their respective scores shown in tables 4.1 and 4.2. This yielded a total of 33 sites, of which 27 sites exhibited median Dscores, less than 0.83 (82 % undruggable cases).

Chapter 4

Table 4.1 Performance in classifying binding sites of glycogen synthase kinase-3 β based on SiteScore

Sr. No.	PDB ID	Pocket 1	Pocket 2	Pocket 3	Pocket 4	Pocket 5	Pocket 6	Pocket 7	Pocket 8
1	1GNG	0.891	0.523	0.726, 0.690, 0.553	0.553	n.f	0.553	0.963	0.743
2	1H8F	1.012	0.525	n.f.	0.720	n.f.	0.722	0.937	0.666
3	1I09	1.035	n.f.	n.f.	0.757	0.703	0.640	0.734, 0.674	0.712
4	1O9U	0.991	n.f.	0.856, 0.639	0.718	n.f.	0.631, 0.592	0.968	0.722
5	1PYX	1.029	0.552	n.f.	0.684	0.636	n.f.	0.934	0.697
6	1Q3D	0.923	0.717	0.566	0.793	0.690	n.f.	0.938	n.f.
7	1Q3W	1.070	n.f.	0.574	0.775	0.652	0.661	0.944	n.f.
8	1Q41	1.097	0.742	n.f.	0.680	0.670	0.581	0.967	n.f.
9	1Q4L	1.045	0.788	0.588	0.860	0.621	n.f.	0.912	n.f.
10	1Q5K	1.014	n.f.	0.659, 0.561	0.681	0.659	0.494	0.914	0.709
11	1R0E	1.033	n.f.	0.773, 0.568	0.805	0.608	0.570	0.946	0.711
12	1UV5	1.043	0.701, 0.605	0.748, 0.621	0.730	0.713	0.823	0.973	0.726
13	2O5K	1.031	0.804	0.709	0.680	n.f.	0.745	0.969	0.664
14	2OW3	1.035	0.636	0.836, 0.623	0.919	n.f.	n.f.	0.957	0.772
15	3DU8	1.058	0.628, 0.627	0.862, 0.686	0.746	n.f.	n.f.	0.947	n.f.
16	3F88	1.118	0.822	0.691, 0.637	0.940	n.f.	0.479	0.870	0.636
17	3GB2	1.046	0.584	n.f.	0.661	n.f.	0.484	0.945	0.631
18	3PUP	1.038	0.597	0.795	0.816	0.631	0.596	0.899	n.f.
19	3ZRM	1.016	0.575	0.728, 0.700, 0.570	0.645	n.f.	n.f.	0.962	0.649
20	4ACD	1.033	0.674	0.686	0.742	0.644	n.f.	0.962	n.f.
21	4J1R	0.930	0.709	0.845	0.627	n.f.	0.636	0.954	0.668
22	4J71	1.034	n.f.	0.664	0.681	0.724	n.f.	0.994	0.664
23	4NM0	0.996	n.f.	0.867, 0.626	0.736	0.718	n.f.	0.754, 0.680	0.744
24	4NU1	1.070	0.930	0.813, 0.651, 0.635	0.735	0.632	0.627	0.810	0.766
Site Score \geq 0.80		24	03	06	05	00	01	22	00
Site Score < 0.80		00	16	27	19	14	15	04	17
Site not found		None	07	05	None	10	09	None	07
Abbreviations: n.f., cavity not found; PDB, Protein Data Bank.									

Table 4.2 Performance in classifying binding sites of GSK-3 β based on Dscore

Sr. No.	PDB ID	Pocket 1	Pocket 2	Pocket 3	Pocket 4	Pocket 5	Pocket 6	Pocket 7	Pocket 8
1	1GNG	0.868	0.430	0.680, 0.678, 0.362	0.461	n.f.	0.484	0.974	0.720
2	1H8F	1.002	0.342	n.f.	0.665	n.f.	0.638	0.943	0.615
3	1I09	1.005	n.f.	n.f.	0.713	0.575	0.596	0.661, 0.620	0.678
4	1O9U	1.013	n.f.	0.904, 0.418	0.590	n.f.	0.568, 0.549	0.994	0.641
5	1PYX	0.987	0.488	n.f.	0.612	0.567	n.f.	0.953	0.671
6	1Q3D	0.896	0.576	0.487	0.769	0.647	n.f.	0.953	n.f.
7	1Q3W	1.054	n.f.	0.505	0.732	0.623	0.655	0.960	n.f.
8	1Q41	1.114	0.723	n.f.	0.622	0.643	0.532	0.999	n.f.
9	1Q4L	1.068	0.752	0.548	0.868	0.542	n.f.	0.930	n.f.
10	1Q5K	1.023	n.f.	0.649, 0.516	0.619	0.602	0.410	0.924	0.233
11	1R0E	1.057	n.f.	0.809, 0.516	0.742	0.564	0.381	0.957	0.653
12	1UV5	0.969	0.516, 0.553	0.747, 0.570	0.670	0.652	0.776	0.936	0.691
13	2O5K	1.003	0.690	0.588	0.552	n.f.	0.732	0.979	0.628
14	2OW3	1.073	0.599	0.851, 0.466	0.935	n.f.	n.f.	0.976	0.721
15	3DU8	1.058	0.571, 0.573	0.894, 0.673	0.725	n.f.	n.f.	0.946	n.f.
16	3F88	1.133	0.800	0.555, 0.604	0.989	n.f.	0.359	0.874	0.573
17	3GB2	1.053	0.520	n.f.	0.603	n.f.	0.405	0.968	0.595
18	3PUP	1.065	0.475	0.820	0.787	0.574	0.560	0.904	n.f.
19	3ZRM	1.026	0.454	0.696, 0.686 0.537	0.596	n.f.	n.f.	0.986	0.598
20	4ACD	1.038	0.624	0.590	0.696	0.601	n.f.	0.983	n.f.
21	4J1R	0.933	0.566	0.854	0.579	n.f.	0.509	0.982	0.617
22	4J71	1.057	n.f.	0.543	0.637	0.691	n.f.	1.031	0.598
23	4NM0	0.982	n.f.	0.928, 0.496	0.715	0.650	n.f.	0.728, 0.510	0.728
24	4NU1	1.083	0.882	0.857, 0.469, 0.561	0.703	0.573	0.499	0.730	0.731
Dscore > 0.98 (druggable)		20	00	00	00	00	00	06	00
Dscore (0.83 – 0.98) (difficult)		04	01	06	03	00	00	15	00
Dscore < 0.83 (undruggable)		00	18	27	21	14	16	05	17

Table 4.3 SiteMap property values of pocket 7 (Allosteric site) of GSK-3 β

Sr. No.	PDB ID	Size	Volume	Exposure	Enclosure	Contact	Phobic*	Philic*	Balance	Donor/acceptor ratio
1	1GNG	111	312.816	0.671	0.643	0.799	0.280	1.079	0.260	1.154
2	1H8F	94	284.690	0.717	0.637	0.808	0.286	1.076	0.265	1.034
3	1I09	50	143.717	0.717	0.621	0.859	0.179	1.154	0.155	0.771
		33	128.968	0.783	0.652	0.810	0.338	0.953	0.355	1.185
4	1O9U	105	320.362	0.693	0.643	0.803	0.359	1.017	0.353	1.093
5	1PYX	91	279.888	0.709	0.638	0.812	0.353	0.001	0.353	0.969
6	1Q3D	95	277.830	0.716	0.633	0.824	0.252	1.052	0.240	1.123
7	1Q3W	92	260.337	0.690	0.655	0.880	0.395	1.026	0.385	0.922
8	1Q41	119	298.753	0.654	0.630	0.820	0.377	0.978	0.386	0.835
9	1Q4L	84	290.864	0.728	0.631	0.823	0.443	0.951	0.466	1.069
10	1Q5K	86	290.178	0.730	0.643	0.798	0.410	1.021	0.402	1.220
11	1R0E	97	300.468	0.731	0.634	0.819	0.327	1.071	0.305	1.145
12	1UV5	111	312.473	0.683	0.658	0.875	0.131	1.222	0.108	0.780
13	2O5K	120	303.555	0.636	0.652	0.844	0.476	1.081	0.440	0.832
14	2OW3	116	319.333	0.707	0.634	0.818	0.231	1.055	0.219	1.315
15	3DU8	93	286.405	0.677	0.658	0.864	0.351	1.090	0.322	1.114
16	3F88	77	287.091	0.779	0.626	0.738	0.140	1.000	0.140	1.128
17	3GB2	97	257.250	0.709	0.626	0.805	0.347	1.022	0.340	1.191
18	3PUP	84	223.979	0.679	0.638	0.790	0.269	1.046	0.257	1.427
19	3ZRM	102	301.154	0.690	0.640	0.801	0.459	1.038	0.443	1.026
20	4ACD	108	297.038	0.667	0.641	0.828	0.424	1.047	0.405	1.122
21	4J1R	112	286.748	0.652	0.623	0.803	0.370	1.017	0.364	1.065
22	4J71	104	281.260	0.633	0.659	0.859	0.536	0.935	0.573	1.220
23	4NM0	40	133.427	0.688	0.671	0.818	0.727	0.826	0.879	1.293
		38	84.721	0.568	0.639	0.849	0.000	1.389	0.000	1.227
24	4NU1	59	186.249	0.704	0.668	0.856	0.117	1.205	0.097	0.619
Average Value		89	259.598	0.693	0.642	0.823	0.330	1.014	0.327	1.072
*Phobic and philic terms are the hydrophobic and hydrophilic scores, respectively.										

The pocket properties of site 7 were evaluated to identify plausible reasons for classification as a 'difficult pocket' as shown in table 4.3. This site was found to be relatively open to solvent with moderately high average exposure scores of 0.69 (calibrated score: ~0.49). Moreover, the site was partially buried with an average enclosure score of 0.64 (calibrated score: ~0.78; higher scores are considered better for a deeply buried pocket). The degree of contact measures the relative tightness between a ligand and the binding site. Here, the contact property displayed relatively lower scores, observed to be 0.8 compared to the standard values (calibrated score: ~1). Moreover, the donor/acceptor character of this pocket quantifies moderate hydrogen-bond possibilities between a well-structured ligand and the site. These features represent the overall characteristics of a “difficult” pocket assessed by SiteMap (Chauhan and Gajjar).

4.1.2.3 Computational Validation Generated Pockets with SiteMap

Identified pockets were validated with known co-crystal structures available at the time of study. Among them seven different cavities are supported by X-ray crystallographic studies in the Protein Data Bank (PDB) where ligands (pocket 1), peptides (pocket 2 and 3) and even heteroatoms (pocket 4, 5, 7, and 8) are known to be captured within these cavities, while pocket 6 represents an orphan site.

Pocket 1: A variety of heterocyclic ligands are known to mimic the GSK-3 β active site. To validate this site, the PDB structure of 1Q4L was selected which has an anilino-maleimide co-crystallized within GSK-3 β along with 2D-structure representation as shown in figure 4.2(A) (Bertrand et al.). A maleimide core structure attached with two aryl rings occupies the yellow hydrophobic region. The carboxylate group and one of the acyl groups of the ligand lie in the red acceptor region, while the NH group of the core maleimide structure occupies the blue donor region. The anilino group just failed to spot the donor region. Here, SiteMap accuracy is judged as the distance between the anilino group and the carbonyl oxygen atom of Val135 is 3.63 Å, which is quiet far for a strong hydrogen-bond interaction.

Pocket 2: This pocket is recognized as the substrate binding site. A pS9 auto-inhibitory peptide recognizing the substrate site is shown in figure 4.3. Key hydrogen-bond interactions are recognized with the primed phosphate groups of the peptide and a triad of three basic residues (Arg96, Arg180, and Lys205) (Eldar-Finkelman; Stamos et al.). Furthermore, the backbone of the peptide is shown to interact with the Lys94 residue of this site. These interactions confirm the binding of such peptides in this pocket.

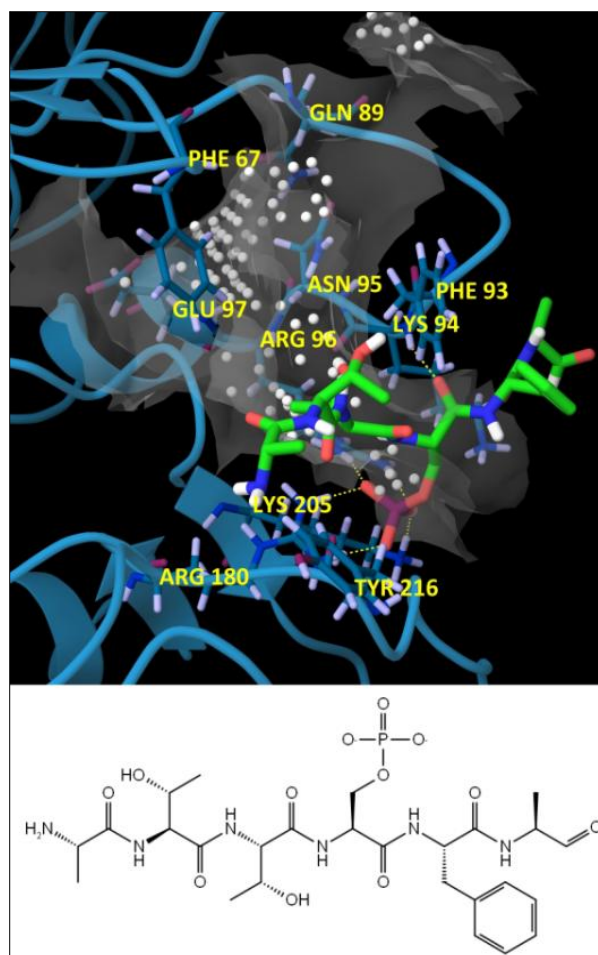


Figure 4.3 Representation of pS9 auto-inhibitory peptide in the substrate site of GSK-3 β

Pocket 3: The Axin and Fratide peptides recognize the peptide-binding channel comprising α -helix (residues 262 - 273) and the extended loop (residues 285 - 299) at the C-lobe of GSK-3 β (Bax et al.; Dajani et al.; Fraser et al.). In several cases across our dataset, two to three small cavities were observed within the entire cavity channel. Among these, a distinct “hydrophobic patch” identified by SiteMap formed with the hydrophobic residues of the α -helix, and the extended loop provides favorable peptide-binding characteristics shown in figure 4.4. Key hydrogen-bond interactions are recognized with residues Tyr288 and Glu290 and the Fratide peptide (PDB ID: 1GNG) represented in figure 4.5(B). Axin peptide is shown to interact with Asp264 residue (PDB ID: 1O9U) represented in figure 4.5(A).

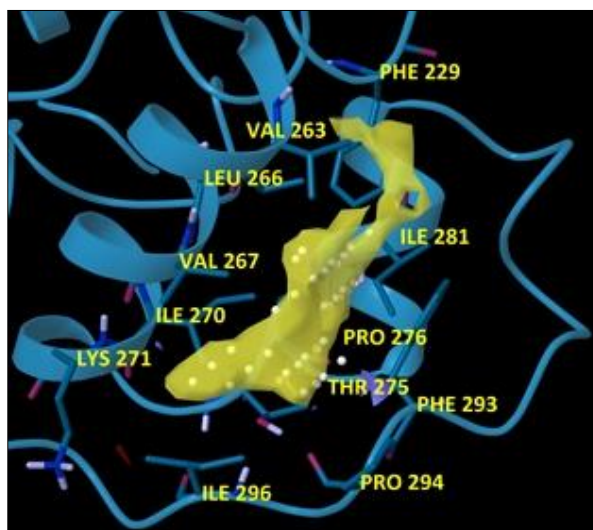


Figure 4.4 A hydrophobic patch identified by SiteMap within the peptide-binding channel of pocket 3

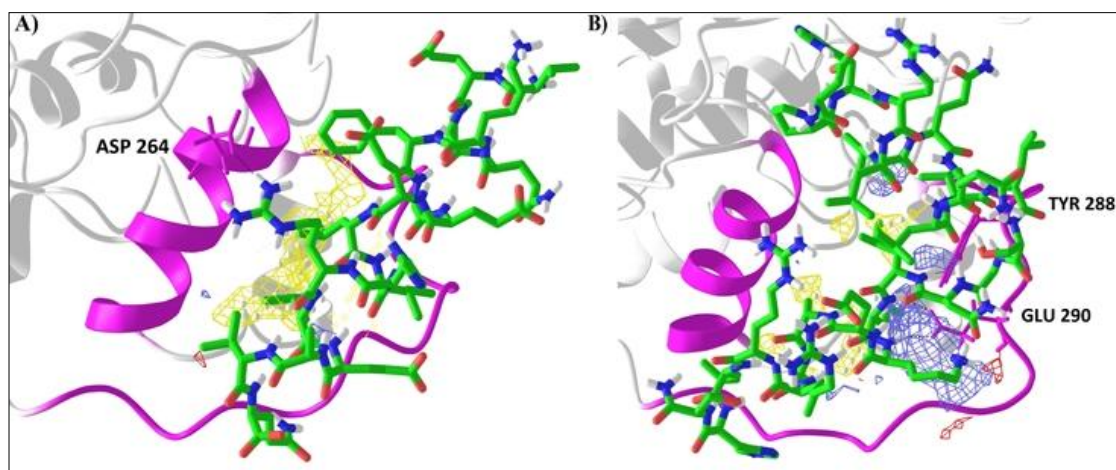


Figure 4.5 Axin (A) and Fratide (B) peptides recognize the peptide binding channel inside pocket 3 of GSK-3 β

Pocket 4: This pocket was visible in case of each PDB analyzed by SiteMap. The cavity generated by SiteMap and the presence of glycerol with a hydrogen bond to the Arg144 residue is observed in the PDB structure of 4NU1 as shown in figure 4.6. Key interactions are observed between the oxygen atom of the glycerol molecule and the guanidine NH group of Arg144.

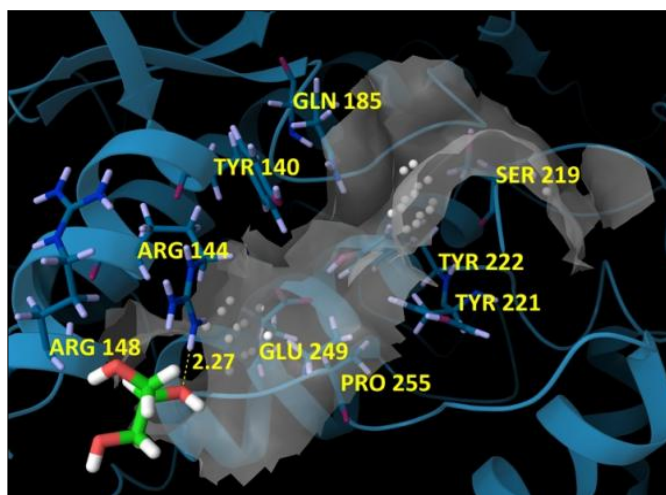


Figure 4.6 Surface view of glycerol molecule occupying pocket 4 of GSK-3 β

Pocket 5: A shallow pocket is located at the N-lobe of GSK-3 β . In the PDB structure of 4NU1, a molecule of glycerol is shown to bind to this pocket. The polar and charged residues (Tyr56, Lys86, and Asn129) surrounding the small cavity are significant enough to form hydrogen-bond contacts with small hydrophilic glycerol molecules, as shown in figure 4.7.

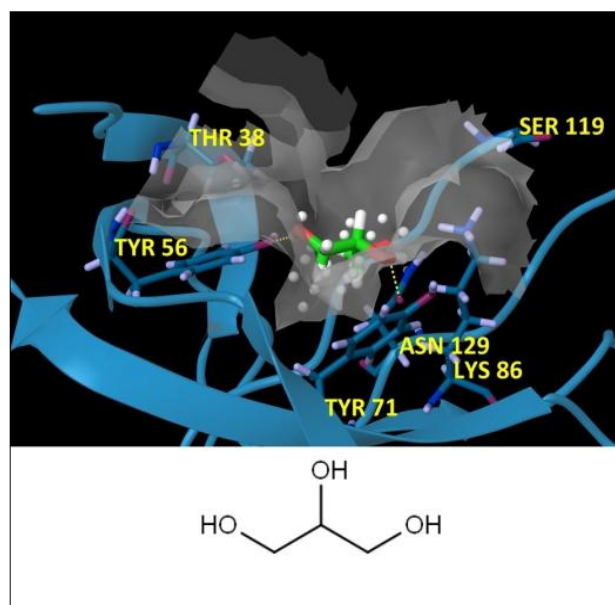


Figure 4.7 Surface view of glycerol molecule occupying pocket 5 of GSK-3 β

Pocket 6: The major residues covering a small cavity in the hinge domain was identified as pocket 6 as shown in figure 4.8. No ligands or heteroatoms are known to bind in this pocket, which represents an orphan site.

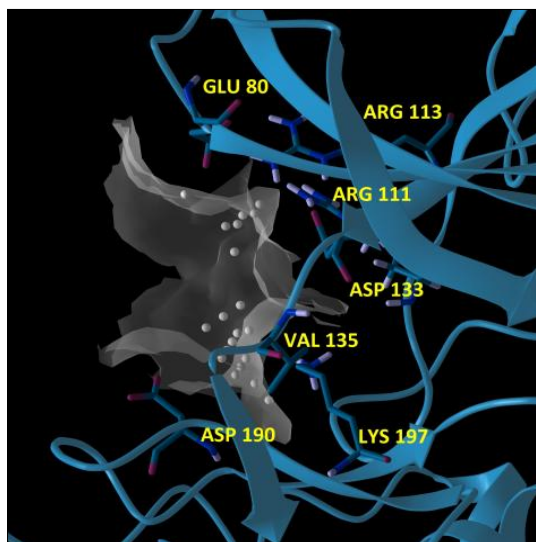


Figure 4.8 The total surface of pocket 6 represented as gray and the site points as white spheres (PDB ID: 1O9U, blue cartoon representation)

Pocket 7: SiteMap scores recognize pocket 7 as a promising allosteric site of GSK-3 β . To support validation results, the PDB structure of 4NM0 was selected, which has Dithiothreitol (DTT) molecule crystallized with GSK-3 β (Stamos et al.). Key hydrogen-bond interaction is recognized between the DTT molecule and residues Thr326, Ala327, and Arg319 of pocket 7, as shown in figure 4.9. In addition, the binding residues Arg209 and His173 of the same pocket in the PDB structures 1UV5, 1I09, and 1GNG also chelate phosphate and sulfate ions present in the crystallization experiments. These interactions are crucial for understanding the important residues for allosteric modulation of the kinase.

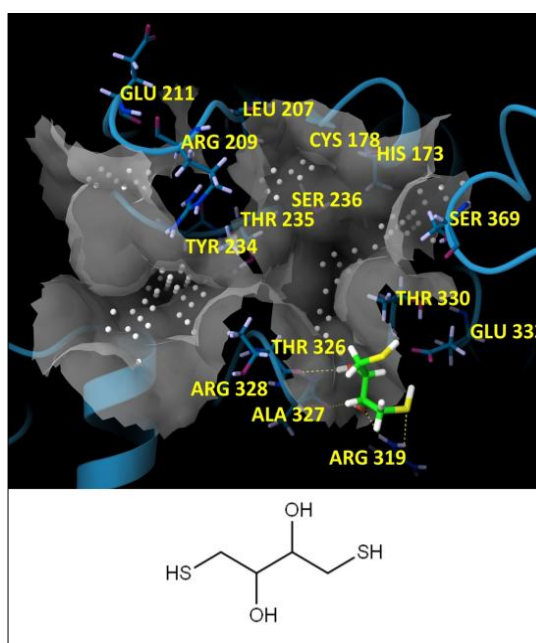


Figure 4.9 Surface view of DTT (Dithiothreitol) molecule occupying pocket 7 of GSK-3 β

Pocket 8: A new small pocket identified by SiteMap is located at the C-lobe of GSK-3 β . The presence of glycerol with a hydrogen-bond to Val155 is observed in the PDB structures of 3ZRM as shown in figure 4.10. The presence of such hydrophilic molecules can provide clues for the prevalence of these pockets on the surface of GSK-3 β .

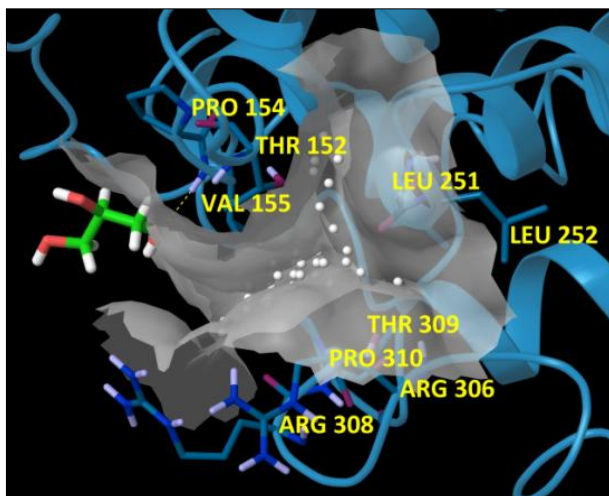


Figure 4.10 Surface view of glycerol molecule occupying pocket 8 of GSK-3 β

Reprinted from *Acta Pharmaceutica Scientia* [Chauhan and Gajjar, “Classifying Druggability on Potential Binding Sites of Glycogen Synthase Kinase-3 β : An in-Silico Assessment.” *Acta Pharmaceutica Scientia*, vol. 55, no. 3, 2017, pp. 43–60] with permission from publisher (Figure 4.1 to 4.10 and Table 4.1 to 4.3).

4.1.3 Summary of SiteMap Analysis

SiteMap evaluates binding site characteristics by assessing SiteScore and Druggability score. A data set of 24 PDB cases were analyzed with an average of eight identified pockets on the surface of GSK-3 β . The SiteScore data was initially analyzed to identify plausible ligand-binding characteristics of a site (Halgren TA). Considering the cut-off scores (SScore \geq 0.80) assigned by the developers of SiteMap, the ATP-binding site (pocket 1) and the allosteric site (pocket 7) showed promising ligand-binding characteristics.

In addition, the druggability of each site of GSK-3 β was assessed with Druggability score (Dscore). Considering the Dscore criteria, binding sites of a protein can be classified into “druggable (Dscore $>$ 0.98),” “undruggable (Dscore $<$ 0.83),” and “medium druggable/difficult (Dscore between 0.83 to 0.98)” sites (Halgren T). Among the 24 PDB cases analyzed by SiteMap, pocket 1 was found to be the highest predicted druggable site with median Dscore values higher than 0.98 with 20 PDB cases, while pocket 7 was predicted a “difficult site” with the highest predicted Dscore values between 0.83 to 0.98 in 15 PDB

cases. Moreover, all other pockets, in most cases, failed the druggability criteria of SiteMap. Pocket 1 proved to be a druggable site and pocket 7 just failed to qualify the druggability criteria.

The pocket properties of site 7 were further evaluated to identify plausible reasons for classification as a 'difficult pocket'. Some of the key features which represent the overall characteristics of site 7 as a "difficult" pocket resulted due to high average exposure scores of 0.69 (calibrated score: ~0.49). This indicates that the site is more open to solvent. Relatively low average enclosure score of 0.64 (calibrated score: ~0.78; higher scores are considered better for a deeply buried pocket) and the contact property displayed relatively lower scores, observed to be 0.8 compared to the standard values (calibrated score: ~1). The contact property is a useful indication for the measure of relative tightness between a ligand and the binding site.

Palomo et al. in a previous study explored seven conserved binding sites on the surface of GSK-3 β using Fpocket software (<http://fpocket.sourceforge.net>). Fpocket is a geometry-based algorithm that relies on the concept of alpha spheres. An alpha sphere is a sphere that contacts four atoms on its boundary and contains no internal atom. For a protein, very small spheres are located within the protein, large spheres at the exterior, and clefts and cavities correspond to spheres of intermediate radii. Thus, it is possible to filter the ensemble of alpha spheres defined from the atoms of a protein according to some minimal and maximal radii values in order to address pocket detection. Here the druggability score is detected by an empirical model that is trained on the basis of known druggable and non-druggable protein sites (Guilloux et al; Schmidtke and Barril). This method is fast and useful in situations where high throughput is desired, but precision may be compromised.

In the present work, SiteMap software tool was used for the prediction of binding sites and their druggability assessment. Moreover, the maps explicitly indicate the shape and suggest the extent of the regions considered as hydrophobic and hydrophilic of a pocket. To assess druggability, a model for predicting the maximal affinity attainable for a given target was trained by known druggability data sets. In this approach the maximal achievable binding energy is modeled and the “undruggable” targets are those that have the poorest predicted maximal affinity (Halgren T). This method is computationally intensive as energy-based calculations are involved but at the same time it has better precision both in terms of site detection as well as druggability prediction.

4.2 *In-Silico* Fragment-Based Approach and Molecular Docking

The present study was focused on *in-silico* design of new chemical series of GSK-3 β inhibitor hits from a fragment-like database of compounds via molecular docking approach. Fragment based approach can be used either as a starting point for "growing" a lead candidate or to identify potential "hits" by docking small molecule fragments into the protein binding sites (Hajduk and Greer; Hao et al.). This study was performed using a diverse set of low molecular weight compounds from the fragment-like subset of ZINC database (Irwin and Shoichet).

4.2.1 Material and Methods

All computational studies were carried out using Schrödinger suite, version 9.3.5 on windows Dell workstation.

4.2.1.1 Database Preparation

A subset of fragment-like compounds was prepared using LigPrep module of Schrödinger Suite. LigPrep produces low energy, 3D conformation structures with correct chiralities for each input structures. The ionization state of each ligand was generated using Epik at a default pH of 7.0 ± 2.0 (considered general pH for biological systems). OPLS 2005 force field was selected for energy minimization. The resulting structures were saved in maestro file format.

4.2.1.2 Molecular Docking

The program GLIDE (version 5.8) from Schrödinger Suite, was used to dock the fragment database into the allosteric pocket 7 of GSK-3 β . This program is designed to search for favourable interactions between ligand molecules and a receptor of protein structure. In GLIDE, docking calculations were performed with the extra precision (XP) mode, which is a refinement tool designed for use only on good ligand poses. GLIDE sorts its results using an empirical scoring function which considers Emodel scores to pick the best pose of a ligand and then ranks the best poses against each other. Molecular docking jobs in GLIDE can be performed by the following steps: (i) Ligand preparation, (ii) Protein preparation, (iii) receptor grid generation, and (iv) GLIDE docking.

The GSK-3 β crystal structure of 1PYX was selected as a model of receptor because it was proved to be one of the best crystal structures for docking studies with the allosteric site (Palomo et al.). Initially, the original ligand of 1PYX (phosphoaminophosphonic acid-adenylate ester) was omitted and the complex was refined with the protein preparation Wizard

in the Maestro program using the default option. Finally, a restrained minimization step with OPLS 2005 (Optimized Potential for Liquid Simulations) force field was performed. A detailed description of the protein preparation is already described in section 4.1.1.1. Binding site identification of 1PYX structure was performed on SiteMap. With this structure, six sites were identified, of which, ATP-binding site (pocket 1) scored the top rank with a druggability score (Dscore) value of 0.987 and the allosteric site (pocket 7) ranked the second best site with a Dscore value of 0.953, as reported in table 4.2.

Till date, crystallographic studies have not been published in the literature for the allosteric pocket 7 of GSK-3 β . Palomo et al. reported a hypothetical binding mode of compound V.P 0.7 with allosteric pocket 7 of GSK-3 β . Therefore, the GLIDE docking protocol was validated using V.P 0.7 structure. In GLIDE, the receptor grid generation panel is used to specify a receptor structure in a protein. The grid was generated for this pocket by keeping the default parameters of Van der Waals scaling factor 1.00 and partial charge cut off value as 0.25. Docking results displayed hydrogen bond interactions with Ser236 and Leu207. Moreover, the polar head of compound V.P 0.7 was sandwiched between Arg209 and Thr235 residues represented in figure 4.11. These results suggest that the docking protocol used in the present study was in perfect agreement with the hypothetical binding mode of compound V.P 0.7 previously reported in the literature.

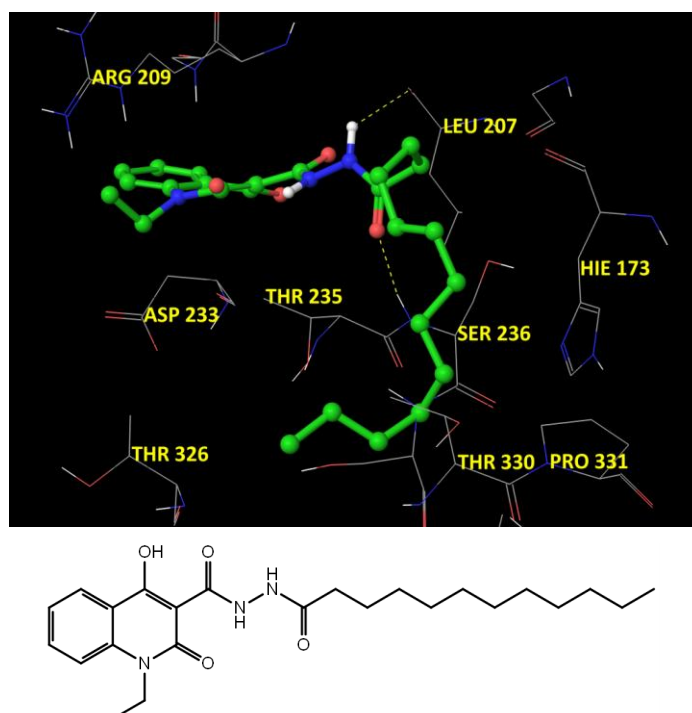


Figure 4.11 Validation of pocket 7 with V.P 0.7 structure represented as green ball and stick model. H-bonds are labelled as yellow dotted lines (PDB ID: 1PYX)

4.2.2 Results and Discussion

4.2.2.1 Identification of New Chemical Series of N^{1,3}-disubstituted imidazolidin-2-one

In docking computations, a small scaffold, 1,3-dimethylbenzimidazol-2-one (ZINC00073681) was identified through fragment-like subset of ZINC database with an XP GLIDE score of -2.6 kcal/mol. A hydrogen bond is established between the oxygen of the benzimidazole scaffold and the NH group of Thr235 residue in the allosteric pocket 7 of GSK-3 β (Figure 4.12).

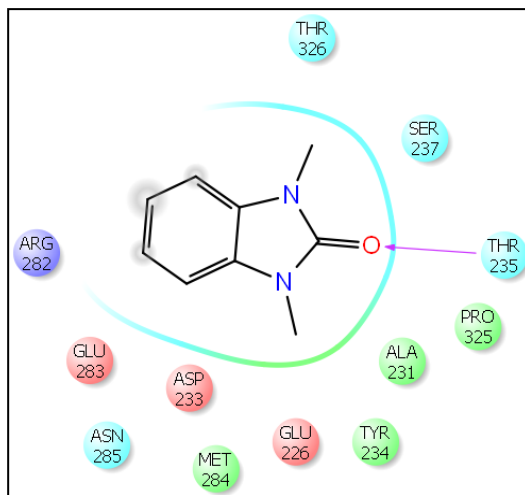


Figure 4.12 LigPlot view of the docked complex 1,3-dimethylbenzimidazol-2-one in the allosteric pocket 7 of GSK-3 β (PDB ID: 1PYX)

In the next stage, Tideglusib side chains were detached and merged with 1,3-dimethylbenzimidazol-2-one scaffold. Additionally, a new benzothiazinone scaffold BTO-jb was reported as non-ATP competitive GSK-3 β inhibitor, which was proposed to bind at allosteric site 7 of GSK-3 β (Zhang et al.). Tideglusib is a non-ATP competitive, irreversible GSK-3 β inhibitor which actually binds to site 1 by forming an electrostatic interaction with Cys199 at the ATP-binding site (Domínguez et al.). The molecules Tideglusib and BTO-jb were proposed to bind at different sites of GSK-3 β i.e. site 1 and 7 respectively in spite of the similarity in the side chains (chapter 3; section 3.1.1.5; figure 3.6). Here, the side chains of BTO-jb were utilized for the design of the proposed compounds. Figure 4.15, illustrates the design strategy using similarity in side chain structural features of BTO-jb and Tideglusib. The optimized structure shown in figure 4.13 (A) was re-docked in the same receptor site and resulted with an improved XP GLIDE score of -3.8 kcal/mol, compared to the previous GLIDE score of -2.9 kcal/mol. A high exposure penalty score of 0.8 was observed as shown in figure 4.13 (B). This penalty score in GLIDE XP indicated that the docked ligand was highly solvent exposed.

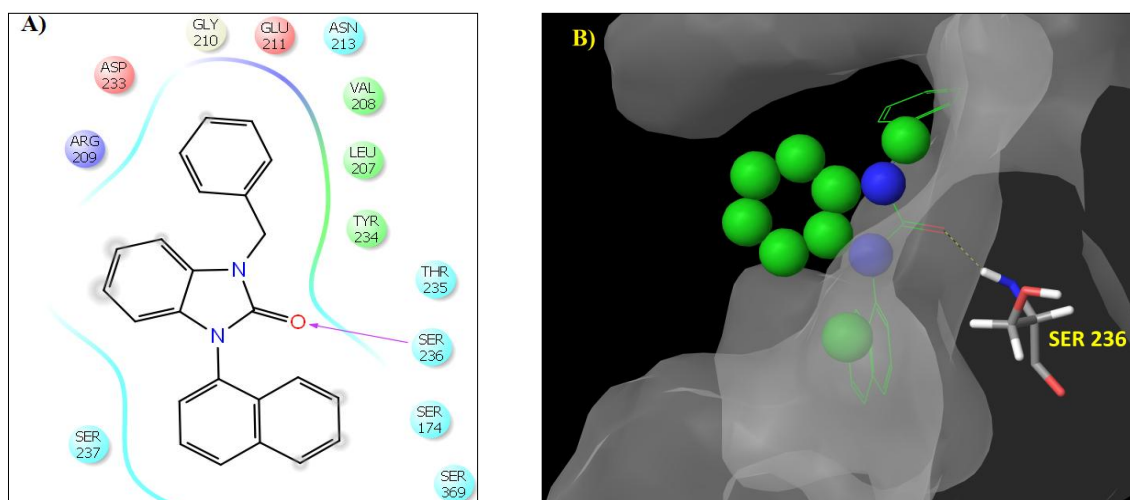


Figure 4.13 A) LigPlot view of 1-benzyl-3-(naphthalen-1-yl)benzimidazol-2-one docked complex in the allosteric pocket 7 of GSK-3 β . B) Solvent exposed region of 1-benzyl-3-(naphthalen-1-yl)benzimidazol-2-one represented as spherical shape

An improved XP GLIDE score of -4.7 kcal/mol was obtained by detaching the solvent exposed part of the benzimidazole core structure of 1-benzyl-3-(naphthalen-1-yl)benzimidazol-2-one structure. The new designed template, 1-benzyl-3-(naphthalen-1-yl)imidazolidin-2-one resulted with reduced exposure penalty score to 0.2 as shown in figure 4.14 (A) and 4.14 (B). Interestingly, a virtual library with all types of substitutions i.e. electron withdrawing, electron donating and also the substituents with hydrogen bonding potentials (H-bond acceptor and H-bond donor containing groups) were designed on both side chains of the newly designed template. Twenty one target compounds with relatively better GLIDE XP score were shortlisted for synthesis and biological evaluation.

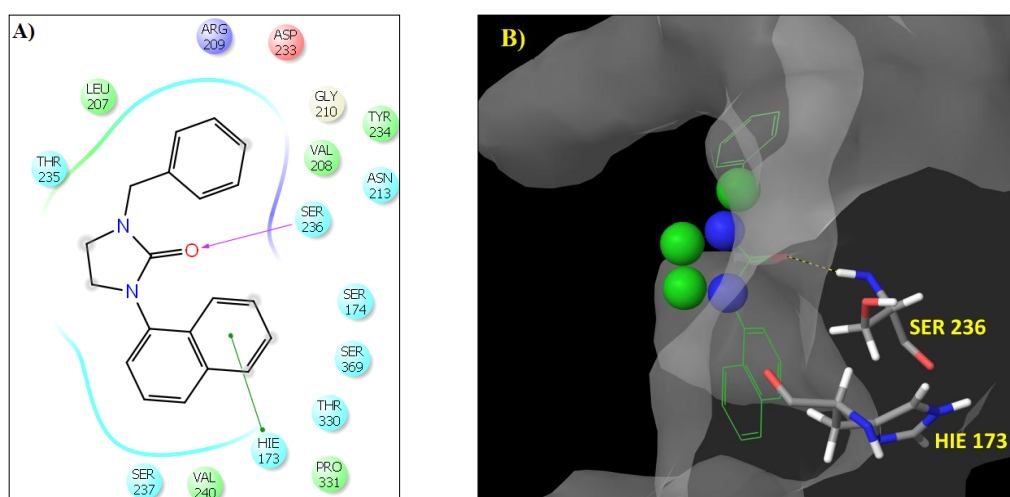


Figure 4.14 A) LigPlot view of 1-benzyl-3-(naphthalen-1-yl)imidazolidin-2-one docked complex in the allosteric pocket 7 of GSK-3 β . B) Solvent exposed region of 1-benzyl-3-(naphthalen-1-yl)imidazolidin-2-one represented as spherical shape

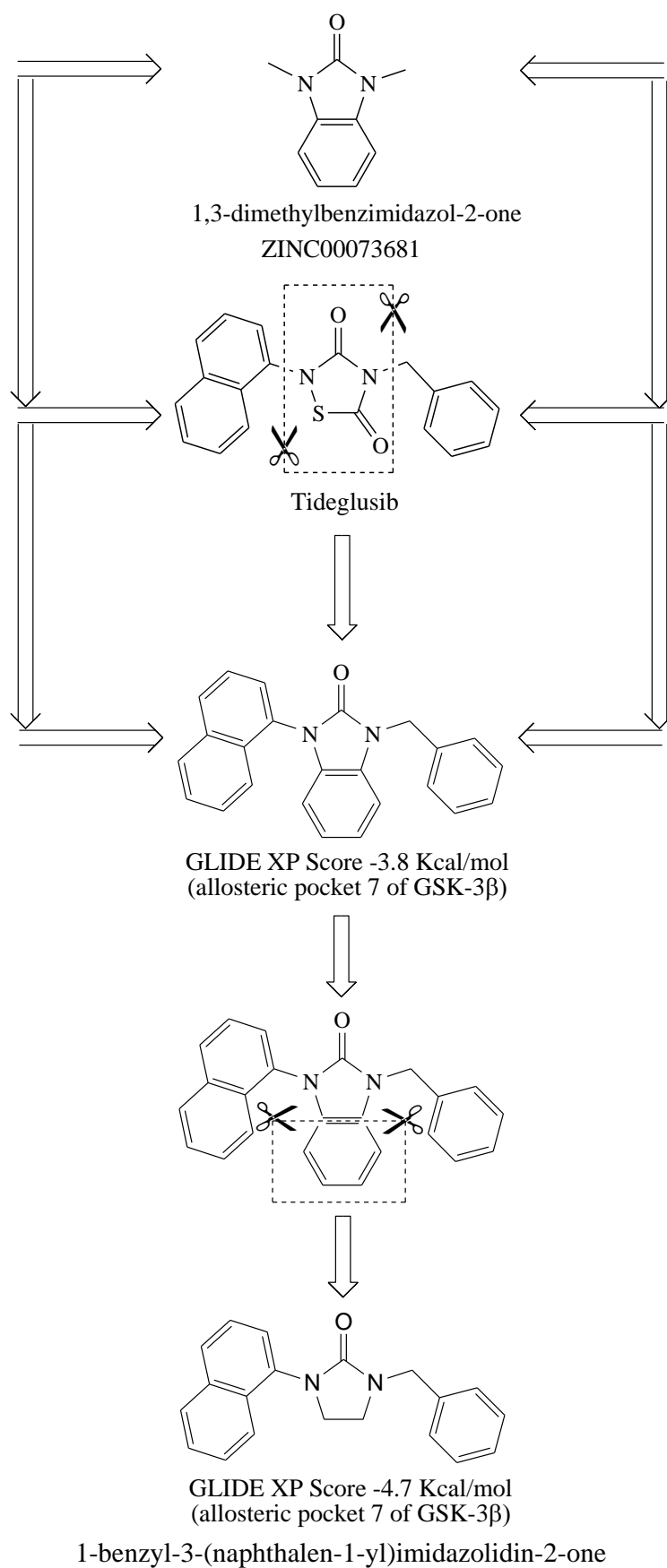


Figure 4.15 Schematic diagram of designed template by *in-silico* fragment-based and molecular docking approach

Table 4.4 Representative structures of N^{1,3}-disubstituted imidazolidin-2-one

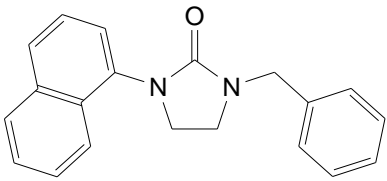
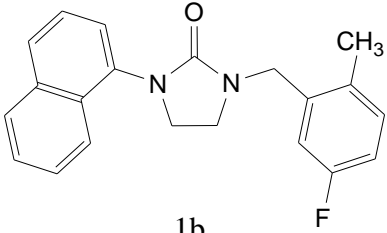
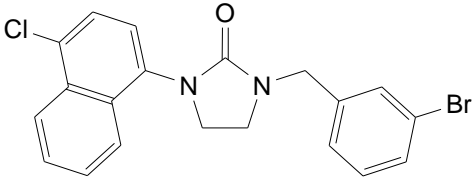
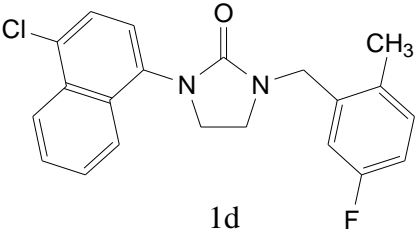
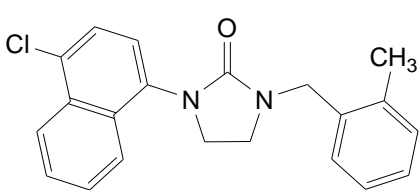
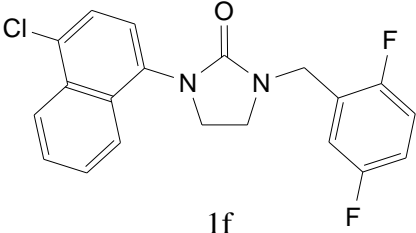
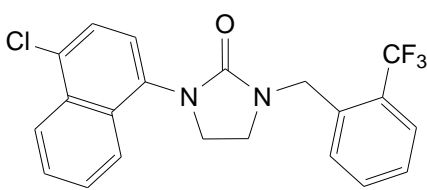
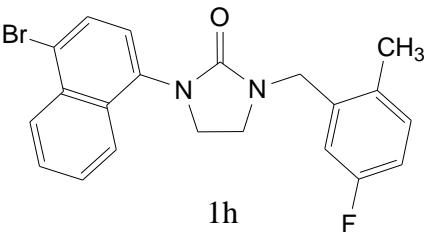
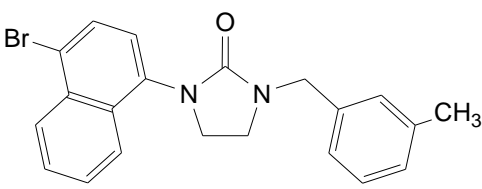
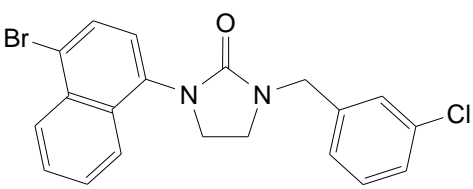
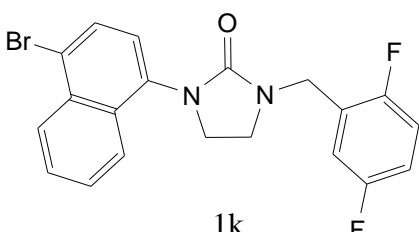
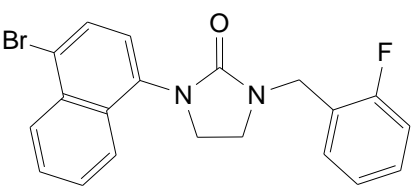
 <p>1a</p>	 <p>1b</p>
 <p>1c</p>	 <p>1d</p>
 <p>1e</p>	 <p>1f</p>
 <p>1g</p>	 <p>1h</p>
 <p>1i</p>	 <p>1j</p>
 <p>1k</p>	 <p>1l</p>

Table 4.4 Representative structures of N^{1,3}-disubstituted imidazolidin-2-one (continued)

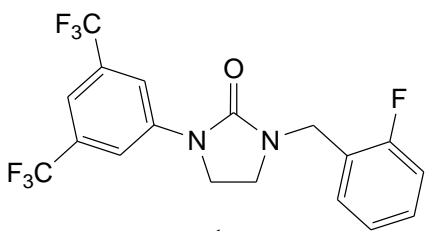
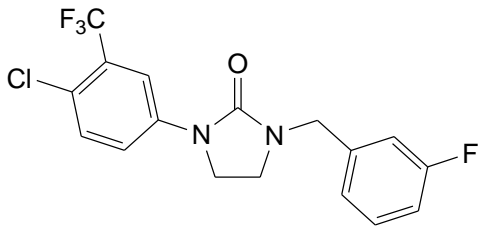
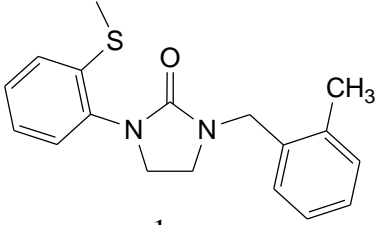
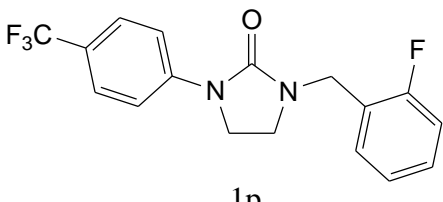
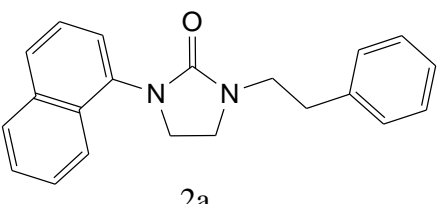
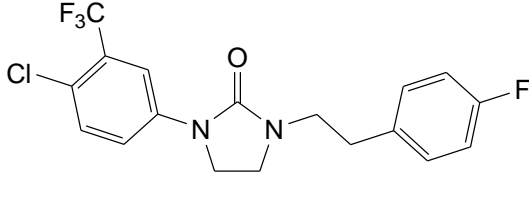
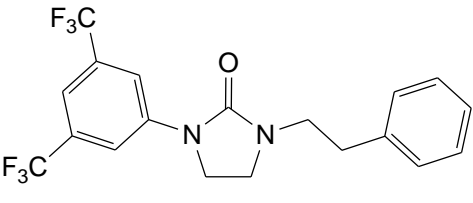
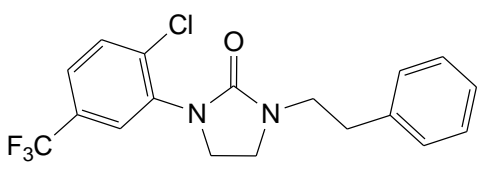
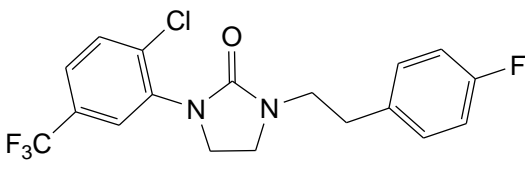
 1m	 1n
 1o	 1p
 2a	 2b
 2c	 2d
 2e	

Table 4.5 Docking results of N^{1,3}-disubstituted imidazolidin-2-one designed compounds in the allosteric pocket 7 of GSK-3 β (PDB ID: 1PYX)

Sr. No.	Compound Code	GLIDE XP Score (kcal/mol)	Interactions		
			H-bond	H-bond distance (Å)	pi-stacking [#]
1	1a	-4.5	SER236	2.08	HIE173
2	1b	-5.1	SER236	2.10	HIE173
3	1c	-4.5	SER236	2.08	HIE173
4	1d	-3.8	SER236	2.80	-
5	1e	-4.5	SER236	2.42	HIE173
6	1f	-4.8	SER236	2.13	-
7	1g	-4.8	SER236	2.38	HIE173
8	1h	-5.1	SER236	2.19	HIE173
9	1i*	-5.6	SER236	2.08	HIE173
10	1j	-4.9	SER236	2.14	-
11	1k	-4.4	SER236	2.27	-
12	1l	-4.8	SER236	1.93	-
13	1m	-3.3	SER236	1.98	-
14	1n	-4.8	SER236	2.00	-
15	1o	-4.2	SER236	2.02	HIE173
16	1p	-4.6	SER236	2.04	-
17	2a	-5.1	SER236	2.01	-
18	2b	-4.0	SER236	2.02	-
19	2c	-5.1	SER236	1.92	HIE173
20	2d	-3.9	SER236	2.07	-
21	2e	-4.8	SER236	2.09	-
*Compound 1i was predicted with highest XP GLIDE score of -5.6 kcal/mol. [#] pi-stacking interactions refer to attractive, non-covalent interactions between aromatic rings. Histidine is explicitly labeled as HIE when the side chains carry a flip label during protein preparation Wizard in Maestro program of Schrödinger Suite.					

Table 4.5 depicts the GLIDE scores, hydrogen-bond interactions and interacting amino acids residues formed with N^{1,3}-disubstituted imidazolidin-2-one compounds. These compounds displayed hydrogen-bond interactions with Ser236 residue in the allosteric pocket 7 with a distance less than 2.5 Å, except compound 1d ($d = 2.80$ Å). In addition, few compounds displayed pi-staking interactions between the aromatic rings of molecules and His173 residue. Figure 4.16 represents docked conformation of 21 designed N^{1,3}-disubstituted imidazolidin-2-one compounds in the allosteric pocket 7 of GSK-3 β .

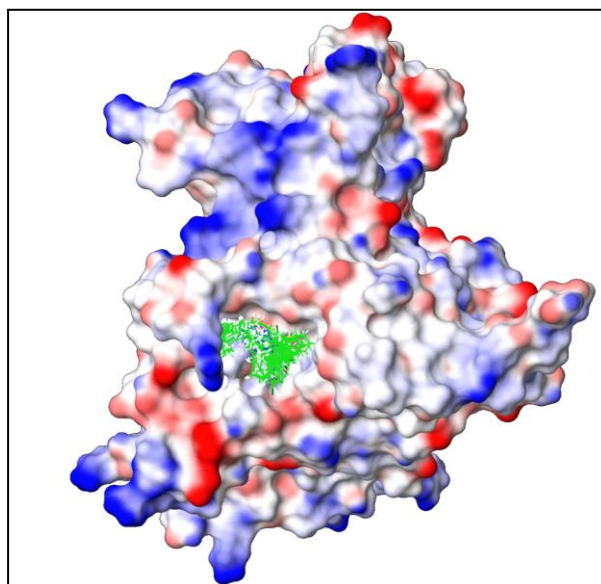


Figure 4.16 Docked conformation of 21 designed $N^{1,3}$ -disubstituted imidazolidin-2-one compounds in the allosteric pocket 7 GSK-3 β (PDB ID: 1PYX)

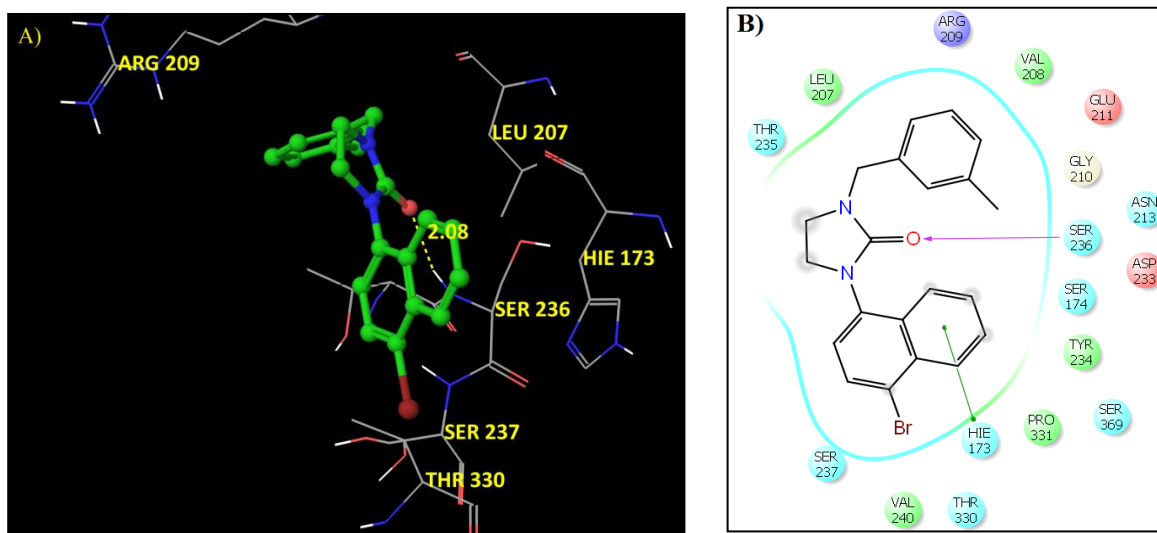


Figure 4.17 Docked conformation of compound 1i in the allosteric pocket 7 of GSK-3 β . A) H-bond interaction is represented as dotted lines and the ligand as ball and stick model. B) LigPlot view of the docked compound 1i in the allosteric pocket 7 of GSK-3 β

In the resulting docked complex of compound 1i, a hydrogen-bond is formed between the oxygen atom of a ligand and NH group of Ser236 residue shown in figure 4.17 (A). Figure 4.17 (B) represents LigPlot view of the docked complex and a pi-stacking interaction with His173. Furthermore, a hydrogen bond is established for compound 1n ($d = 2.07$ Å) and 2d ($d = 2.00$ Å) with Ser236 residue as represented in figure 4.18 and 4.19. These interactions

provide clues for binding of N^{1,3}-disubstituted imidazolidin-2-one compounds in the allosteric pocket 7 of GSK-3 β .

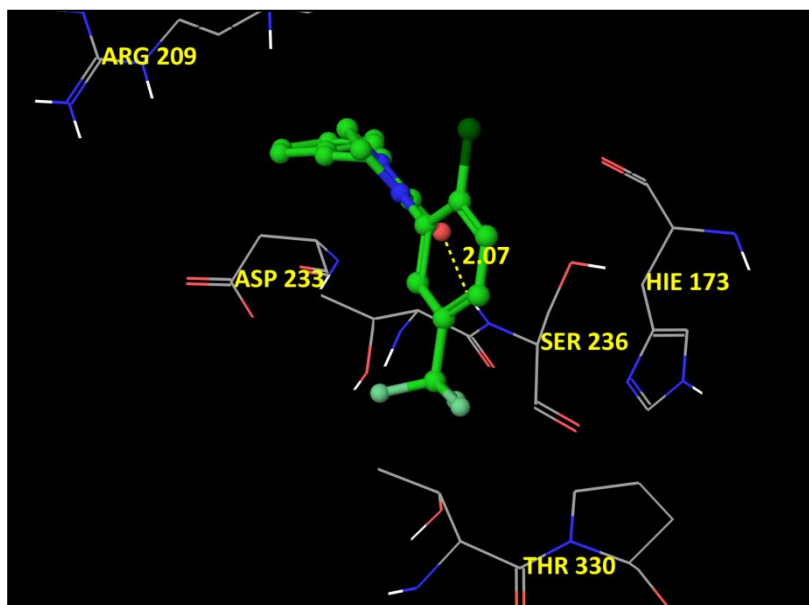


Figure 4.18 Docked conformation of compound 1n in the allosteric pocket 7 of GSK-3 β

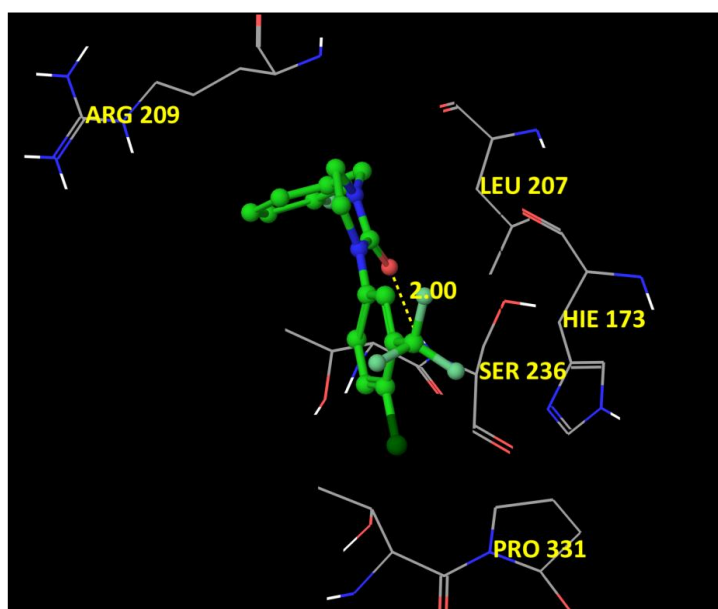


Figure 4.19 Docked conformation of compound 2d in the allosteric pocket 7 of GSK-3 β

4.2.2.2 Prediction of Physicochemical Properties of N^{1,3}-disubstituted imidazolidin-2-one Compounds

The QikProp version 3.5, available in Maestro program of Schrödinger Suite was used to predict a range of physicochemical properties of 21 designed target compounds. The following properties were computed as listed in table 4.6.

Table 4.6 Predicted physicochemical properties of N^{1,3}-disubstituted imidazolidin-2-one compounds using QikProp[#]

Sr. No	Compound Code	Molecular Weight	QPlogPo/w Predicted octanol/water partition coefficient	PSA (Polar Surface Area)	Predicted Aqueous Solubility (QPlogS)	Lipinski Violations (Rule of Five)
1	1a	302.375	5.267	27.752	-5.795	1
2	1b	334.392	5.731	27.193	-6.291	1
3	1c	415.716	6.323	29.293	-7.400	1
4	1d	368.837	6.175	27.189	-6.947	1
5	1e	350.847	5.940	27.203	-6.598	1
6	1f	372.801	6.112	28.023	-6.998	1
7	1g	404.818	6.358	25.748	-7.044	1
8	1h	413.288	6.247	27.189	-7.047	1
9	1i	395.298	6.154	29.346	-7.270	1
10	1j	415.716	6.322	29.323	-7.366	1
11	1k	417.252	6.183	28.024	-7.076	1
12	1l	399.262	5.969	27.542	-6.843	1
13	1m	406.302	6.493	30.071	-7.757	1
14	1n	372.749	5.973	29.615	-7.108	1
15	1o	312.429	5.162	29.171	-5.914	1
16	1p	338.304	5.471	30.093	-6.362	1
17	2a	316.402	5.656	29.027	-6.429	1
18	2b	386.776	6.388	30.751	-7.646	1
19	2c	402.339	6.770	30.747	-8.203	1
20	2d	368.785	6.243	30.866	-7.348	1
21	2e	386.776	6.483	30.866	-7.725	1

[#]QikProp recommended range: molecular weight < 500 daltons; predicted octanol-water partition coefficient (QPlogPo/w) -2.0 to 6.5; polar surface area (PSA) 7.0 to 200.0 Å², predicted aqueous solubility (QPlogS, S in mol dm⁻³) -6.5 to 0.5; Lipinski violations (rule of five) maximum value 4.

QikProp is a fast and accurate physicochemical and ADME (absorption, distribution, metabolism, and excretion) prediction program designed by Professor William L. Jorgensen. (Jorgensen and Duffy). The theoretical predictive power of the QikProp software was tested by comparing properties of molecule's with those of 95 % known drugs. The development of QikProp involved ~710 drugs and drug-like compounds (Schrödinger, LLC). Ioakimidis et al. published data on reliability of Qikprop software with a correlation between experimental data of physicochemical properties from the literature and predicted values. The developers of QikProp state that 95 % of assessed drugs and drug-like collection for prediction of octanol-water partition (QPlogPo/w), is in the range of -2.0 to 6.5, and prediction of aqueous solubility (QPlogS) is between -6.5 to 0.5. Ioakimidis and colleagues, analyzed octanol-water partition results with 476 orally administered marketed drug compounds; 93.9 % cases were within these limits, supporting their observations. In other cases for prediction of aqueous solubility, with 289 neutral organic molecules; 87.3 % cases were within these limits.

QikProp version 3.5, evaluates a total of 46 molecular and biological properties. For the target compounds, the octanol-water partition coefficient (QPlogPo/w) and aqueous solubility (QPlogS), known to be critical parameters for estimation of absorption and distribution of drugs within the body, were predicted in the range 5.162 to 6.493 and -5.795 to -7.757, respectively. In QikProp, a higher positive value of octanol-water partition coefficient indicates that the designed compounds are predicted with high lipophilicity. With few compounds, a slightly higher range was observed with predicted aqueous solubility (for compounds with value greater than -6.5) indicating poor aqueous solubility. According to Lipinski's "rule of five", compounds are considered "drug like" if their molecular weight is < 500 daltons, log P values < 5, H-bond donors ≤ 5 and H-bond acceptors ≤ 10 (Lipinski et al.). The designed target compounds obey the Lipinski's "rule of five". However, predicted octanol-water partition coefficient of all target compounds are above the permissible limits in Lipinski's rule of five. Polar Surface Area (PSA) is the sum of surface contributions of polar atoms (usually oxygen, nitrogen and attached hydrogens) in a molecule and has been shown to correlate well with drug transport properties, such as intestinal absorption, or blood-brain barrier penetration (Clark). All target compounds were predicted in the range 27.193 to 30.866 Å², and are within the permissible QikProp recommendations.

4.2.3 Summary of *In-Silico* Fragment-Based Approach and Molecular Docking

The design strategy of GSK-3 β inhibitor hits was performed by combined applicability of *in-silico* fragment-based and molecular docking approach. This study was performed by docking a diverse set of fragment-like subset of ZINC database in the allosteric pocket 7 of GSK-3 β . In docking computations, a small scaffold, 1,3-dimethylbenzimidazol-2-one was identified. In the next stage, Tideglusib side chains were detached and merged with 1,3-dimethylbenzimidazol-2-one scaffold. The optimized structure of 1-benzyl-3-(naphthalen-1-yl)benzimidazol-2-one resulted in an XP GLIDE score of -3.8 kcal/mol. Furthermore, removing the solvent exposed part of the optimized structure resulted in the design of 1-benzyl-3-(naphthalen-1-yl)imidazolidin-2-one with an improved XP GLIDE score of -4.7 kcal/mol. Twenty one N^{1,3}-disubstituted imidazolidin-2-one compounds with relatively better XP GLIDE scores were shortlisted for synthesis and biological evaluation. Results of *in-silico* physicochemical prediction by QikProp were within permissible range. However, these compounds are predicted to be more lipophilic in nature and deprived aqueous solubility.

4.3 Virtual Screening

Virtual screening is one of the fastest and precise technique to obtain new hits with desired activity profile (Lionta et al.). Three separate studies were performed based on the structural features of Tideglusib molecule. The first study was based on combined shape-based similarity screening and molecular docking approach using SPECS database. The second approach was based on rescoring the top-ranked hits obtained with similarity screening and comparing electrostatic similarity of the obtained top scoring hits with Tideglusib. The third approach was based on pharmacophore feature identification of Tideglusib using ZINC database, docking and validating the obtained hits by molecular dynamics.

4.3.1 ROCS Shape Based Similarity Screening and Molecular Docking

The shape-based similarity screening was performed with ROCS version 3.1.2 (Rapid Overlay of Chemical Structures; Open Eye Scientific Software) (Muchmore et al.). This program is designed to screen large scale chemistry databases based on the 3D shape and chemical ("color") similarity.

4.3.1.1 Materials and Methods

This study was performed using Tideglusib drug as a reference compound to screen the SPECS database (<http://www.specs.net>). The ExAcD (Exciting Academic database), a subset of SPECS compound database was screened which consists of 4,60,250 diverse structures.

Database filtration was performed with FILTER 2.0.2 module in OpenEye. FILTER eliminates structures with toxic functionalities, Lipinski violations and low probability of orally bioavailable compounds. After applying FILTER, the database returned to 70,243 filtered compounds. In the present computation studies, single low-energy conformations of Tideglusib and filtered database were generated with OMEGA 2.4.6 (Optimized Ensemble Generation Application) in OpenEye, which served as an input database (.oeb.gz file format) for performing ROCS calculations. The shape based similarity scores were ranked by Tanimoto Combo score (default score) that includes both shape fit and color similarity. This score varies in the range 0 to 2; where 2 represents the exact similarity match.

The top-ranking 500 virtual hits of ROCS output file (.oeb.gz file) were converted to .sdf file format using VIDA in OpenEye. The output file was subjected to ligand preparation

using LigPrep module of Schrödinger. Molecular docking was performed with XP GLIDE as per the methodology described in section 4.2.1.2. Docking computations were performed on the substrate site (site 2) of GSK-3 β .

4.3.1.2 Results and Discussions

The initial shape-screening protocol yielded 500 top-scoring virtual hits. Compound AO-476/41610153 resulted with a Tanimoto Combo score of 1.028 (Figure 4.20). Subsequently, molecular docking was performed with 500 top scoring virtual hits.

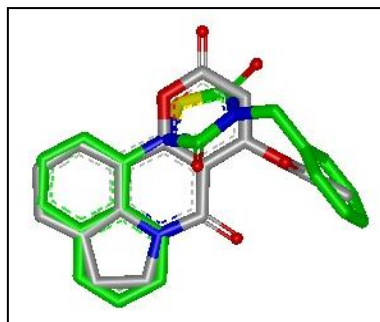


Figure 4.20 Overlay of Tideglusib reference compound (green stick representation) and SPECS database compound AO-476/41610153 (gray stick representation) with ROCS similarity screening (Chauhan N. et al.)

Molecular docking of top scoring virtual hits resulted with compound AO-476/41610153 with the highest XP Glide Score of -4.2 kcal/mol in the substrate site as shown in figure 4.21(A).

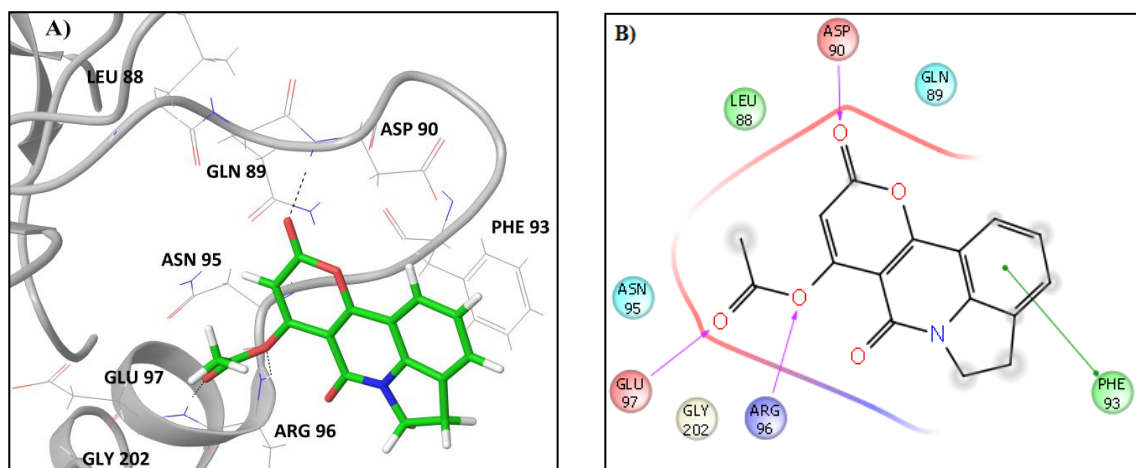


Figure 4.21 A) Docked complex of SPECS database compound [7,10-dioxo-4,5-dihydro-7H,10H-pyrano[3,2,1-*ij*]quinolin-8-yl acetate] in the substrate binding site of GSK-3 β . B) LigPlot interaction view of the SPECS database compound in the substrate binding site

Key hydrogen-bond interactions are formed between the ligand with Arg96, Glu97 and Gln89 residues and a pi-stacking interaction with Phe93 residue in the substrate site of

GSK-3 β shown in figure 4.21(B) (Chauhan N et al.) Till date, crystallographic studies have not been published on thiadiazolidinedione (TDZD) compounds; the class to which Tideglusib belongs. Martinez proposed the initial hypothesis of TDZD binding site, with the help of molecular docking and suggested that TDZD class of compounds are sandwiched between the glycine-rich loop (P-loop), the activation loop and the C-loop, which have been proposed to be the substrate binding pocket of GSK-3 β .

4.3.2 Electrostatic Similarity Search

EON is an electrostatics comparison program of Open Eye Scientific Software, a program designed to calculate electrostatic correlations of pre-aligned molecules and determines the Tanimoto measures for the comparison.

4.3.2.1 Materials and Methods

Another approach was based on rescoring the top ranked ROCS output structures with EON. The output files were clustered and ranked according to the electrostatic Tanimoto (T_e) score (Muchmore et al.).

4.3.2.2 Results and Discussions

Results of the electrostatic similarity screening with the 500 ROCS output files yielded a top scoring compound AT-057/43486355 with an electrostatic Tanimoto (T_e) score of 0.7650. Figure 4.22 shows comparative electrostatic contour maps of Tideglusib on the left, and identified hit molecule on the right along with 2D structure representation.

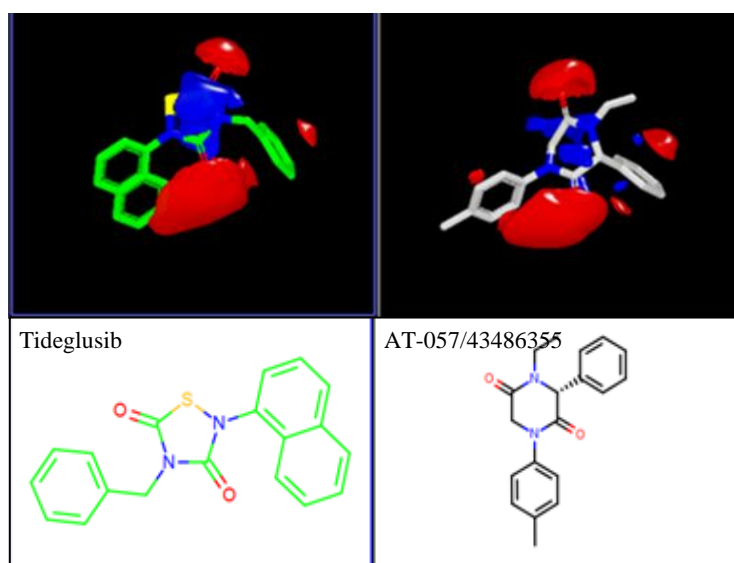


Figure 4.22 Predicted top-scoring virtual hit AT-057/43486355 of SPECS database identified by electrostatic screening. Contour maps of positive and negative charges are shown as blue and red maps respectively

4.3.3 Pharmacophore Feature-Based Virtual Screening

Identification of structurally similar compounds based on the pharmacophore features of Tideglusib was performed using the ZINCPharmer online server tool (Koes and Camacho).

4.3.3.1 Materials and Methods

Tideglusib structure was accessed in .mol2 file format from the ZINC database (ZINC13985228) and energy minimization step was performed with CHARMM force field implemented in the Accelry's discovery studio. The resultant relaxed structure was saved as .pdb file and then uploaded to the ZINCPharmer online server to identify pharmacophore features of Tideglusib. These features explored four aromatic rings with a radius of 1.10 Å, and two hydrogen-bond acceptor side chains with a radius of 0.50 Å on the core heterocyclic ring of Tideglusib represented in figure 4.23(A). The identified pharmacophore features of the query molecule (Tideglusib) were submitted to ZINCPharmer for searching structurally similar compounds with matching pharmacophore features. A total of 416 compounds out of 17,818,291 commercially available small molecules exhibited pharmacophore features similar to those of Tideglusib; the details of these 416 compounds were saved as a database of compounds in the .sdf file format for further virtual screening studies.

ArgusLab version 4.0.1 docking program was implemented for virtual screening. The GSK-3 β protein structure (PDB ID: 1PYX) and ligands were prepared for virtual screening by adding the hydrogen atoms and by removing all water molecules that were crystallized with this target protein. The addition of new hydrogen atoms ensures an accurate determination of the ionization states of amino acid residues. The energy of the protein structure was then minimized using the CHARMM (Chemistry at Harvard Macromolecular Mechanics) force field in the Discovery studio package. Additionally, the obtained 417 compounds (including Tideglusib) were prepared by first removing the hybridization errors in the molecules and then adding the missing hydrogen bonds in order to check the fidelity of all bonds in the compounds. All prepared compounds were saved in the .mol file format for further docking studies after a geometry optimization stage with the Universal Force Field (UFF).

The energy-scoring grid box was centered at the active ligand binding site location and its dimensions were set to 60 Å along each axis (x, y, and z) with a grid spacing of 0.40 Å. The grid was assigned such that the active site of GSK-3 β was enclosed by the three-dimensional grid box. Blind docking was performed which covers the total protein with the grid box instead of limiting to a particular site. “Ascore” scoring function with all docking

parameters set to the default values was selected as the docking program in ArgusLab. A total of 63 compounds exhibited better binding potentials (more negative binding energy) compared to that of Tideglusib.

The compound with the best binding energy was subjected to molecular dynamics (MD) simulation conducted for 20-ns using the Desmond module version 3.6 from Schrödinger, Inc. For a brief period, the OPLS2005 force field was used to simulate the predefined three-site transferable intermolecular potential (TIP3P) water model. An orthorhombic periodic boundary conditions solvent box buffered at a distance of 10 Å was setup to specify the shape and size of the water simulation box. Boundary conditions box volume was calculated to be 478,000 Å³. To electrically neutralize the system, appropriate counter ions such as Cl⁻ and Na⁺ were placed randomly in the solvated system.

4.3.3.2 Results and Discussions

Pharmacophore feature-based virtual screening resulted with a total of 63 compounds having better binding potentials (more negative binding energy) and were compared with that of Tideglusib using ArgusLab software. Tideglusib was docked with a resulting binding energy of -11.37 kcal/mol in the active site by forming an electrostatic interaction with Cys199 and hydrogen bonds with Met101 and Asp200, as shown in figure 4.23(B). The ZINC4192390 compound was identified to be the best binding compound, with a binding energy of -13.39 kcal/mol. This high binding energy resulted from a strong electrostatic interaction of the Cys199 and hydrogen bonds along with pi-stacking with the Val110, Leu132, and Asp200 residues, as shown in figure 4.23(C).

MD simulations were performed to confirm the binding energy and molecular level interactions determined by virtual screening. Initially, we performed individual MD simulations for GSK-3 β complexed with Tideglusib and with the best compound identified via virtual screening in this study i.e., ZINC4192390 (2-benzylindeno [1,2,3-*de*]phthalazin-3(2H)-one). Energy plots of GSK-3 β complexed with Tideglusib and with the ZINC4192390 compound for 20-ns MD simulations are shown in figure 4.23(D). An inspection of the graph clearly shows that the present virtual screening predictions are in good agreement with the results for the simulated receptor-ligand complexes. According to docking results, the GSK-3 β complexed with Tideglusib showed a binding energy of -11.37 kcal/mol whereas the GSK-3 β complexed with ZINC4192390 showed a binding energy of -13.39 kcal/mol. The energy difference shows the same trend shown by the simulated energies of -114500 kcal/mol and -149500 kcal/mol, which were observed for the total GSK-3 β and Tideglusib system (protein

+ ligand + solvated water + ions) and for the GSK-3 β and ZINC4192390 system, respectively. Therefore, it is clear that ZINC4192390 exhibits a much better binding potential for GSK-3 β compared to Tideglusib. Furthermore, this trend was confirmed when the simulated energies of the GSK-3 β protein in the presence of Tideglusib was analyzed and thereby obtained a simulated energy of -2500 kcal/mol. Following a similar procedure for the ZINC4192390 compound, the obtained average simulated energy was -4000 kcal/mol. (Chauhan et al.)

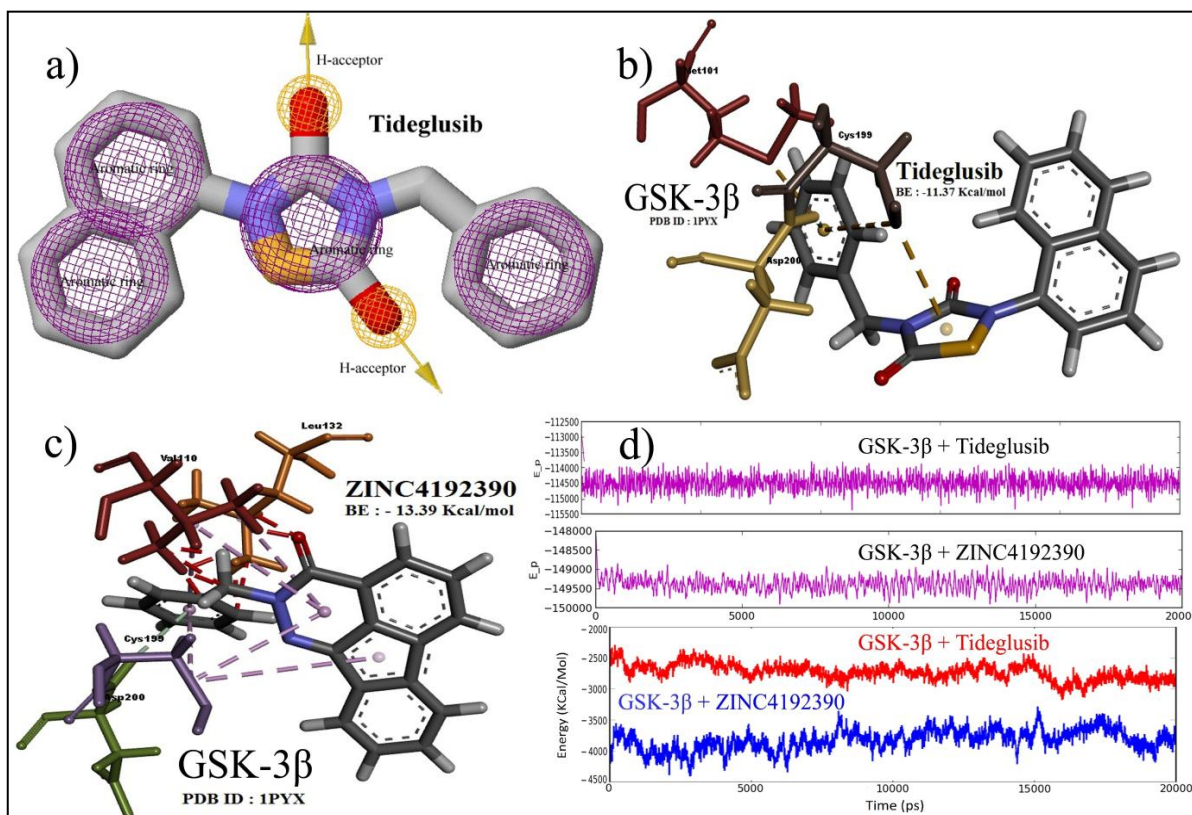


Figure 4.23 A) Pharmacophore features of Tideglusib which was used for finding structurally similar compounds for virtual screening; B) docking snapshot of Tideglusib in the active site; C) docking snapshot of ZINC4192390 compound at the active binding site of GSK-3 β ; D) MD simulation energy plots for the GSK-3 β complexed with Tideglusib and ZINC4192390 (Chauhan et al.)

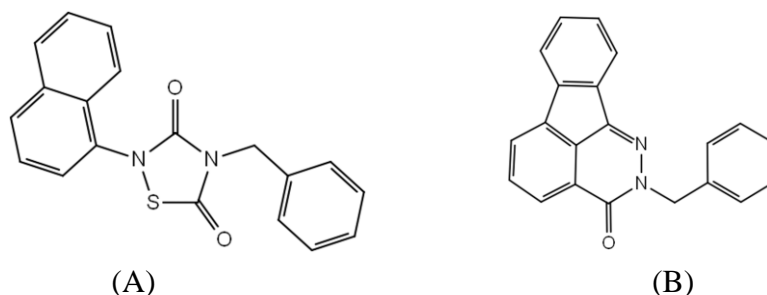


Figure 4.24 Chemical structure of A) Tideglusib and chemical structure of B) ZINC4192390 compound (2-benzylindeno[1,2,3-de]phthalazin-3(2H)-one)

To further validate the stability of the GSK-3 β complexed with the ZINC4192390 compound compared with that of the GSK-3 β complexed with Tideglusib, the root mean square deviation (RMSD) shown in figure 4.25 (A) and the root mean square fluctuation (RMSF) shown in figure 4.25 (B) of the GSK-3 β protein during 20-ns MD simulations were analyzed. From the comparative graphs of RMSD, it can be inferred that GSK-3 β protein in complex with Tideglusib is fluctuating around 2.5 Å, with few high peaks up to 3.0 Å in between 20-ns of simulated time, whereas RMSD trajectory of GSK-3 β protein in complex with ZINC4192390 compound showed a steady graph maintained at 1.5 Å, indicating better and stable complex compared to Tideglusib. From the comparative graphs of RMSF, it can be inferred that there are more number of fluctuating residues with GSK-3 β protein in complex with Tideglusib compared to ZINC4192390. In general, lower the RMSD and RMSF, better is the stability of protein ligand complex.

As shown in figure 4.25 (C) superimposition of the MD simulation snapshots revealed that the compound ZINC4192390 was located much closer to the Cys199 residue, favoring the formation of a stronger binding complex than that obtained with Tideglusib. Moreover, as shown in figure 4.25 (B), 199 and 200 numbered residues are fluctuating in the active site of GSK-3 β , which signifies that this region of the protein in specific could be playing a crucial role for stronger ligand binding with the protein structure (Chauhan et al.)

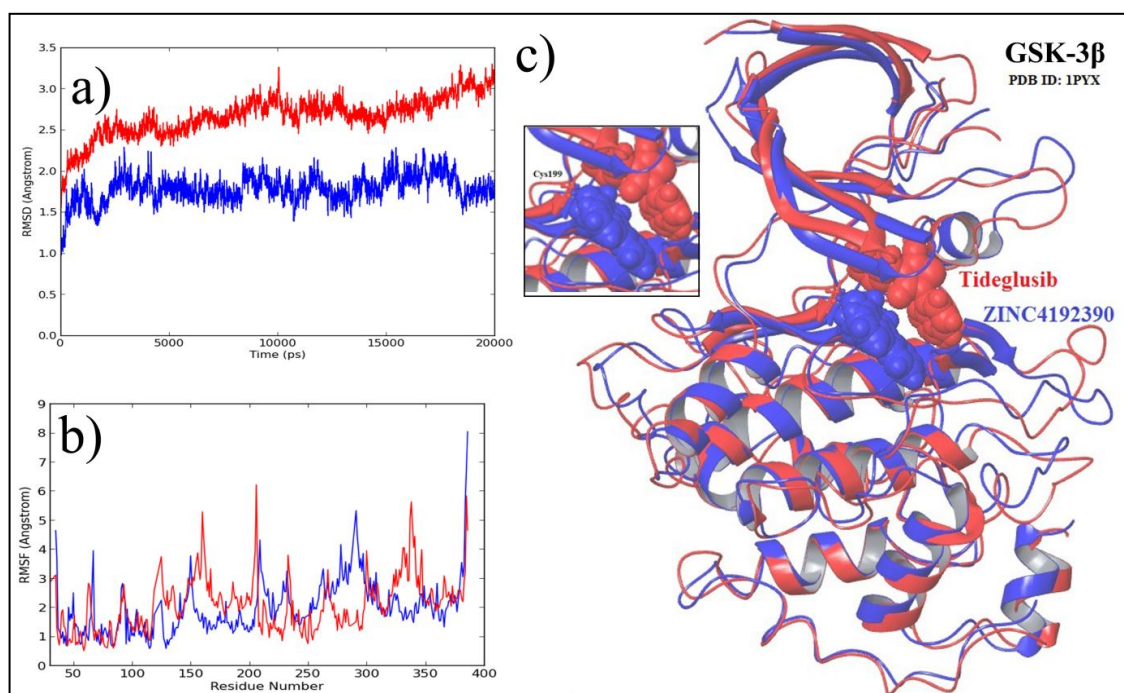


Figure 4.25 A) Root mean square deviation (RMSD) of GSK-3 β protein in presence of Tideglusib (red) and ZINC4192390 compound (blue) B) Root mean square fluctuations (RMSF) of GSK-3 β protein in presence of Tideglusib (red) and ZINC4192390 (blue) C) Superimposition of the final snapshots of MD simulations (Chauhan et al.)

4.3.4 Prediction of Physicochemical Properties of Identified Virtual Hits

The QikProp module version 3.5, available in Maestro program of Schrödinger Suite was used to predict a range of physicochemical properties of identified hits and Tideglusib. The following properties were computed as listed in table 4.7.

Table 4.7 Predicted physicochemical properties of identified hit compounds and Tideglusib using QikProp#

Sr. No.	Compound Code	Molecular Weight	QPlogPo/w Predicted octanol/water partition coefficient	PSA (Polar Surface Area)	Predicted Aqueous Solubility (QPlogS)	Lipinski Violations (Rule of Five)
1	Tideglusib*	334.392	4.379	55.754	-5.041	0
2	AO-476/41610153	297.267	0.319	104.218	-1.629	0
3	AT-057/43486355	308.379	2.464	53.110	-3.175	0
4	AK-080/40907857	310.354	5.080	41.045	5.653	1
#QikProp recommended range: molecular weight < 500 daltons; predicted octanol-water partition coefficient (QPlogPo/w) -2.0 to 6.5; polar surface area (PSA) 7.0 to 200.0 Å ² , predicted aqueous solubility (QPlogS, S in mol dm ⁻³) -6.5 to 0.5; Lipinski violations (rule of five) maximum value 4.						
*Tideglusib predicted log <i>P</i> value 4.72 reported in drug bank (http://www.drugbank.ca)						

Selected physicochemical predictions of virtual hits are within the permissible QikProp recommendations. The designed hit compounds obey the Lipinski's "rule of five". However, slightly higher range of octanol-water partition coefficient was predicted for compound AK-080/40907857 with a value of 5.080 which are above the permissible limits in Lipinski's rule of five.

4.4 Conclusion

Druggability assessment of GSK-3 β target provides useful insights in classifying druggable, difficult and undruggable binding sites. The ATP-binding site (pocket 1) was classified as a "druggable site" while the allosteric site (pocket 7) as a "difficult site" by SiteMap analysis. All other pockets of GSK-3 β did not qualify the druggability criteria. The results of druggability assessment conclude that the allosteric site (pocket 7) is the second best scoring site.

Combined *in-silico* fragment-based and molecular docking approach yielded the design of new series of allosteric targeted N^{1,3}-disubstituted imidazolidin-2-one compounds. These target compounds displayed strong H-bond and pi-stacking interactions with Ser236 and His173 residues respectively. Twenty-one target compounds with relatively better XP GLIDE scores were shortlisted for synthesis and biological evaluation.

Application of virtual screening methodology based on structural features of Tideglusib; identified three novel heterocyclic compounds via shape-based similarity screening using ROCS followed by molecular docking, electrostatic similarity screening using EON and pharmacophore feature-based searching and molecular dynamics simulation approach. Three identified top scoring virtual hits AO-476/41610153, AT-057/43486355 and AK-080/40907857 (ZINC4192390) may possess strong binding potential on GSK-3 β target. The shortlisted compounds were purchased from SPECS (Bleiswijkseweg, The Netherlands) for biological evaluation.

4.5 References

- Arfeen, Minhajul, and Prasad Bharatam. "Design of Glycogen Synthase Kinase-3 Inhibitors: An Overview on Recent Advancements." *Current Pharmaceutical Design*, vol. 19, no. 26, 2013, pp. 4755–4775.
- Bertrand, J.A., et al. "Structural Characterization of the GSK-3 β Active Site Using Selective and Non-Selective ATP-Mimetic Inhibitors." *Journal of Molecular Biology*, vol. 333, no. 2, 2003, pp. 393–407.
- Bax, Benjamin, et al. "The Structure of Phosphorylated GSK-3 β Complexed with a Peptide, FRATtide, That Inhibits β -Catenin Phosphorylation." *Structure*, vol. 9, no. 12, 2001, pp. 1143–1152.
- Chauhan, Navneet, and Anuradha Gajjar. "Classifying Druggability on Potential Binding Sites of Glycogen Synthase Kinase-3 β : An in-Silico Assessment." *Acta Pharmaceutica Scientia*, vol. 55, no. 3, 2017, pp. 43–60.
- Chauhan, Navneet, et al. "Pharmacophore Feature-Based Virtual Screening for Finding Potent GSK-3 Inhibitors Using Molecular Docking and Dynamics Simulations." *Bioinformation*, vol. 12, no. 10, 2016, pp. 391–395.
- Chauhan, Navneet, et al. "Identification of Novel Glycogen Synthase Kinase-3 β Inhibitor through Combined Shape-Based Screening and Molecular Docking Approach." *International Journal of Pharmaceutical Sciences and Drug Research*, vol. 9, no. 3, 2017, pp. 145–148.
- Clark, David E. "what has polar surface area ever done for drug discovery?" *Future Medicinal Chemistry*, vol. 3, no. 4, 2011, pp. 469–484.
- Dajani, R. "Structural Basis for Recruitment of Glycogen Synthase Kinase 3 β to the Axin-APC Scaffold Complex." *The EMBO Journal*, vol. 22, no. 3, 2003, pp. 494–501.
- Domínguez, Juan Manuel, et al. "Evidence for Irreversible Inhibition of Glycogen Synthase Kinase-3 β by Tideglusib." *Journal of Biological Chemistry*, vol. 287, no. 2, 2011, pp. 893–904.
- Eldar-Finkelman, Hagit, et al. "Substrate Competitive GSK-3 Inhibitors Strategy and Implications." *Biochimica et Biophysica Acta (BBA) - Proteins and Proteomics*, vol. 1804, no. 3, 2010, pp. 598–603.

- Fraser, Elizabeth, et al. "Identification of the Axin and Frat Binding Region of Glycogen Synthase Kinase-3." *Journal of Biological Chemistry*, vol. 277, no. 3, 2001, pp. 2176–2185.
- Guilloux, Vincent Le, et al. "Fpocket: An Open Source Platform for Ligand Pocket Detection." *BMC Bioinformatics*, vol. 10, no. 1, 2009, p. 168.
- Halgren, Thomas A. "Identifying and Characterizing Binding Sites and Assessing Druggability." *Journal of Chemical Information and Modeling*, vol. 49, no. 2, 2009, pp. 377–389.
- Halgren, Tom. "New Method for Fast and Accurate Binding-Site Identification and Analysis." *Chemical Biology & Drug Design*, vol. 69, no. 2, 2007, pp. 146–148.
- Hajduk, Philip J., and Jonathan Greer. "A Decade of Fragment-Based Drug Design: Strategic Advances and Lessons Learned." *Nature Reviews Drug Discovery*, vol. 6, no. 3, 2007, pp. 211–219.
- Hao, Ge-Fei, et al. "ACFIS: a Web Server for Fragment-Based Drug Discovery." *Nucleic Acids Research*, vol. 44, no. W1, May 2016.
- Ioakimidis, Leukothea, et al. "Benchmarking the Reliability of QikProp. Correlation between Experimental and Predicted Values." *QSAR & Combinatorial Science*, vol. 27, no. 4, 2008, pp. 445–456.
- Irwin, John J., and Brian K. Shoichet. "ZINC – A Free Database of Commercially Available Compounds for Virtual Screening." *Journal of Chemical Information and Modeling*, vol. 45, no. 1, 2005, pp. 177–182.
- Jorgensen, William L., and Erin M. Duffy. "Prediction of Drug Solubility from Structure." *Advanced Drug Delivery Reviews*, vol. 54, no. 3, 2002, pp. 355–366.
- Koes, D. R., and C. J. Camacho. "ZINCPharmer: Pharmacophore Search of the ZINC Database." *Nucleic Acids Research*, vol. 40, no. W1, 2012.
- Lionta, Evanthia, et al. "Structure-Based Virtual Screening for Drug Discovery: Principles, Applications and Recent Advances." *Current Topics in Medicinal Chemistry*, vol. 14, no. 16, 2014, pp. 1923–1938.

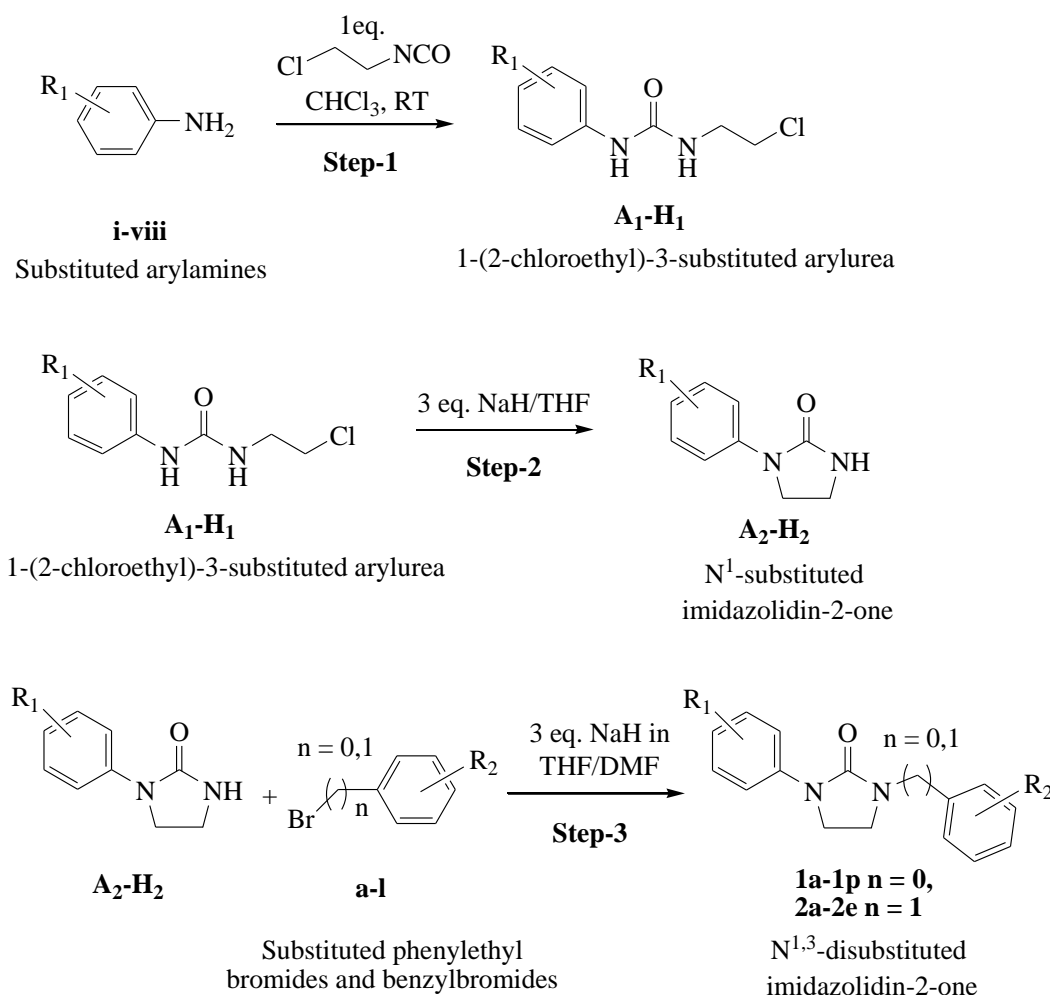
- Lipinski, Christopher A., et al. "Experimental and Computational Approaches to Estimate Solubility and Permeability in Drug Discovery and Development Settings." *Advanced Drug Delivery Reviews*, vol. 23, no. 1-3, 1997, pp. 3–25.
- Martinez, Ana, et al. "First Non-ATP Competitive Glycogen Synthase Kinase 3 β (GSK-3 β) Inhibitors: Thiadiazolidinones (TDZD) as Potential Drugs for the Treatment of Alzheimers Disease." *Journal of Medicinal Chemistry*, vol. 45, no. 6, 2002, pp. 1292–1299.
- Muchmore, Steven W., et al. "The Use of Three-Dimensional Shape and Electrostatic Similarity Searching in the Identification of a Melanin-Concentrating Hormone Receptor 1 Antagonist." *Chemical Biology Drug Design*, vol. 67, no. 2, 2006, pp. 174–176.
- Palomo, Valle, et al. "Exploring the Binding Sites of Glycogen Synthase Kinase 3. Identification and Characterization of Allosteric Modulation Cavities." *Journal of Medicinal Chemistry*, vol. 54, no. 24, 2011, pp. 8461–8470.
- Schmidtke, Peter, and Xavier Barril. "Understanding and Predicting Druggability. A High-Throughput Method for Detection of Drug Binding Sites." *Journal of Medicinal Chemistry*, vol. 53, no. 15, 2010, pp. 5858–5867.
- Schrödinger, L.L.C. "QikProp, version 3.5." *New York, NY*, 2012.
- Stamos, Jennifer L, et al. "Structural Basis of GSK-3 Inhibition by N-terminal Phosphorylation and by the Wnt Receptor LRP6." *ELife*, vol. 3, 2014.
- Thompson, Mark A. "ArgusLab 4.0.1." *Planaria Software LLC, Seattle, WA*, 2004.
- Visualizer, Discovery Studio. "Release 4.0." *Accelrys Software Inc., San Diego, CA, USA*, 2013.
- Wagner, Jeffrey R., et al. "Emerging Computational Methods for the Rational Discovery of Allosteric Drugs." *Chemical Reviews*, vol. 116, no. 11, 2016, pp. 6370–6390.
- Zhang, Peng, et al. "Novel Benzothiazinones (BTOs) as Allosteric Modulator or Substrate Competitive Inhibitor of Glycogen Synthase Kinase 3 β (GSK-3 β) with Cellular Activity of Promoting Glucose Uptake." *Bioorganic & Medicinal Chemistry Letters*, vol. 24, no. 24, 2014, pp. 5639–5643.

5.1 Chemicals and Instruments

All chemicals and solvents used for this project were purchased from commercial sources like Sigma-Aldrich, Merck, Finar, TCI chemicals and Spectrochem. These reagents were used without further purification. Reaction progress and purity of all synthesized compounds were monitored on aluminum foil pre-coated with silica gel 60 F254. Melting points were determined on a Thomas micro hot stage apparatus and are uncorrected. Infrared spectra of the compounds were recorded on a JASCO FTIR 6100 spectrometer by KBr dispersion method. Mass spectra were recorded using a Waters micro mass Q-tof micro spectrometer with an ESI source. ^1H NMR spectra were obtained at 400 MHz on a Bruker Avance instrument using DMSO-*d*₆ as solvent and tetramethylsilane (TMS) as an internal standard. Mass and ^1H NMR spectra of all final compounds were recorded at Oxygen Healthcare Research Pvt. Ltd., Ahmedabad. ^{13}C NMR spectra of the compounds were obtained at 101 MHz using Bruker Avance NMR spectrometer using DMSO-*d*₆ as solvent. LC-MS analysis was carried on a Waters ACQUITY H class UPLC system. For LC-MS solvent A consisted of 2 mM ammonium acetate and 0.1 % formic acid in water while solvent B consisted of 0.1 % formic acid in acetonitrile with Column BEH-C18 (1.7 μm , 2.1 x 50 mm). Compound was detected by ultraviolet (UV) light absorption at 254 nm. ^{13}C NMR and LC-MS spectra were recorded at Piramal Discovery Solutions, Ahmedabad.

Synthetic imidazolidinone derivatives have resulted in many potential drugs and exhibit a broad spectrum of biological activity on various therapeutic targets (Verma and Singh). Particularly, 2-imidazolidinones have been investigated as antihyperglycemic (Wang et al.), anti-cancer (Xue et al.), anti-viral (Chern et al.), anti-microbial, antileishmanial (Lima and Lovely; Robert et al.), and for the treatment of CNS disorders (Andrés et al.; Goodacre et al.).

5.2 Synthetic Scheme



Substituted Aryl amines

- i) naphthalen-1-amine
- ii) 4-chloronaphthalen-1-amine
- iii) 4-bromonaphthalen-1-amine
- iv) 3,5-bis(trifluoromethyl)benzenamine
- v) 4-chloro-3-(trifluoromethyl)benzenamine
- vi) 3-(methylthio)benzenamine
- vii) 4-(trifluoromethyl)benzenamine
- viii) 2-chloro-5-(trifluoromethyl)benzenamine

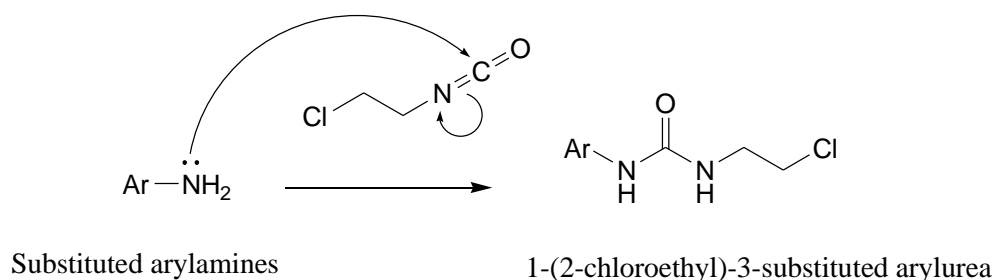
Substituted Phenylethylbromides/benzylbromides

- a) (bromomethyl)benzene
- b) 2-(bromomethyl)-4-fluoro-1-methylbenzene
- c) 1-bromo-3-(bromomethyl)benzene
- d) 2-(bromomethyl)-4-fluoro-1-methylbenzene
- e) 1-(bromomethyl)-2-methylbenzene
- f) 2-(bromomethyl)-1,4-difluorobenzene
- g) 1-(bromomethyl)-2-(trifluoromethyl)benzene
- h) 1-(bromomethyl)-3-chlorobenzene
- i) 1-(bromomethyl)-2-fluorobenzene
- j) 1-(bromomethyl)-3-fluorobenzene
- k) (2-bromoethyl)benzene
- l) 1-(2-bromoethyl)-4-fluorobenzene

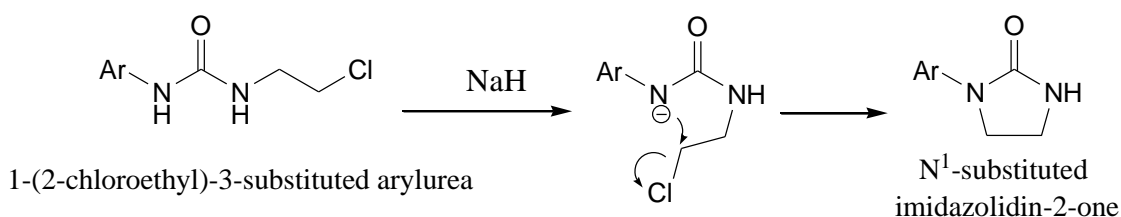
Figure 5.1 Synthetic scheme of N^{1,3}-disubstituted imidazolidin-2-one derivatives

5.3 Reaction Mechanism

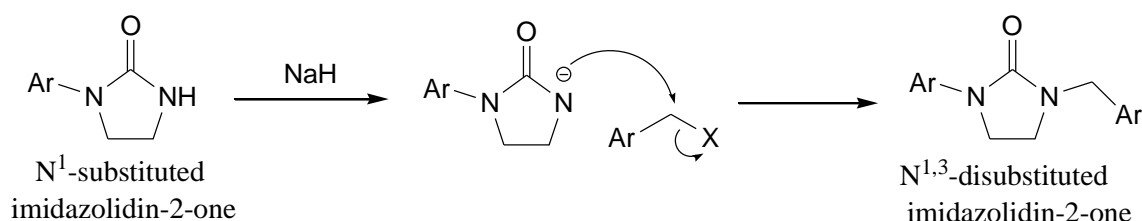
Step 1: 2-chloroethylisocyanate was condensed with appropriate arylamine to give corresponding arylurea.



Step 2: Subsequent intramolecular cyclization of the arylurea intermediate under strong alkaline condition resulted in the formation of monosubstituted imidazolidin-2-one.



Step 3: N-alkylation with substituted phenylethylbromide and substituted benzylbromide yielded desired $\text{N}^{1,3}$ -disubstituted imidazolidin-2-one.



The present work is focussed on the design and synthesis of novel imidazolidin-2-one derivatives. Few imidazolidin-2-one moieties have been synthesized with diverse biological activity reported in literature (Burow and Roger Lee; Fortin et al.; Gaudreault and Sebastien). A series of $\text{N}^{1,3}$ -disubstituted imidazolidin-2-one moieties (**1a-1p**, **2a-2e**) were synthesized as shown in figure 5.1. As per prescribed procedure 2-chloroethylisocyanate was condensed with appropriate arylamine to give corresponding arylureas (**A₁-H₁**) in good yield (Table 5.1). This condensation was followed by cyclization under strong alkaline conditions with sodium hydride to give monosubstituted imidazolidin-2-one derivatives (**A₂-H₂**) (Table 5.2). N^3 -alkylation with various substituted phenylethylbromides and benzylbromides were carried out

in the presence of DMF:THF (1:1) and 3 equivalent of sodium hydride to obtain the desired final compounds (**1a-1p**, **2a-2e**). The time required to carry out the alkylation reaction with substituted benzylbromides (**1a-1p**) was 2 hours, while a longer time of 24 hours was required for alkylation with substituted phenylethylbromides (**2a-2e**). The progress of each reaction was monitored by TLC. Synthesized compounds were purified by column chromatography in the final step and the structures were confirmed by IR spectra, Mass spectra, ^1H NMR and ^{13}C NMR. Percentage yield of intermediates and final compounds were obtained in the range of 77 - 86 % and 48 - 67 % respectively.

5.4 Experimental Procedure

5.4.1 General procedure for synthesis of 1-(2-chloroethyl)-3-substituted aryl-urea (A₁-H₁**)**

Arylamine (**i-viii**) (35 mmol, 1.0 equivalent) was dissolved in chloroform (100 mL) at room temperature. 2-chloroethylisocyanate (35 mmol, 1.0 equivalent) was added drop wise to the above reaction mixture and the reaction mixture was stirred at room temperature. After completion of the reaction, the precipitated solid was filtered, washed with cold chloroform (10 mL) and dried under vacuum to obtain the desired product (**A₁-H₁**).

5.4.2 General procedure for synthesis of N¹-substituted imidazolidin-2-ones (A₂-H₂**)**

Compound (**A₁-H₁**) (2 mmol, 1.0 equivalent) was dissolved in dry THF (25 mL) and cooled to 0 °C under dry nitrogen atmosphere. Sodium hydride (60 % moistened with paraffin) (6 mmol, 3.0 equivalent) was added in portions and the reaction mixture was stirred at room temperature for about 1.5 hours. On completion, the reaction mixture was again cooled to 0 °C and quenched with drop wise addition of methanol (5 mL). The resulting solution was added to ice-cold water. The obtained precipitated solid was filtered and dried under vacuum to obtain the desired product (**A₂-H₂**).

Table 5.1 Structure and physical properties of substituted arylurea derivatives (A₁-H₁)

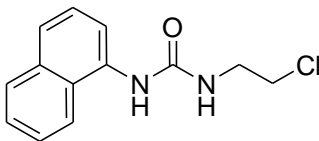
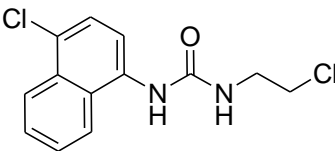
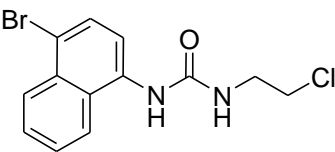
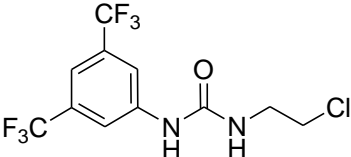
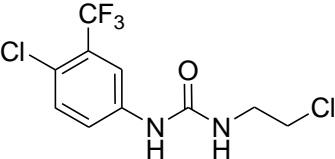
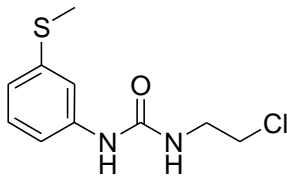
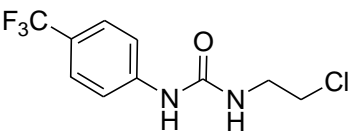
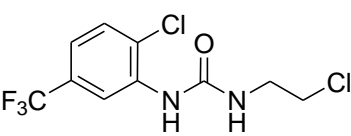
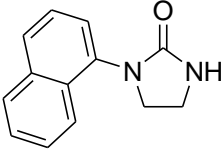
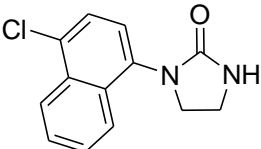
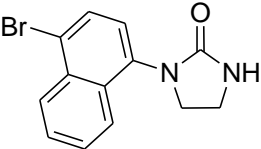
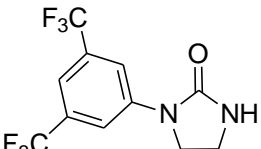
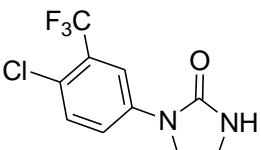
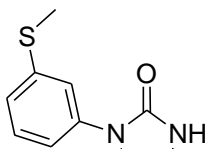
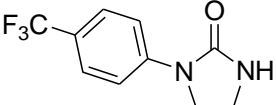
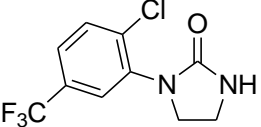
Sr. No.	Compound Code	Intermediate Structures (Step I)	Melting Point (°C)	Yield (%)
1	A ₁		124 - 129	92
2	B ₁		118 - 123	90
3	C ₁		116 - 120	89
4	D ₁		112 - 117	85
5	E ₁		122 - 127	93
6	F ₁		135 - 140	90
7	G ₁		119 - 124	85
8	H ₁		123 - 128	89

Table 5.2 Structure and physical properties of N¹-substituted imidazolidin-2-ones derivatives (A₂-H₂)

Sr. No.	Compound Code	Intermediate Structures (Step II)	Melting Point (°C)	Yield (%)
1	A ₂		160 - 165	86
2	B ₂		> 250	80
3	C ₂		> 250	85
4	D ₂		104 - 109	77
5	E ₂		122 - 126	80
6	F ₂		168 - 173	83
7	G ₂		113 - 117	85
8	H ₂		124 - 128	86

5.4.3 General procedure for synthesis of N^{1,3}-disubstituted imidazolidin-2-ones (1a-1p, 2a-2e)

Compound (**A₂-H₂**) (1.18 mmol, 1.0 equivalent) was dissolved in dry THF:DMF (1:1) (10 mL) and cooled to 0 °C under nitrogen atmosphere. Sodium hydride (60 % moistened with paraffin) (3.53 mmol, 3.0 equivalent) was added in portions and the reaction mixture was stirred at room temperature for 10 minutes. Appropriate bromide (**a-l**) (1.29 mmol, 1.1 equivalent) was added drop wise and the reaction mixture was stirred at room temperature. On completion, the reaction mixture was quenched with methanol (2 mL). The resulting solution was added to ice-cold water, the obtained precipitated solid was filtered and dried under vacuum to afford a crude product which was purified by 100 - 200 mesh silica gel by column chromatography (0.5 % ethylacetate in *n*-hexane) to obtain the desired product (**1a-1p** and **2a-2e**) (Table 5.3).

5.4.3.1. 1-benzyl-3-(naphthalen-1-yl)imidazolidin-2-one (1a)

Yield: 65 %; pale brown solid; *R_f* value 0.38; m.p. 197 - 202 °C; FT-IR (KBr, cm⁻¹): 1715.42 (N-CO-N); ¹H NMR (400 MHz, DMSO-*d*₆): δ 7.99 - 7.88 (m, 3H), 7.57 - 7.48 (m, 4H), 7.44 - 7.33 (m, 5H), 4.44 (s, 2H), 3.85 - 3.81 (t, *J* = 7.8 Hz, 2H), 3.49 - 3.45 (t, *J* = 7.6 Hz, 2H); ESI-MS calculated for (C₂₀H₁₈N₂O) [M+1]⁺ 303.37, found 303.1 [M + 1]⁺.

5.4.3.2. 1-(5-fluoro-2-methylbenzyl)-3-(naphthalen-1-yl)imidazolidin-2-one (1b)

Yield: 66 %; pale white solid; *R_f* value 0.47; m.p. 108 - 113 °C; FT-IR (KBr, cm⁻¹): 1690.35 (N-CO-N); ¹H NMR (400 MHz, DMSO-*d*₆): δ 8.01 - 7.93 (m, 2H), 7.91 - 7.89 (d, *J* = 8.0 Hz, 1H), 7.58 - 7.50 (m, 4H), 7.29 - 7.25 (t, *J* = 8.0 Hz, 1H), 7.19 - 7.15 (dd, *J* = 4.0, 12.0 Hz, 1H), 7.09 - 7.04 (dt, *J* = 4.0, 10 Hz, 1H), 4.42 (s, 2H), 3.88 - 3.84 (t, *J* = 8.0 Hz, 2H), 3.52 - 3.48 (t, *J* = 8.0 Hz, 2H), 2.31 (s, 3H); ESI-MS calculated for (C₂₁H₁₉FN₂O) [M+1]⁺ 335.39, found 335.4 [M + 1]⁺.

5.4.3.3. 1-(3-bromobenzyl)-3-(4-chloronaphthalen-1-yl)imidazolidin-2-one (1c)

Yield: 59 %; pale white solid; *R_f* value 0.48; m.p. 105 - 110 °C; FT-IR (KBr, cm⁻¹): 1690.41 (N-CO-N); ¹H NMR (400 MHz, DMSO-*d*₆): δ 8.25 - 8.22 (d, *J* = 12 Hz, 1H), 8.02 - 8.00 (d, *J* = 8.0 Hz, 1H), 7.77 - 7.67 (m, 3H), 7.59 (s, 1H), 7.56 - 7.52 (m, 2H), 7.42 - 7.37 (d, *J* = 4.0 Hz, 2H), 4.44 (s, 2H), 3.88 - 3.84 (t, *J* = 8.0 Hz, 2H), 3.52 - 3.48 (t, *J* = 8.0 Hz, 2H); ESI-MS calculated for (C₂₀H₁₆BrClN₂O) [M+1]⁺ 415.02, found 415.2 [M + 1]⁺.

5.4.3.4. 1-(4-chloronaphthalen-1-yl)-3-(5-fluoro-2-methylbenzyl)imidazolidin-2-one (1d)

Yield: 61 %; pale white solid; R_f value 0.51; m.p. 94 - 99 °C; FT-IR (KBr, cm^{-1}): 1691.46 (N-CO-N); ^1H NMR (400 MHz, $\text{DMSO-}d_6$): δ 8.24 - 8.22 (d, J = 8.0 Hz, 1H), 8.06 - 8.04 (d, J = 8.0 Hz, 1H), 7.77 - 7.67 (m, 3H), 7.54 - 7.52 (d, J = 8.0 Hz, 1H), 7.28 - 7.25 (t, J = 6.0 Hz, 1H), 7.19 - 7.6 (dd, J = 4.0, 12 Hz, 1H), 7.08 - 7.03 (dt, J = 4.0, 10 Hz, 1H), 4.42 (s, 2H), 3.89 - 3.85 (t, J = 8.0 Hz, 2H), 3.52 - 3.49 (t, J = 8.0 Hz, 2H), 2.23 (s, 3H); ESI-MS calculated for ($\text{C}_{21}\text{H}_{18}\text{ClFN}_2\text{O}$) $[\text{M}+1]^+$ 369.11, found 369.4 $[\text{M}+1]^+$, 371.4 $[\text{M}+2]^+$.

5.4.3.5. 1-(4-chloronaphthalen-1-yl)-3-(2-methylbenzyl)imidazolidin-2-one (1e)

Yield: 64 %; pale white solid; R_f value 0.52; m.p. 96 - 101 °C; FT-IR (KBr, cm^{-1}): 1738.44 (N-CO-N); ^1H NMR (400 MHz, $\text{DMSO-}d_6$): δ 8.24 - 8.22 (d, J = 8.0 Hz, 1H), 8.05 - 8.03 (d, J = 8.0 Hz, 1H), 7.77 - 7.67 (m, 3H), 7.52 - 7.50 (d, J = 8.0 Hz, 1H), 7.33 - 7.23 (m, 4H), 4.43 (s, 2H), 3.86 - 3.82 (t, J = 8.0 Hz, 2H), 3.47 - 3.43 (t, J = 8.0 Hz, 2H), 2.34 (s, 3H); ESI-MS calculated for ($\text{C}_{21}\text{H}_{19}\text{ClN}_2\text{O}$) $[\text{M}+1]^+$ 351.12, found 351.3 $[\text{M}+1]^+$.

5.4.3.6. 1-(4-chloronaphthalen-1-yl)-3-(2,5-difluorobenzyl)imidazolidin-2-one (1f)

Yield: 56 %; pale white solid; R_f value 0.54; m.p. 90 - 95 °C; FT-IR (KBr, cm^{-1}): 1736.38 (N-CO-N); ^1H NMR (400 MHz, $\text{DMSO-}d_6$): δ 8.24 - 8.22 (d, J = 8.0 Hz, 1H), 8.04 - 8.02 (d, J = 8.0 Hz, 1H), 7.77 - 7.66 (m, 3H), 7.53 - 7.51 (d, J = 8.0 Hz, 1H), 7.36 - 7.21 (m, 3H), 4.48 (s, 2H), 3.89 - 3.85 (t, J = 8.0 Hz, 2H), 3.57 - 3.53 (t, J = 8.0 Hz, 2H); ESI-MS calculated for ($\text{C}_{20}\text{H}_{15}\text{ClF}_2\text{N}_2\text{O}$) $[\text{M}+1]^+$ 373.09, found 373.3 $[\text{M}+1]^+$.

5.4.3.7. 1-(4-chloronaphthalen-1-yl)-3-(2-(trifluoromethyl)benzyl)imidazolidin-2-one (1g)

Yield: 54 %; pale white solid; R_f value 0.61; m.p. 109 - 114 °C; FT-IR (KBr, cm^{-1}): 1715.45 (N-CO-N); ^1H NMR (400 MHz, $\text{DMSO-}d_6$): δ 8.24 - 8.22 (d, J = 8.0 Hz, 1H), 8.09 - 8.07 (d, J = 8.0 Hz, 1H), 7.80 - 7.68 (m, 6H), 7.57 - 7.53 (m, 2H), 4.62 (s, 2H), 3.91 - 3.87 (t, J = 8.0 Hz, 2H), 3.57 - 3.53 (t, J = 8.0 Hz, 2H); ESI-MS calculated for ($\text{C}_{21}\text{H}_{16}\text{ClF}_3\text{N}_2\text{O}$) $[\text{M}+1]^+$ 405.09, found 405.3 $[\text{M}+1]^+$.

5.4.3.8. 1-(4-bromonaphthalen-1-yl)-3-(5-fluoro-2-methylbenzyl)imidazolidin-2-one (1h)

Yield: 62 %; pale brown solid; R_f value 0.61; m.p. 84 - 89 °C; FT-IR (KBr, cm^{-1}): 1738.02 (N-CO-N); ^1H NMR (400 MHz, $\text{DMSO-}d_6$): δ 8.19 - 8.17 (d, J = 8.0 Hz, 1H), 8.05 - 8.03 (d, J = 8.0 Hz, 1H), 7.95 - 7.93 (d, J = 8.0 Hz, 1H), 7.75 - 7.65 (m, 2H), 7.47 - 7.45 (d, J = 8.0 Hz, 1H), 7.28 - 7.24 (m, J = 8.0 Hz, 1H), 7.18 - 7.16 (d, J = 8.0 Hz, 1H), 7.08 - 7.04 (t, J = 8.0 Hz, 1H), 4.41 (s, 2H), 3.89 - 3.85 (t, J = 8.0 Hz, 2H), 3.52 - 3.48 (t, J = 8.0 Hz, 2H), 2.30 (s, 3H); ESI-MS calculated for ($\text{C}_{21}\text{H}_{18}\text{BrFN}_2\text{O}$) $[\text{M}+1]^+$ 413.06, found 413.3 $[\text{M}+1]^+$, 415.2 $[\text{M}+2]^+$.

5.4.3.9. 1-(4-bromonaphthalen-1-yl)-3-(3-methylbenzyl)imidazolidin-2-one (1i)

Yield: 63 %; pale white solid; R_f value 0.62; m.p. 101 - 106 °C; FT-IR (KBr, cm^{-1}): 1684.52 (N-CO-N); ^1H NMR (400 MHz, $\text{DMSO}-d_6$): δ 8.19 - 8.17 (d, J = 8.0 Hz, 1H), 8.01 - 7.99 (d, J = 8.0 Hz, 1H), 7.94 - 7.92 (d, J = 8.0 Hz, 1H), 7.76 - 7.72 (t, J = 8.0 Hz, 1H), 7.69 - 7.65 (d, J = 8.0 Hz, 1H), 7.46 - 7.44 (d, J = 8.0 Hz, 1H), 7.32 - 7.28 (t, J = 8.0 Hz, 1H), 7.18 - 7.13 (m, 3H), 4.38 (s, 2H), 3.85 - 3.82 (t, J = 8.0 Hz, 2H), 3.49 - 3.45 (t, J = 8.0 Hz, 2H), 2.34 (s, 3H); ^{13}C NMR (101 MHz, $\text{DMSO}-d_6$) δ 159.61, 138.25, 137.94, 137.77, 132.32, 131.99, 130.34, 129.03, 128.93, 128.60, 128.47, 127.62, 127.28, 125.41, 124.91, 120.55, 47.97, 46.45, 42.77, 40.21, 21.56; ESI-MS calculated for ($\text{C}_{21}\text{H}_{19}\text{BrN}_2\text{O}$) $[\text{M}+1]^+$ 395.07, found 395.2 $[\text{M}+1]^+$, 397.2 $[\text{M}+2]^+$.

5.4.3.10. 1-(4-bromonaphthalen-1-yl)-3-(3-chlorobenzyl)imidazolidin-2-one (1j)

Yield: 55 %; pale white solid; R_f value 0.52; m.p. 88 - 93 °C; FT-IR (KBr, cm^{-1}): 1690.43 (N-CO-N); ^1H NMR (400 MHz, $\text{DMSO}-d_6$): δ 8.20 - 8.18 (d, J = 8.0 Hz, 1H), 8.01 - 7.99 (d, J = 8.0 Hz, 1H), 7.95 - 7.93 (d, J = 8.0 Hz, 1H), 7.76 - 7.72 (dt, J = 4.0, 8.0 Hz, 1H), 7.68 - 7.65 (dt, J = 4.0, 8.0 Hz, 1H), 7.47 - 7.44 (m, 3H), 7.41 - 7.34 (m, 2H), 4.44 (s, 2H), 3.88 - 3.84 (t, J = 8.0 Hz, 2H), 3.53 - 3.49 (t, J = 8.0 Hz, 2H); ESI-MS calculated for ($\text{C}_{20}\text{H}_{16}\text{BrClN}_2\text{O}$) $[\text{M}+1]^+$ 415.02, found 415.3 $[\text{M}+1]^+$, 417.2 $[\text{M}+2]^+$.

5.4.3.11. 1-(4-bromonaphthalen-1-yl)-3-(2,5-difluorobenzyl)imidazolidin-2-one (1k)

Yield: 57 %; pale white solid; R_f value 0.70; m.p. 98 - 103 °C; FT-IR (KBr, cm^{-1}): 1715.49 (N-CO-N); ^1H NMR (400 MHz, $\text{DMSO}-d_6$): δ 8.19 - 8.17 (d, J = 8.0 Hz, 1H), 8.03 - 8.01 (d, J = 8.0 Hz, 1H), 7.95 - 7.93 (d, J = 8.0 Hz, 1H), 7.76 - 7.72 (dt, J = 4.0, 8.0 Hz, 1H), 7.69 - 7.65 (dt, J = 4.0, 8.0 Hz, 1H), 7.47 - 7.45 (d, J = 8.0 Hz, 1H), 7.36 - 7.21 (m, 3H), 4.48 (s, 2H), 3.89 - 3.85 (t, J = 8.0 Hz, 2H), 3.58 - 3.54 (t, J = 8.0 Hz, 2H); ESI-MS calculated for ($\text{C}_{20}\text{H}_{15}\text{BrF}_2\text{N}_2\text{O}$) $[\text{M}+1]^+$ 417.04, found 417.2 $[\text{M}+1]^+$, 419.2 $[\text{M}+2]^+$.

5.4.3.12. 1-(4-bromonaphthalen-1-yl)-3-(2-fluorobenzyl)imidazolidin-2-one (1l)

Yield: 60 %; pale brown solid; R_f value 0.54; m.p. 80 - 85 °C; FT-IR (KBr, cm^{-1}): 1715.37 (N-CO-N); ^1H NMR (400 MHz, $\text{DMSO}-d_6$): δ 8.19 - 8.17 (d, J = 8.0 Hz, 1H), 8.02 - 8.00 (d, J = 8.0 Hz, 1H), 7.95 - 7.93 (d, J = 8.0 Hz, 1H), 7.76 - 7.72 (dt, J = 4.0, 8.0 Hz, 1H), 7.69 - 7.65 (dt, J = 4.0, 8.0 Hz, 1H), 7.47 - 7.45 (d, J = 8.0 Hz, 2H), 7.27 - 7.13 (m, 3H), 4.45 (s, 2H), 3.88 - 3.84 (t, J = 8.0 Hz, 2H), 3.59 - 3.49 (t, J = 8.0 Hz, 2H); ESI-MS calculated for ($\text{C}_{20}\text{H}_{16}\text{BrFN}_2\text{O}$) $[\text{M}+1]^+$ 399.05, found 399.3 $[\text{M}+1]^+$, 401.3 $[\text{M}+2]^+$.

5.4.3.13. 1-(3,5-bis(trifluoromethyl)phenyl)-3-(2-fluorobenzyl)imidazolidin-2-one (1m)

Yield: 67 %; pale white solid; R_f value 0.89; m.p. 95 - 100 °C; FT-IR (KBr, cm^{-1}): 1715.38 (N-CO-N); ^1H NMR (400 MHz, $\text{DMSO}-d_6$): δ 8.24 (s, 2H), 7.68 (s, 1H), 7.45 - 7.39 (q, J = 8.0 Hz, 1H), 7.18 - 7.11 (m, 3H), 4.45 (s, 2H), 4.00 - 3.96 (t, J = 8.0 Hz, 2H), 3.48 - 3.44 (t, J = 8.0 Hz, 2H); ESI-MS calculated for ($\text{C}_{18}\text{H}_{13}\text{F}_7\text{N}_2\text{O}$) $[\text{M}+1]^+$ 407.09, found 407.3 $[\text{M}+1]^+$.

5.4.3.14. 1-(4-chloro-3-(trifluoromethyl)phenyl)-3-(3-fluorobenzyl)imidazolidin-2-one (1n)

Yield: 61 %; cream color solid; R_f value 0.86; m.p. 96 - 101 °C; FT-IR (KBr, cm^{-1}): 1715.37 (N-CO-N); ^1H NMR (400 MHz, $\text{DMSO}-d_6$): δ 8.29 (s, 1H), 7.71 - 7.66 (m, 2H), 7.45 - 7.39 (q, J = 8.0 Hz, 1H), 7.17 - 7.11 (m, 3H), 4.43 (s, 2H), 3.91 - 3.87 (t, J = 8.0 Hz, 2H), 3.44 - 3.40 (t, J = 8.0 Hz, 2H); ^{13}C NMR (101 MHz, $\text{DMSO}-d_6$) δ 164.03, 161.60, 157.22, 140.48, 132.35, 131.10, 131.02, 127.17, 124.20, 122.67, 121.98, 115.91, 114.79, 114.74, 47.00, 42.20, 41.30; ESI-MS calculated for ($\text{C}_{17}\text{H}_{13}\text{ClF}_4\text{N}_2\text{O}$) $[\text{M}+1]^+$ 373.07, found 373.1 $[\text{M}+1]^+$.

5.4.3.15. 1-(2-methylbenzyl)-3-(2-(methylthio)phenyl)imidazolidin-2-one (1o)

Yield: 48 %; Pale brown solid; R_f value 0.41; m.p. 83 - 88 °C; FT-IR (KBr, cm^{-1}): 1738.37 (N-CO-N); ^1H NMR (400 MHz, $\text{DMSO}-d_6$): δ 7.36 - 7.2 (m, 8H), 4.36 (s, 2H), 3.67 - 3.63 (t, J = 8.0 Hz, 2H), 3.33 - 3.29 (t, J = 8.0 Hz, 2H), 2.42 (s, 3H), 2.30 (s, 3H); ESI-MS calculated for ($\text{C}_{18}\text{H}_{20}\text{N}_2\text{OS}$) $[\text{M}+1]^+$ 313.13, found 313.5 $[\text{M}+1]^+$.

5.4.3.16. 1-(2-fluorobenzyl)-3-(4-(trifluoromethyl)phenyl)imidazolidin-2-one (1p)

Yield: 58 % Pale cream solid; R_f value 0.86; m.p. 97 - 102 °C; FT-IR (KBr, cm^{-1}): 1690.68 (N-CO-N); ^1H NMR (400 MHz, $\text{DMSO}-d_6$): δ 7.81 - 7.79 (d, J = 8.4 Hz, 2H), 7.69 - 7.67 (d, J = 8.8 Hz, 2H), 7.44 - 7.39 (m, 1H), 7.17 - 7.10 (m, 3H), 4.48 (s, 2H), 3.90 - 3.86 (t, J = 8.0 Hz, 2H), 3.44 - 3.40 (t, J = 8.0 Hz, 2H); ESI-MS calculated for ($\text{C}_{17}\text{H}_{14}\text{F}_4\text{N}_2\text{O}$) $[\text{M}+1]^+$ 339.2, found 339.2 $[\text{M}+1]^+$.

5.4.3.17. 1-(naphthalen-1-yl)-3-phenethylimidazolidin-2-one (2a)

Yield: 51 %; dark cream solid; R_f value 0.41; m.p. 125 - 130 °C; FT-IR (KBr, cm^{-1}): 1698.02 (N-CO-N); ^1H NMR (400 MHz, $\text{DMSO}-d_6$): δ 7.97 - 7.95 (d, J = 8.0 Hz, 1H), 7.86 - 7.84 (d, J = 8.0 Hz, 1H), 7.75 - 7.73 (d, 8.0 Hz, 1H), 7.56 - 7.48 (m, 3H), 7.40 - 7.38 (d, J = 8.0 Hz, 1H), 7.37 - 7.32 (m, 4H), 7.26 - 7.24 (m, 1H), 3.79 - 3.75 (t, J = 8.0 Hz, 2H), 3.59 - 3.55 (t, J = 8.0 Hz, 2H), 3.49 - 3.46 (t, J = 8.0 Hz, 2H), 2.90 - 2.87 (t, J = 8.0 Hz, 2H); ESI-MS calculated for ($\text{C}_{21}\text{H}_{20}\text{N}_2\text{O}$) $[\text{M}+1]^+$ 317.16, found 317.5 $[\text{M}+1]^+$.

5.4.3.18. 1-(4-chloro-3-(trifluoromethyl)phenyl)-3-(4-fluorophenethyl)imidazolidin-2-one (2b)

Yield: 54 %; pale white solid; R_f value 0.48; m.p. 103 - 108 °C; FT-IR (KBr, cm^{-1}): 1697.05 (N-CO-N); ^1H NMR (400 MHz, $\text{DMSO}-d_6$): δ 8.23 (s, 1H), 7.64 (m, 2H), 7.32 - 7.29 (t, J = 8.0 Hz, 2H), 7.14 - 7.09 (t, J = 9.0 Hz, 2H), 3.84 - 3.80 (t, J = 8.0 Hz, 2H), 3.49 - 3.41 (m, 4H), 2.84 - 2.80 (t, J = 8.0 Hz, 2H); ESI-MS calculated for ($\text{C}_{18}\text{H}_{15}\text{ClF}_4\text{N}_2\text{O}$) $[\text{M}+1]^+$ 387.77, found 387.3 $[\text{M}+1]^+$.

5.4.3.19. 1-(3,5-bis(trifluoromethyl)phenyl)-3-phenethylimidazolidin-2-one (2c)

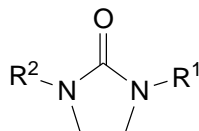
Yield: 50 %; cream color solid; R_f value 0.85; m.p. 93 - 98 °C; FT-IR (KBr, cm^{-1}): 1698.06 (N-CO-N); ^1H NMR (400 MHz, $\text{DMSO}-d_6$): δ 8.19 (s, 2H), 7.64 (s, 1H), 7.33 - 7.19 (m, 5H), 3.94 - 3.90 (t, J = 8.0 Hz, 2H), 3.53 - 3.45 (m, 4H), 2.86 - 2.82 (t, J = 8.0 Hz, 2H); ESI-MS calculated for ($\text{C}_{19}\text{H}_{16}\text{F}_6\text{N}_2\text{O}$) $[\text{M}+1]^+$ 403.33, found 403.4 $[\text{M}+1]^+$.

5.4.3.20. 1-(2-chloro-5-(trifluoromethyl)phenyl)-3-(2-phenylethyl)imidazolidin-2-one (2d)

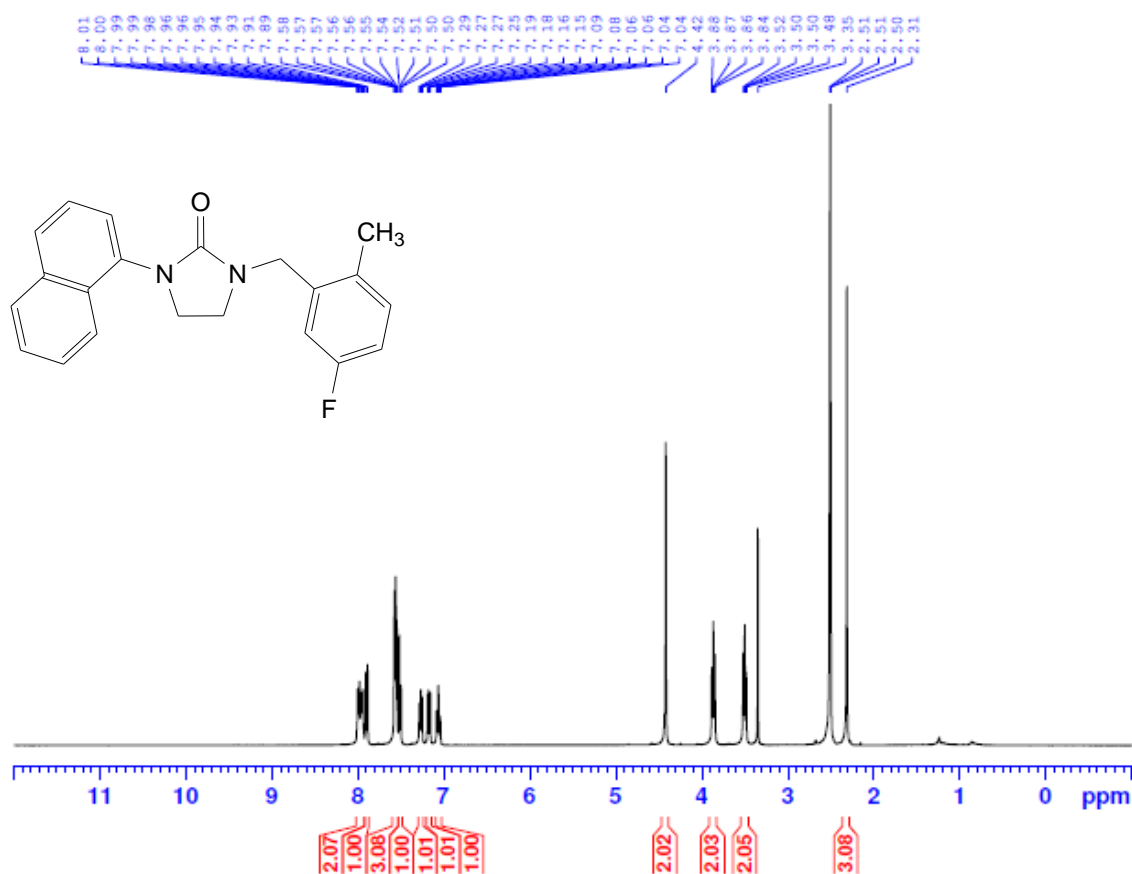
Yield: 53 %; pale white solid; R_f value 0.81; m.p. 92 - 97 °C; FT-IR (KBr, cm^{-1}): 1697.05 (N-CO-N); ^1H NMR (400 MHz, $\text{DMSO}-d_6$): δ 7.78 - 7.73 (m, 2H), 7.67 - 7.65 (d, J = 8.0 Hz, 1H), 7.33 - 7.29 (m, 4H), 7.23 - 7.19 (m, 1H), 3.77 - 3.73 (t, J = 8.0 Hz, 2H), 3.52 - 3.48 (t, J = 8.0 Hz, 2H), 3.45 - 3.41 (t, J = 8.0 Hz, 2H), 2.86 - 2.82 (t, J = 8.0 Hz, 2H); ^{13}C NMR (101 MHz, $\text{DMSO}-d_6$) δ 158.26, 139.56, 139.15, 136.02, 131.78, 129.36, 129.04, 128.72, 128.02, 126.64, 126.46, 125.31, 124.97, 122.61, 45.31, 44.76, 42.84, 33.63; ESI-MS calculated for ($\text{C}_{18}\text{H}_{16}\text{ClF}_3\text{N}_2\text{O}$) $[\text{M}+1]^+$ 369.09, found 369.4 $[\text{M}+1]^+$, 371.3 $[\text{M}+2]^+$; LC-MS (m/z): 369.39 $[\text{M}+1]^+$.

5.4.3.21. 1-(2-chloro-5-(trifluoromethyl)phenyl)-3-(2-(4-fluorophenyl)ethyl)imidazolidin-2-one (2e)

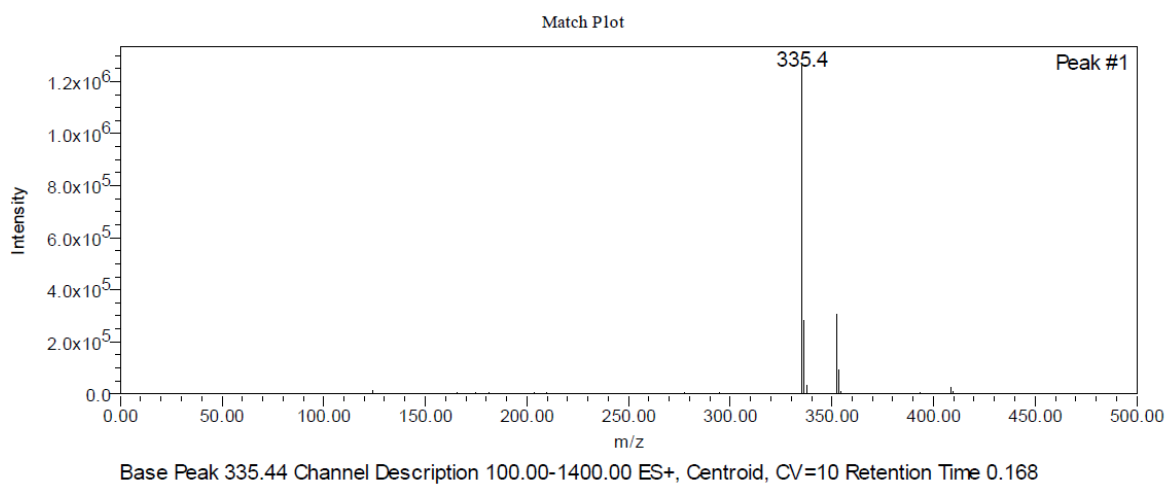
Yield: 52 %; pale yellow solid; R_f value 0.78; m.p. 91 - 96 °C; FT-IR (KBr, cm^{-1}): 1697.04 (N-CO-N); ^1H NMR (400 MHz, $\text{DMSO}-d_6$): δ 7.78 - 7.76 (d, J = 8.0 Hz, 1H), 7.72 (s, 1H), 7.67 - 7.65 (d, J = 8.0 Hz, 1H), 7.34 - 7.30 (t, J = 8.0 Hz, 2H), 7.14 - 7.10 (t, J = 8.0 Hz, 2H), 3.77 - 3.73 (t, J = 8.0 Hz, 2H), 3.53 - 3.49 (t, J = 8.0 Hz, 2H), 3.44 - 3.40 (t, J = 8.0 Hz, 2H), 2.85 - 2.81 (t, J = 8.0 Hz, 2H); ESI-MS calculated for ($\text{C}_{18}\text{H}_{15}\text{ClF}_4\text{N}_2\text{O}$) $[\text{M}+1]^+$ 387.08, found 387.3 $[\text{M}+1]^+$, 389.3 $[\text{M}+2]^+$.

Table 5.3 Structure and physical properties of N^{1,3}-disubstituted imidazolidin-2-ones derivatives (1a-1p and 2a-2e)

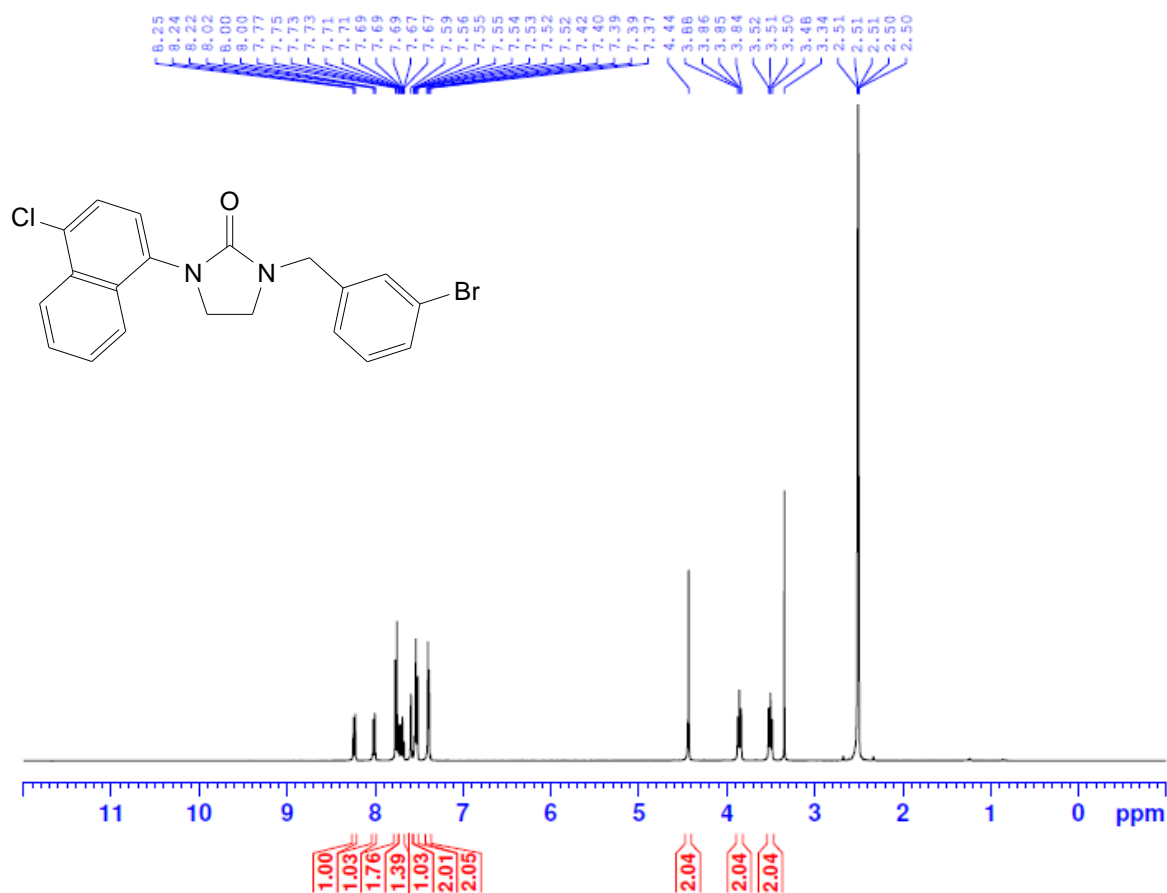
Sr. No.	Compound Code	R ¹	R ²	Melting Point (°C)	Yield (%)
1	1a	Bn	1-naphthyl	197 - 202	65
2	1b	2-Me-5-F-Bn	1-naphthyl	108 - 113	66
3	1c	3-Br-Bn	4-Cl-naphthyl	105 - 110	59
4	1d	2-Me-5-F-Bn	4-Cl-naphthyl	94 - 99	61
5	1e	2-Me-Bn	4-Cl-naphthyl	96 - 101	64
6	1f	2,5-F-Bn	4-Cl-naphthyl	90 - 95	56
7	1g	2-CF ₃ -Bn	4-Cl-naphthyl	109 - 114	54
8	1h	2-Me-5-F-Bn	4-Br-naphthyl	84 - 89	62
9	1i	3-Me-Bn	4-Br-naphthyl	101 - 106	63
10	1j	3-Cl-Bn	4-Br-naphthyl	88 - 93	55
11	1k	2,5-F-Bn	4-Br-naphthyl	98 - 103	57
12	1l	2-F-Bn	4-Br-naphthyl	80 - 85	60
13	1m	2-F-Bn	3,5-CF ₃ -Ph	95 - 100	67
14	1n	3-F-Bn	3-CF ₃ -4-Cl-Ph	96 - 101	61
15	1o	2-Me-Bn	2-SMe-Ph	83 - 88	48
16	1p	2-F-Bn	4-CF ₃ -Ph	97 - 102	58
17	2a	Ph-Et	1-naphthyl	125 - 130	51
18	2b	4F-Ph-Et	3-CF ₃ -4-Cl-Ph	103 - 108	54
19	2c	Ph-Et	3,5-CF ₃ -Ph	93 - 98	50
20	2d	Ph-Et	2-Cl-5-CF ₃ -Ph	92 - 97	53
21	2e	4F-Ph-Et	2-Cl-5-CF ₃ -Ph	91 - 96	52

5.5.3 ^1H NMR Spectrum (400 MHz, DMSO) of compound 1b

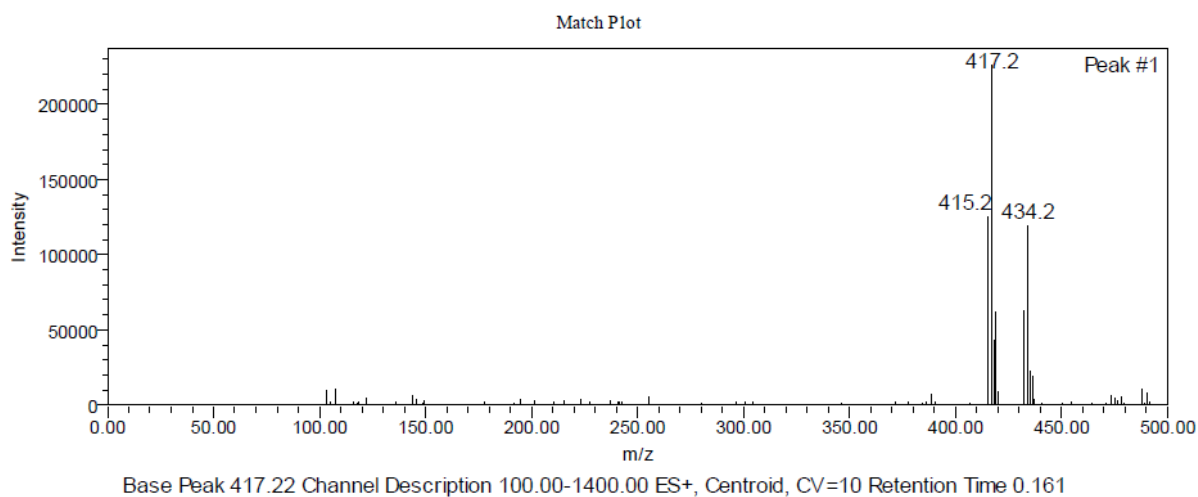
5.5.4 ESI-MS Spectrum of compound 1b



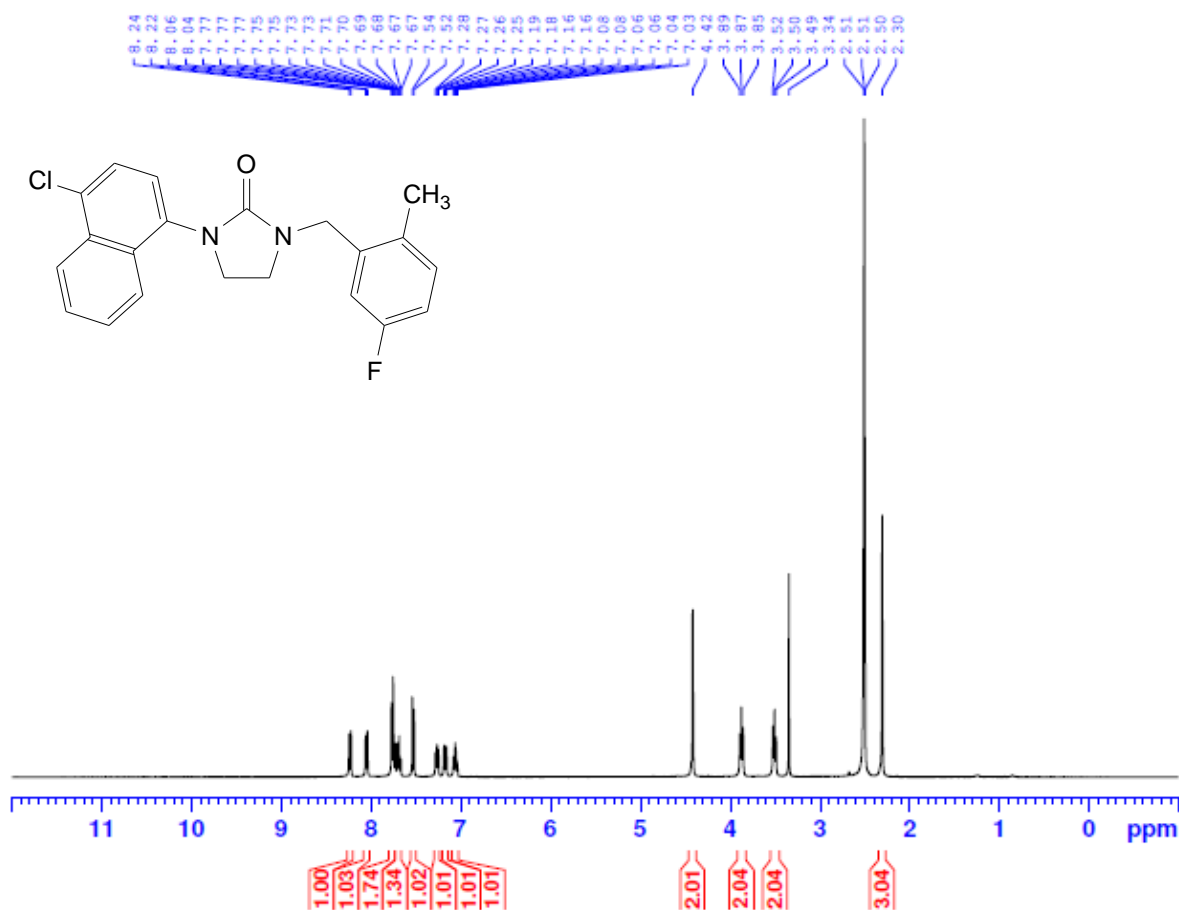
5.5.5 ^1H NMR Spectrum (400 MHz, DMSO) of compound 1c



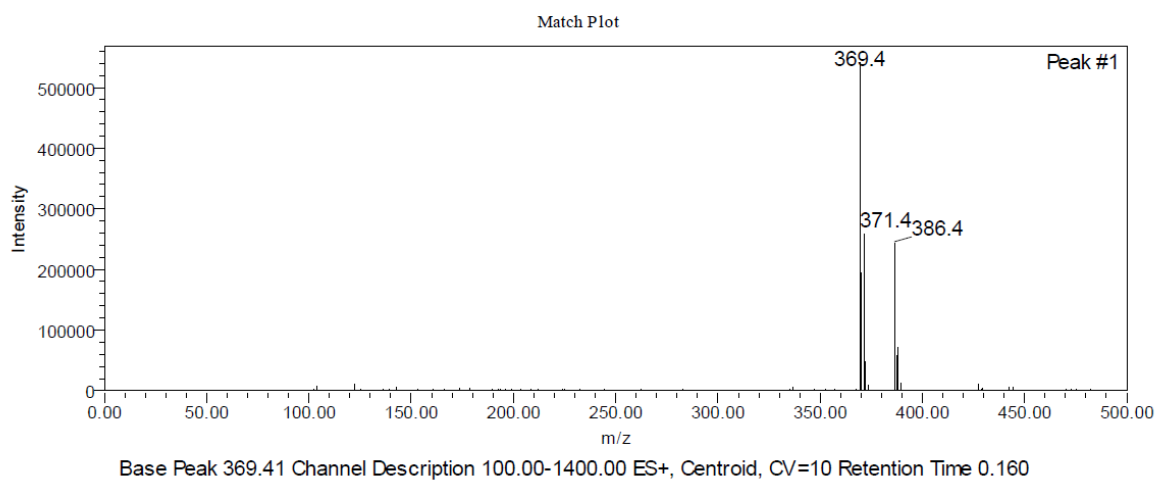
5.5.6 ESI-MS Spectrum of compound 1c



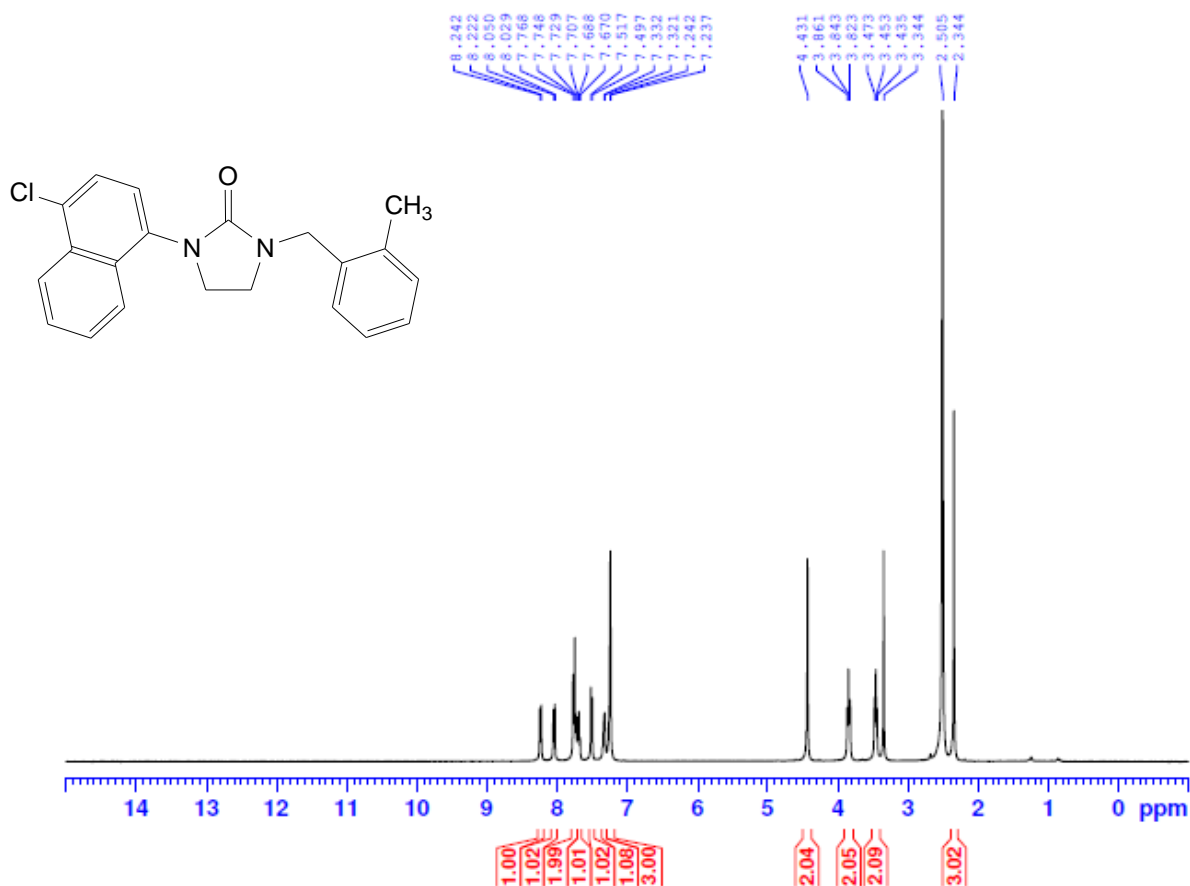
5.5.7 ^1H NMR Spectrum (400 MHz, DMSO) of compound 1d



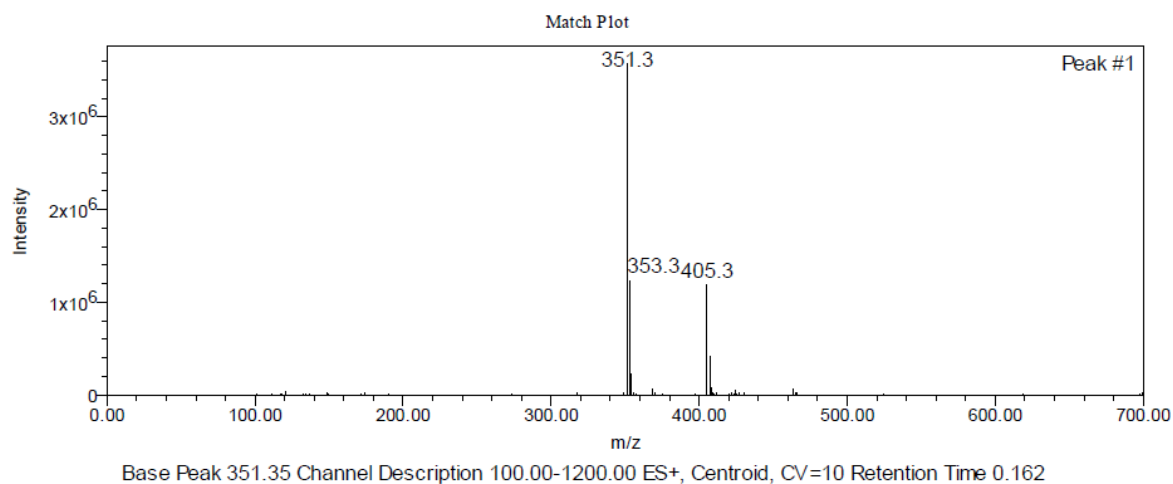
5.5.8 ESI-MS Spectrum of compound 1d

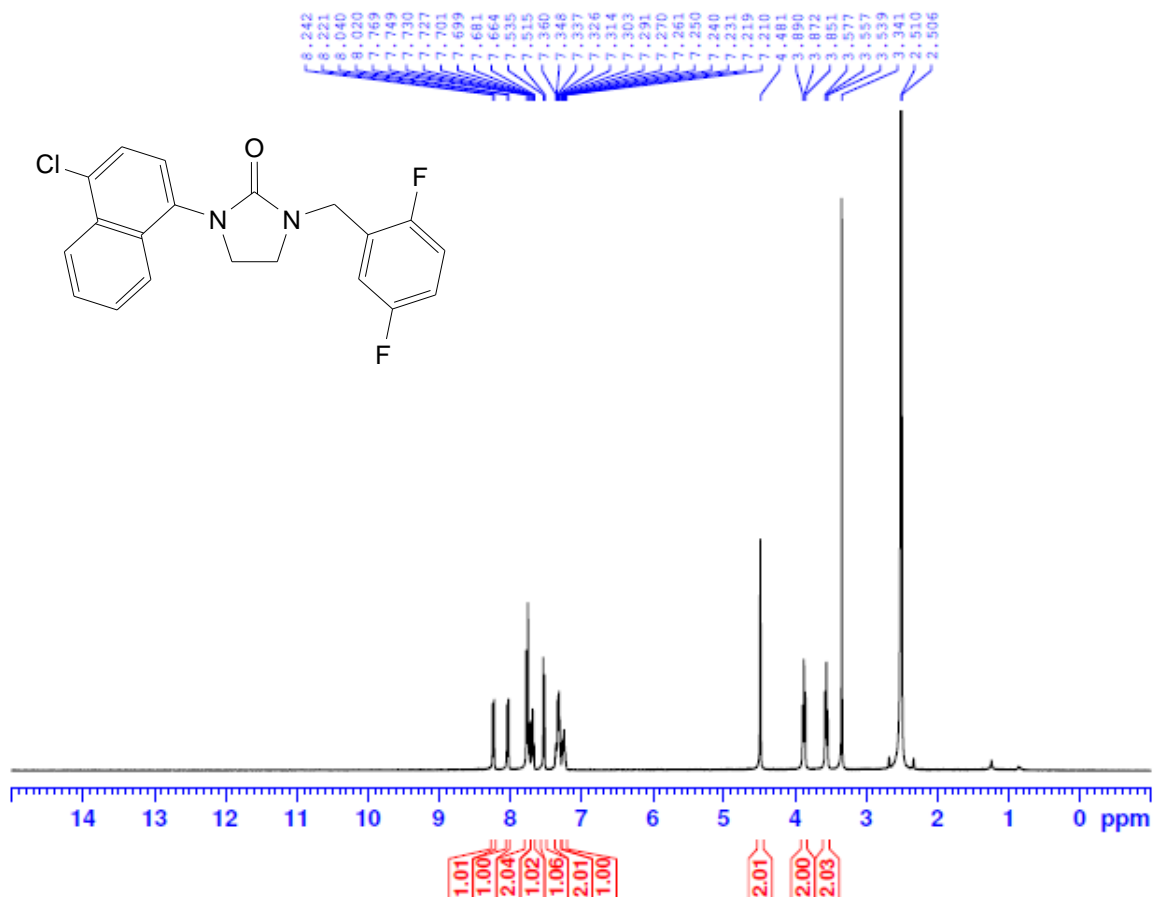


5.5.9 ^1H NMR Spectrum (400 MHz, DMSO) of compound 1e

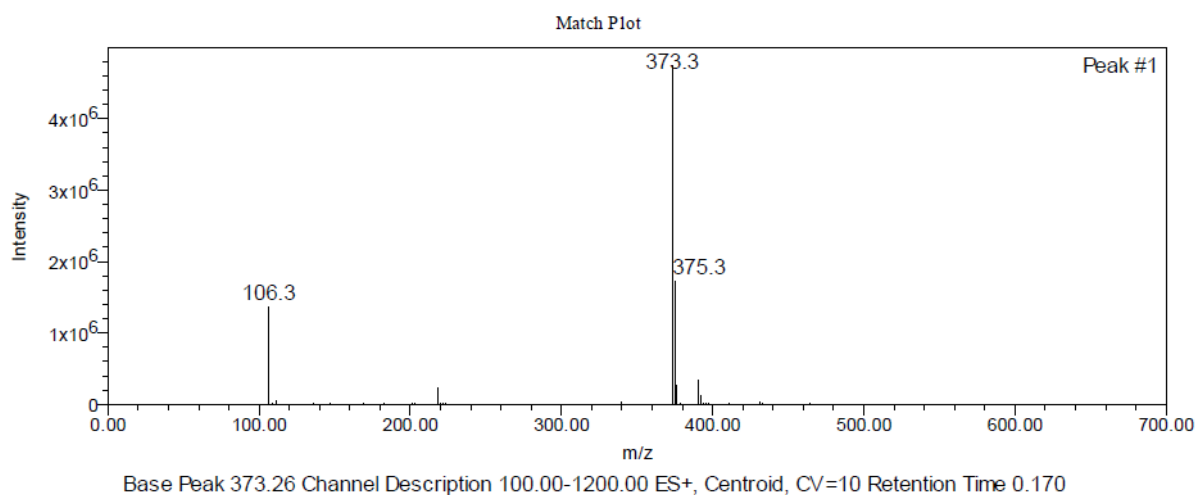


5.5.10 ESI-MS Spectrum of compound 1e

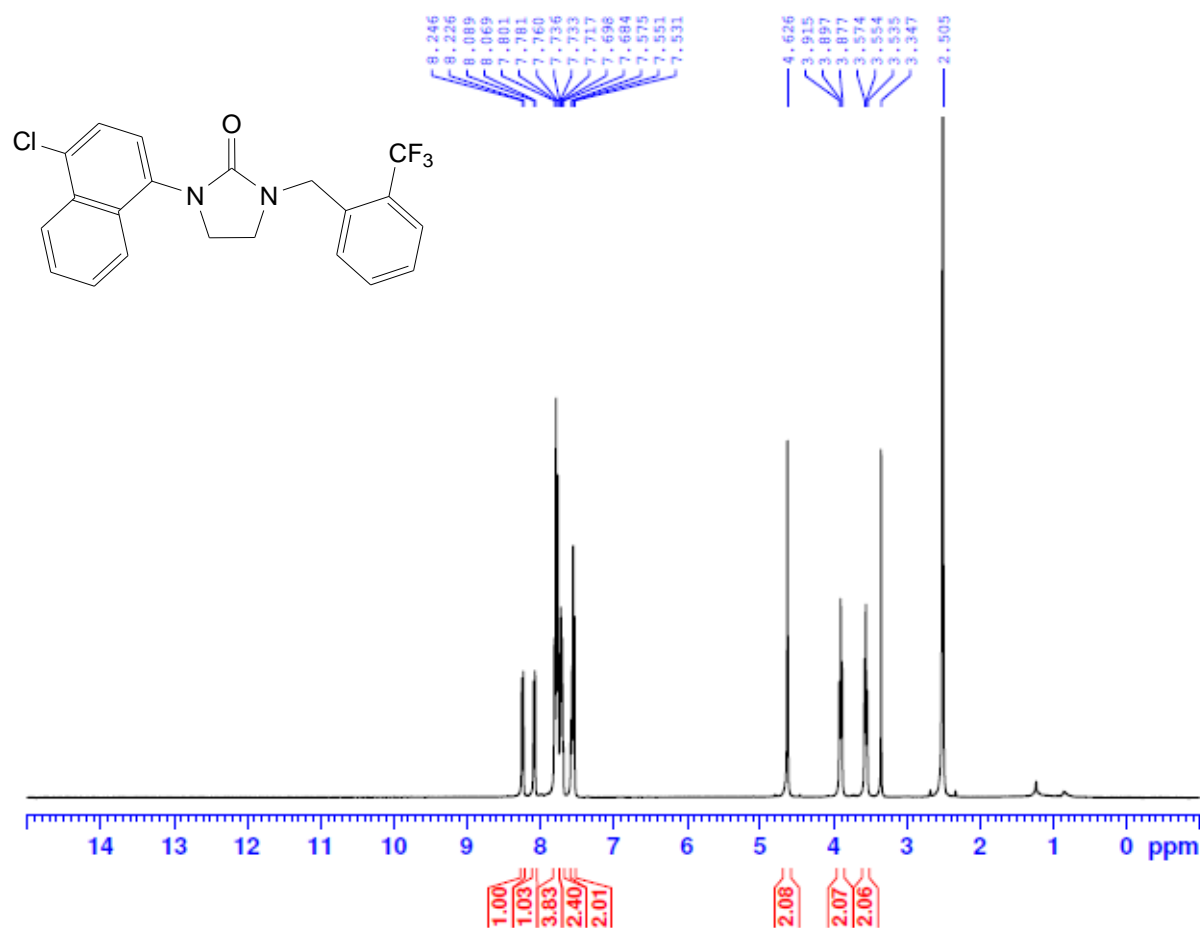


5.5.11 ^1H NMR Spectrum (400 MHz, DMSO) of compound 1f

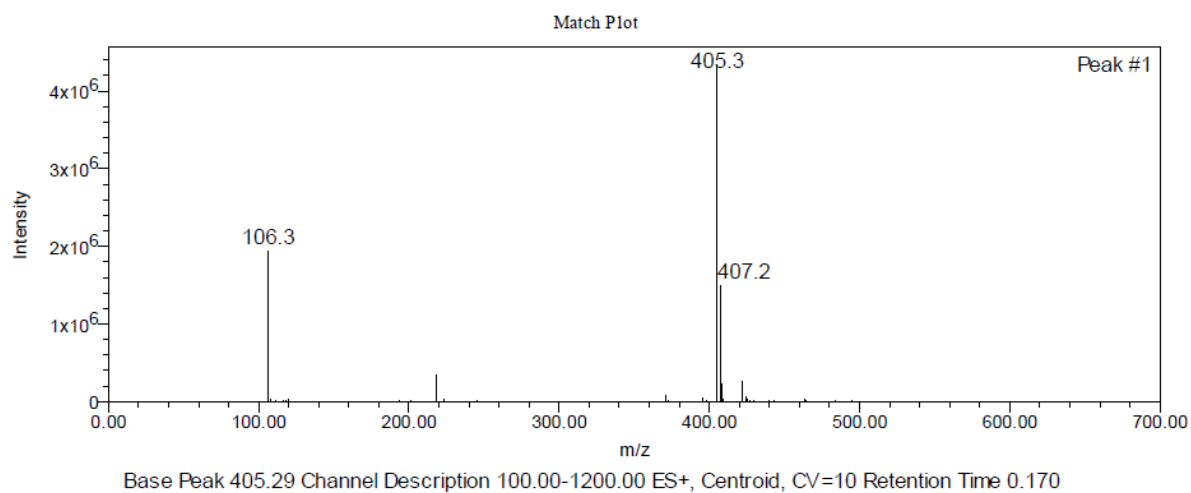
5.5.12 ESI-MS Spectrum of compound 1f

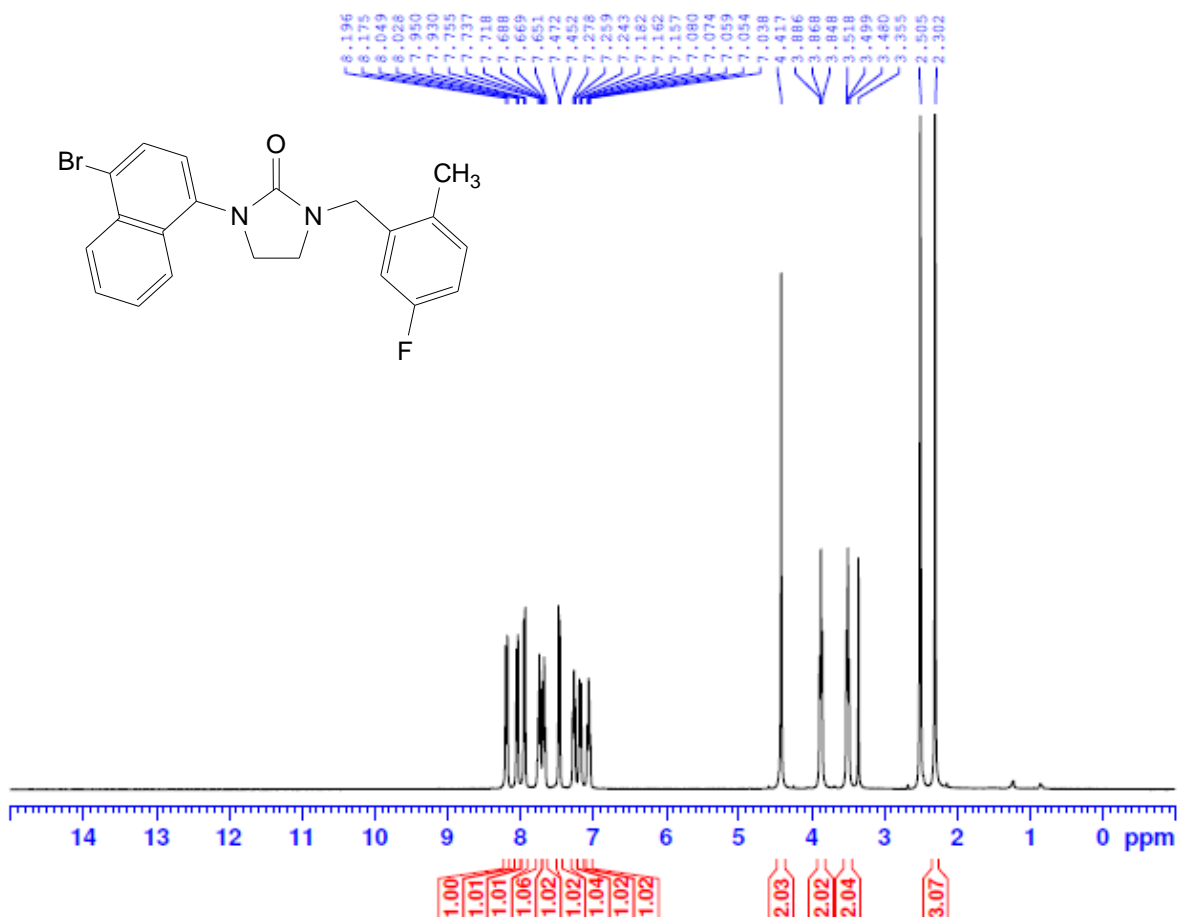


5.5.13 ^1H NMR Spectrum (400 MHz, DMSO) of compound 1g

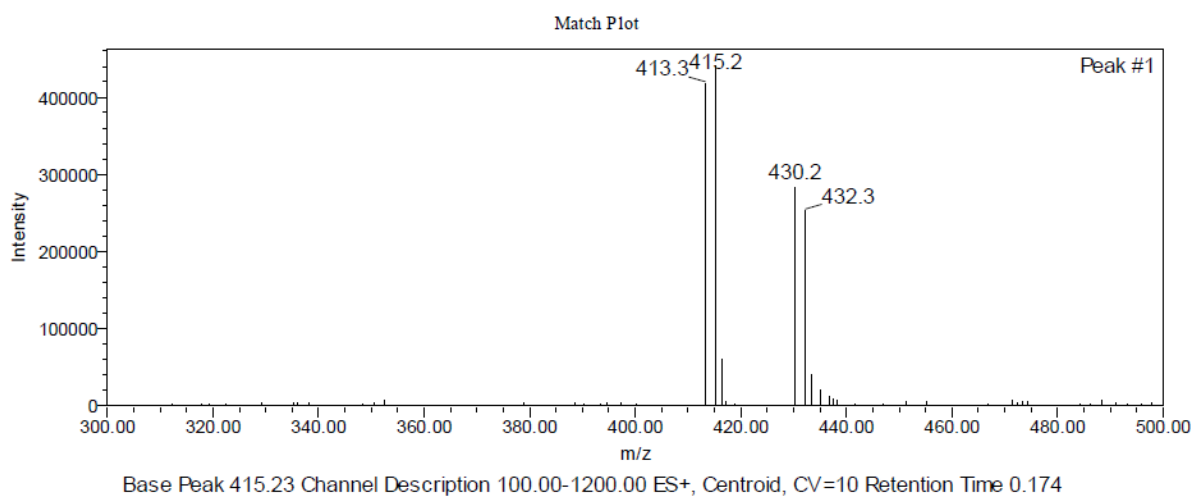


5.5.14 ESI-MS Spectrum of compound 1g

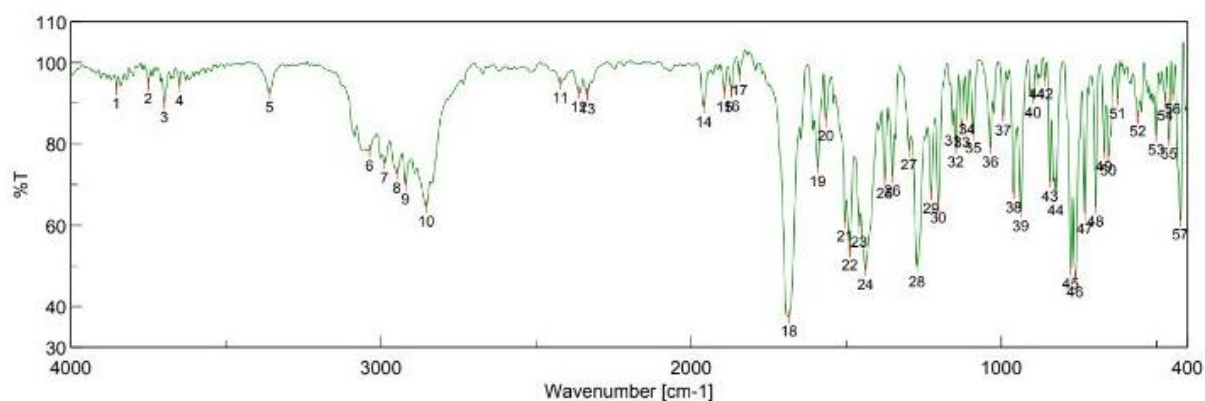


5.5.15 ^1H NMR Spectrum (400 MHz, DMSO) of compound 1h

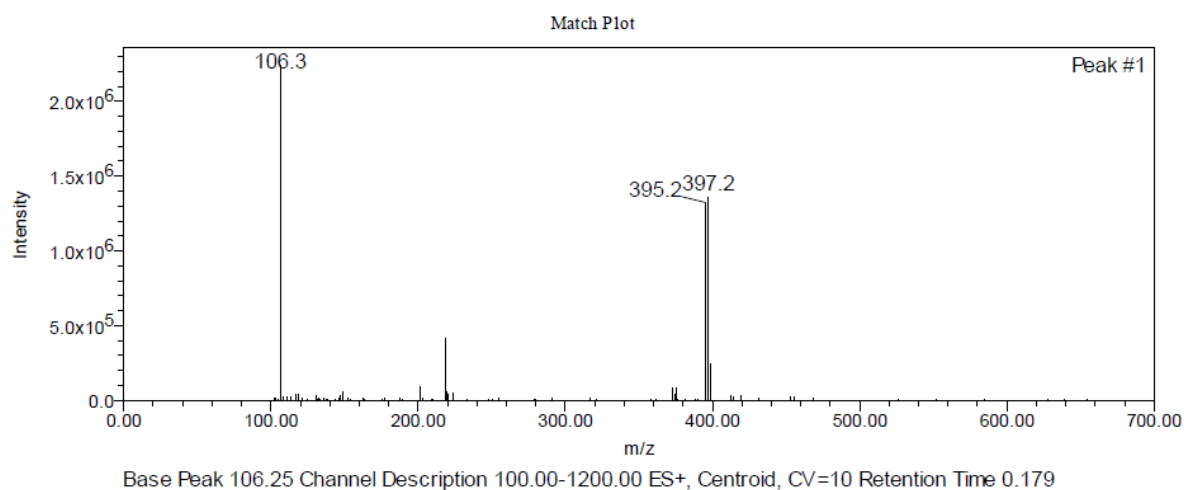
5.5.16 ESI-MS Spectrum of compound 1h

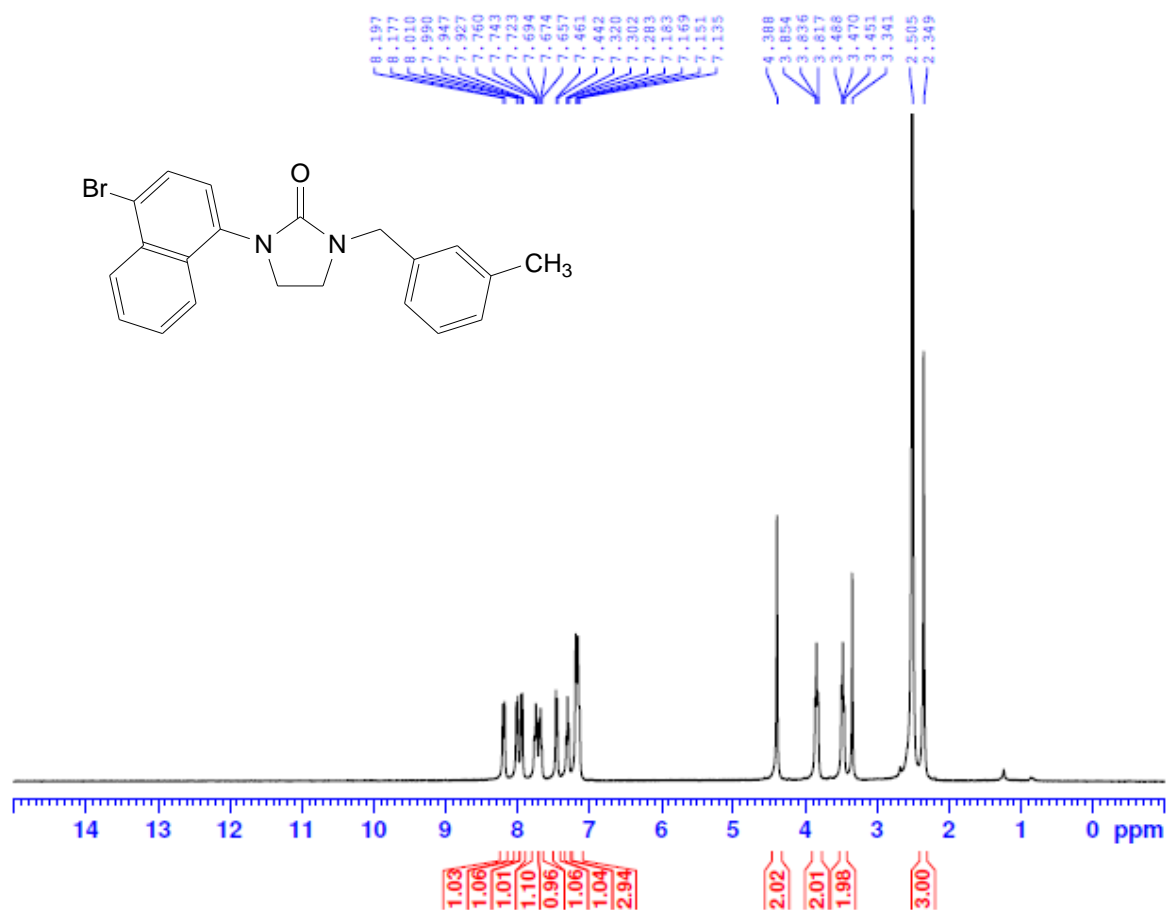


5.5.17 IR Spectrum (KBr, cm^{-1}) of compound 1i

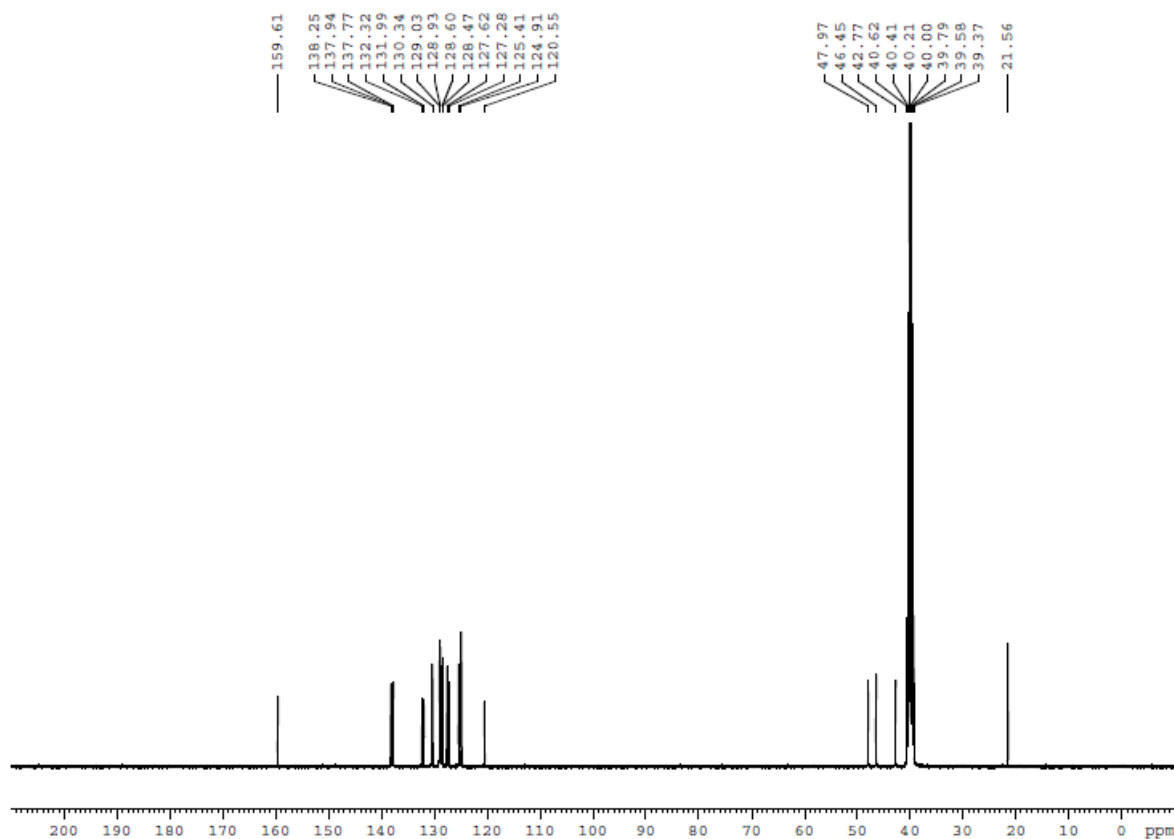


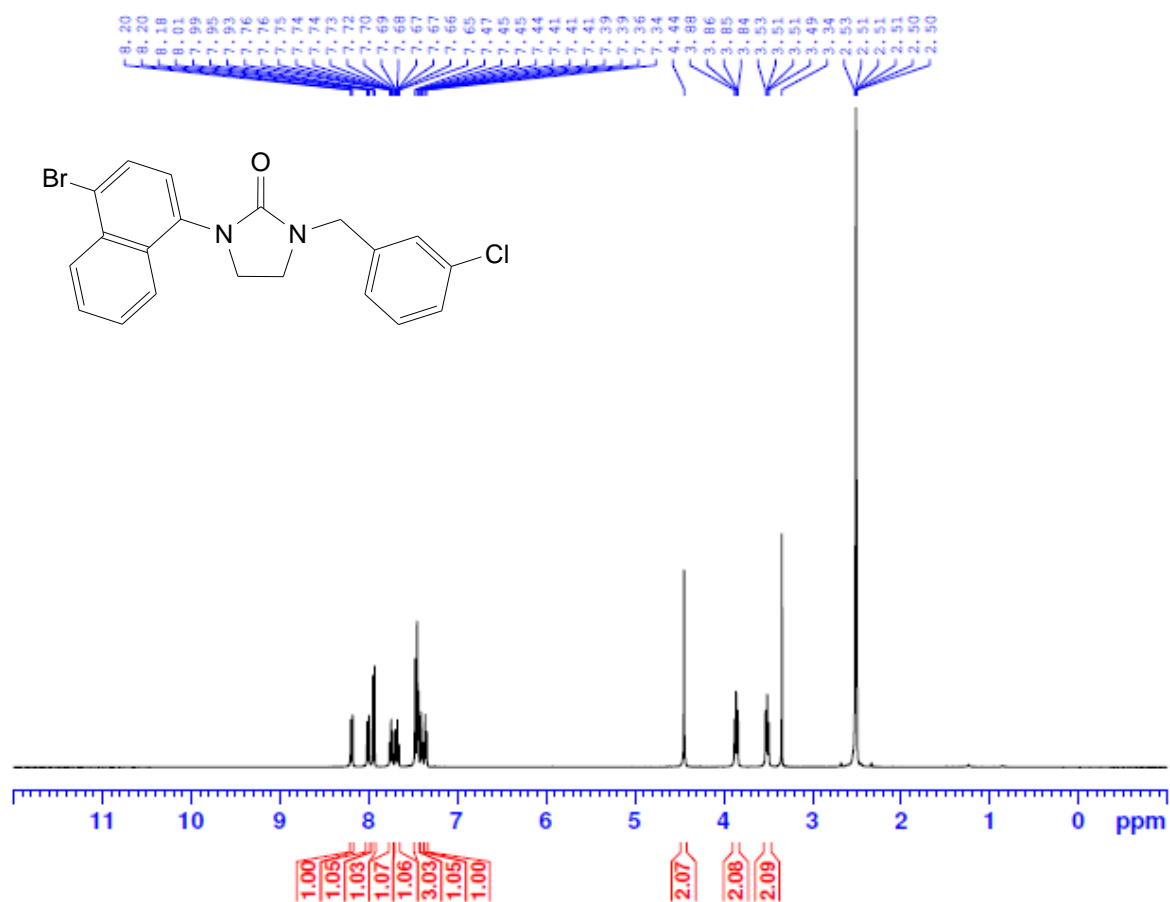
5.5.18 ESI-MS Spectrum of compound 1i



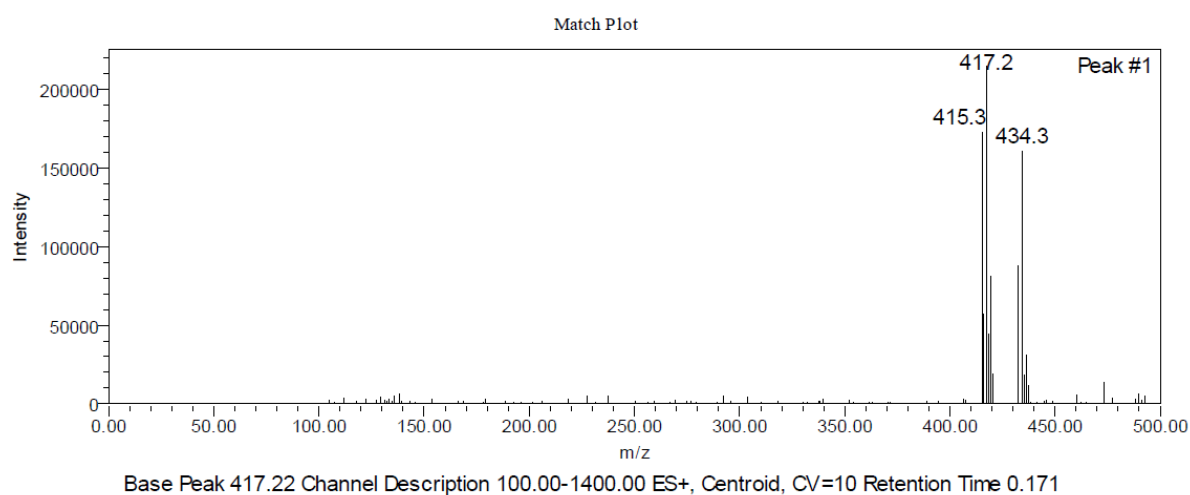
5.5.19 ^1H NMR Spectrum (400 MHz, DMSO) of compound 1i

5.5.20 ^{13}C NMR Spectrum of compound (101 MHz, DMSO) of compound 1i

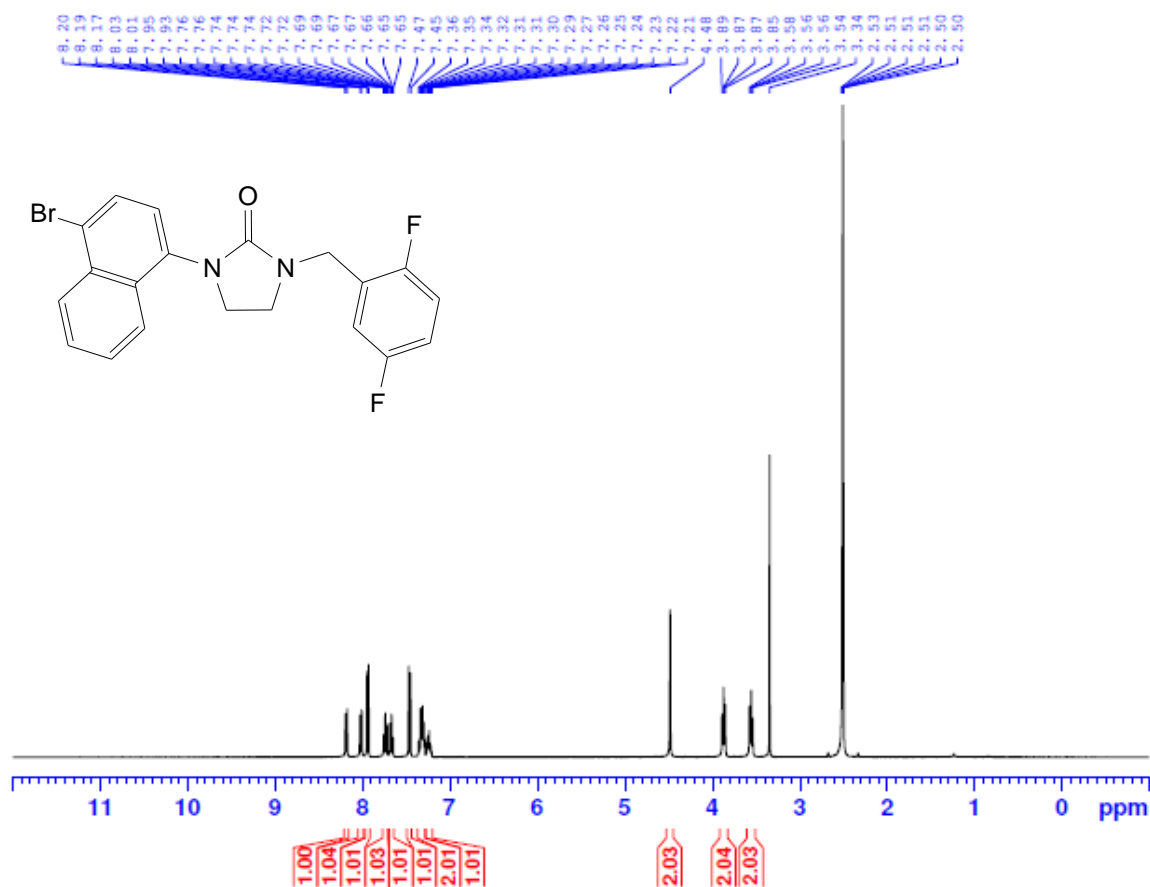


5.5.21 ^1H NMR Spectrum (400 MHz, DMSO) of compound 1j

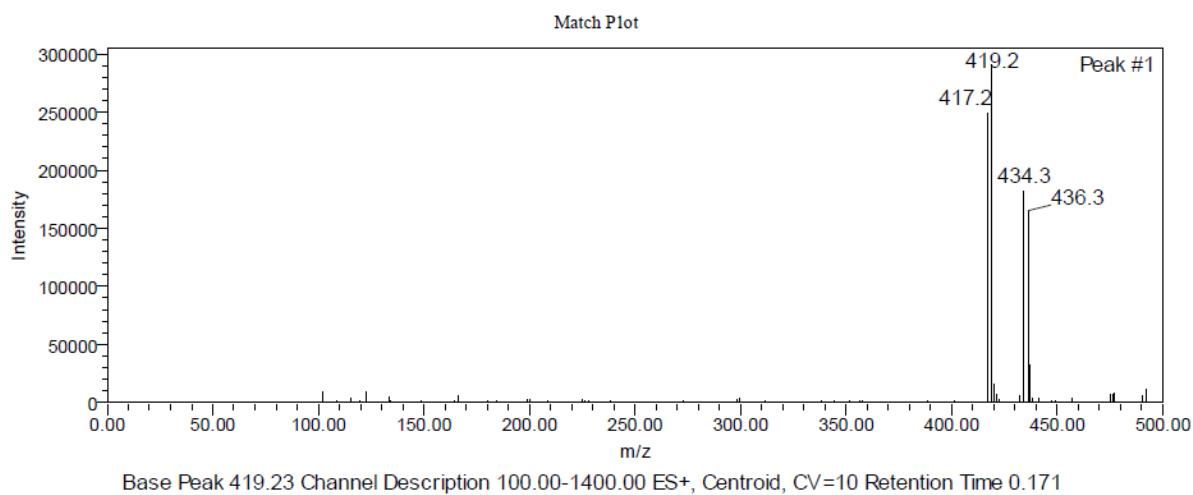
5.5.22 ESI-MS Spectrum of compound 1j

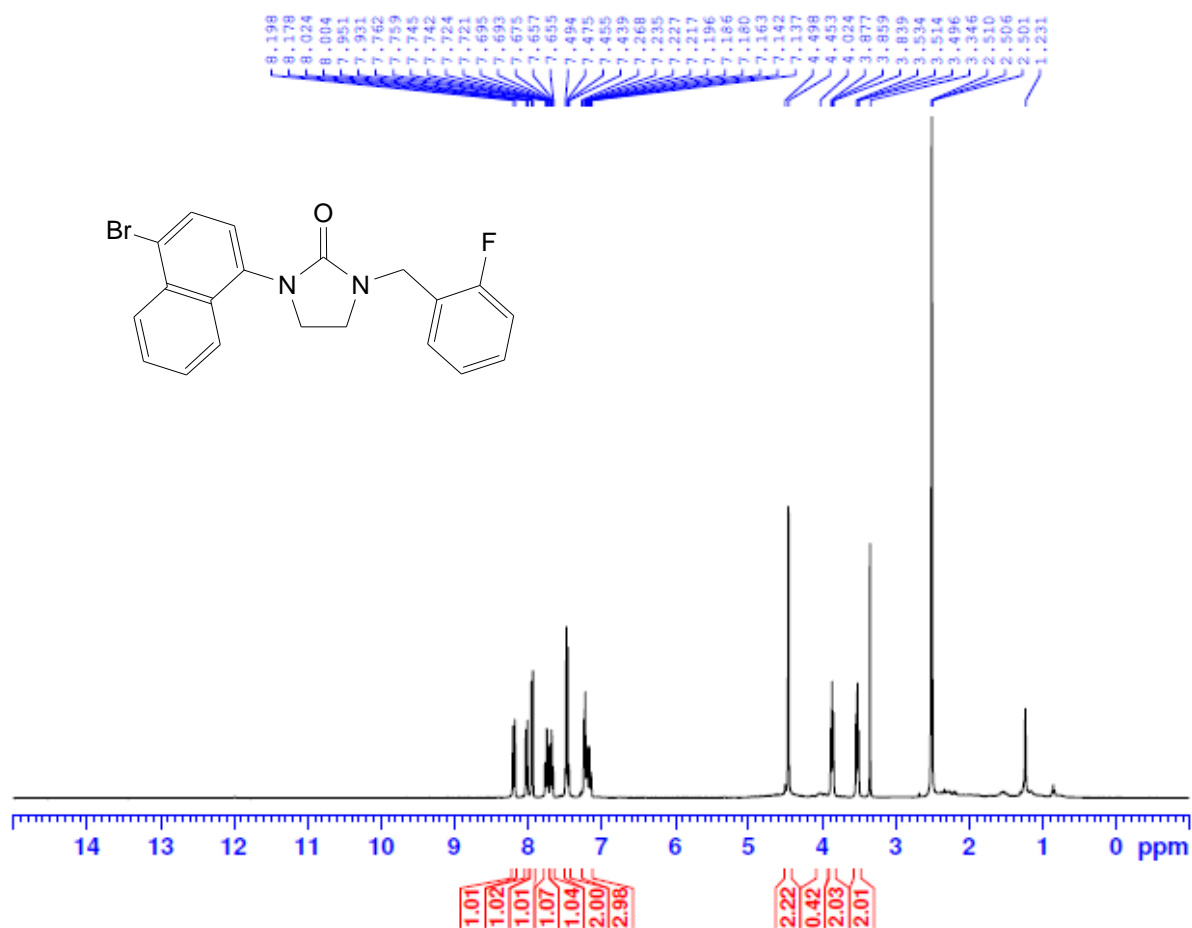


5.5.23 ^1H NMR Spectrum of compound (400 MHz, DMSO) of compound 1k

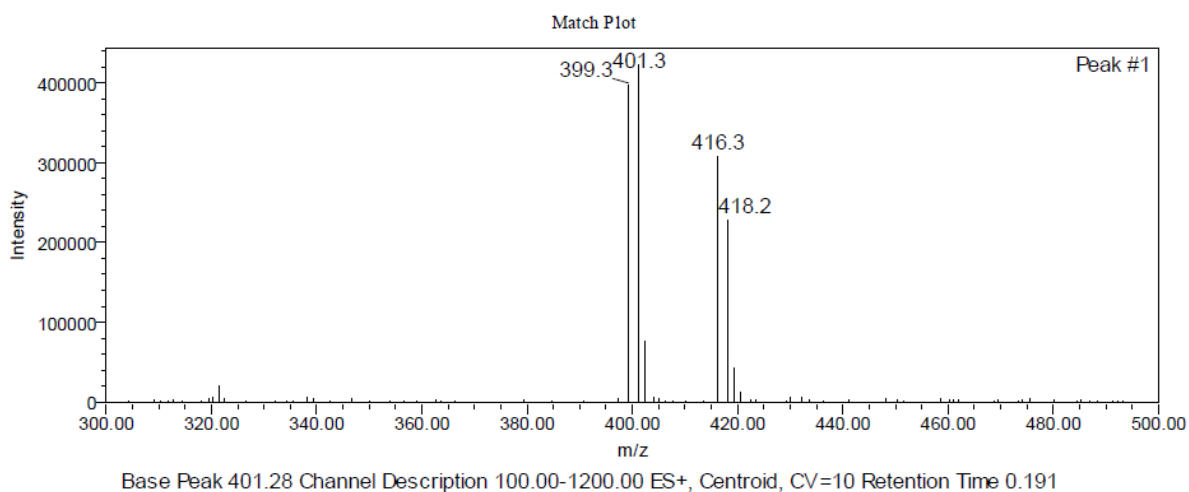


5.5.24 ESI-MS Spectrum of compound 1k

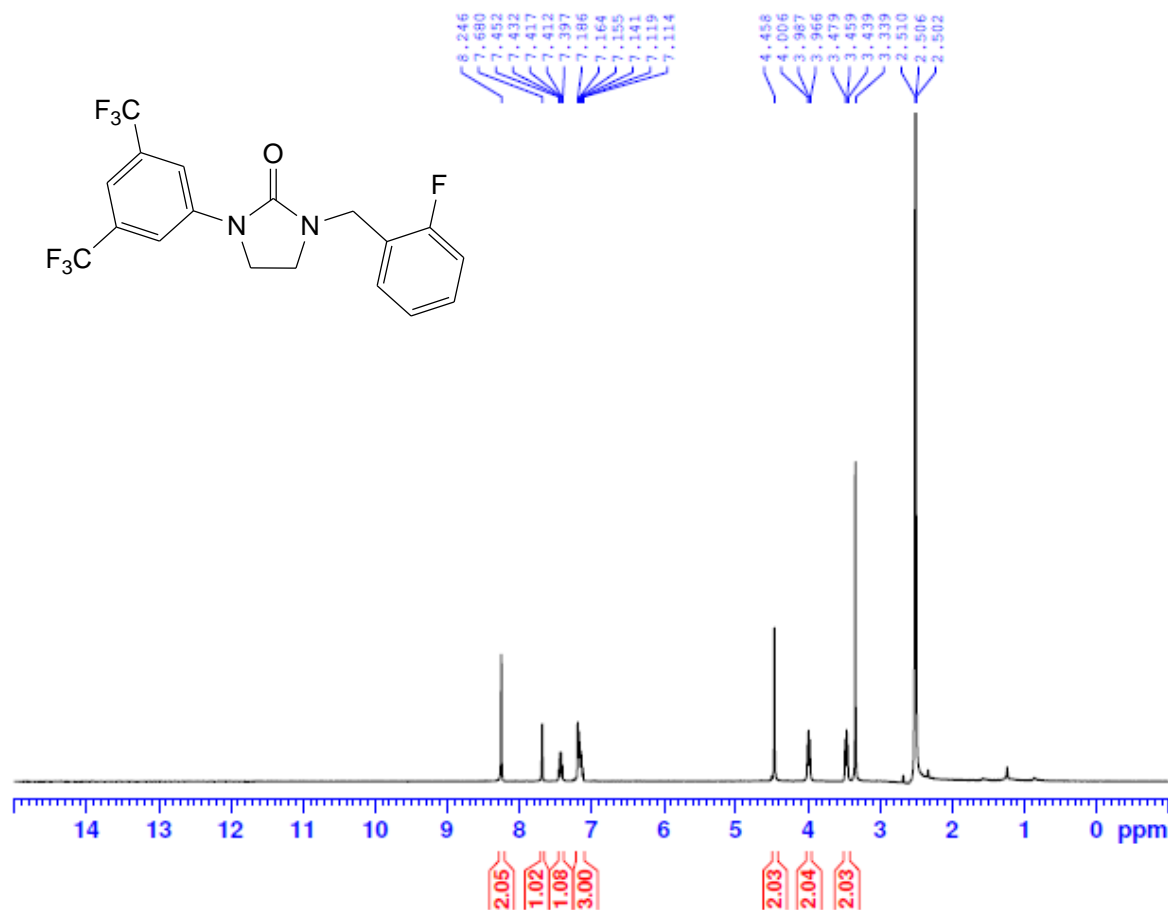


5.5.25 ^1H NMR Spectrum of compound (400 MHz, DMSO) of compound 11

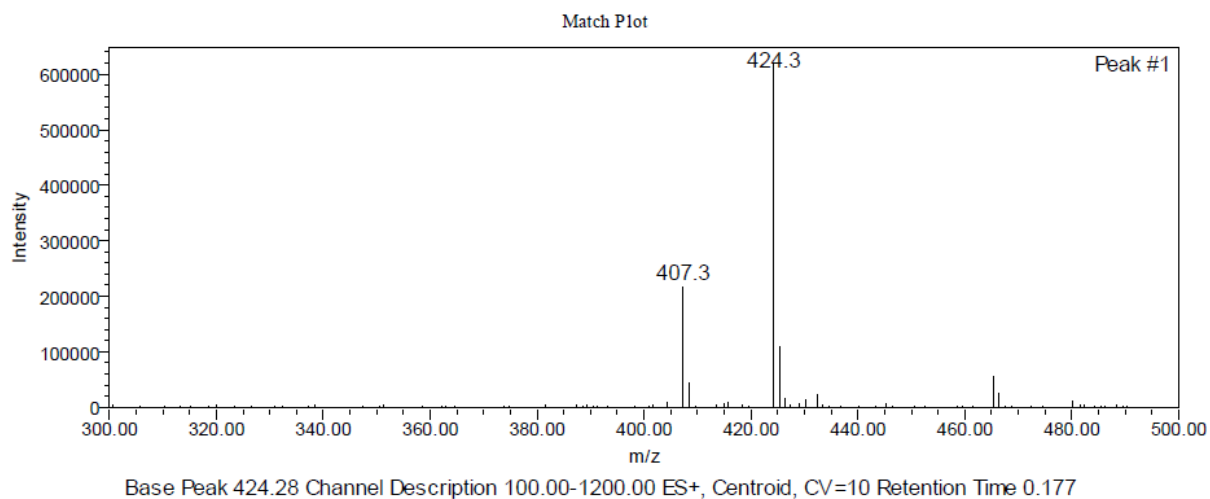
5.5.26 ESI-MS Spectrum of compound 11



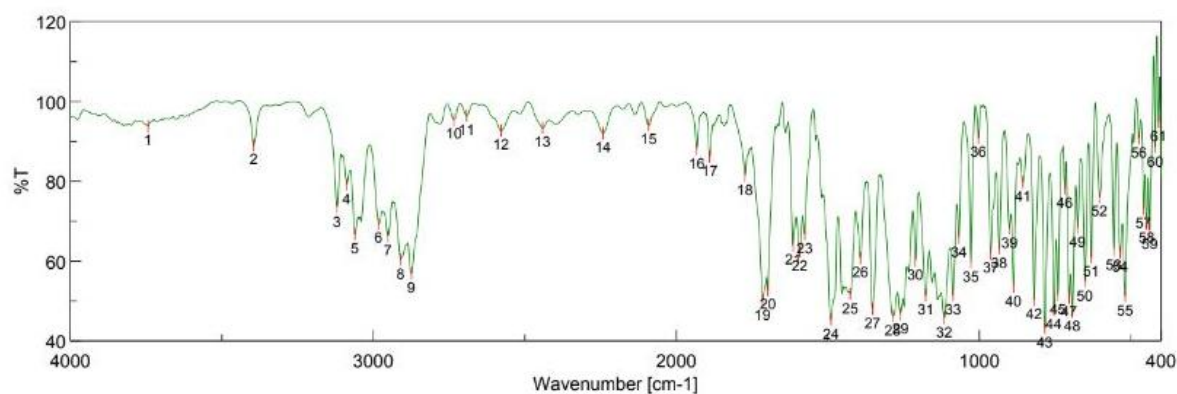
5.5.27 ^1H NMR Spectrum of compound (400 MHz, DMSO) of compound 1m



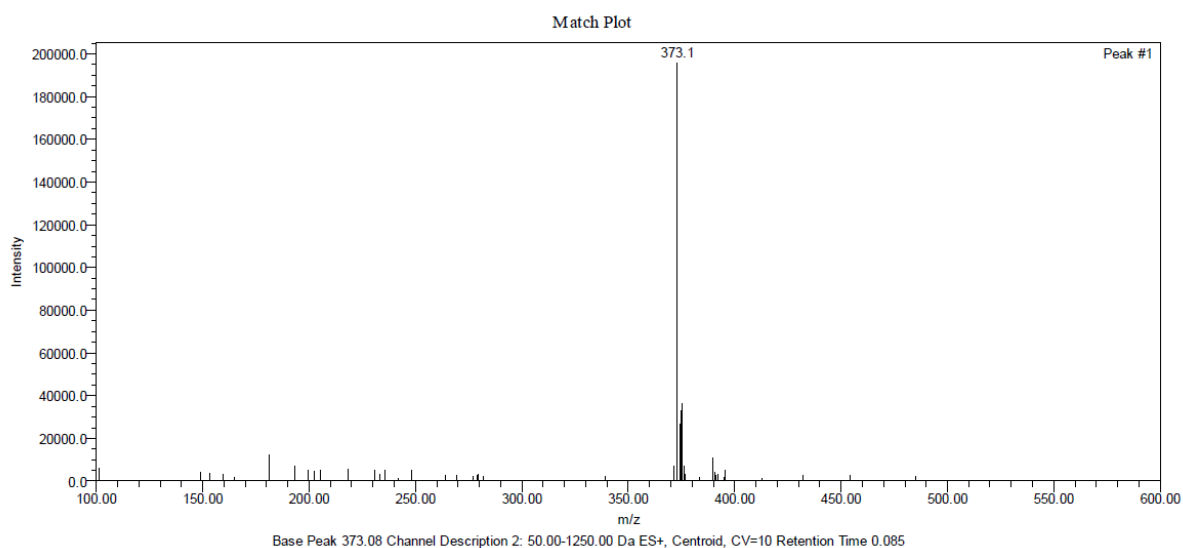
5.5.28 ESI-MS Spectrum of compound 1m



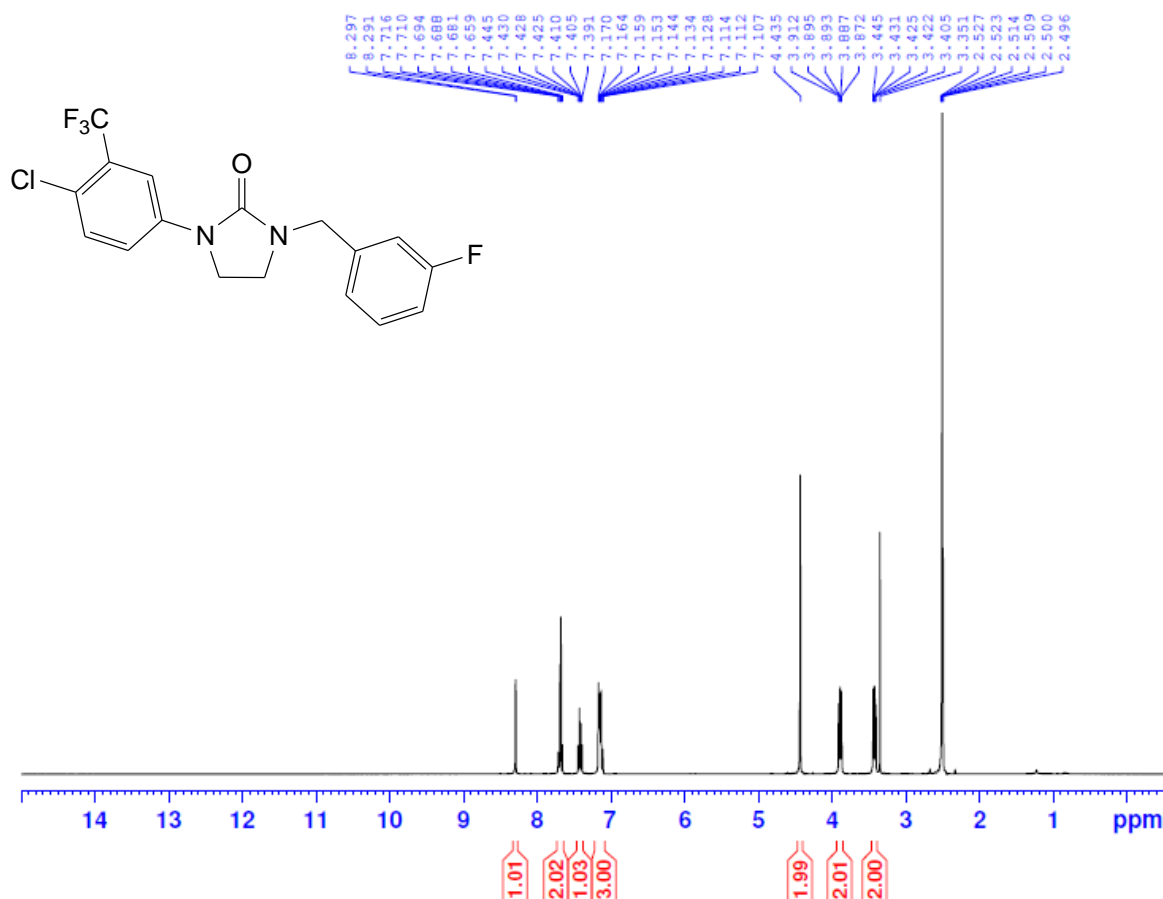
5.5.29 IR Spectrum (KBr, cm^{-1}) of compound 1n

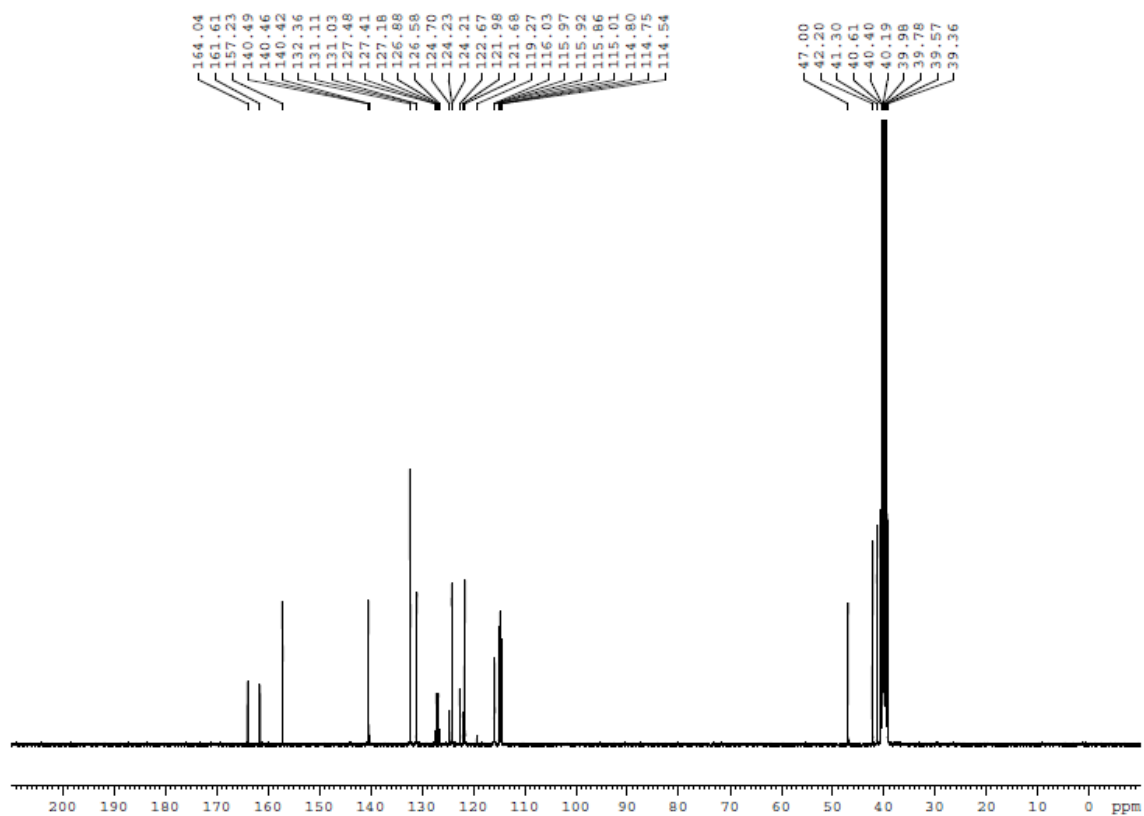


5.5.30 ESI-MS Spectrum of compound 1n

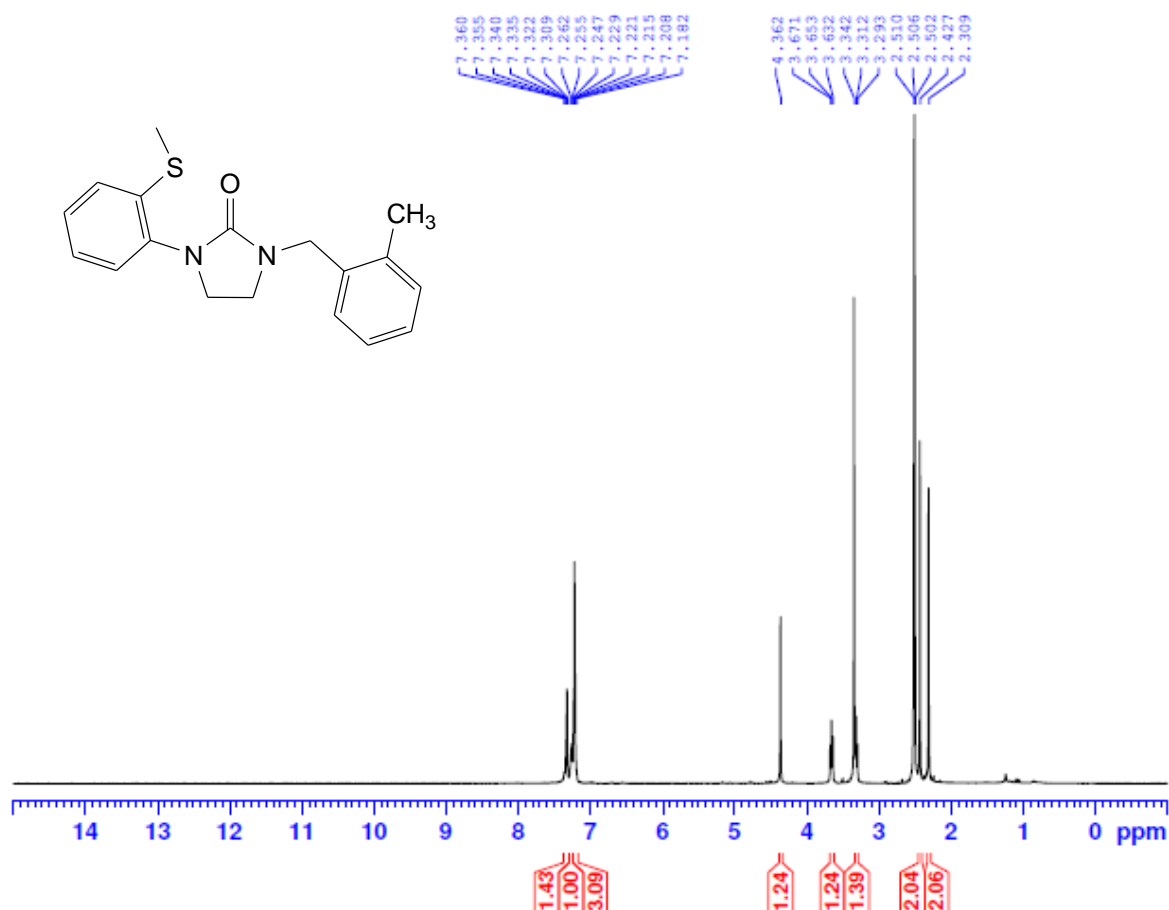


5.5.31 ^1H NMR Spectrum (400 MHz, DMSO) of compound 1n

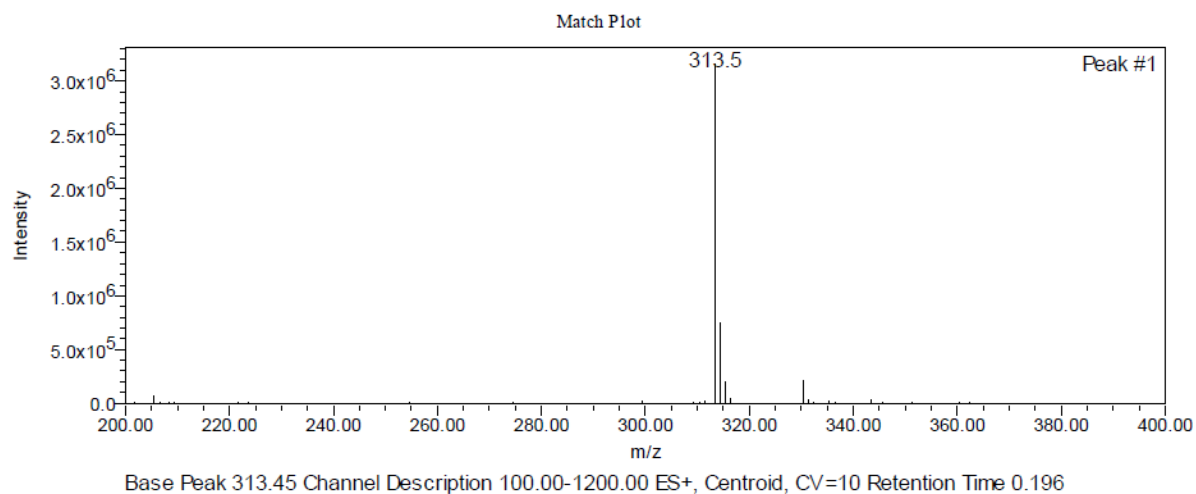


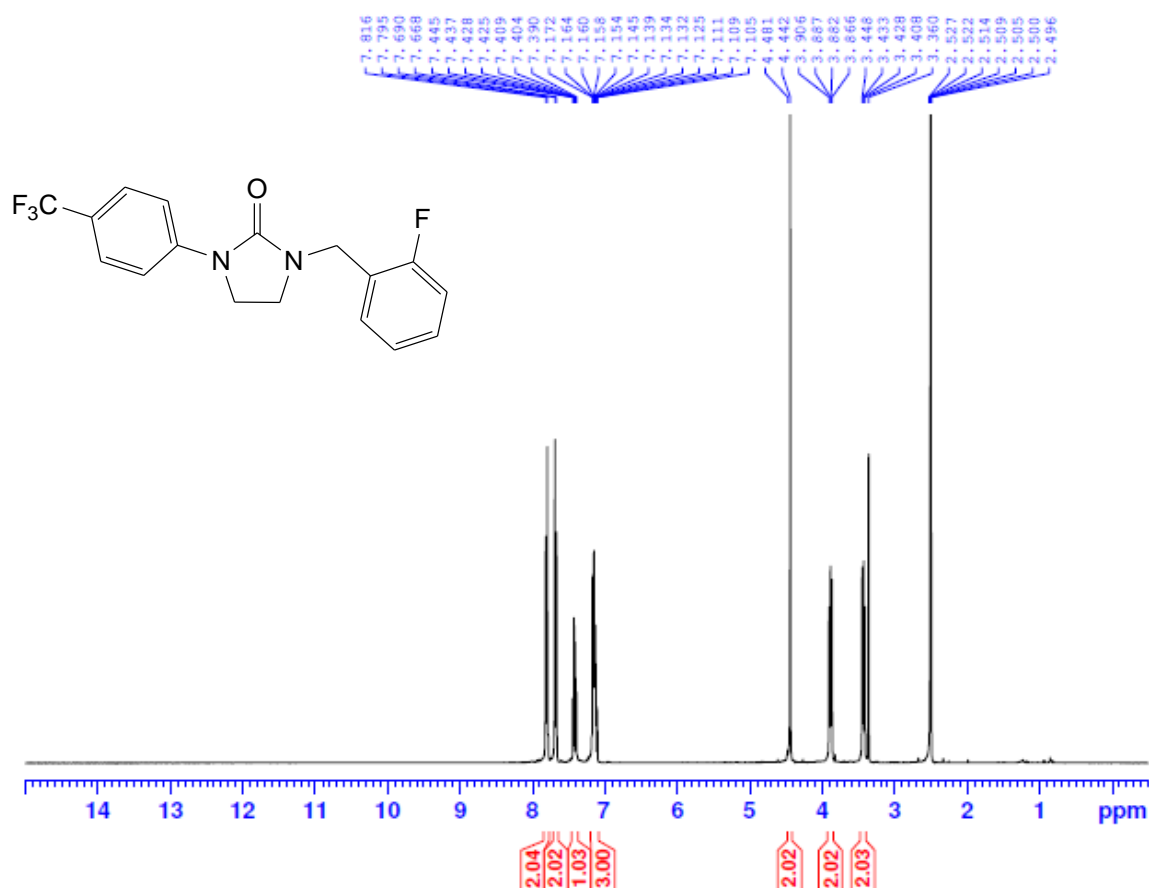
5.5.32 ^{13}C NMR Spectrum of compound (101 MHz, DMSO) of compound 1n

5.5.33 ^1H NMR Spectrum (400 MHz, DMSO) of compound 1o

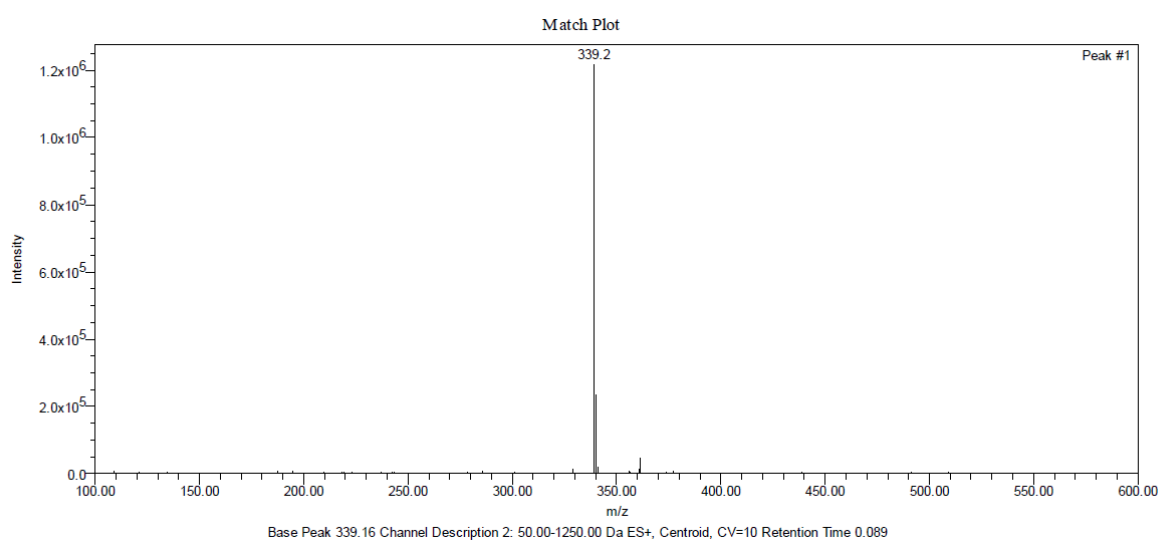


5.5.34 ESI-MS Spectrum of compound 1o

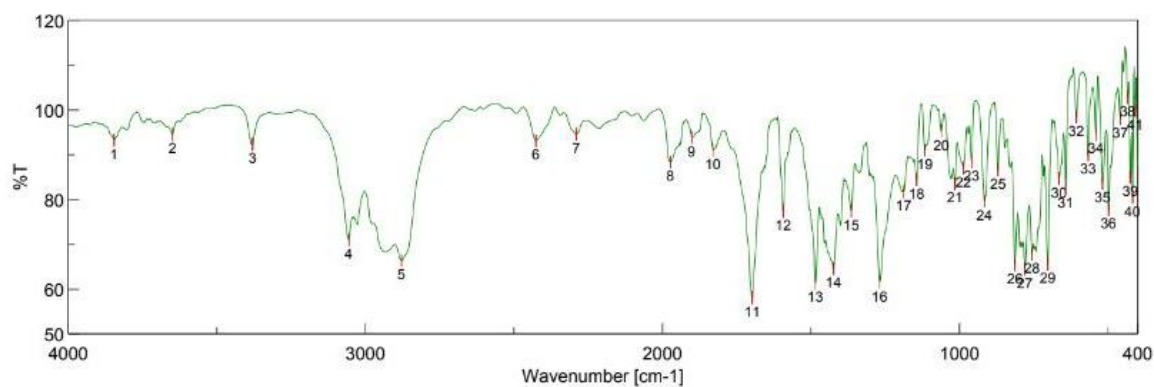


5.5.35 ^1H NMR Spectrum (400 MHz, DMSO) of compound 1p

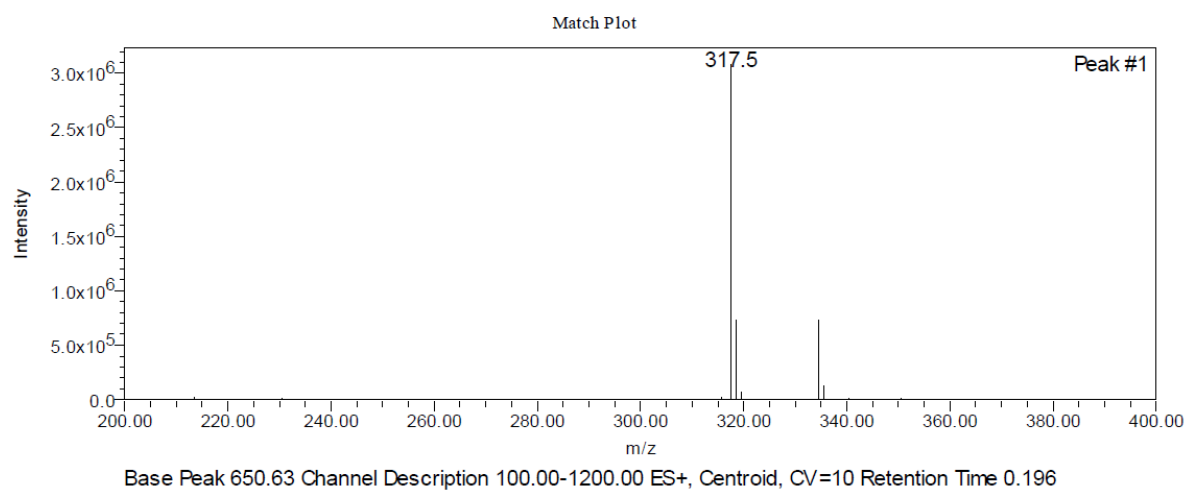
5.5.36 ESI-MS Spectrum of compound 1p

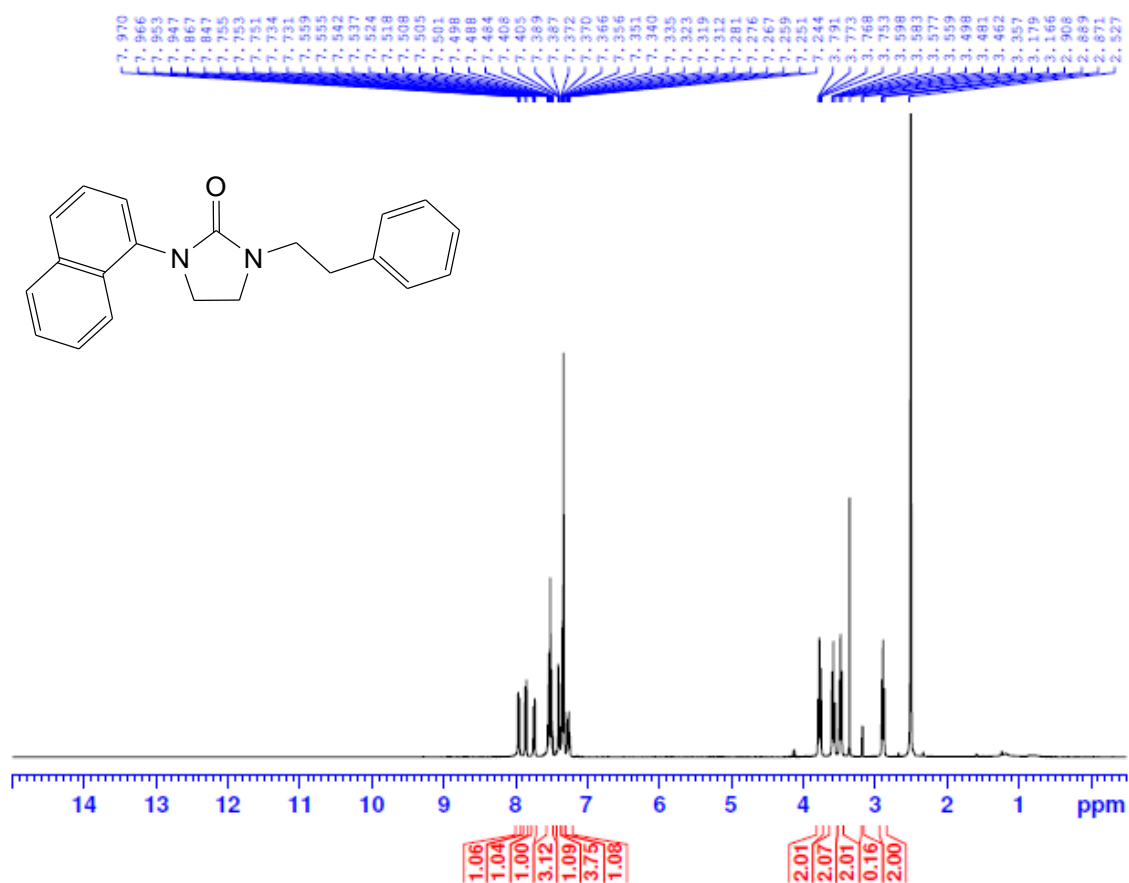


5.5.37 IR Spectrum (KBr, cm^{-1}) of compound 2a

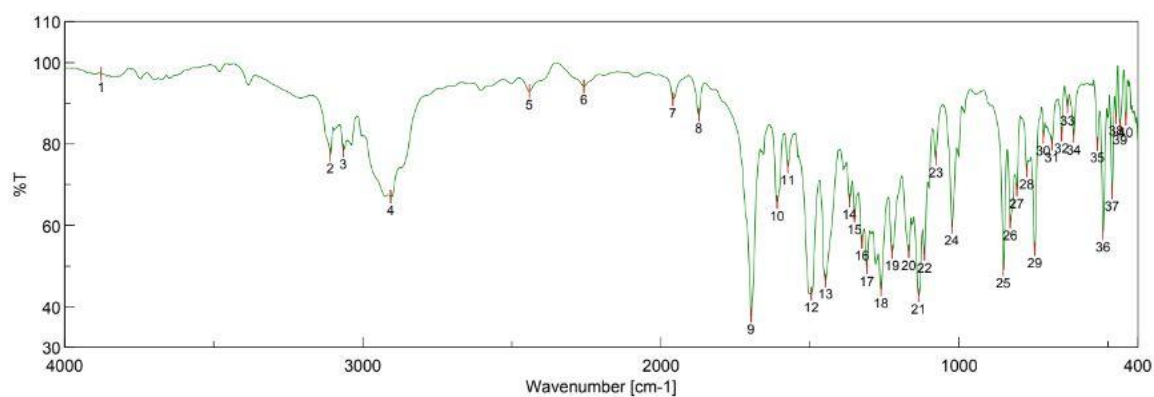


5.5.38 ESI-MS Spectrum of compound 2a

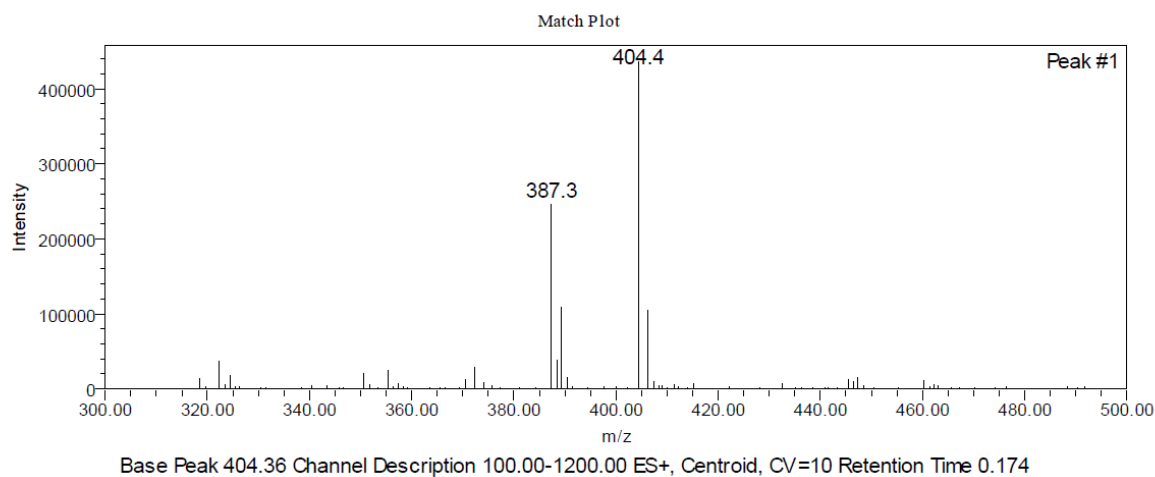


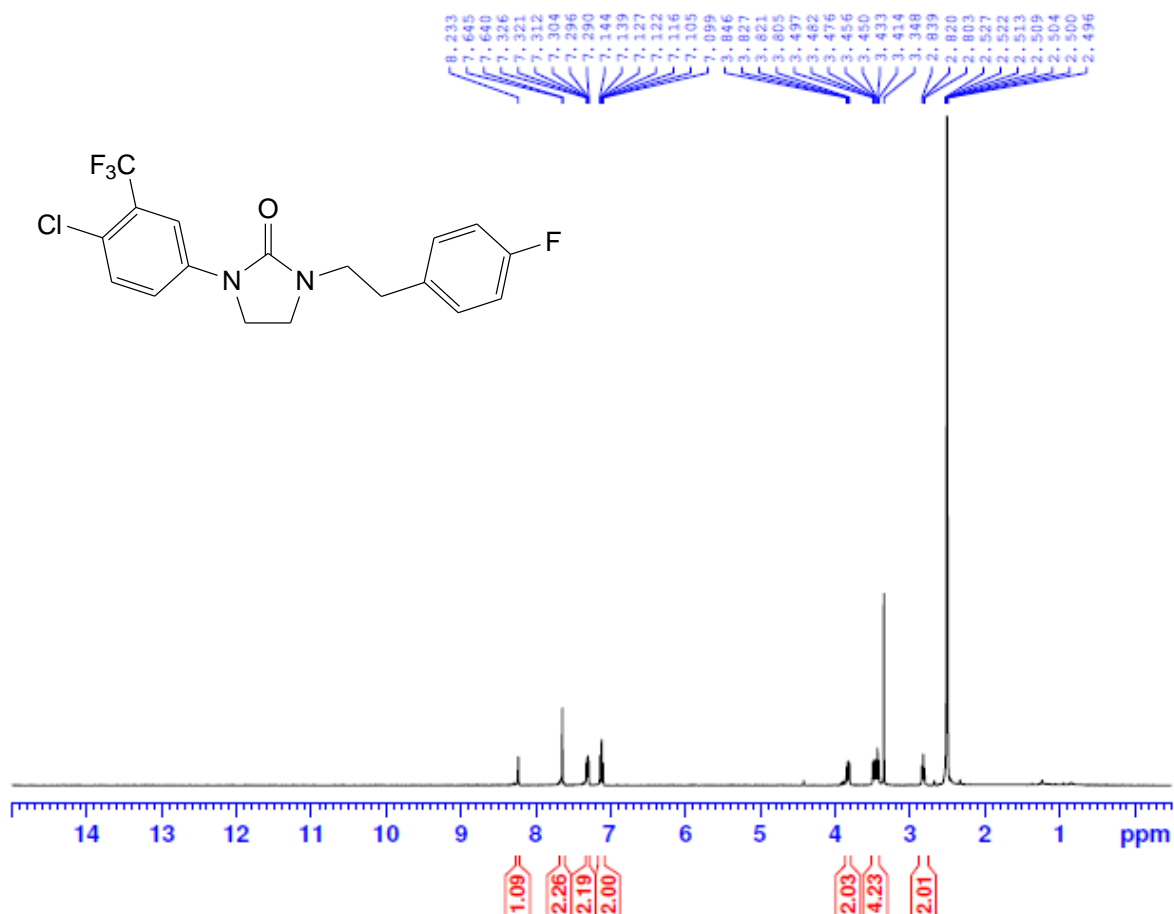
5.5.39 ^1H NMR Spectrum (400 MHz, DMSO) of compound 2a

5.5.40 IR Spectrum (KBr, cm^{-1}) of compound 2b

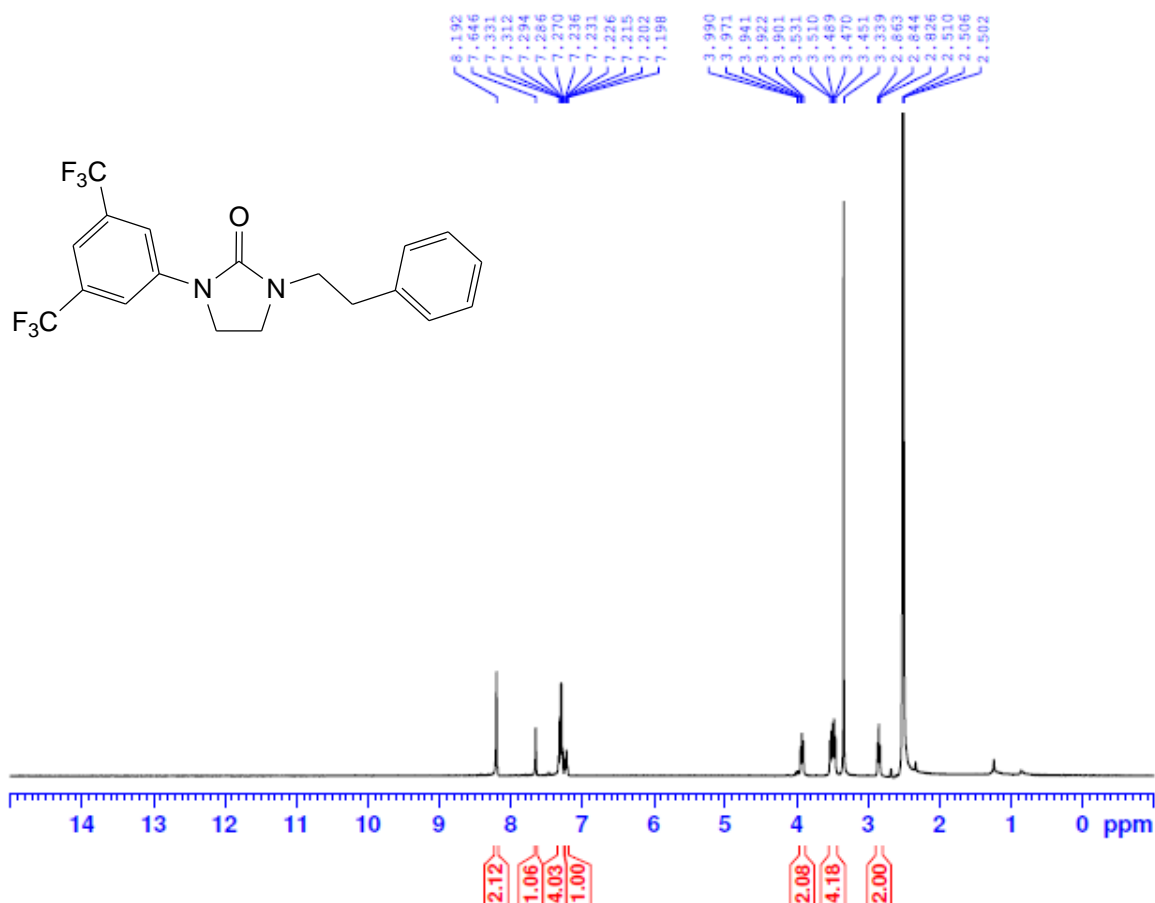


5.5.41 ESI-MS Spectrum of compound 2b

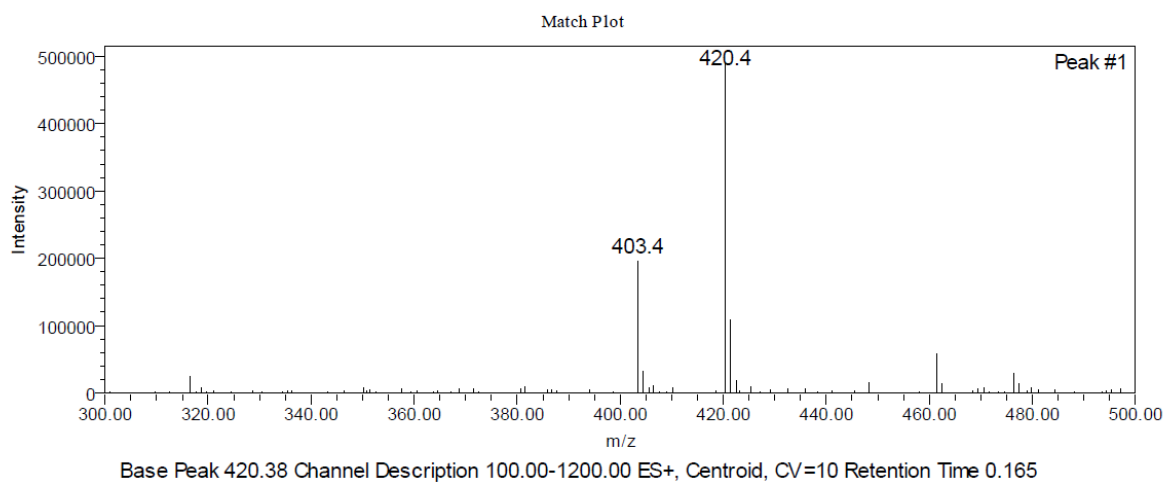


5.5.42 ^1H NMR Spectrum (400 MHz, DMSO) of compound 2b

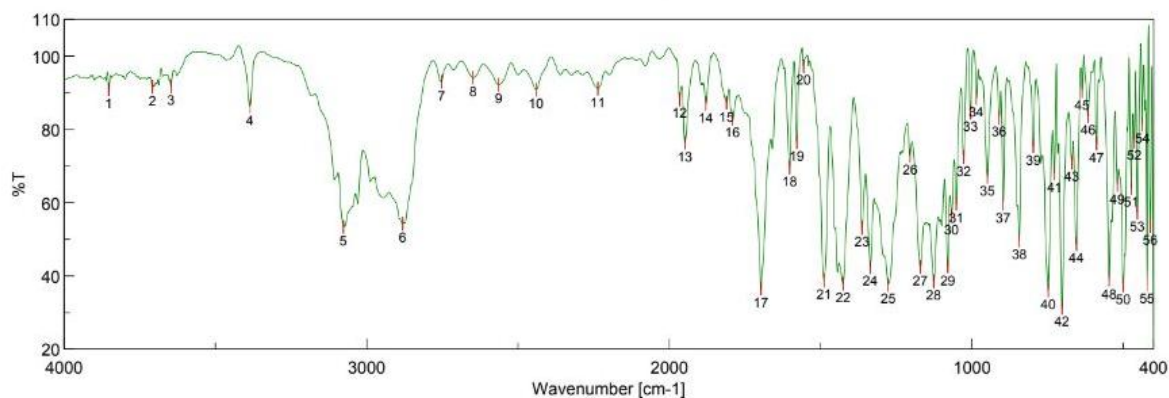
5.5.43 ^1H NMR Spectrum (400 MHz, DMSO) of compound 2c



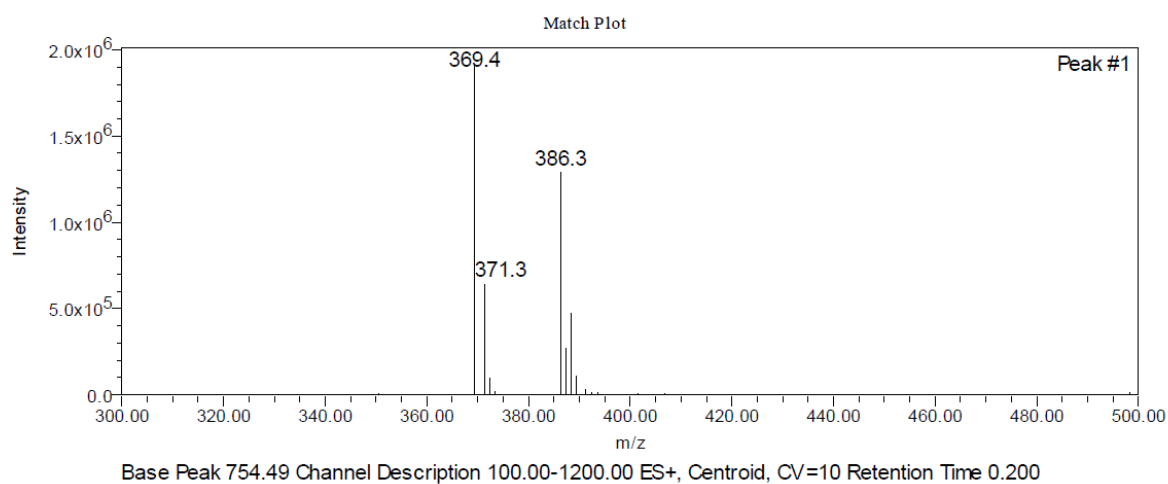
5.5.44 ESI-MS Spectrum of compound 2c



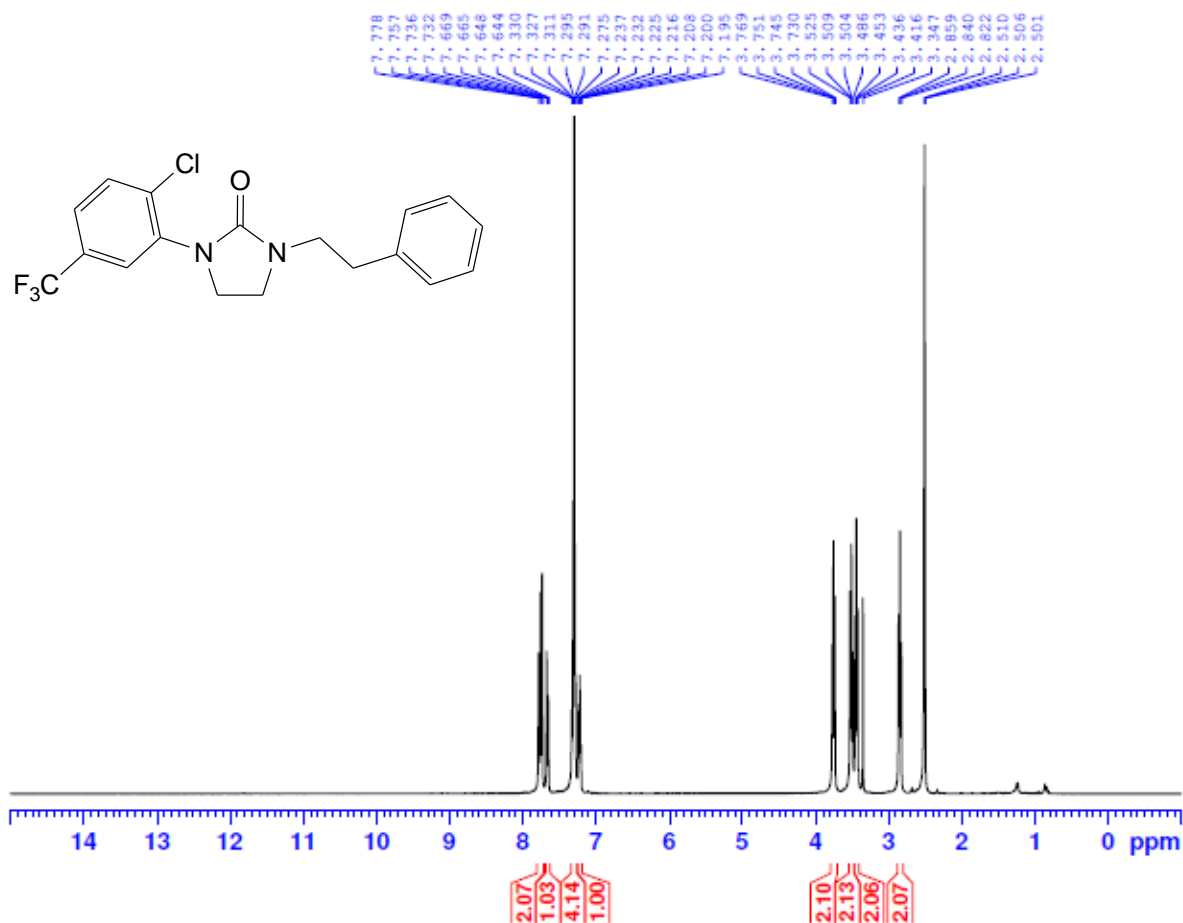
5.5.45 IR Spectrum (KBr, cm^{-1}) of compound 2d

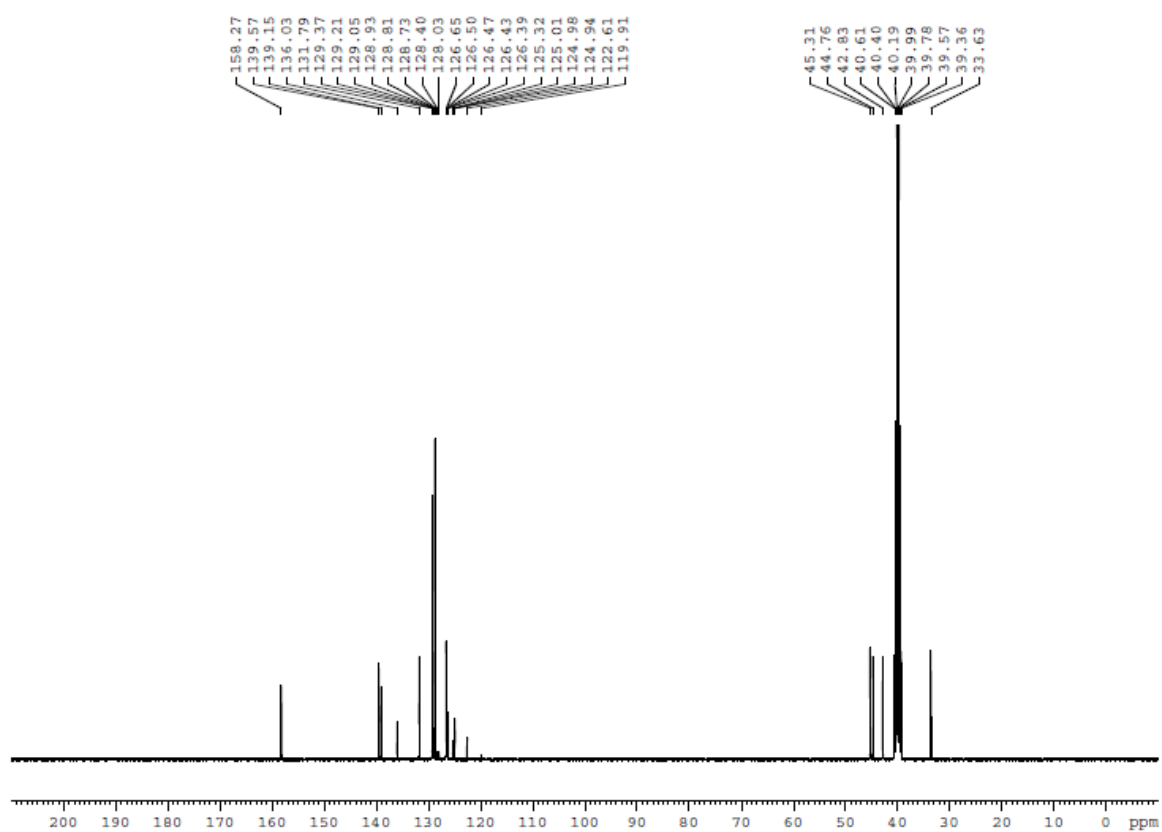


5.5.46 ESI-MS Spectrum of compound 2d

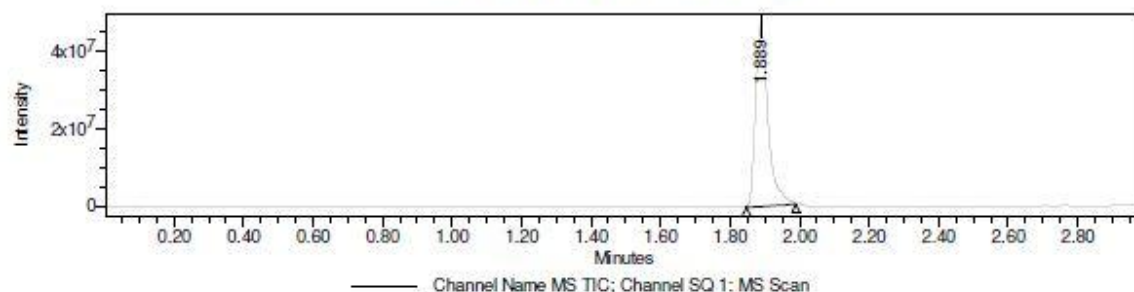
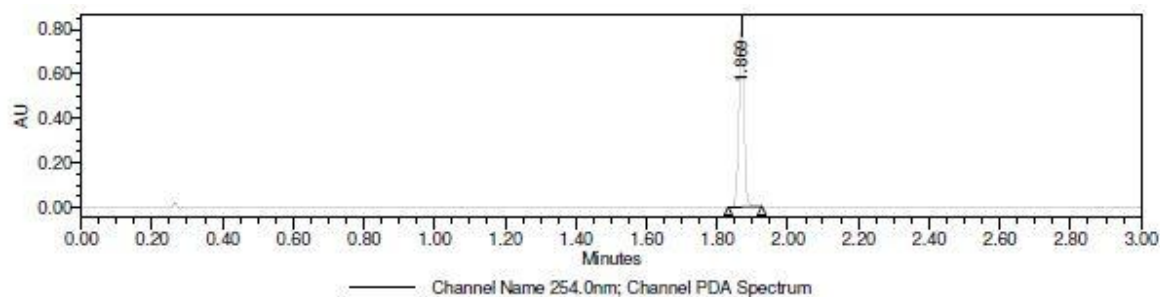


5.5.47 ^1H NMR Spectrum (400 MHz, DMSO) of compound 2d



5.5.48 ^{13}C NMR Spectrum (101 MHz, DMSO) of compound 2d

5.5.49 LC-MS Spectrum of compound 2d

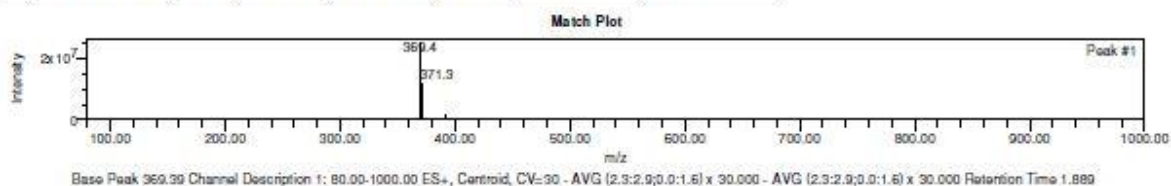


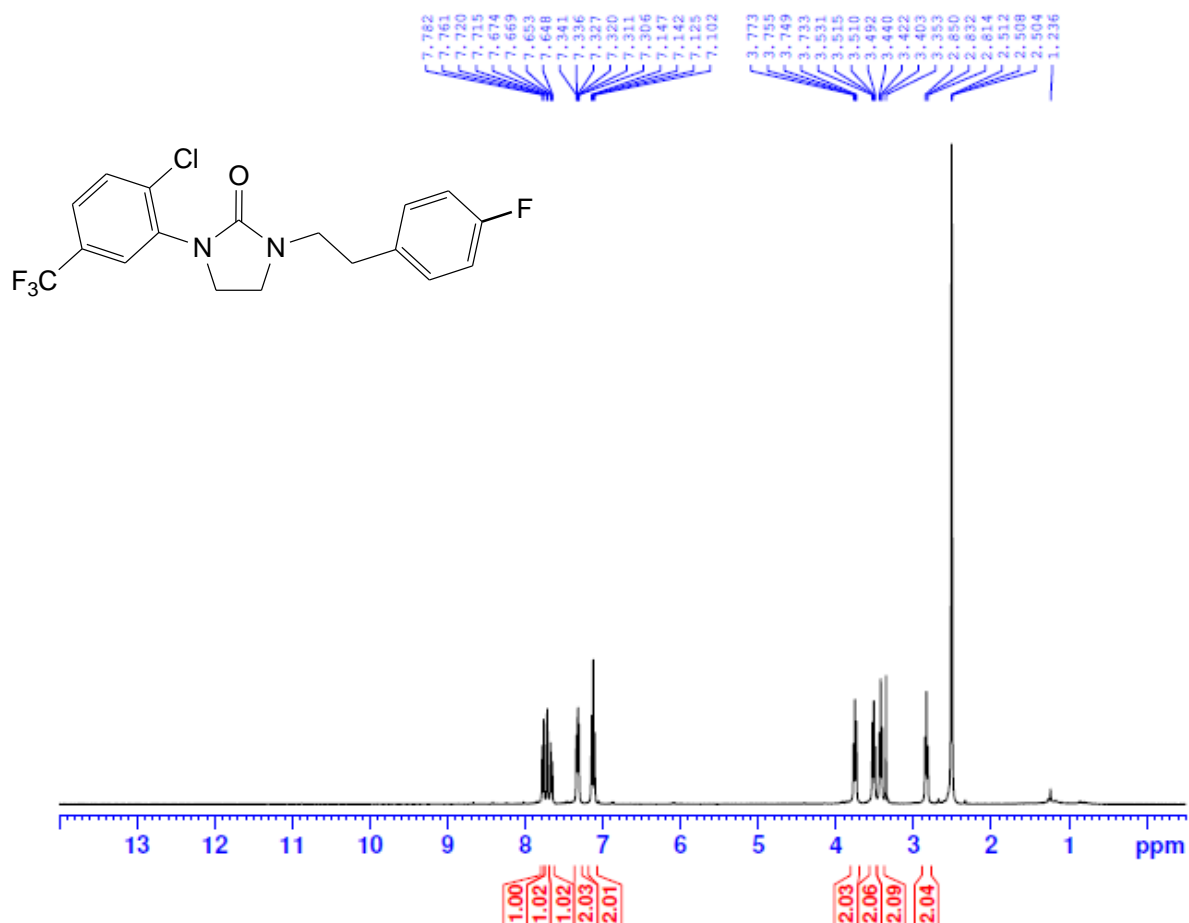
Peak Results
Channel: PDA Spectrum

	Retention Time (min)	Base Peak (m/z)	Height (μV)	Area (μV*sec)	% Area	Channel	Channel Name
1	1.889		827459	828141	100.00	PDA Spectrum	254.0nm

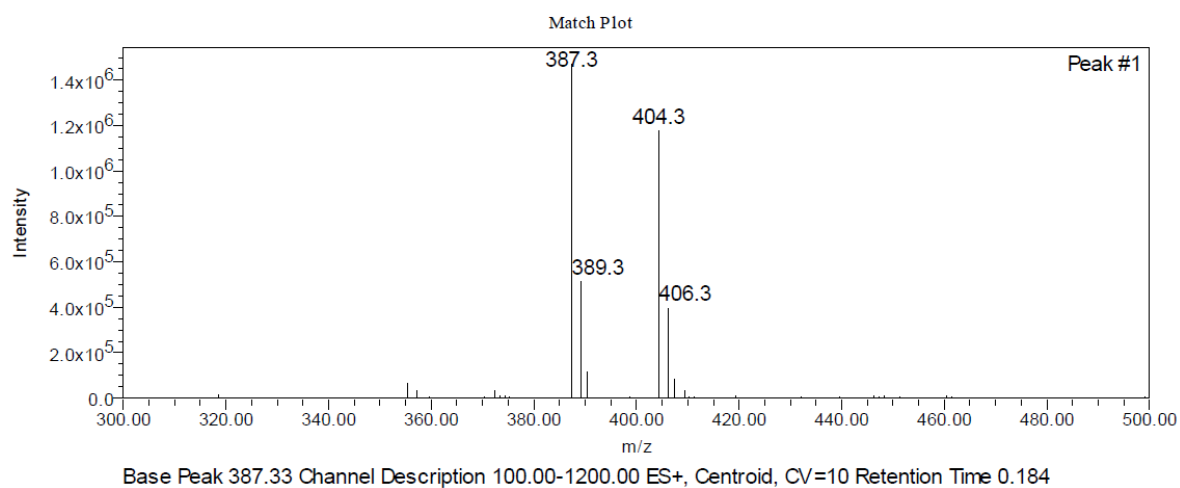
Peak Results
Channel: SQ 1: MS Scan

	Retention Time (min)	Base Peak (m/z)	Height (μV)	Area (μV*sec)	% Area	Channel	Channel Name
1	1.889	369.39	47636893	118471397	100.00	SQ 1: MS Scan	MS TIC



5.5.50 ^1H NMR Spectrum (400 MHz, DMSO) of compound 2e

5.5.51 ESI-MS Spectrum of compound 2e



5.6 TLC analysis of synthesized compounds

The purity of synthesized compounds (**1a-1p**, **2a-2e**) were checked on aluminum foil pre-coated with silica gel 60 F254, visualized under UV cabinet. TLC analysis was performed using *n*-hexane and ethyl acetate (8:2 v/v) mobile phase. All the synthesized final compounds when analyzed by TLC, showed a single spot giving preliminary indication of the purity shown in figure 5.2.

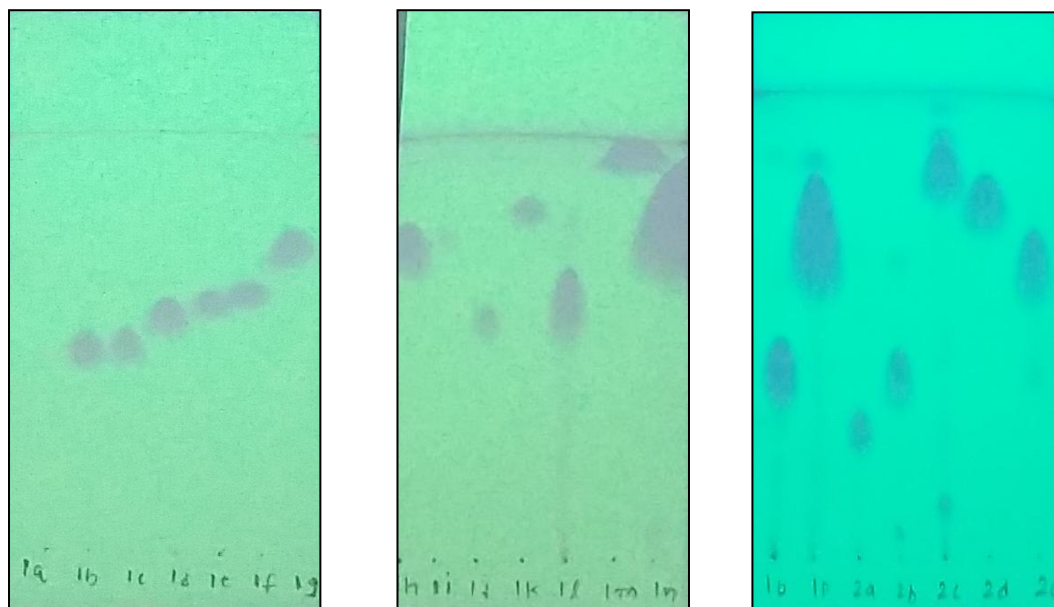


Figure 5.2 TLC analysis of synthesized compounds

5.7 Conclusion

Total 21 compounds (**1a-1p**, **2a-2e**) of N^{1,3}-disubstituted imidazolidin-2-one derivatives were successfully synthesized where 1a-1p series of compounds were obtained in better yield as compared to 2a-2e series. Structural conformation of the final compounds was carried through ESI-MS spectra. Compounds with bromo and chloro substitutions showed [M+2]⁺ peaks which confirms the appearance of these substitutions in the synthesized moieties. In IR spectra, a sharp peak was observed at around 1680 - 1760 cm⁻¹ which indicates the presence of a carbonyl group. Further, structure confirmation was performed using ¹H NMR and ¹³C NMR analysis. In ¹H NMR, the two cyclic -CH₂- protons of the imidazolidinone ring showed a splitting pattern as triplet at around 3.91 - 3.87 and 3.44 - 3.40 ppm, and the aliphatic -CH₂- protons were observed as singlet at around 4.40 ppm which confirms the formation of the desired N-alkylated product in the final step of the reaction scheme. The aromatic region protons showed a splitting pattern as multiplets in the range of 7.3 - 7.9 ppm. In proton decoupled ¹³C NMR, all carbon atoms with different environment appeared at different δ values as a singlet peak. Carbon attached to the N-urea of imidazolidinone appeared at around 159.1 ppm and the carbons present as cyclic -CH₂- appeared at around 42 and 43 ppm, while the aliphatic -CH₂- appeared at around 47 ppm. All the aromatic carbon atoms of the phenyl ring appeared in the range of 125 - 150 ppm depending upon their substitutions.

LC-MS analysis of compound **2d** represents a single peak (100 % AUC) at 1.869 retention time in PDA spectrum at 254 λ_{max} , and the corresponding MS spectrum indicates mass intensity of that peak at 1.889 retention time. The mass spectrum analysis shows a base peak at 369.39 [M+1]⁺ as the most stable ion peak. Hence, ¹H NMR, ¹³C NMR, LC-MS spectra and TLC analysis confirmed the structures together with purity of newly synthesized compounds. Similar results were obtained for other synthesized compounds.

5.8 References

- Andrés, Ignacio J., et al. "Synthesis and biological evaluation of imidazol-2-one and 2-cyanoiminoimidazole derivatives: novel series of PDE4 inhibitors." *Bioorganic & Medicinal Chemistry Letters*, vol. 12, no. 4, 2002, pp. 653–658.
- Chern, Jyh-Haur, et al. "Synthesis and antipicornavirus activity of (R)- and (S)-1-[5-(4'-Chlorobiphenyl-4-yloxy)-3-Methylpentyl]-3-Pyridin-4-yl-Imidazolidin-2-one." *Bioorganic & Medicinal Chemistry Letters*, vol. 15, no. 19, 2005, pp. 4206–4211.
- Fortin, Sébastien, et al. "Design, Synthesis, Biological Evaluation, and Structure–Activity Relationships of Substituted Phenyl 4-(2-Oxoimidazolidin-1-yl)Benzenesulfonates as New Tubulin Inhibitors Mimicking Combretastatin A-4." *Journal of Medicinal Chemistry*, vol. 54, no. 13, 2011, pp. 4559–4580.
- Gaudreault, Rene C., and Fortin, Sebastien. "Substituted 2-imidazolidones and analogs" WO 2011100840 A1. 25 Aug 2011. (b) Burow, Kenneth Wayne, Jr.; St. Clair, Roger Lee. "Imidazolidinone derivatives" EP0044185 A2. 20 Jan 1982.
- Goodacre, Caroline J., et al. "A series of bisaryl imidazolidin-2-Ones has shown to be selective and orally active 5-HT_{2C} receptor antagonists." *Bioorganic & Medicinal Chemistry Letters*, vol. 15, no. 22, 2005, pp. 4989–4993.
- Lima, Heather M., and Carl J. Lovely. "Synthesis of 2-Imidazolones and 2-Iminoimidazoles." *Organic Letters*, vol. 13, no. 21, 2011, pp. 5736–5739.
- Robert, Jean-Michel H, et al. "Synthesis and antileishmanial activity of new imidazolidin-2-One derivatives." *European Journal of Medicinal Chemistry*, vol. 38, no. 7-8, 2003, pp. 711–718.
- Verma, Amita, et al. "Imidazole: Having Versatile Biological Activities." *Journal of Chemistry*, vol. 2013, 2013, pp. 1–12.
- Wang, Liutang, et al. "Synthesis and evaluation of structurally constrained imidazolidin derivatives as potent dipeptidyl peptidase IV inhibitors." *European Journal of Medicinal Chemistry*, vol. 44, no. 8, 2009, pp. 3318–3322.
- Xue, Na, et al. "Synthesis and biological evaluation of imidazol-2-One derivatives as potential antitumor agents." *Bioorganic & Medicinal Chemistry*, vol. 16, no. 5, 2008, pp. 2550–2557.

6.1 *In-vitro* Screening for GSK-3 β Inhibitory Activity

This chapter presents *in-vitro* screening of 24 test compounds on GSK-3 β target. The IC₅₀ values were determined for all test compounds using ADP-Glo™ Kinase assay.

6.1.1 Principle of ADP-Glo™ Kinase Assay

The ADP-Glo™ Kinase assay is a luminescent kinase assay that measures ADP formed from a kinase reaction; ADP is converted into ATP, which is converted into light by Ultra-Glo™ Luciferase. The luminescent signal is correlated with the amount of ATP present and is inversely correlated with the amount of kinase activity (Figure 6.1).

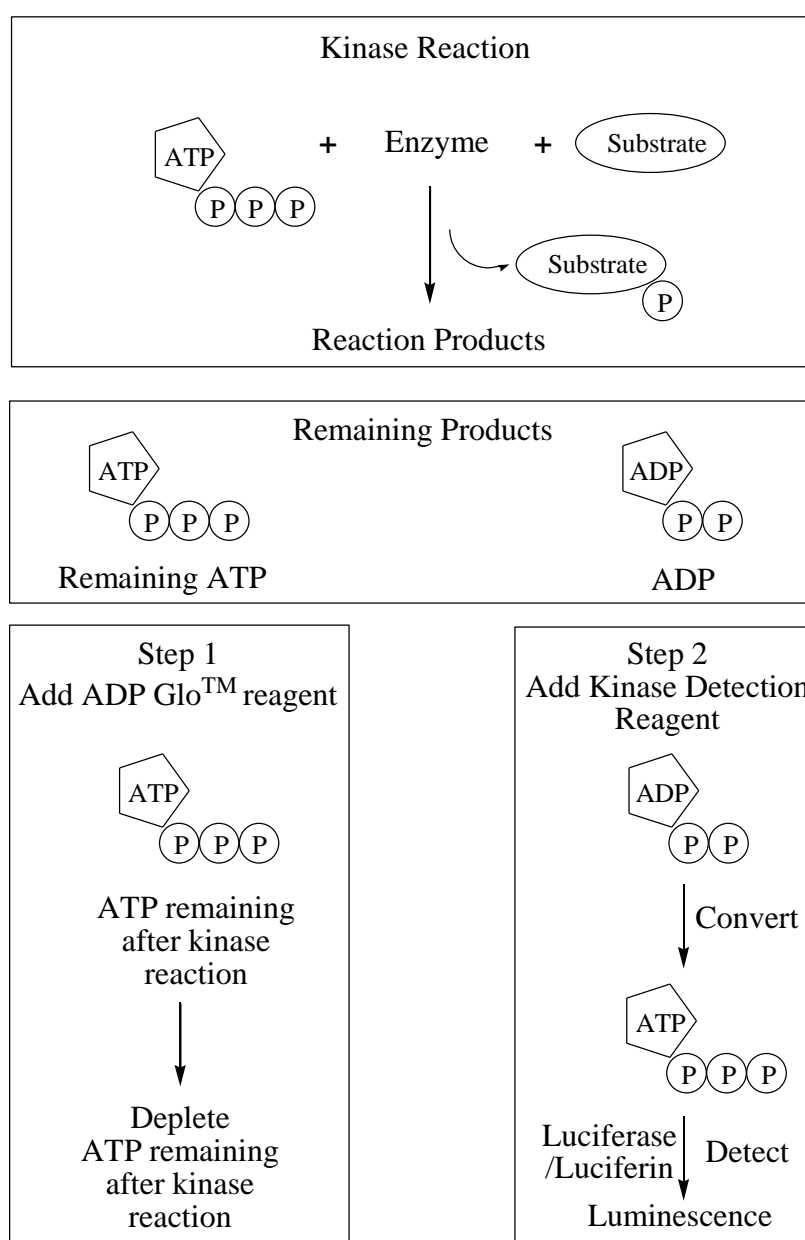


Figure 6.1 Principle of ADP-Glo™ Kinase Assay (adapted from Promega corporation)

The ADP-Glo™ Kinase assay kit (Catalogue number V9101) consists of: (i) ADP-Glo™ reagent (ii) kinase detection reagent (prepared by mixing kinase detection buffer with a lyophilized kinase detection substrate) and (iii) ultrapure adenosine triphosphate (ATP) and ADP.

Upon completion of kinase reaction the assay procedure consists of two steps: (i) addition of ADP-Glo™ reagent for termination of kinase reaction and depletion of remaining ATP (40 minute incubation time) (ii) the kinase detection reagent is added to convert ADP to ATP and the newly generated ATP by reaction with luciferase/luciferin produces luminescence (incubation is 30 - 60 minutes depending on the ATP concentration used in the kinase reaction). The luminescent signal generated is proportional to the ADP concentration produced and is inversely correlated with the kinase activity (Auld et al.; Glickman; Tanega et al.; Zegzouti et al.).

6.1.2 Materials and Reagents

1. ADP-Glo™ Kinase Assay Kit: Catalogue Number (V9101), procured from Promega
2. Enzyme: GSK-3 β , catalogue number (G09-10G), procured from SignalChem
3. Substrate: Human glycogen synthase 1 (GS1), catalogue number (G50-58) procured from SignalChem
4. Standard drug: Tideglusib, product catalogue number (SML0339), procured from Sigma-Aldrich
5. Test groups: Synthesized compounds of series 1a-1p, 2a-2e and compound codes of AT-057/43486355, AO-476/41610153, and AK-080/40907857 procured from SPECS. Eleven different concentrations of test compounds were prepared ranging from 0.003 - 100 μ M concentrations
6. Vehicle: DMSO
7. Plate Reader: Envision of Perkin Elmer

6.1.3 Assay Procedure

The ADP-Glo™ Kinase assay was performed according to the supplier protocol (Promega; catalogue number V9101).

6.1.3.1 Assay Standardization of GSK-3 β

Assay standardization was performed to find the optimum concentration of enzyme (GSK-3 β), ATP and substrate (GS1) for use in subsequent inhibitor concentration response

curve (CRC) determination. Standardization of GSK-3 β assay was performed with three steps using 384-well plate format.

- i) Enzyme titration protocol (Protocol I)
- ii) Determination of ATP (Km) protocol (Protocol II)
- iii) Determination of substrate (Km) Protocol (Protocol III)

Steps followed for GSK-3 β assay standardization protocol:

Assay standardization was performed with 10 μ L kinase reaction containing kinase buffer followed by incubation at 30 °C for a period of 15 minutes. The enzymatic reaction was stopped with 5 μ L of ADP-Glo™ reagent thus depleting unconsumed ATP, leaving only ADP and a very low background of ATP. The enzymatic reaction was incubated for a period of 40 minutes at room temperature. Subsequently, 10 μ L of kinase detection reagent was added to convert ADP to ATP and luciferase and luciferin were added to detect ATP. Luminescence was recorded after 30 minutes of incubation at room temperature.

Protocol 1: Enzyme titration protocol was performed with fixed concentration of substrate (10 μ M), ATP (10 μ M) and using 8 different concentrations of enzyme as outlined in table 6.1. As a control, a repeat titration was carried out in the absence of enzyme.

Table 6.1 Enzyme titration protocol for standardization of GSK-3 β

Assay Components	Positive control* (μ L)	Background (μ L)
Enzyme (different conc.)	2.5	---
Assay Buffer	2.5	5
ATP (10 μ M)	2.5	2.5
Substrate (10 μ M)	2.5	2.5
Incubation at 30 °C for 15 minutes		
ADP-Glo™ Reagent	5	5
Incubation at RT for 40 minutes		
Kinase Detection	10	10
Incubation at RT for 30 minutes		
Luminescence determination in EnVision		
<i>Abbreviations:</i> RT, room temperature; μ L, microlitre; μ M, micromolar. *As a positive control, enzyme, ATP and substrate were added to each well.		

Protocol 2: Determination of optimum concentration (K_m) for ATP with 8 different concentrations of ATP, and fixed concentration of enzyme (7.5 ng/well) and substrate (10 μ M) was performed as per the protocol outlined in table 6.2. As a control, a repeat titration was carried out in the absence of enzyme.

Table 6.2 ATP titration protocol for standardization of GSK-3 β

Assay Components	Positive control* (μ L)	Background (μ L)
ATP (different conc.)	2.5	2.5
Assay Buffer	2.5	5
Enzyme (7.5 ng/well)	2.5	---
Substrate (10 μ M)	2.5	2.5
Incubation at 30 °C for 15 minutes		
ADP-Glo™ Reagent	5	5
Incubation at RT for 40 minutes		
Kinase Detection	10	10
Incubation at RT for 30 minutes		
Luminescence determination in EnVision		
<i>Abbreviations:</i> RT, room temperature; μ L, microlitre; μ M, micromolar; ng, nanogram. *As a positive control, enzyme, ATP and substrate were added to each well.		

Protocol 3: Determination of optimum concentration (K_m) of the substrate with 8 different concentrations of substrate, fixed concentration of enzyme (7.5 ng/well) and ATP (10 μ M) was performed as per the protocol outlined in table 6.3. As a control, a repeat titration was carried out in the absence of enzyme.

Table 6.3 Determination of substrate (K_m) protocol for standardization of GSK-3 β

Assay Components	Positive control (μ L)	Background (μ L)
Substrate (different conc.)	2.5	2.5
Assay Buffer	2.5	5
Enzyme (7.5 ng/well)	2.5	---
ATP (10 μ M)	2.5	2.5
Incubation at 30 °C for 15 minutes		
ADP-Glo™ Reagent	5	5
Incubation at RT for 40 minutes		
Kinase Detection	10	10
Incubation at RT for 30 minutes		
Luminescence determination in EnVision		

6.1.3.2 Protocol for assay validation of GSK-3 β

Assay validation was performed to determine the IC₅₀ value of the reference compound Tideglusib with 11 point concentration response curve (CRC). The assay validation was performed as per the given protocol indicated in table 6.4.

Table 6.4 Protocol for determination of IC₅₀ for the reference compound (Tideglusib)

Assay Components	Positive Control (μL)	Negative Control (μL)	Background (μL)
Enzyme	2.5	2.5	---
Inhibitor (different conc.)	---	2.5	---
Assay Buffer*	---	---	5
Incubation at RT for 60 minutes			
DMSO (4 %)	2.5	---	2.5
ATP	2.5	2.5	2.5
Substrate	2.5	2.5	---
Incubation at RT for 15 minutes			
ADP-Glo™ Reagent	5	5	5
Incubation at RT for 40 minutes			
Kinase Detection	10	10	10
Incubation at RT for 30 minutes			
Luminescence determination in EnVision			
*Assay Buffer composition: HEPES pH 7.4: 15 mM, NaCl: 20 mM, Tween 20: 0.02 %, MgCl ₂ : 10 mM, EGTA: 1 mM, EDTA: 1 mM, DTT: 0.25 mM Abbreviations: RT, room temperature; μL, microlitre; DMSO, dimethylsulphoxide; ATP, adenosine triphosphate.			

6.1.3.3 Data Analysis

The data generated was exported to excel file and the percentage inhibition was calculated using the following formula:

$$\text{Percent inhibition} = 100 - (100 \times (\text{RU-NC}) / (\text{PC-NC}))$$

where RU = relative unit

NC = 100 % inhibition control (negative control)

PC = Maximum signal wells (positive control)

The data analysis for concentration response curves (i.e. IC₅₀ assessment) were calculated using a 4-parameter logistic non-linear regression model in GraphPad Prism software (version 6.0).

6.1.4 Results and Discussion

6.1.4.1 Determination of optimal enzyme concentration (protocol I)

The enzyme titrations were performed using eight different concentrations of enzyme (range: 0.3 - 40 ng; 2-fold dilutions) and keeping fixed concentrations of ATP (10 μ M) and substrate (10 μ M) in triplicates. Different concentrations of enzyme and their respective measurement of relative light unit (RLU) were recorded as shown in table 6.5.

Table 6.5 Determination of optimal enzyme concentration

GSK-3 β (ng/well)	RLU1	RLU2	RLU3	Avg*	Avg - B [#]	S/B [^]
Blank (B)	1520	1640	1560	1573		
40	50040	50760	52920	51240	49667	32
20	27000	29520	30480	29000	27427	17
10	18080	18240	20920	19080	17507	11
5	10840	11160	12200	11400	9827	6
2.5	6560	6400	6440	6467	4893	3
1.25	3320	3320	2720	3120	1547	1
0.625	1600	1840	1600	1680	107	0
0.3125	1040	1160	1320	1173	-400	0

*Avg, Average of relative light unit (RLU) in triplicates.
[#]Avg-B, the average change in relative light unit (RLU) minus the zero enzyme control (blank).
[^]S/B, Signal-to-background ratio is a measure of average change in relative light unit (RLU) compared to the zero enzyme control.

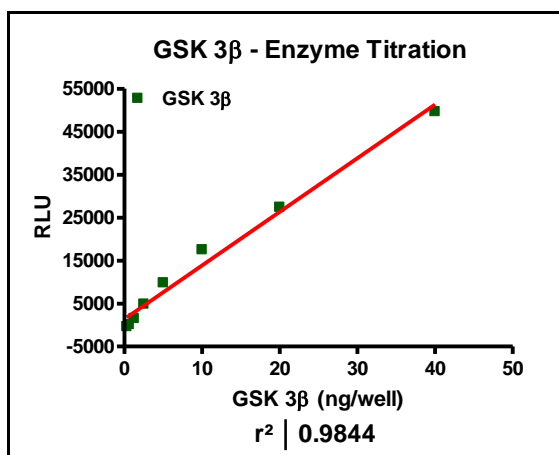


Figure 6.2 Plot of relative light unit (RLU) versus different concentrations of GSK-3 β enzyme (ng)

The graph shown in figure 6.2 concludes that the enzyme activity was linear for all concentrations of the enzyme. Results from table 6.5 showed that the signal-to-background (S/B) ratio was 11-fold for 10 ng concentration of enzyme. The observed difference was more than 5-fold as compared to the lower concentrations of enzyme. Therefore, a concentration of 7.5 ng for the enzyme was fixed as the optimal enzyme concentration for enzyme inhibition studies.

6.1.4.2 Determination of optimal ATP concentration (protocol II)

The ATP titration was performed to fix the optimal concentration of ATP for the entire study which was obtained using different concentrations of ATP and keeping fixed concentrations of enzyme (7.5 ng) and substrate (10 μ M). Different concentrations of ATP and their respective measurement of relative light unit (RLU) were recorded as shown in table 6.6.

Table 6.6 Determination of optimal ATP concentration

GSK-3 β enzyme (ng)	ATP (μ M)	RLU1	RLU2	RLU3	Avg	Avg-B	S/B
	Blank	2040	2080	1600	1906		
7.5 ng	40	37000	48400	43280	42893	40987	21
	20	33360	33360	29960	32227	30320	16
	10	23960	21760	24080	23267	21360	11
	5	16240	17200	15120	16187	14280	7
	2.5	10840	11280	11080	11067	9160	5
	1.25	7560	6800	6480	6947	5040	3
	0.625	5200	4840	4480	4840	2933	2
	0.3125	3240	3080	2360	2893	987	1

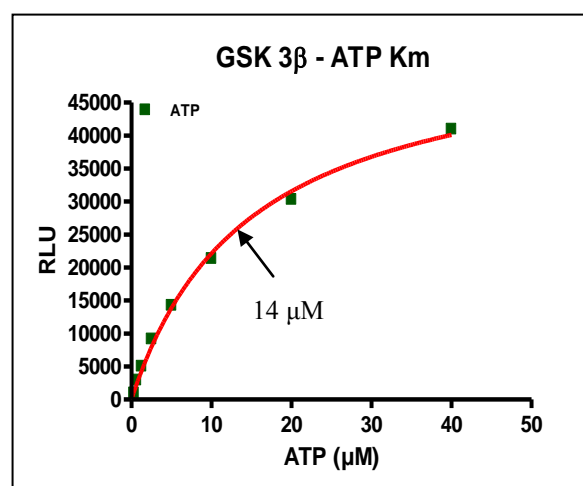


Figure 6.3 Plot of relative light unit (RLU) versus different concentrations of ATP (μ M)

From the above graph, the K_m assessed was found to be 14 μM (Figure 6.3). Therefore 10 μM ATP concentration was fixed as the optimal ATP concentration for enzyme inhibition studies.

6.1.4.3 Determination of optimal substrate concentration (protocol III)

The substrate titration was performed to fix the optimal concentration of substrate (GS1) for the entire study which was obtained using different concentrations of substrate and keeping fixed concentrations of enzyme (7.5 ng) and ATP (10 μM). Different concentrations of ATP and their respective measurement of relative light unit (RLU) were recorded as shown in table 6.7.

Table 6.7 Determination of optimal substrate concentration

GS1 (μM)	RLU1	RLU2	RLU3	Avg	Avg-B	S/B
Blank	1240	1480	1160	1293		
40	24800	32200	29200	28733	27440	21
20	24720	28320	28240	27093	25800	20
10	23200	25880	22280	23787	22493	17
5	21280	22960	19800	21347	20053	16
2.5	17680	20000	18760	18813	17520	14
1.25	12600	15120	14960	14227	12933	10
0.625	11520	12520	11160	11733	10440	8
0.3125	7600	7480	8080	7720	6427	5

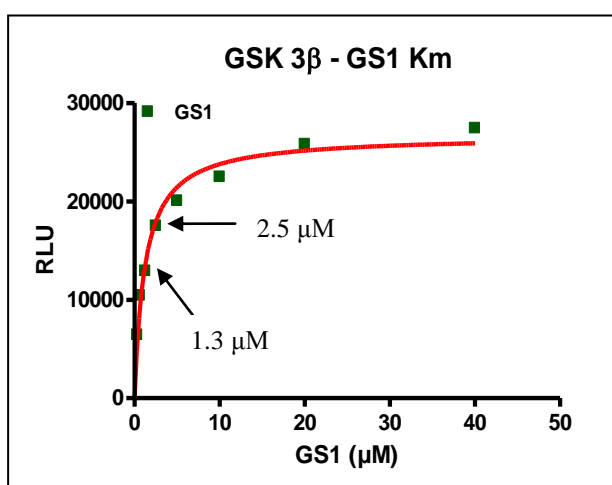


Figure 6.4 Plot of relative light unit (RLU) versus different concentrations of substrate (GS1) (μM)

From the above graph, the K_m assessed was found to be 1.3 μM (Figure 6.4). Therefore, a 2 μM GS1 concentration was selected as the optimal substrate concentration for enzyme inhibition studies.

6.1.4.4 Results of DMSO Tolerance Test

DMSO tolerance test was used to fix the percentage of DMSO for compound treatment. In some enzymatic assays, DMSO concentrations affects enzyme activity. Therefore appropriate concentration of DMSO is to be selected prior to enzyme inhibition studies. Different concentrations of DMSO were tested with GSK-3 β as shown in table 6.8.

Table 6.8 Determination of optimal DMSO concentration

% DMSO	RLU1	RLU2	RLU3	Avg	Avg-B	S/B
Blank	1247	1380	1260	1296		
10	3480	4240	4120	3947	2651	2
5	6360	7640	6680	6893	5598	4
2.5	8080	9920	8440	8813	7518	6
1.25	12000	14920	12640	13187	11891	9
0.625	15320	16200	16080	15867	14571	11
0.3125	13480	14640	14600	14240	12944	10
0.15625	14760	15440	13480	14560	13264	10
0.078125	14600	15840	13320	14587	13291	10

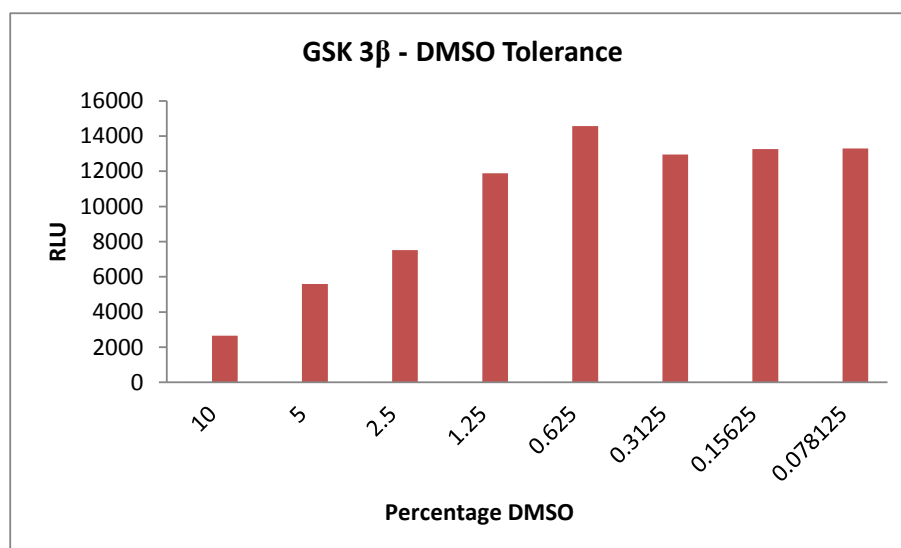


Figure 6.5 Plot of relative light unit (RLU) versus percentage of DMSO

The loss of GSK-3 β activity was observed with ~1.25 % DMSO (Figure 6.5). Therefore, 1 % DMSO was selected as the optimum percentage for enzyme inhibition studies.

6.1.4.5 Results of GSK-3 β assay validation

After determining appropriate concentrations of GSK-3 β (7.5 ng), ATP (10 μ M) and GS1 substrate (2 μ M), assay validation was performed with reference compound Tideglusib. The IC₅₀ value of Tideglusib was determined by preparing 11 different concentrations of Tideglusib ranging from 0.003, 0.009, 0.0029, 0.0093, 0.0296, 0.0937, 0.2971, 0.9418, 2.9854, 9.4637 and 30 micromolar concentrations. Luminescence was measured using Envision plate reader (Perkin Elmer) with an integration time of 1 second per well.

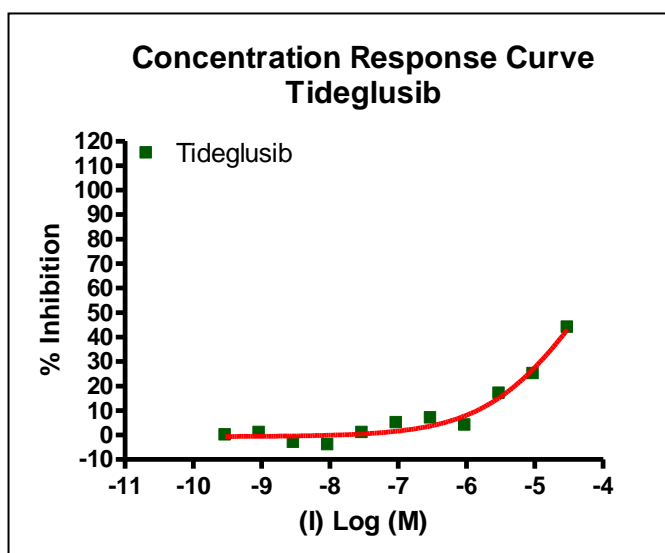


Figure 6.6 Concentration response curve of Tideglusib using ADP-GloTM Kinase assay

The IC₅₀ value of Tideglusib was determined based on the concentration response curves generated by x-y scatter plot using GraphPad Prism software (version 6.0). Briefly, the concentration versus percent inhibition values were transformed and analyzed through non-linear sigmoid curve option of the software (variable slope). Based on the observed data, the IC₅₀ value of Tideglusib should be greater than 30 μ M as 100 percent inhibition was not observed at the top tested concentration. It was observed as 44 percent maximal inhibition.

In order to identify probable IC₅₀ of Tideglusib, the top percentage inhibition was locked at 100 percent by applying a constraint in GraphPad Prism software. This enabled to visualize a probable IC₅₀ for the compound. From the above graph, Tideglusib showed 44 percent inhibition at 30 μ M with GSK-3 β . Therefore, the IC₅₀ assessed was found to be 46 μ M.

6.2 Results of GSK-3 β screening of 24 test compounds

The ADP-GloTM Kinase assay was performed according to the supplier protocol (Promega; catalogue number V9101) and the method described by Jolanta Vidugiriene et al. The IC₅₀ values of 24 test compounds and Tideglusib were determined with concentrations ranging from 0.003 μ M to 100 μ M with 3-fold serial dilutions from the top concentration dissolved in 1 % DMSO. The compound concentration used for GSK-3 β inhibition was taken on the x-axis and the luminescence data obtained for the compounds was taken on the y-axis. The concentration response curves (i.e. IC₅₀ assessment) were calculated using a 4-parameter logistic non-linear regression model in GraphPad Prism software.

The IC₅₀ values were determined for all test compounds (1a-1p, 2a-2e, AT-057/43486355, AO-476/41610153 and AK-080/40907857) and the reference compound Tideglusib. All experiments of Tideglusib were performed in triplicates and their results are shown in figure 6.6 and 6.7. Tideglusib was found to have an inhibitory effect on GSK-3 β activity in micromolar range (i.e. plate 1 IC₅₀: 16 μ M and plate 2 IC₅₀: 26 μ M respectively by applying a top constraint at 100 percent in GraphPad Prism software). However, the results of assay validation of GSK-3 β inhibition with Tideglusib assessed was found to be 46 μ M. The variability around IC₅₀ value of Tideglusib was found to be 3-fold. Therefore, mean IC₅₀ value of Tideglusib was obtained using the formula of standard deviation of the mean in Microsoft excel.

$$\sigma_M = \frac{\sigma}{\sqrt{N}}$$

Where,

σ_M = Standard error of the mean

σ = Standard deviation of the original distribution

N = Sample size (three values i.e. 46 μ M, 16 μ M and 26 μ M)

\sqrt{N} = Root of sample size

The mean IC₅₀ of Tideglusib was obtained as 29.33 \pm 8.81 μ M, where 8.81 is the standard error of the mean. Among the test compounds, four compounds (compounds 1i, 1n, 2d and AO-476/41610153) showed IC₅₀ values greater than 100 micromolar concentration as these compounds never attained 100 percent maximal inhibition at the top tested concentration (Figure 6.8). As IC₅₀ represents the compound concentration that inhibits 50 percent of the enzyme activity, a precise IC₅₀ was not attained for these compounds. In order

to draw out a probable IC_{50} of these compounds, the top percentage inhibition was locked at 100 percent by applying a constraint using GraphPad Prism software. This enabled to visualize a probable IC_{50} of the four test compounds which were found to be greater than 100 μM . The remaining test compounds failed to show appropriate activity (Table 6.9).

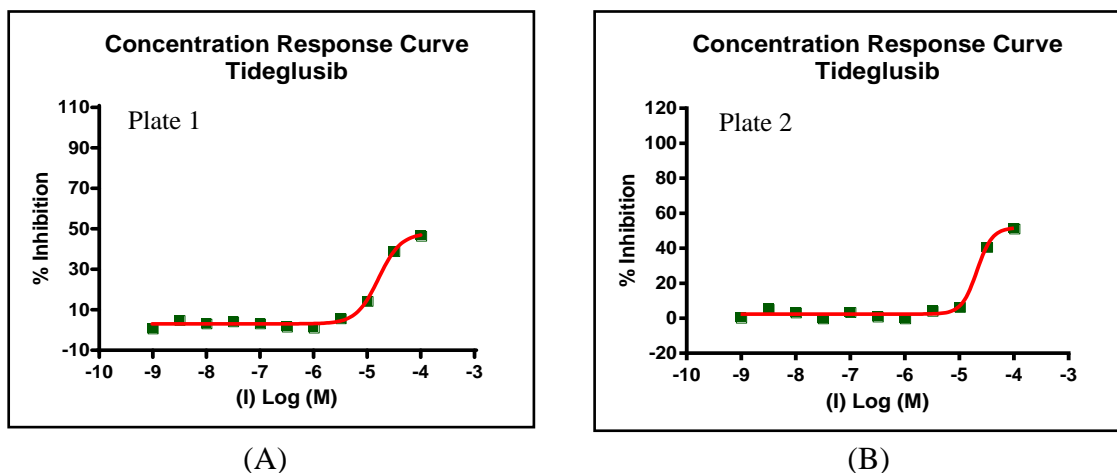


Figure 6.7 Concentration response plot of reference compound Tideglusib (A, plate 1 IC_{50} : 16 μM and B, plate 2 IC_{50} : 26 μM)

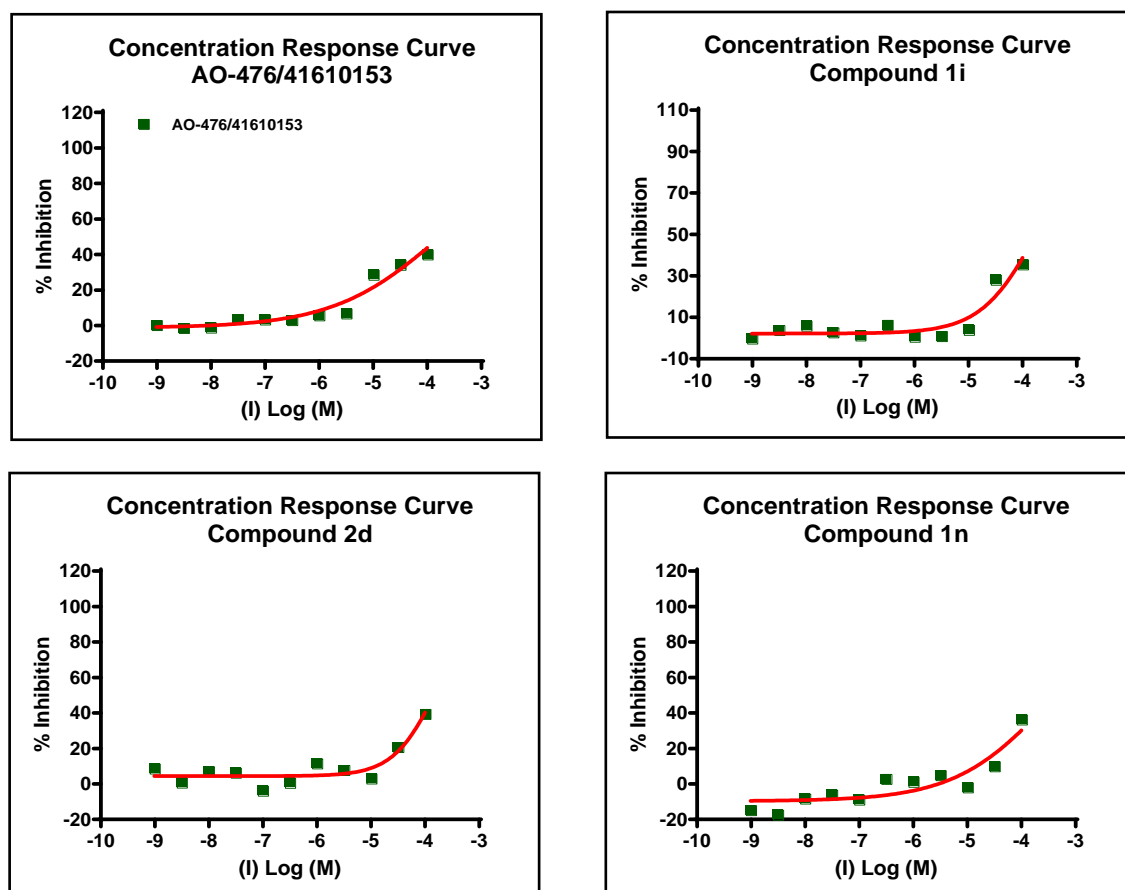
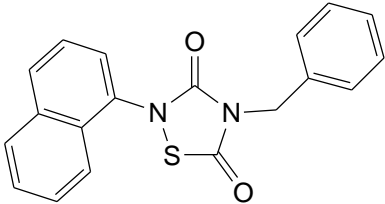
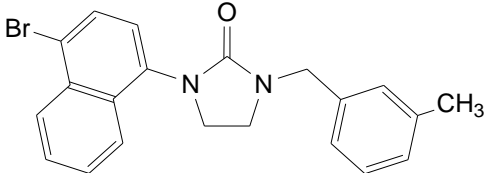
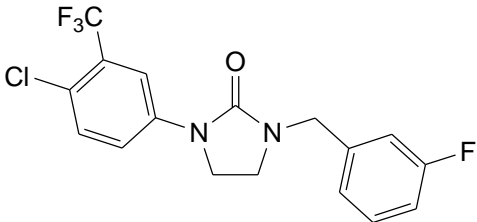
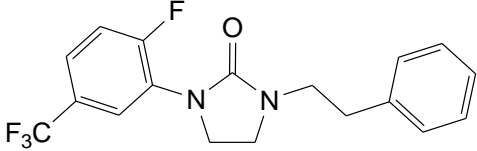
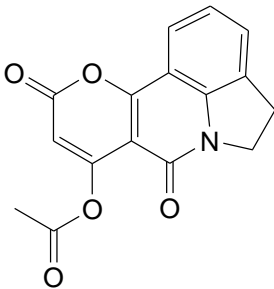


Figure 6.8 Concentration response plots of compounds AO-476/41610153, 1i, 1n and 2d using ADP-GloTM Kinase assay

Table 6.9 GSK-3 β inhibitory activity of four test compounds

Compound Code	Structure	IC ₅₀ (μ M)#
Tideglusib (standard drug)		29.33 \pm 8.81*
1i		>100
1n		>100
2d		>100
AO-476/41610153		>100
All other test compounds failed to show appropriate activity		
<p><i>Abbreviation:</i> μM, micromolar.</p> <p>#A top constraint was applied at 100 percent using GraphPad Prism software.</p> <p>*Mean IC₅₀ value of Tideglusib was determined as 29.33 \pm 8.81 μM.</p>		

6.3 Conclusion

Inhibition of GSK-3 β was measured using an ADP-GloTM kinase assay of Promega corporation. Assay standardization was performed to find the optimal concentrations of ATP (10 μ M), substrate glycogen synthase 1 (2 μ M) and GSK-3 β (7.5 ng) for the entire study. The half maximal inhibitory concentration (IC₅₀) values were determined from 11 data point concentration response plots of 24 test compounds and Tideglusib. Tideglusib was found to have inhibitory effect on GSK-3 β activity with micromolar potency. Based on the results displayed using ADP-GloTM kinase assay, the mean IC₅₀ value determined for Tideglusib is in micromolar range i.e. 29.33 ± 8.81 μ M.

However, the potency reported in the literature of Tideglusib was measured with different assay using fluorescence resonance energy transfer FRET-based Z'-LYTETM technology and involves the use of specific peptide substrate, "Ser/Thr-9", a fluorescein and coumarin double-labeled peptide based on the sequence of human glycogen synthase 1 containing Ser-641. Domínguez et al. reported the IC₅₀ value of Tideglusib as 60 nM using FRET-based Z'-LYTETM technology. Morales-Garcia et al. reviewed the IC₅₀ value of Tideglusib for GSK-3 β inhibition in micromolar range i.e. 1 μ M (unpublished experimental data).

Based on the ADP-GloTM kinase assay, the substrate used is a generic GSK-3 substrate procured from SignalChem that differs from the reported literature. The GSK-3 substrate peptide sequence is based on human muscle glycogen synthase 1. Additionally, based on literature reported by Martinez; it has been demonstrated that TDZD series of compounds (the class in which Tideglusib belongs) were found to have micromolar potency.

Among the twenty four test compounds evaluated for GSK-3 β inhibitory potency, four compounds (compound 1i, 1n, 2d and AO-476/41610153) were found to exhibit IC₅₀ greater than 100 μ M (these compounds never attained 100 percent maximal inhibition at the top tested concentration). The remaining test compounds failed to show any appreciable activity. These results conclude that the four identified hit compounds showed weak inhibitory activity on GSK-3 β . Further chemical modification of these compounds could provide compounds with better activity on GSK-3 β .

6.4 References

- Auld, Douglas S., et al. "A Basis for Reduced Chemical Library Inhibition of Firefly Luciferase Obtained from Directed Evolution." *Journal of Medicinal Chemistry*, vol. 52, no. 5, Dec. 2009, pp. 1450–1458.
- Cohen, Philip. "Protein Kinases - the Major Drug Targets of the Twenty-First Century?" *Nature Reviews Drug Discovery*, vol. 1, no. 4, 2002, pp. 309–315.
- Domínguez, Juan Manuel, et al. "Evidence for Irreversible Inhibition of Glycogen Synthase Kinase-3 β by Tideglusib." *Journal of Biological Chemistry*, vol. 287, no. 2, 2011, pp. 893–904.
- Glickman, J. Fraser, and Doug Auld. "Protein Nanoarrays." *Assay and Drug Development Technologies*, vol. 2, no. 4, Jan. 2004, pp. 446–446.
- Martinez, Ana, et al. "First Non-ATP Competitive Glycogen Synthase Kinase 3 β (GSK-3 β) Inhibitors: Thiadiazolidinones (TDZD) as Potential Drugs for the Treatment of Alzheimers Disease." *Journal of Medicinal Chemistry*, vol. 45, no. 6, 2002, pp. 1292–1299.
- Morales-Garcia, Jose A., et al. "Glycogen Synthase Kinase 3 Inhibition Promotes Adult Hippocampal Neurogenesis *in Vitro* and *in Vivo*." *ACS Chemical Neuroscience*, vol. 3, no. 11, 2012, pp. 963–971.
- Tanega, Cordelle, et al. "Comparison of Bioluminescent Kinase Assays Using Substrate Depletion and Product Formation." *Assay and Drug Development Technologies*, vol. 7, no. 6, 2009, pp. 606–614.
- Vidugiriene, Jolanta, et al. "Evaluating the Utility of a Bioluminescent ADP-Detecting Assay for Lipid Kinases." *Assay and Drug Development Technologies*, vol. 7, no. 6, 2009, pp. 585–597.
- Vidugiriene, Jolanta, et al. "GSK-3 β kinase assay" ADP-GloTM Kinase Assay Application Notes, Promega Corporation.
- Zegzouti, Hicham, et al. "ADP-Glo: A Bioluminescent and Homogeneous ADP Monitoring Assay for Kinases." *Assay and Drug Development Technologies*, vol. 7, no. 6, 2009, pp. 560–572.
- ADP-GloTM Kinase Assay Protocol, technical manual V9101.

7.1 Summary

Glycogen synthase kinase-3 (GSK-3) is a serine/threonine kinase identified three decades ago. Many pathologies such as Alzheimer's disease, type 2 diabetes, mood disorders, various types of cancer such as colon, liver, ovarian, and pancreatic tumors are developed by over-activity of GSK-3 β . Although a huge number of GSK-3 β inhibitors belonging to various chemical classes have been developed so far, none of them have reached the market. The most significant concern is the selectivity and safety against other kinases. Allosteric modulators of GSK-3 β could emerge as safe compounds for chronic treatments. In order to regulate the abnormal GSK-3 β brain levels, such inhibitors require crossing the blood-brain barrier. The preferred oral administration route for the treatment of CNS disorders, like chronic AD, exaggerates this problem, as it is very difficult to manage the equilibrium between molecular lipophilicity through entering into the brain and molecular hydrophilicity to be orally administered, and this requirement has ruled out several promising GSK-3 β inhibitors in the pre-clinical and clinical phases.

On the basis of the findings reported in literature the present research was focussed to design potent, selective and safe GSK-3 β inhibitors. Many substituted imidazolidin-2-one derivatives active on a variety of biological targets have been reported so far in literature. Particularly, N^{1,3}-disubstituted imidazolidin-2-one scaffold has been explored on the allosteric pocket of GSK-3 β . The design strategy for GSK-3 β inhibitors was combined applicability of *in-silico* fragment-based and molecular docking approaches using GLIDE XP. This study was performed by docking a diverse set of fragment-like subset of ZINC database in the allosteric pocket 7 of GSK-3 β . With this rational, 21 derivatives of N^{1,3}-disubstituted imidazolidin-2-one were shortlisted based on docking scores, *in-silico* physicochemical predictions and synthetic feasibility. These derivatives were synthesized using 2-chloroethylisocyanate condensed with appropriate arylamine which formed corresponding arylurea. Subsequent intramolecular cyclization of the arylurea intermediate under strong alkaline condition with sodium hydride resulted in the formation of monosubstituted imidazolidin-2-one. N-alkylation with substituted phenylethylbromide and substituted benzylbromide yielded desired N^{1,3}-disubstituted imidazolidin-2-one. The final synthesized compounds were characterized using spectroscopic techniques like FT-IR, Mass, ¹H NMR and ¹³C NMR which support the structure elucidation and purity of final compounds.

Application of virtual screening methodology based on structural features of Tideglusib; identified three novel hit compounds via shape-based similarity screening using

ROCS followed by molecular docking, electrostatic similarity search using EON and pharmacophore feature-based searching and molecular dynamics simulation approach. This approach yielded compounds AO-476/41610153, AT-057/43486355 and AK-080/40907857 (ZINC4192390) from the SPECS and ZINC database.

The inhibitory effect of 24 test compounds and Tideglusib on GSK-3 β was studied using ADP-GloTM Kinase assay. The IC₅₀ assessed for Tideglusib was found to be 29.33 \pm 8.81 μ M. Results of *in-vitro* screening of test compounds **1i**, **1n**, **2d** and **AO-476/41610153** were found to exhibit IC₅₀ values above 100 μ M. This concludes that the four identified hits were shown have weak inhibitory activity on GSK-3 β target. In docking computations, compounds **1i** and **AO-476/41610153** showed the highest GLIDE XP scores in the allosteric and substrate sites of GSK-3 β respectively. These results confirm that the docking protocol is in perfect agreement with the *in-vitro* results.

7.2 Future Prospects

Looking into the results of the present study, ideas that can be explored in future are:

- The exact binding mode and molecular inhibition mechanism of the identified hit compounds could be confirmed by kinetic experiments.
- The compounds **1i**, **1n**, **2d** and **AO-476/41610153** could be further screened *in-vivo* into animal models for diabetes and Alzheimer's disease.
- The identified hits (**1i,1n**, **2d** and **AO-476/41610153**) could be further studied with appropriate structural modifications giving lead molecules having better promise as therapeutic agents.